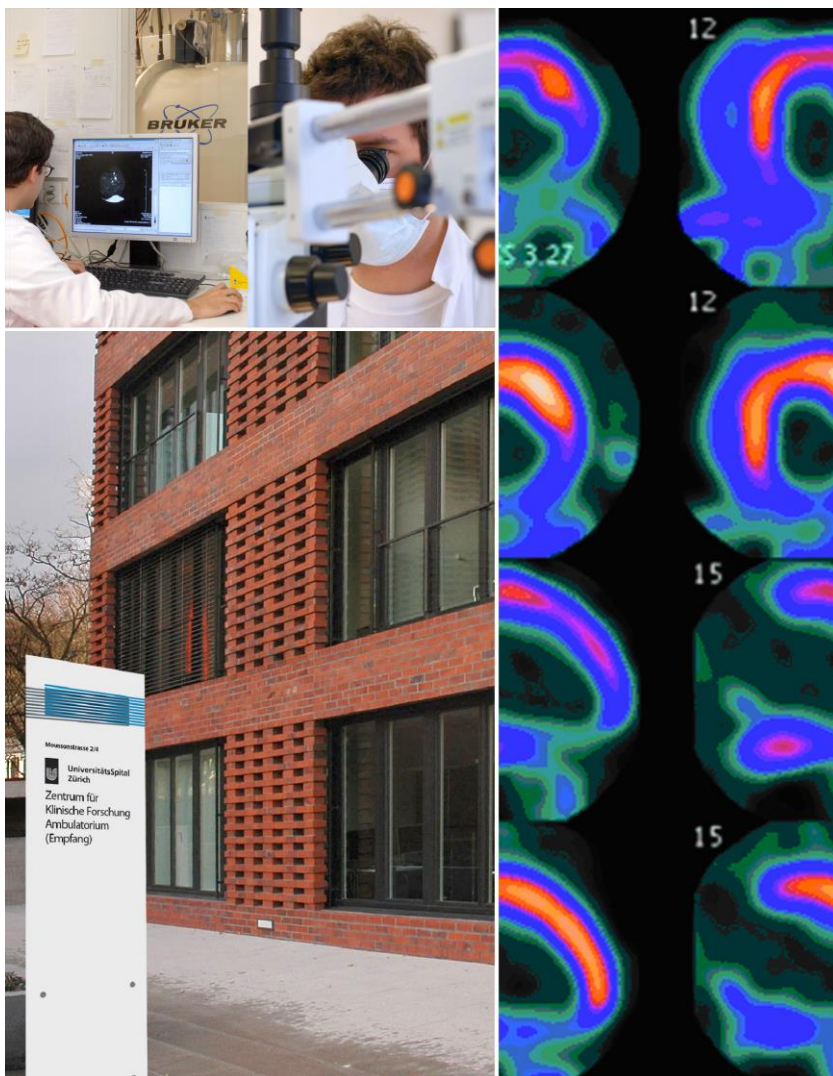


Program

- 14th Day of Clinical Research
- Georg-Friedrich-Götz-Preisverleihung 2015

Zurich, April 9, 2015



Structure of the Center for Clinical Research/

Clinical Trials Center

Kuratorium

Prof. Dr. K. W. Grätz (Dekan, ex officio)
Prof. Dr. Ch. Hock (Prorektor, ex officio)
Prof. Dr. E. Seifritz
Prof. Dr. J. Hodler
Prof. Dr. T. Lüscher
Prof. Dr. P.-A. Clavien
Prof. Dr. M. Pruschy
Prof. Dr. S. Gay
Prof. Dr. R. Nitsch
lic. oec. HSG R. Ziegler
Prof. Dr. B. Stieger
Prof. Dr. G. Zünd (Managing Director)

Direktorium

Prof. Dr. M. Weller
Prof. Dr. B. Beck Schimmer
Prof. Dr. A. von Eckardstein (Co-Direktor)
Prof. Dr. R. Graf
Prof. Dr. A. Aguzzi (Co-Direktor)
Prof. Dr. G. A. Kullak-Ublick
Prof. Dr. H. Moch
Prof. Dr. G. Spinaz
Prof. Dr. G. Zünd (Managing Director)

Geschäftsstelle ZKF

Robin Schneider, MBA
Geschäftsführer

Clinical Trials Center

PD Dr. G. Senti
Leitende Ärztin Clinical Trials Center

Biologisches Zentrallabor

Dr. Hugo Battaglia
Leiter Biologisches Zentrallabor

Zentrum für Regenerative Medizin

Prof. Dr. Dr. Simon P. Hoerstrup
Leiter Zentrum für Regenerative Medizin

Forschungsgruppenleiterkonferenz

Leitung: Prof. Dr. B. Beck-Schimmer
Prof. Dr. R. Graf
Scientific Research Group Leaders of the University Hospitals of Zurich (University Hospital, Children's Hospital, Balgrist University Clinic, Psychiatric University Hospital) and related institutions of the Faculty of Medicine

Table of contents

| | |
|--------------------------|-----------------|
| Program | 1 - 3 |
| List of Abstracts | 4 - 17 |
| Abstracts | 18 - 164 |

Bild Vorderseite: Verification of potential ischemia or scar tissue by PET in stress/rest test

Programm

Donnerstag, 9. April 2015

Grosser Hörsaal Ost

08.15 **Eröffnung**

Prof. Dr. Gregor Zünd
Managing Director ZKF, Direktor Forschung und Lehre UniversitätsSpital Zürich

08.20 **Begrüssung**

Rita Ziegler, lic. oec. HSG
Vorsitzende der Spitaldirektion

08.25 **Begrüssung**

Prof. Dr. Dr. Klaus W. Grätz
Dekan der Medizinischen Fakultät der Universität Zürich

Session 1: Cardiovascular Diseases/Metabolics/Endocrinology

Chairpersons: Prof. Dr. Frank Ruschitzka / Prof. Dr. Matthias Baumgartner

08.35 **Wissenschaftliches Hauptreferat**

“From preclinical to clinical research in international surgery”
Prof. Dr. Francesco Maisano, Klinikdirektor, Klinik für Herz- und Gefässchirurgie, USZ

08.55 **Trophic chain of lactate in infant’s gut revealed by a novel functional approach (Abstract No. 2299)**

V. Pham, C. Chassard, C. Braegger, C. Lacroix

09.05 **Safety of VEGF Inhibitors in Age-Related Macular Degeneration (SAVE-AMD) (Abstract No. 2353)**

F. Enseleit, S. Michels, M. Nägele, I. Sudano, M. Stahel, S. Zweifel, O. Schlager, M. Becker, S. Winnik, A. Flammer, M. Neidhart, N. Graf, CM. Matter, B. Seifert, T. Lüscher, F. Ruschitzka

09.15 **Deoxysphingolipids, a novel biomarker for type 2 diabetes, are cytotoxic for insulin-producing cells (Abstract No. 2306)**

R. Zuellig, T. Hornemann, A. Othman, A. Hehl, H. Bode, T. Güntert, O. Ogunshola, E. Saponara, K. Grabliauskaite, J. Jang, U. Ungethüm, Y. Wei, A. Von Eckardstein, R. Graf, S. Sonda

09.25 **Deletion of endothelial Rictor (mTORC2) constrains extensive FGF2 -induced vascular remodeling and growth in vivo and disables endothelial network formation in vitro (Abstract No. 2381)**

F. Aimi, S. Georgiopolou, I. Kalus, F. Lehner, N. Lindenblatt, I. Bhattacharya, V. Gomes de Lima, E. Haas, M. Rüegg, M. Hall, E. Battegay, R. Humar

09.35 **Differential Role of AKT-pathway in Mediating the Growth Effects of GPER in Human Coronary Arterial Smooth Muscle Cells and Human Umbilical Vein Endothelial Cells (Abstract No. 2301)**

E. Unterleutner, F. Barchiesi, B. Imthurn, R. Dubey

09.45 **Coffee Break**

Session 2: Hematology/Oncology

Chairpersons: Prof. Dr. Bernhard Pestalozzi, Prof. Dr. Holger Moch

10.00 **Wissenschaftliches Hauptreferat**

„Modeling drug resistant acute lymphoblastic leukemia at the interface of biology and clinical research“
PD Dr. Jean-Pierre Bourquin, Medizinische Klinik, Kinderspital Zürich

- 10.20 **Cell cycle Induction of Dormant Hematopoietic Stem Cells by Thrombopoietin Mimetic but not G-CSF (Abstract No. 2343)**
L. Kovtonyuk, M. Manz, H. Takizawa
- 10.30 **Identification of ADAM17 as a Novel Target for Radiosensitization of Non–Small Cell Lung Cancer (Abstract No. 2319)**
S. Bender, A. Sharma, O. Riesterer, A. Brogгинi-Tenzer, M. Pruschy
- 10.40 **Inositol trispyrophosphate (ITPP) and its anti-hypoxic potential in colorectal metastases of the liver (Abstract No. 2272)**
P. Limani, M. Linecker, N. Borgeaud, E. Kachaylo, C. Tschuor, A. Schlegel, J. Jang, S. Georgiopoulou, J. Lehn, R. Graf, B. Humar, PA. Clavien
- 10.50 **MiR-Score: A 6-microRNA signature for prognosis in malignant pleural mesothelioma (Abstract No. 2384)**
M. Kirschner, Y. Cheng, N. Armstrong, R. Lin, S. Kao, A. Linton, S. Klebe, B. McCaughan, N. Van Zandwijk, G. Reid
- 11.00 **The natural HLA ligandome of glioma stem-like cells: Another step towards peptide-based immunotherapy (Abstract No. 2398)**
M. Neidert, D. Kowalewski, F. Wolpert, S. Stevanovic, L. Regli, M. Weller, G. Eisele
- 11.10 **Lunch/Poster viewing**

Session 3: Stem Cell Research, Regenerative Medicine and Advanced Technologies

Chairpersons: Prof. Dr. Philipp Kaufmann, Prof. Dr. Martin Meuli

- 13.10 **Wissenschaftliches Hauptreferat**
 “Advanced Technologies in Systems Pathology”
 Prof. Dr. Peter Johannes Wild, Leitender Arzt, Institut für Klinische Pathologie, USZ
- 13.30 **In vivo maintenance of human hematopoietic stem cells and hematopoiesis by engineered bone organs (Abstract No. 2354)**
K. Fritsch, P. Bourguine, S. Pigeot, E. Piccinini, I. Martin, M. Manz, H. Takizawa
- 13.40 **Melatonin Rescues Small for Size Liver Graft Failure in Mice (Abstract No. 2365)**
Z. Song, E. Maurizio, B. Humar, R. Graf, PA. Clavien, Y. Tian
- 13.50 **The ubiquitin proteasome system regulates epigenetic remodeling in pluripotent cells (Abstract No. 2380)**
 U. Graf, F. Weber, E. Vollenweider, G. Wanner, H. Koseki, J. Wong, R. Santoro, P. Cinelli
- 14.00 **Cancer Stem Cells and Tumor Heterogeneity in Renal Cancer (Abstract No. 2324)**
C. Corrà, C. Razafinjatovo, A. Von Teichman, S. Dettwiler, V. Voung, P. Schraml, H. Moch, M. Rechsteiner
- 14.10 **Identification of microRNAs involved in the activation of adult skeletal muscle stem cells (Abstract No. 2392)**
 J. Krützfeldt, A. Mizbani

Session 4: Infection/Immunity/Inflammation

Chairpersons: Prof. Dr. Onur Boyman, Prof. Dr. Dr. Annelies Zinkernagel

- 14.25 **Wissenschaftliches Hauptreferat**
 “Implementation of good clinical practice in acute healthcare”
 PD Dr. Hugo Sax, Leitender Arzt, Klinik für Infektionskrankheiten und Spitalhygiene, USZ
- 14.45 **High-throughput sequencing of human immunoglobulin variable regions with subtype identification (Abstract No. 2371)**
M. Schanz, T. Liechti, O. Zagordi, E. Miho, S. Reddy, H. Günthard, A. Trkola, M. Huber

- 14.55 **Treatment of Staphylococcus aureus persisting infections by phagolysosome alkalinization (Abstract No. 2326)**
N. Leimer, C. Rachmühl, A. Bahlmann, M. Palheiros Marques, A. Furrer, K. Seidl, R. Schüpbach, A. Zinkernagel
- 15.05 **Implementation of the multisite, multidisciplinary trial “Metagenomic profiling of viral infections for improved virus diagnostic and infectious disease management in immune compromised patients” into clinical daily routine (Abstract No. 2369)**
P. Schreiber, C. Benden, C. Berger, J. Böni, D. Braun, M. Felder, F. Geissberger, T. Güngör, H. Günthard, M. Hoernes, M. Huber, D. Lewandowska, K. Metzner, T. Müller, D. Nadal, J. Pavlovic, J. Reichenbach, J. Pachlopnik Schmid, M. Schuurmans, R. Seger, R. Weber, O. Zagordi, A. Trkola, N. Müller
- 15.15 **Targeting the Unknown Unknowns: Characterization of HIV Positive Patients not Enrolled in the Swiss HIV Cohort Study (SHCS) (Abstract No. 2289)**
M. Shilahi, A. Marzel, J. Schüpbach, J. Böni, S. Yerly, T. Klimkait, V. Aubert, H. Günthard, R. Kouyos
- 15.25 **Brain-infiltrating JC virus-specific CD8⁺ effector T cells counteract CD4⁺ T cell immune escape of neurotropic JC virus variant (Abstract No. 2315)**
I. Jelcic, C. Kempf, F. Largey, R. Planas, S. Schippling, H. Budka, M. Sospedra, R. Martin
- 15.35 **Coffee Break**

Session 5: Neurosciences/Pharmacology

Chairpersons: Prof. Dr. Gerd-Achim Kullak-Ublick, Prof. Dr. Franz X. Vollenweider

- 15.50 **Wissenschaftliches Hauptreferat**
 “Targeting immune tolerance in MS with peptide-coupled cells”
 Prof. Dr. Andreas Lutterotti, Oberarzt, Klinik für Neurologie, USZ
- 16.10 **Methodological Approach to Identify and Isolate Disease Relevant Brain-infiltrating T Cell Clones in Multiple Sclerosis Patients (Abstract No. 2325)**
R. Planas, M. Ortiz, Metz, Vilarrasa, Heesen, Brück, Martin, Sospedra
- 16.20 **Nogo-A and S1PR2 as novel regulators of developmental and tumor angiogenesis in the CNS (Abstract No. 2401)**
T. Wälchli, A. Wacker, J.Y. Shiu, S. Pantasis, H. Schneider, J. Vogel, V. Vogel, M. Schwab, M. Weller, O. Bozinov, K. Frei, L. Regli, S.P. Hoerstrup
- 16.30 **Exercise effects in Huntington’s disease (Abstract No. 2382)**
S. Frese, M. Auer, E. Rushing, M. Toigo, J. Petersen, H. Jung
- 16.40 **Metabolic and genetic research into early onset epileptic encephalopathies (Abstract No. 2304)**
L. Abela, K. Steindl, L. Simmons, D. Mathis, M. Papuc, B. Oneda, B. Schmitt, G. Wohlrab, J. Kröll, R. Schmid, T. Iff, T. Schmitt-Mechelke, R. Asadollahi, L. Crowther, C. Bühner, O. Sass, M. Hersberger, P. Joset, A. Rauch, B. Plecko
- 16.50 **Reduced Sleep Spindle Activity May Reflect Impaired Thalamocortical Connectivity in Very Preterm Born Children and Adolescents (Abstract No. 2340)**
F. Wehrle, B. Latal, R. O’Gorman, C. Hagmann, R. Huber
- 17.05 **Posterpreis**
- 17.15 **Verleihung Georg Friedrich Götz Preis 2015**
- 18.30 **Apéro**

Cardiovascular Diseases/Metabolics/Endocrinology

Basic Research

2273

A. Jaeger, A. Von Eckardstein, H. Drexel

MicroRNAs as novel biomarkers for an earlier diagnosis of Type 2 Diabetes and/or diabetic complications

2276

E. Ter Voert, H. Davison, F. De Galiza Barbosa, M. Huellner, P. Veit-Haibach, G. Delso

Incorporation of TOF information reduces artifacts in simultaneous TOF PET/MR scanning

2299

V. Pham, C. Chassard, C. Braegger, C. Lacroix

Trophic chain of lactate in infant's gut revealed by a novel functional approach

2301

E. Unterleutner, F. Barchiesi, B. Imthurn, R. Dubey

Differential Role of AKT-pathway in Mediating the Growth Effects of GPER in Human Coronary Arterial Smooth Muscle Cells and Human Umbilical Vein Endothelial Cells

2306

RA. Zuellig, T. Hornemann, A. Othman, A. Hehl, H. Bode, T. Güntert, O. Ogunshola, E. Saponara, K. Grabliauskaite, J. Jang, U. Ungethüm, Y. Wei, A. Von Eckardstein, R. Graf, S. Sonda

Deoxysphingolipids, a novel biomarker for type 2 diabetes, are cytotoxic for insulin-producing cells.

2309

M. Dietrich, R. Zuellig, B. Hemmings, G. Spinas, R. Lehmann, O. Tschopp, M. Niessen

Specific and redundant roles of PKB β /AKT1 and PKB β /AKT2 in human pancreatic islets

2310

D. Perisa, A. Kaech, L. Rohrer, A. Von Eckardstein

The Adventures of High Density Lipoproteins In Endothelial Cells

2311

A. Zhakupova, M. Krols, S. Janssens, A. Von Eckardstein, T. Hornemann

REGULATION OF THE ACTIVITY OF MAMMALIAN SERINE PALMITOYLTRANSFERASE

2312

Z. Mahdi, B. Stieger

In vitro interaction of drugs with canalicular lipid transporters

2316

I. Alec¹, A. Othman, A. Von Eckardstein, T. Hornemann

Elucidating Novel Metabolic Pathways of the Neurotoxic 1-Deoxysphingolipids

2317

L. Rigassi, F. Federica, B. Imthurn, R. Dubey

Role of microRNA-221 in mediating the protective action of Estradiol in vascular cells

2318

L. Kurmann, L. Rigassi, F. Barchiesi, B. Imthurn, R. Dubey

Estradiol regulates miR-221 expression via both ER-dependent and ER-independent mechanisms.

2356

J. Vontobel, R. Liga, M. Possner, O. Clerc, F. Mikulicic, P. Veit-Heibach, E. Ter Voert, T. Fuchs, R. Buechel, P. Kaufmann

MR-based attenuation correction for cardiac FDG-PET on a hybrid PET/MR scanner: Comparison with standard CT attenuation correction

2358

S. Velagapudj, L. Rohrer, A. Von Eckardstein

Transport of High-density lipoproteins (HDL) through endothelial cells

2360

R. Hasballa, L. Rohrer, P. Fotakis, V. Zannis, J. Parks, A. Von Eckardstein

Characterization of ApoA-I and HDL metabolism in an endothelial specific ABCA1 deficient mouse model

2367

U. Lindert, M. Gnoli, L. Sangiorgi, M. Bedeschi, M. Rohrbach, C. Giunta

Pathomechanism of a COL1A1 Signal Peptide Heterozygous Mutation Leading to Severe Osteogenesis Imperfecta

2378

K. Dräger, I. Bhattacharya, P. Seebeck, U. Held, A. Azzi, S. Brown, M. Hall, R. Humar, E. Battegay, E. Haas

Knockout of Rictor in adipocytes and brain increases mean arterial pressure and locomotor activity

2381

F. Aimi, S. Georgiopoulou, I. Kalus, F. Lehner, N. Lindenblatt, I. Bhattacharya, V. Gomes de Lima, E. Haas, M. Rüegg, M. Hall, E. Battegay, R. Humar

Deletion of endothelial Rictor (mTORC2) constrains extensive FGF2 -induced vascular remodeling and growth in vivo and disables endothelial network formation in vitro

2394

A. Hartung, J. Krützfeldt

A high-throughput screen to identify microRNAs which influence human skeletal muscle metabolism

2402

P. Zanoni, L. Rohrer, A. Von Eckardstein

Development of a genome-wide siRNA screening as a tool to unveil new players in liver HDL holoparticle uptake

Translational Research

2274

M. Linecker, P. Limani, E. Kachaylo, P. Kron, P. Kambakamba, M. Foti, J-F. Dufour, R. Graf, B. Humar, P-A. Clavien

Fighting the liver fat: Impact of exercise and ω -3 fatty acids on ischemia reperfusion injury and regeneration of fatty liver

2294

G. Klinke, M. Rohrbach, R. Giugliani, P. Burda, M. Baumgartner, C. Tran, M. Gautschi, D. Mathis, M. Hersberger

LC-MS/MS BASED ASSAY AND REFERENCE INTERVALS IN CHILDREN AND ADOLESCENTS FOR OXYSTEROLS ELEVATED IN NIEMANN-PICK DISEASES

2314

M. Schmid, J. Marti-Jaun, M. Bühler, M. Herová, M. Hersberger

Polymorphisms in SOCS 1 and 3 and Human Coronary Artery Disease

2359

J. Münger, J. Meienberg, J. Crabb, A. Mauri, S. Gysi, C. Kaiser, G. Barmettler, J. De Vos, I. Bhattacharya, J. Courseau, C. Giunta, E. Bakker, E. Battegay, R. Jaeger, E. Van Bavel, E. Haas, U. Ziegler, M. Kopf, S. Zeisberger, E. Mazza, G. Matyas
Assessment of the Mechanical Stability of the Aorta in a Col3a1 Mouse Model

2412

O. Clerc, B. Kaufmann, M. Possner, R. Liga, J. Vontobel, F. Mikulicic, C. Gräni, D. Benz, B. Herzog, O. Gämperli, P. Kaufmann, R. Büchel
Long-term prognostic performance of prospectively ECG-triggered low-dose coronary CT angiography

2413

O. Clerc, M. Possner, R. Maire, R. Liga, T. Fuchs, S. Dougoud, J. Stehli, J. Vontobel, F. Mikulicic, C. Gräni, D. Benz, B. Herzog, R. Büchel, P. Kaufmann, O. Gämperli
Is left bundle branch block a predictive factor of coronary artery disease?

2414

J. Stehli, O. Clerc, T. Fuchs, S. Dougoud, M. Possner, R. Liga, J. Vontobel, F. Mikulicic, C. Gräni, D. Benz, P. A. Kaufmann
Impact of Monochromatic Reconstructions from Single-Source Dual-Energy Coronary CT Angiography on Stenosis Evaluation. A Comparison to Invasive Angiography.

Clinical Trials

2352

M. Nägele, A. Flammer, F. Enseleit, S. Roas, S. Cantatore, A. Hirt, P. Kaiser, M. Romanens, T. Lüscher, F. Ruschitzka, G. Noll, I. Sudano
Stress-Induced Vascular Dysfunction: Evaluation of Sympathetic Activity and Endothelial Function in Patients with Takotsubo Syndrome

2353

F. Enseleit, S. Michels, M. Nägele, I. Sudano, M. Stahel, S. Zweifel, O. Schlager, M. Becker, S. Winnik, A. Flammer, M. Neidhart, N. Graf, CM. Matter, B. Seifert, T. Lüscher, F. Ruschitzka
Safety of VEGF Inhibitors in Age-Related Macular Degeneration (SAVE-AMD)

2355

M. Martin, J. Bonvini, S. Kuhn, T. Neff, B. Beck-Schimmer
Sevoflurane Postconditioning might reduce severity of cardiac and non-cardiac complications after elective cardiac valve surgery. Results of a 6 Month follow-up

Hematology/Oncology

Basic Research

2272

P. Limani, M. Linecker, N. Borgeaud, E. Kachaylo, C. Tschuor, A. Schlegel, J. Jang, S. Georgiopoulou, J. Lehn, R. Graf, B. Humar, PA. Clavien

Inositol trispyrophosphate (ITPP) and its anti-hypoxic potential in colorectal metastases of the liver

2300

E. Saponara, G. Seleznik, R. Buzzi, F. Baschieri, H. Farhan, O. Pertz, A. Caflisch, K. Grabliauskaite, R. Graf, S. Sonda

Intracellular serotonin regulates cytoskeletal remodeling at the base of pancreatic acinar-to-ductal-metaplasia formation

2321

J. Kresoja-Rakic, G. Ziltener, L. Pecze, B. Schwaller, W. Weder, R. Stahel, E. Felley-Bosco
MECHANISMS REGULATING CALRETININ EXPRESSION IN MALIGNANT PLEURAL MESOTHELIOMA

2332

C. Fankhauser, A. Curioni-Fontecedro, J. Beyer, V. Tischler, T. Sulser, H. Holger, P. Bode
Frequent expression of PD-L1 in testicular germ cell tumors

2343

L. Kovtonyuk, M. Manz, H. Takizawa

Cell cycle Induction of Dormant Hematopoietic Stem Cells by Thrombopoietin Mimetic but not G-CSF

2357

C. Eberhardt, MC. Wurnig, A. Wirsching, C. Rossi, M. Rottmar, P. Özbay, L. Filli, M. Lesurtel, A. Boss
Intravoxel incoherent motion analysis of abdominal organs: computation of reference parameters in a large cohort of C57Bl/6 mice

2361

R. Gerosa, S. Boettcher, M. Manz

The regulatory role of non-hematopoietic bone marrow cells in steady-state and during inflammation

2388

B. Vrugt, E. Felley-Bosco, S. Simmler, M. Storz, M. Friess, A. Soltermann, W. Weder, H. Moch, I. Opitz

Changes in biomarker profil and dedifferentiation during progression of malignant pleural mesothelioma

2390

T. Reding, G. Seleznik, A. Dittmann, A. Perren, R. Graf

Gastrokine as a novel potential biomarker for premalignant pancreatic lesions

2391

G. Seleznik, T. Reding, A. Perren, E. Diamantis, M. Heikenwaelder, R. Graf

Lymphotoxin Promotes Acinar Cell Reprogramming and Accelerates Pre-neoplastic Conversion in Kras Induced Pancreatic Tumorigenesis

2398

M. Neidert, D. Kowalewski, F. Wolpert, S. Stevanovic, L. Regli, M. Weller, G. Eisele

The natural HLA ligandome of glioma stem-like cells: Another step towards peptide-based immunotherapy

2403

H. Wong, C. Nombela-Arrieta, M. Manz, A. Müller

BONE MARROW INJURY AND ITS CONSEQUENCES ON HEMATOPOIETIC RECONSTITUTION FOLLOWING RADIATION CONDITIONING AND HEMATOPOIETIC CELL TRANSPLANTATION

2404

P. Cheng, O. Shahkova, D. Widmer, D. Zingg, S. Frommel, B. Belloni, M. Raaijmakers, O. Eichhoff, S. Goldinger, R. Santoro, S. Hemmi, K. Hoek, L. Sommer, R. Dummer, M. Levesque

Methylation dependent SOX9 expression mediates invasion in human melanoma cells and is a negative prognostic factor in advanced melanoma

2407

A. Rafiei, H. Takizawa, Y. Saito, M. Manz

Establishment of a human B-RAJV600E mutated LCH model in humanized mice

Translational Research

2277

D. Widmer, M. Raaijmakers, A. Narechania, J. Wenzina, P. Cheng, V. Teichgräber, L. French, M. Krauthammer, R. Desalle, R. Dummer, M. Levesque¹

Investigating the role of genetic heterogeneity in melanoma progression by whole-exome sequencing

2319

S. Bender, A. Sharma, O. Riesterer, A. Broggini-Tenzer, M. Pruschy

Identification of ADAM17 as a Novel Target for Radiosensitization of Non-Small Cell Lung Cancer

2320

A. Broggini-Tenzer, F. Bachmann, V. Vuong, A. Messikommer, K. Nytko-Karouzakis, T. O'Reilly, H A. Lane, M. Pruschy

The novel microtubule-destabilizing drug BAL101553 (prodrug of BAL27862) sensitizes a treatment refractory tumor model to ionizing radiation

2328

N. Lautenbach, L. Saleh, T. Sulser, A. Von Eckardstein, C. Poyet

Prevalence of PSA disturbance caused by heterophilic antibodies in plasma of patients

2334

N. Echeverry, G. Ziltener, W. Weder, R. Stahel, E. Felley-Bosco

INHIBITION OF AUTOPHAGY SENSITIZES MALIGNANT PLEURAL MESOTHLIOMA CELLS TO DUAL PI3K/mTOR INHIBITORS

2376

M. Meerang, K. Bérard, B. Bitanihirwe, M. Friess, E. Felley-Bosco, A. Soltermann, B. Vrugt, B. Seifert, R. Stahel, H. Moch, W. Weder, I. Opitz

NF2 and Hippo Pathway Dysregulation as Predictors of Survival for Mesothelioma Patients Treated with Multimodal therapy

2384

M. Kirschner, Y. Cheng, N. Armstrong, R. Lin, S. Kao, A. Linton, S. Klebe, B. McCaughan, N. Van Zandwijk, G. Reid

MiR-Score: A 6-microRNA signature for prognosis in malignant pleural mesothelioma

2389

J. Mata Pavia, D. Wyser, A. Kalyanov, C. Germanier, M. Rudin, M. Wolf

Hypoxia Measurements on Mice with Near-infrared Optical Tomography (NIROT) and Fluorescence Molecular Tomography (FMT)

2397

C. Razafinjatovo, M. Rechsteiner, Q. Zhong, P. Wild, P. Schraml, H. Moch
Comprehensive investigation of the mutational landscape in clear cell Renal Cell Carcinoma and its correlation to treatment response

2409

Q. Zhong, M. Gabrani, T. Guo, P.J. Schöffler, R. Aebbersold, H. Moch, P.J. Wild
Computational profiling of heterogeneity reveals high concordance between morphology and proteomics-based methods in prostate cancer

2411

K. Deml, S. Merkelbach-Bruse, H. Künstlinger, K. Albus, M. Ihle, K. König, L. Heukamp, J. Wolf, R. Büttner, H. Schildhaus
Genetic and phenotypic diversity of BRAF mutations in lung cancer

Stem Cell Research/Regenerative Medicine/Advanced Technologies

Basic Research

2275

M. Langiewicz, A. Schegel, B. Humar, R. Graf, PA. Clavien

Molecular Mechanisms underlying the unprecedented liver regeneration induced by ALPPS surgery

2283

O. Evrora, J. Houska, E. Bonavoglia, M. Calcagni, P. Giovanoli, V. Vogel, J. Buschmann

Development of an elastic, biocompatible and biodegradable protein delivery device for tendon repair: emulsion electrospun DegraPol scaffold

2284

F. Kivrak-Pfiffner, C. Waschkies, Y. Tian, A. Woloszyk, M. Calcagni, P. Giovanoli, M. Rudin,

J. Buschmann

A new in vivo MRI method to non-invasively monitor and quantify the perfusion capacity of 3D-biomaterials grown on the chorioallantoic membrane of chick embryos

2337

A. Hegglin, C.A. Schmidt, M. McLuckie, D. Bezuidenhout, S. Hoerstrup, N. Lindenblatt

Surface modified polyurethane discs promote early angiogenesis in skin defects

2354

K. Fritsch, P. Bourguine, S. Pigeot, E. Piccinini, I. Martin, M. Manz, H. Takizawa

In vivo maintenance of human hematopoietic stem cells and hematopoiesis by engineered bone organs

2370

E. Malagola, K. Schlesinger, E. Saponara, K. Grabliauskaite, T. Reding Graf, S. Sonda, R. Graf

Effect of thyroid hormone T3 in pancreatic acinar cells

2392

J. Krützfeldt, A. Mizbani

Identification of microRNAs involved in the activation of adult skeletal muscle stem cells

2393

T. Gorski, J. Krützfeldt

Adipogenic potential and UCP1 expression in monoclonal colonies of skeletal muscle fibro-adipogenic progenitors

Translational Research

2324

C. Corrà, C. Razafinjatovo, A. Von Teichman, S. Dettwiler, V. Voung, P. Schraml, H. Moch, M. Rechsteiner

Cancer Stem Cells and Tumor Heterogeneity in Renal Cancer

2329

H. Richter, M. Michael, D. Andermatt, R. Frigg, P. Kronen, K. Klein, K. Nuss, S. Ferguson, U. Stöckle, B. Von Rechenberg

Dynamization at the Near Cortex in Locking Plate Osteosynthesis by Means of Dynamic Locking Screws - An Experimental Study of Transverse Tibial Osteotomies in Sheep

2330

M. Kijanska, A. Marmaras, A. Hegglin, V. Kurtcuoglu, P. Giovanoli, N. Lindenblatt

In vivo and in vitro study of the wound healing properties of the silk-derived surgical scaffold SERI™

2350

D. Marino, J. Luginbühl, A. Klar, E. Reichmann
Bioengineering Dermo-Epidermal Skin Grafts with Blood and Lymphatic Capillaries

2365

Z. Song, E. Maurizio, B. Humar, R. Graf, PA. Clavien, Y. Tian
Melatonin Rescues Small for Size Liver Graft Failure in Mice

2380

U. Graf, F. Weber, E. Vollenweider, G. Wanner, H. Koseki, J. Wong, R. Santoro, P. Cinelli
The ubiquitin proteasome system regulates epigenetic remodeling in pluripotent cells

2416

S. Salemi, A. Mortezaei, T. Sulser, D. Eberli
The Role of Autophagy in the Differentiation of Adipose Derived Stem Cells to Functional Smooth Muscle Cells for Urologic Tissue Engineering

2417

S. Salemi, D. Keller, M. Rottmar, T. Sulser, D. Eberli
Synergistic effects of combining undifferentiated adult stem cells and differentiated cells for the engineering of functional bladder smooth muscle tissue.

2418

D. Haralampeiva, S. Salemi, T. Betzel, I. Dinulovic, S. Kramer, S. Ametamey, C. Hanschin, T. Sulser, D. Eberli
Metabolic Tracking Of Muscle Precursor Cells For Muscle Tissue Engineering by PET Imaging

2419

M. Rottmar, D. Keller, A. Boss and D. Eberli
Monitoring of in vivo fiber formation of muscle precursor cells via magnetization transfer (MT)-MRI

Clinical Trials

2313

N. Naenni, D. Schneider, C. Hämmerle, R. Jung, J. Hüsler, D. Thoma
Randomized controlled clinical study evaluating two membranes for guided bone regeneration

2331

U. Siler, E. Kuzmenko, R. Valencia, J. Reichenbach
A Clinical Phase I/II Gene Therapy Study for Chronic Granulomatous Disease

2339

H. Klein, D. Simic, P. Giovanoli, J. Plock
Handling the complications of cosmetic surgery tourism - Analysis of cost effectiveness and potential treatment

2341

H. Klein, N. Fuchs, M. Calcagni, G. Huber, P. Giovanoli, J. Plock
Extending the limits – reconstructive microsurgery in the elderly

Infection/Immunity/Inflammation

Basic Research

2281

J. Jang, Y. Yamada, W. Weder, W. Jungraithmayr

Organ-preconditioning by CD26/DPP4-inhibitor improves lung transplants via SDF-1 – mediated pathway

2282

C. Oberle, B. Joos, N. Campbell, D. Beauparlant, H. Kuster, C. Schenkel, P. Rusert, A. Trkola, K. Metzner, H. Günthard

Phenotypic Characterization of Transmitted/Founder Virus in HIV-1 Transmission Pairs

2289

M. Shilaih, A. Marzel, J. Schüpbach, J. Böni, S. Yerly, T. Klimkait, V. Aubert, H. Günthard, R. Kouyos
Targeting the Unknown Unknowns: Characterization of HIV Positive Patients not Enrolled in the Swiss HIV Cohort Study (SHCS)

2291

A. Wyss, T. Raselli, K. Atrott, I. Frey-Wagner, A. Sailer, G. Rogler, B. Misselwitz

Role of EBI2 and Oxysterols in the Development of Intestinal Lymphoid Structures and Colon Inflammation

2292

T. Raselli, A. Wyss, K. Atrott, I. Frey-Wagner, A. Geier, A. Sailer, G. Rogler, B. Misselwitz

Role of EBI2 and Oxysterols in the Pathogenesis of Fatty Liver Disease

2298

Y. Achermann, B. Tran, M. Kang, J. Harro, M. Shirtliff

Immunoproteomic identification of in vivo-expressed Propionibacterium acnes proteins in a rabbit biofilm infection model

2305

Seidl, Leimer, Furrer, Senn, Holzmann-Bürgel, Palheiros Marques, Matt, S. Zinkernagel

USA300 methicillin resistant Staphylococcus aureus in Zurich, Switzerland between 2001 and 2013

2327

A. Marzel, M. Shilaih, W. Yang, J. Böni, S. Yerly, T. Klimkait, V. Aubert, H. Günthard, R. Kouyos, SHC.
Swiss HIV Cohort Study

Estimation of HIV-1 Transmission During Recent Infection in Switzerland

2338

E. Guenova, D. Ignatova, Y. Chang, R. Dummer, L. French, A. Cozzio

Malignant T cells inhibit anti-infectious immunity in cutaneous T cell lymphoma

2347

S. Grossj, HD. Beer

The molecular mechanisms underlying UVB-induced apoptosis of human primary keratinocytes

2351

D. Lewandowska, O. Zagordi, A. Zbinden, MM. Schuurmans, P. Schreiber, F. Geissberger, J. Huder, J. Böni, C. Benden, N. Mueller, A. Trkola, M. Huber

DIAGNOSIS OF AN ENTEROVIRUS C104 STRAIN IN A LUNG TRANSPLANT RECIPIENT BY HIGH-THROUGHPUT SEQUENCING

2362

G. Gers Huber, A. Audigé, H. Rehrauer, RF. Speck
Identification of IFN- γ -stimulated candidate genes as novel HIV-1 restriction factors

2366

F. Largey, I. Jelcic, M. Sospedra, R. Garcea, R. Martin, I. Jelcic
The anti-VLA-4 monoclonal antibody natalizumab depletes intrathecal production of anti-JCV and -BKV antibodies, but not other antiviral antibodies

2371

M. Schanz, T. Liechti, O. Zagordi, E. Miho, S. Reddy, H. Günthard, A. Trkola, M. Huber
High-throughput sequencing of human immunoglobulin variable regions with subtype identification

2375

U. Nüesch, B. Volkmer, A. Mauracher, A. Urwyler, S. Vavassori, J. Pachlopnik Schmid
Role of TTC7 in the pathogenesis of combined immunodeficiency in hereditary multiple intestinal atresia

2385

D. Heuberger, A. Franchini, R. Schuepbach
Thrombomodulin-thrombin complex activates pro-inflammatory signaling pathway via protease-activated receptor 2

2399

G. Strittmatter, L. French, H. Beer
Keratinocytes, the Inflammasome and Viral Infection

2400

K. Schilcher, A. Zinkernagel
Impact of subinhibitory concentrations of clindamycin on biofilm formation and matrix composition in *Staphylococcus aureus*

2405

Y. Kok, V. Vongrad, M. Shilaih, H. Kuster, R. Kouyos, H. Günthard, K. Metzner
HIV-1 Integration Sites in Macrophages and CD4+ T Cells are Distinct

Translational Research

2293

I. Leonardi, A. Gerstgrasser, F. Nicholls, B. Tewes, R. Greinwald, G. Rogler, I. Frey-Wagner
Administration of *T. suis* ova protects immunocompetent rabbit from DSS colitis, but is detrimental to immunosuppressed individuals.

2315

I. Jelcic, I. Jelcic, C. Kempf, F. Largey, R. Planas, S. Schippling, H. Budka, M. Sospedra, R. Martin
Brain-infiltrating JC virus-specific CD8+ effector T cells counteract CD4+ T cell immune escape of neurotropic JC virus variant

2323

M. Bombardo Ayats, E. Saponara, T. Reding Graf, R. Graf, S. Sonda
Epigenetic acetylation mechanisms are activated during progenitor cell-based regeneration in the adult pancreas.

2326

N. Leimer, C. Rachmühl, A. Bahlmann, M. Palheiros Marques, A. Furrer, K. Seidl, R. Schüpbach, A. Zinkernagel
Treatment of *Staphylococcus aureus* persisting infections by phagolysosome alkalinization

2369

P. Schreiber, C. Benden, C. Berger, J. Böni, D. Braun, M. Felder, F. Geissberger, T. Güngör, H. Günthard, M. Hoernes, M. Huber, D. Lewandowska, K. Metzner, T. Müller, D. Nadal, J. Pavlovic, J. Reichenbach, J. Pachlopnik Schmid, M. Schuurmans, R. Seger, R. Weber, O. Zagordi, A. Trkola, N. Müller

Implementation of the multisite, multidisciplinary trial "Metagenomic profiling of viral infections for improved virus diagnostic and infectious disease management in immune compromised patients" into clinical daily routine

2379

C. Waschkies, T. Reding Graf, G. Seleznik, U. Ungethuen, R. Graf

Magnetic Resonance Imaging of the Pancreas in a Transgenic Mouse Model of Pancreatic Carcinogenesis

2386

P. Valko, B. Roschitzki, W. Faigle, J. Grossmann, C. Panse, P. Biro, M. Dambach, D. Spahn, M. Weller, C. Baumann

In Search of CSF Biomarkers of Fatigue in Multiple Sclerosis. A Proteomic Study.

2395

D. Rittirsch, E. Wanner, V. Schoenborn, S. Märsmann, P. Cinelli, C. Werner, H-P. Simmen, G. Wanner
Role of the heme degradation pathway in systemic inflammation after multi-system injury

2410

R. Higgins, R. Wälchli, L. Weibel, J. Hafner, A. Navarini

Comparable whole exome sequence data from FFPE and snap-frozen skin samples

Clinical Trials

2406

A. Scherer, J. Böni, W. Yang, R. Kouyos, S. Yerly, T. Klimkait, H. Günthard

HIV-1 Drug Resistance among ART-Experienced Patients in the Swiss HIV Cohort Study between 1999 and 2013

Neurosciences/Pharmacology

Basic Research

2278

T. Fleischmann, J. Henke, P. Jirkof, P. Jirkof, M. Arras, M. Arras, N. Cesarovic
Triple shot (fentanyl-midazolam-medetomidin) for injection anesthesia in mice: characterisation of safety and side-effects with and without antagonization

2279

L. Holper, F. Scholkmann, E. Seifritz
Changes in brain connectivity during resting-state and respiratory challenges: a multimodal functional near-infrared spectroscopy

2285

P. Jirkof, P. Cinelli, A. Tourvieille, M. Arras
Buprenorphine for pain relief in mice: repeated injections vs sustained release depot formulation

2288

M. Samardzija, P. Geiger, M. Barben, C. Grimm
Blue light-induced cone cell death and edema formation in the retina of the R91W;*Nrl*^{-/-} mouse

2290

C. Schori, S. Ahanger, K. Evans, E. Levine, C. Grimm
Investigation of the neuroprotective role of Müller glia cell specific activation of a hypoxic response

2297

A. Palla, M. Rohrbach, M. Baumgartner, A. Klein, D. Straumann, C. Bockisch
Evaluation of a video-oculographic system for the examination of saccadic eye movements in a 3-year old boy with Niemann-Pick Type C Disease

2303

M. Barben, C. Schori, C. Grimm, M. Samardzija
Cone pathophysiology under chronic hypoxia

2307

A. Maric, C. Lustenberger, E. Werth, J. Leemann, R. Huber, C. Baumann, R. Poryazova
Slow Wave Activity and Vigilance Changes after Acute Sleep Deprivation and Chronic Sleep Restriction

2308

A. Maric, C. Lustenberger, J. Leemann, E. Werth, A. Tarnutzer, A. Pangalu, R. Huber, C. Baumann, R. Poryazova
Vigilance and Cortical Excitability after Acute Sleep Deprivation and Chronic Sleep Restriction

2325

Planas, M. Ortiz, Metz, Vilarrasa, Heesen, Brück, Martin, Sospedra
Methodological Approach to Identify and Isolate Disease Relevant Brain-infiltrating T Cell Clones in Multiple Sclerosis Patients

2335

N. Shepherd, T. Zeffiro, K. Hassanpour, M. Claussen, M. Matthis, M. Michael, C. Mueller-Pfeiffer
Attention in Posttraumatic Stress Disorder: Gaze registration and functional magnetic resonance imaging study of saccadic eye movements

2336

M. Hugelshofer, MC. Wurnig, A. Keller, A. Boss, A. Aguzzi
Photothrombotic cortical lesions in the mouse brain: a suitable rodent model for ischemic stroke?

2344

I. Tritschler, K. Seystahl, E. Szabo, G. Tabatabai, M. Weller

TGF-BETA INDUCES AND BMP SUPPRESSES VEGF RELEASE DEPENDING ON SMAD2/3 VERSUS SMAD1/5/8 SIGNALING IN GLIOBLASTOMA

2363

A. Richter, Ch. Woernle, N. Krayenbühl, S. Kollias, D. Bellut

Affective symptoms and white matter alterations in brain tumor patients

2373

S. Dias, L. Regli, A. Keller

Oxidative stress modifies microvascular calcifications in brain

2383

V. Sennrich, A. Maric, J. Leemann, S. Weissengruber, C. Ruff, C. Baumann, R. Poryazova

Reduced Risk Aversion After Chronic Sleep Restriction But Not After Acute Sleep Deprivation

Translational Research

2286

J. Müller, C.J. Bockisch, G. Bertolini, D. Straumann, A. Tarnutzer

Spatial orientation in patients with chronic unilateral vestibular deficits

2287

E. Eschmann, S. Karlen, J. Blaser

Need for Drug-Drug Interaction Alerts Triggered by Prolonged QTc Intervals

2302

S. Burnos, O. Schmid, T. Fedele, N. Krayenbühl, J. Sarnthein

Quantifying the relationship between SEP and evoked high frequency oscillations (HFO) under anesthesia

2304

L. Abela, K. Steindl, L. Simmons, D. Mathis, M. Papuc, B. Oneda, B. Schmitt, G. Wohlrab, J. Kröll, R. Schmid, T. Iff, T. Schmitt-Mechelke, R. Asadollahi, L. Crowther, C. Bühner, O. Sass, M. Hersberger, P. Joset, A. Rauch, B. Plecko

Metabolic and genetic research into early onset epileptic encephalopathies

2340

F. Wehrle, B. Latal, R. O'Gorman, C. Hagmann, R. Huber

Reduced Sleep Spindle Activity May Reflect Impaired Thalamocortical Connectivity in Very Preterm Born Children and Adolescents

2342

F. Wehrle, B. Latal, R. O'Gorman, C. Hagmann, R. Huber

Working Memory Ability and Topographical Distribution of Sleep Slow Wave Activity in Children and Adolescents

2348

L. Simmons, L. Abela, K. Steindl, B. Schmitt, P. Joset, M. Papuc, L. Crowther, A. Rauch, B. Plecko

Untargeted clinical metabolomics reveals N-acetylspermidine as a biomarker for spermine synthase deficiency (Snyder-Robinson Syndrome).

2349

Y. Valko, S. Rosengren, H. Jung, D. Straumann, K. Landau, K. Weber

A novel diagnostic tool for myasthenia gravis: ocular vestibular evoked myogenic potentials (oVEMP)

2368

T. Restin, M. Kajdi, M. Schläpfer, B. Beck-Schimmer

Sevoflurane improves junction properties of brain endothelial cells after hypoxia

2377

S. Karlen, E. Eschmann, M. Schneemann, S. Weiler, J. Blaser

Too frequent Methotrexate Administrations in Non-Oncological Therapies and Technical Challenges for Preventing Prescription Errors

2396

C. Egger, S. Lukas, C. Waschkies, R. Martin, M. Rudin, S. Schippling

Using the afferent visual pathway model to quantify neurodegeneration in Multiple Sclerosis and experimental autoimmune encephalomyelitis – A translational optical coherence tomography (OCT) and diffusion-tensor-imaging (DTI) approach

2401

T. Wälchli, A. Wacker, J.Y. Shiu, S. Pantasis, H. Schneider, A. Kempf, J. Vogel, V. Vogel, M. Schwab, M. Weller, O. Bozinov, K. Frei, L. Regli, S.P. Hoerstrup

Nogo-A and S1PR2 as novel regulators of developmental and tumor angiogenesis in the CNS

Clinical Trials

2280

C. Giger-Tobler, J. Eisenack, D. Holzmann, A. Pangalu, V. Sturm, H. Killer, K. Landau, G. Jaggi
Measurements of optic nerve sheath diameter by CT, MRI and ultrasound

2295

C. Naegeli, T. Zeffiro, A. Weilenmann, K. Hassanpour, M. Schick, M. Rufer, R. Pitman, S. Orr, C. Mueller-Pfeiffer

The neural correlates of autonomic stress sensitization in posttraumatic stress disorder

2296

M. Toeteberg-Harms, L. Jozic, J. Magner, J. Funk

IOP Lowering Efficacy of Phacoemulsification Cataract-Extraction with Intraocular Lens Implantation alone (phaco) versus plus Excimer Laser Trabeculotomy (phaco-ELT) versus plus ab interno Trabeculotomy with the Trabectome® (phaco-AIT) – 1 Year Results.

2333

J. Schneider, A. Luft, S. Wegener

Transcranial ultrasound predictors of recurrent ischemic stroke in symptomatic internal carotid artery occlusion

2345

A. Lutterotti, T. Brodie, C. Blumer, M. Kayser, R. Stenger, M. Foege, M. Sospedra, R. Martin
Antigen-specific tolerance in multiple sclerosis with myelin peptide-coupled red blood cells.

2374

C. Van Niftrik, M. Piccirelli, O. Bozinov, J. Burkhardt, G. Esposito, S. Wegener, A. Luft, A. Pangalu, A. Valavanis, J. Fierstra, L. Regli

Assessment of cerebral autoregulation: a combined fMRI and ASL study

2382

S. Frese, M. Auer, E. Rushing, M. Toigo, J. Petersen, H. Jung

Exercise effects in Huntington's disease

2387

LM. Macrea, DR. Spahn, K. Maurer

Pain-Out - Quality of postoperative pain management in lung surgery. A survey study.

P. Limani¹, M. Linecker¹, N. Borgeaud¹, E. Kachaylo¹, C. Tschuor¹, A. Schlegel¹, J. Jang¹, S. Georgiopoulou², J. Lehn³, R. Graf¹, B. Humar¹, PA. Clavien¹

Inositol trispyrophosphate (ITPP) and its anti-hypoxic potential in colorectal metastases of the liver

Swiss Hepato-Pancreatico-Biliary (HPB) Center, Department of Surgery, University Hospital Zurich, Zurich¹, Research Unit, Division of Internal Medicine, University Hospital Zurich², Institut de Science et d'Ingénierie Supramoléculaires, Université de Strasbourg/France³

Introduction:

The hypoxic tumor response not only promotes angiogenesis, but also a number of other processes associated with malignant behavior. Therefore, inhibition of hypoxia rather than angiogenesis may be a potent anticancer strategy. The recently designed molecule ITPP promotes oxygen release from hemoglobin under hypoxic conditions. We assessed whether ITPP can inhibit hypoxia and improve outcome in a mouse model of colorectal cancer (CRC) liver metastasis.

Methods:

Two syngeneic orthotopic mouse models of hepatic CRC metastasis were established by selective portal vein injection of CRC cells. Small animal MR imaging was used to follow metastatic development in vivo. Oxygen dissociation kinetics from hemoglobin were determined by tonometry. Localization of hypoxic areas was achieved by pimonidazole staining on histological sections.

Results:

Mice treated with ITPP had a significant survival benefit along with a reduced tumor burden. ITPP had an antihypoxic effect as demonstrated by pimonidazole staining, HIF downregulation, Warburg inhibition, inflammatory changes, the normalization of systemic angiogenesis/metastasis markers, and a reduced cancer cell invasiveness. Notably, the ITPP effects were maintained following cessation of treatment. Combining ITPP with standard chemotherapy prolonged survival by three times and was superior to chemotherapy plus targeted anti-angiogenic therapy.

Conclusion:

ITPP is a potent inhibitor of the hypoxic tumor response. Its anti-hypoxic action favors a more benign tumor phenotype that is accompanied by reduced tumor invasiveness and increased survival. ITPP appears to act synergistically with cytotoxic agents. A planned Phase Ib/IIa clinical trial will reveal whether ITPP holds promise as a novel anti-hypoxic agents.

A. Jaeger¹, A. Von Eckardstein¹, H. Drexel²

MicroRNAs as novel biomarkers for an earlier diagnosis of Type 2 Diabetes and/or diabetic complications

Institute for Clinical Chemistry, University Hospital Zürich, Zürich¹, VIVIT, Landeskrankenhaus Feldkirch, Feldkirch²

Introduction:

Background: Diabetes mellitus type 2 (T2DM) is often diagnosed at an advanced stage after patients developed clinical complications. Therefore, there is a need for biomarkers that enable earlier diagnosis. Such novel biomarkers could be miRNAs. MiRNAs are small non-coding RNAs that play key roles in metabolic and inflammatory processes in T2DM and may contribute to disease complications.

Aim: Identification of circulating miRNAs, which are associated with T2DM in a discovery study.

Methods:

Study cohort: The study is carried out in serum samples of the prospective VIVIT cohort. The VIVIT cohort encompasses about 600 clinically well characterized heart disease patients followed from 2000 to 2006.

MicroRNA profiling: We investigated the circulating miRNAs profile of 27 patients by means of quantitative real-time PCR (qRT-PCR). Out of the patients, 9 suffered from metabolic syndrome (MetS) at baseline and developed T2DM, 9 suffered from MetS and did not develop T2DM and 9 individuals were healthy.

Results:

Results: We identified 10 candidate biomarker miRNAs associated with T2DM. The levels of miR-10b, miR-373*, miR-627, miR-888 and miR-934 were lower in subjects who converted into overt diabetes compared to non-converters, whereas the levels of miR-192, miR-193b, miR-194, miR-215 and miR-22* were higher.

Conclusion:

Conclusion/Outlook: The 10 miRNAs, which are associated with T2DM, are promising candidate biomarkers for T2DM. The miRNAs are to be validated by qRT-PCR in the entire VIVIT cohort at baseline. We will compare the prognostic performance of these miRNAs with that of already established biomarkers.

M. Linecker¹, P. Limani¹, E. Kachaylo¹, P. Kron¹, P. Kambakamba¹, M. Foti², J-F. Dufour³, R. Graf¹, B. Humar¹, P-A. Clavien¹

Fighting the liver fat: Impact of exercise and ω 3- fatty acids on ischemia reperfusion injury and regeneration of fatty liver

Swiss Hepato-Pancreatico-Biliary (HPB) Center, Department of Visceral Surgery and Transplantation, University Hospital of Zurich¹, Département Physiologie Cellulaire & Métabolisme, Faculté de Médecine, Genève², Department for Hepatology, University Hospital Berne³

Introduction:

The Western life style is associated with a surge in the number of patients that present with obesity and/or fatty liver (steatosis). Hepatic lipid accumulation increases the risk of hepatocellular carcinoma and hence contributes to an increased demand for liver surgery. However, steatosis enhances the sensitivity of liver towards ischemia reperfusion injury (IRI) and slows its regeneration (LR). Both exercise and ω 3- polyunsaturated fatty acids (n3-PUFAs) are known to reverse steatosis, but their effects on IRI and regeneration in fatty livers are less clear.

Methods:

We are investigating the impact of daily exercise and n3-PUFA on hepatic IRI and regeneration in lean mice and mice with high fat diet-induced steatosis.. Mice were consecutively treated for 4 weeks with either equicaloric n3-PUFA supplementation (20kJ%) or daily exercise (1h). Whilst exercise increases energy expenditure, the effects of n3-PUFAs on energy metabolism need clarification.

Results:

Both treatments markedly reduced steatosis and IRI, whilst improving regeneration after 70% hepatectomy. Unlike exercise, n3-PUFAs had little effect on peripheral fat, yet both led to the activation of hepatic Amkp, the upregulation of Pten, and potentially to hepatocyte browning and a M1>M2 Kupffer cell polarization shift. The contribution of these alterations to the beneficial effects of exercise & n3-PUFAs will be the subject of our future studies.

Conclusion:

Any intervention that can safely reduce hepatic fat accumulation and mitigate IRI without negatively affecting the regenerative capacity would be most welcome in the clinic. Inasmuch n3-PUFA acids can substitute the beneficial effects of exercising is another point of interest, as regular exercise will always remain limited in its therapeutic potential due to matters of compliance and the critical health state of obese individuals. The identification of key pathways underlying the beneficial effects of n3-PUFAs may provide new alternatives for a therapeutic intervention.

M. Langiewicz¹, A. Schegel¹, B. Humar¹, R. Graf¹, PA. Clavien¹

Molecular Mechanisms underlying the unprecedented liver regeneration induced by ALPPS surgery

Visceral and Transplantation Surgery, University Hospital Zürich, Zürich¹

Introduction:

In many patients with liver cancer, the tumor is too advanced to permit a curative resection. A novel surgical approach, ALPPS (combining PVL with transection), may be used for unresectable disease due to its ability to induce massive acceleration of liver regeneration. Using a novel ALPPS mouse model, we aim at studying the molecular mechanisms underlying this accelerated liver growth.

Methods:

Liver tissue was collected at early time points post ALPPS surgery (30min, 1h, 4h, 8h, 12h) and analysed by RNA deep sequencing. Plasma samples were collected 30min after ALPPS for proteomics analysis by protein enrichment, albumin depletion, and mass spectrometry. Each protein fraction is confirmed for activity by inducing accelerated regeneration upon injection into mice treated with PVL only.

Results:

Plasma proteins have been identified as the sole contributors to the accelerated liver growth underlying ALPPS surgery. Genomics analysis shows that gene differential expression occurs 8 hours after ALPPS step 1, while liver growth occurs mainly by hyperplastic mechanisms reflected as an increased number of hepatocytes entering the cell cycle.

Conclusion:

ALPPS is conducive to accelerated liver regeneration through the proteins that are regulated and circulating in the plasma just 30 minutes after ALPPS Step 1 procedure. We aim to elucidate a mechanistic pathway that can explain the molecular alterations causing the unprecedented liver growth in ALPPS.

Incorporation of TOF information reduces artifacts in simultaneous TOF PET/MR scanning

Department of Medical Imaging, Division of Nuclear Medicine, University Hospital Zurich, Zurich, Zurich, Switzerland¹, GE Healthcare, Waukesha, WI, United States²

Introduction:

In simultaneous PET/MR scanning, MR data is employed for PET photon attenuation correction (MR-AC). Bone or metal implants could lead to inconsistencies in the MR-AC maps, thereby affecting the PET images. Lesions close to bone or implants may be obscured and remain unnoticed or cannot be accurately assessed. A possible solution could be the inclusion of time-of-flight (TOF) information into the PET image reconstruction algorithm. This study aims to evaluate the influence of TOF information on artifact reduction and improvement in PET image quality in clinical simultaneous TOF PET/MR scanning.

Methods:

Part A (clinical): A total of 35 patients with various malignant tumors were included and scheduled for a comparative scan in a new simultaneous TOF PET/MR scanner (GE SIGNA). TOF and non-TOF PET images were reconstructed, clinically examined and compared by a radiologist/nuclear medicine physician. Differences in the image quality, especially those related to (implant) artifacts, were assessed using a 5-point scale, ranging from zero (no artifact) to four (severe).

Part B (simulation): In seven patients the reconstructions were repeated after the introduction of artificial signal voids in the attenuation map to simulate three different sized clinically relevant metal artifacts in the maxilla, humeral head, chest, sternum, thoracic spine, lumbar spine and below the femoral head. The reconstructed images were then compared with reconstructed images that had no simulated artifacts for the TOF and non-TOF reconstructions.

Results:

Part A: A total 46 image artifacts were being evaluated. Two patients had large and six patients had small implant-related artifacts, ten patients had dental implants/fillings and 19 patients had implant-unrelated artifacts. In 1 patient with spondylolysis the TOF images scored 1, and non-TOF images 4 as a bone metastasis was not seen. Cardio artefacts in two patients had the same scores (1/2) in both the TOF and non-TOF images, although the TOF images were found to have improved overall image quality. In patients with dental implants/fillings, stents and intrauterine devices, no (significant) artefact was seen. Overall, the average score was 1.3 ± 1.0 (mean \pm std) for the non-TOF PET and 0.7 ± 0.8 for the TOF images ($P < 0.01$, Wilcoxon matched-pairs signed rank test).

Part B: In all cases the magnitude and impact of the error was reduced when TOF information was included in the reconstruction. However, for all anatomical regions investigated except for the lumbar spine, the number of small magnitude (-5% to -30%) errors present in the TOF image was greater than in the non-TOF image.

Conclusion:

From a clinical point of view the image quality and the reader confidence was improved significantly near artifacts with the inclusion of TOF. The simulations showed that TOF information reduced the impact of artifact related errors in all metal implant cases. TOF not only improves e.g. signal-to-noise ratio, accuracy, lesion detectability and the convergence rate of the iterative algorithm, its inclusion also makes the system become better-conditioned and therefore less sensitive to errors in the attenuation map. The use of TOF in conjunction with other (MR) techniques to correct for metal artifacts could possibly even further improve overall image quality and clinical reader confidence.

Conclusion: These results suggest that PET imaging may significantly benefit from the integration of TOF information in simultaneous TOF PET/MR scanning.

D. Widmer¹, M. Raaijmakers¹, A. Narechania², J. Wenzina¹, P. Cheng¹, V. Teichgräber³, L. French¹, M. Krauthammer⁴, R. Desalle², R. Dummer¹, M. Levesque¹

Investigating the role of genetic heterogeneity in melanoma progression by whole-exome sequencing

Department of Dermatology, University Hospital Zürich, ZH, 8091 Zürich, Switzerland¹, American Museum of Natural History, NY, 10024-5192 New York, USA², F. Hoffmann-La-Roche AG, 4070 Basel, Switzerland³, Department of Pathology, Yale University School of Medicine, CT, 06511 New Haven, USA⁴

Introduction:

Targeted BRAF inhibitors have produced a dramatic anti-tumor response rate of 80% in patients with BRAF (V600E) mutated melanomas. However, after initial success, most patients develop resistance within 6-8 months, largely through reactivation of the MAPK pathway. Although several mechanisms of pathway reactivation have been identified, how genetic heterogeneity contributes to intrinsic or acquired resistance to pathway inhibition is still poorly understood.

Methods:

Taking advantage of the extensive melanoma biobank at the University Hospital of Zurich, we applied optimized protocols for DNA extraction from FFPE tumor material. We generated whole-exome sequence data from multiple lesions of three metastatic melanoma patients treated with targeted (BRAF and MEK) and non-targeted (multi-receptor tyrosine kinase) inhibitors, generating deep sequencing data from germline DNA, dysplastic nevi, primary tumors, and metastases before and after therapy.

Results:

Performing whole-exome phylogenetic analysis, we observed a rapid monophyletic evolution of melanoma subpopulations in response to targeted therapy that was not observed in non-targeted therapy. We also show that multiple resistance mechanisms are present within an individual stage IV melanoma patient. Digital-PCR and clonal sequencing of a patient-derived early-passage melanoma culture showed for the first time that activating BRAF and NRAS mutations can occur naturally in the same cells.

T. Fleischmann¹, J. Henke², P. Jirkof¹, P. Jirkof³, M. Arras¹, M. Arras³, N. Cesarovic¹

Triple shot (fentanyl-midazolam-medetomidin) for injection anesthesia in mice: characterisation of safety and side-effects with and without antagonization

Division of Surgical Research, University Hospital Zurich, Zurich, Switzerland¹, Boehringer Ingelheim Pharma GmbH & Co. KG, Biological Laboratory Service, Germany², Neuroscience Center Zurich, University of Zurich and ETH Zurich, Winterthurerstrasse 190, Zurich, Switzerland³

Introduction:

Injection anesthesia still is the predominant type of anesthesia in laboratory rodents for most types of interventions. The main drawbacks are reflected in a narrow safety margin, the inability to respond to the needs of individual animals and the long post-interventional recovery period with a delayed onset of normal activity. A fully reversible anesthesia with fentanyl, midazolam and medetomidin (triple shot) aims for a greater safety margin during anesthesia and a shorter recovery period, as all substances can be antagonized. Here we investigated not only the feasibility of this protocol to provide 50 minutes of anesthesia, but also quality and the effects on post-anesthetic recovery in mice, especially regarding the impact on heart rate (HR), body temperature (BT) and home cage activity in mice.

Methods:

Adult female C57BL/6J mice were implanted with a telemetry system for recording of heart rate (HR) and body temperature (BT) and were randomly allocated into two anesthesia groups (with or without antagonization). Measurements of HR and BT were collected for 3 days prior (baseline), during anesthesia and for 3 days afterwards. Anesthesia was induced with fentanyl (0.05 mg/kg), midazolam (5 mg/kg) and medetomidin (0.5 mg/kg). During anesthesia animals laid on a warming mat and reflex testing (tail and cutaneous pinches, pedal withdrawal) was periodically applied to estimate anesthetic depth. Arterial blood gas analysis was performed after 50 minutes. Then half of the mice were antagonized with naloxone (1.2 mg/kg), flumazenil (0,5 mg/kg) and atipamezol (2,5 mg/kg); the other half was left untreated. Finally mice were placed back into their cages and were video recorded for 24 hours to monitor home cage activity.

Results:

During anesthesia all animals displayed bradycardia (200-300 bpm) and moderate hypothermia (34-35°C). Respiratory rate averaged 130/min and in the course of anesthesia, hyperglycaemia, hypercapnia, mild hypoxia and respiratory acidosis developed. After antagonization HR and BT regained pre-anaesthetic baseline values within 1 hour. Without antagonization HR and BT were markedly decreased during the first 24h after anesthesia, reaching critical values of 90 bpm and 21°C respectively. All animals survived. Mice with antagonization of the triple shot anesthesia – although quickly regaining physiological values of HR and BT – revealed a disrupted pattern of activity and sleep rhythm compared to the control group. Mice without antagonization were immobile in the first 12 hours after anesthesia, slowly starting to recover in the following 12 hours.

Conclusion:

Triple shot produced a safe and stable anesthesia for 50 min with hypothermia and bradycardia as side-effects. After antagonization HR and BT quickly regained normal values. However mice without antagonization showed marked hypothermia and severe bradycardia up to 24 hours after anesthesia. Circadian rhythm of activity was disturbed in all mice for up to 24 hours after anesthesia. As it is of great importance for mice to regain normal HR and BT as quickly as possible, antagonization of the narcotic components provides a reliable method for quick recovery and also improves well-being in mice after anesthesia.

L. Holper², F. Scholkmann¹, E. Seifritz²

Changes in brain connectivity during resting-state and respiratory challenges: a multimodal functional near-infrared spectroscopy

Biomedical Optics Research Laboratory, Division of Neonatology, University Hospital Zurich, 8091 Zurich, Switzerland¹, Department of Psychiatry, Psychotherapy, and Psychosomatics, University Hospital of Psychiatry Zurich, Lenggstrasse 31, 8032 Zurich, Switzerland²

Introduction:

Brain hemodynamic (i.e. changes in cerebral blood flow as well as cerebral tissue oxygenation) are strongly influenced by respiration. Here we investigated the time-frequency dynamics of states of hypo- and hypercapnia using three respiratory challenges (i.e., hyperventilation, breath-holding, and rebreathing) compared to resting-state.

Methods:

Cortical hemodynamic responses were assessed using functional near-infrared spectroscopy (fNIRS) within two regions of interest, (i.e. the medial prefrontal cortex and the dorsolateral prefrontal cortex). Respiratory measures were assessed in form of partial end-tidal carbon dioxide (PetCO₂), heart rate, arterial oxygen saturation and respiration rate. Time–frequency analysis was performed using the wavelet transform coherence to quantify positive and negative phase-coupling within each region of interest.

Results:

We found that the respiration challenges modulated the time-frequency dynamics differently: (i) Hyperventilation and breath-holding exhibited an inverse effect on positive and negative phase-coupling with respect to resting-state. (ii) In contrast, rebreathing had no significant effect with respect to resting-state. (iii) Low-frequency oscillations contributed to a greater extent to coherence dynamics compared to high-frequency oscillations.

Conclusion:

The results highlight that distinct differences exist in time-frequency dynamics not only between hypo- (hyperventilation) and hypercapnia, but also between different states of hypercapnia (breath-holding versus rebreathing). This study gives new insights into the impact of respiratory changes on brain hemodynamics – insights that could be relevant to differentiate between physiological and pathological respiratory behavior in a medical context.

C. Giger-Tobler¹, J. Eisenack¹, D. Holzmann⁵, A. Pangalu², V. Sturm⁴, H. Killer³, K. Landau¹, G. Jaggi¹

Measurements of optic nerve sheath diameter by CT, MRI and ultrasound

Department of Ophthalmology, UniversityHospital Zurich, Zurich¹, Department of Neuroradiology, University Hospital of Zürich, Zürich², Department of Ophthalmology, Cantonal Hospital Aarau, Aarau³, Department of Ophthalmology, Cantonal Hospital St.Gallen, St.Gallen⁴, Department of ENT, UniversityHospital Zurich, Zurich⁵

Introduction:

Quantification of the optic nerve sheath diameter (ONSD) is promising for detection of altered intracranial pressure. The objective of this study was to assess the relationship between ONSD, as measured using CT, MRI and ultrasound (US).

Methods:

15 patients (60.8 [y]±16.73SD; 7 female) with paranasal sinuses pathology and existing CT and MRI underwent ONSD measurements by US, as well as an ophthalmological examination. US-, CT- and MRI-derived maximal ONSD values 3mm behind the globe were compared.

Results:

ONSD measured (n=30) by US (mean 6.2[mm]±0.82SD) were significantly ($p<0.01$) higher than ONSD in CT (5.2±1.11) or MRI (5.4±1.14). There was no significant ($p=0.21$) difference but well correlation ($\rho=0.851$, $p<0.01$) between ONSD measured in CT and MRI. Those of US and CT ($\rho=0.624$, $p<0.01$) and US and MRI ($\rho=0.558$, $p<0.01$) showed a modest but significant correlation. There was a negative correlation between age and ONSD in CT ($\rho=0.428$, $p=0.02$) and in MRI ($\rho=0.490$, $p<0.01$).

Conclusion:

The comparability of ONSD measurements seems to be given between CT and MRI while comparability between US and CT or MRI seems to be questionable. Overall a significant but modest correlation was found.

J. Jang¹, Y. Yamada¹, W. Weder¹, W. Jungraithmayr¹

Organ-preconditioning by CD26/DPP4-inhibitor improves lung transplants via SDF-1 – mediated pathway

University Hospital, Dept. of Thoracic Surgery, Zurich¹

Introduction:

CD26/DPP4 is a co-stimulatory molecule on T cells but has also enzymatic activity cleaving biological peptides. Inhibiting the enzymatic activity can enhance the availability of key immune-modulatory proteins, e.g. SDF-1. Here, we aimed to prevent primary graft dysfunction (PGD) through CD26/DPP4 inhibition in donor lungs exposed to prolonged ischemia.

Methods:

Syngeneic orthotopic mouse lung transplantation (Tx) between WT C57BL/6 (n=6) was performed after 12 hours of cold ischemia. Donor lungs were perfused by saline or with a specific CD26/DPP4-inhibitor (Vildagliptin, 1ug/ml) for preconditioning. Grafts were analyzed after cold ischemia time and 7 days after Tx for CD4⁺ CD8⁺ T cells, and F4/80 (macrophages) by FACS, and CD3 and F4/80 by IHC. SDF-1, TNF- α , and IL-10 were determined by ELISA. Raw267 macrophage cell line was used to confirm an anti-inflammatory effect of Vildagliptin and SDF1 *in vitro*.

Results:

Vildagliptin preconditioning significantly preserved SDF1 12 hours after cold ischemia. Seven days after transplantation, donor lungs were macroscopically and microscopically preserved. CD4⁺ and CD8⁺ T cell infiltration was reduced by Vildagliptin preconditioning, confirmed by reduced overall CD3⁺ T cell infiltration, but increased macrophage numbers in IHC. Furthermore, Vildagliptin (50ug/ml) treatment increased the expression of IL-10 in donor lungs 7 days after Tx. Vildagliptin (50ug/ml) or SDF1 - treatment in Raw267 macrophage cell line confirmed the reduction of TNF- α .

Conclusion:

The preconditioning by CD26/DPP4 inhibitor Vildagliptin induces a long-term improvement of donor lung transplants via reduction of T cells and SDF-1 mediated reduction of TNF- α , and an increase of IL-10, most likely released by immunosuppressive macrophages phenotype. These data suggest Vildagliptin as an effective compound for donor organ preconditioning in order to attenuate PGD.

C. Oberle¹, B. Joos¹, N. Campbell¹, D. Beauparlant², H. Kuster¹, C. Schenkel¹, P. Rusert², A. Trkola², K. Metzner¹, H. Günthard¹

Phenotypic Characterization of Transmitted/Founder Virus in HIV-1 Transmission Pairs

Department of Infectious Diseases and Hospital Epidemiology, University Hospital Zurich, Zurich¹, Institute of Medical Virology, University of Zurich, Zurich²

Introduction:

In 60-90% of mucosal HIV-1 transmissions a single transmitted/founder (T/F) virus from a genetically diverse virus population of the transmitter infects the recipient. Whether HIV-1 transmission is a stochastic process or the T/F viruses have beneficial features facilitating transmission and infection is controversially discussed. Here, we investigated the phenotypes of viruses isolated from transmission pairs in order to discover properties that might favor transmission.

Methods:

Based on phylogenetic analyses of HIV-1 *polymerase* and *envelope* sequences and clinical data from patients enrolled in the Zurich Primary HIV-1 Infection Study (ZPHI) and Swiss HIV Cohort Study (SHCS), 9 potential transmission pairs of subtype B were identified and primary virus isolates of transmitter and recipient (acutely infected patients with single T/F virus) at the nearest time point of transmission were generated. Virus isolates were characterized in respect to replication capacity in peripheral blood mononuclear cells (PBMCs) in the absence and presence of IFN- α and in monocyte-derived macrophages (MDMs). Furthermore, sensitivity to different entry inhibitors (Maraviroc, DARPIn 57.2, soluble CD4, T-20) and neutralizing antibodies (b12, 2G12, 4E10, 2F5), and the entry kinetics of these virus isolates were studied.

Results:

All virus isolates replicated efficiently in PBMCs and 15 of 18 virus isolates were capable to replicate in MDMs, however, to a lesser extent. No clear pattern could be observed: In some transmission pairs, the virus isolate from the transmitter replicated more efficiently in MDMs and/or PBMCs and vice versa in other pairs. All virus isolates were sensitive to IFN- α ; yet the degree to which replication was reduced varied within and between transmission pairs. In terms of entry, virus isolates from the same transmission pair were inhibited to similar degrees by different entry inhibitors and neutralizing antibodies. Moreover, virus obtained from transmitter and recipient showed similar entry kinetics.

Conclusion:

For some transmission pairs, differences in replication capacities in both PBMCs in the absence or presence of IFN- α and MDMs were detected, yet we could not identify a common property shared by T/F viruses. T/F viruses and the virus population of the transmitter showed similar sensitivity to entry inhibitors/neutralizing antibodies and similar entry kinetics. Hence, according to the investigated parameters no significant phenotypic pattern could be attributed to T/F viruses.

O. Evrora¹, J. Houska¹, E. Bonavoglia³, M. Calcagni¹, P. Giovanoli¹, V. Vogel², J. Buschmann¹

Development of an elastic, biocompatible and biodegradable protein delivery device for tendon repair: emulsion electrospun DegraPol scaffold

Division of Plastic Surgery and Hand Surgery, University Hospital Zurich, 8091 Zurich, Switzerland¹, Laboratory of Applied Mechanobiology, ETH Zurich, Switzerland², ab medica, Via Nerviano 31, Lainate (Milan), Italy³

Introduction:

In the field of musculoskeletal disorders affecting muscles, bones, ligaments or tendons, regenerative engineering approaches employing biomaterials combined with biological factors for improved healing have been recently proposed as a viable option. There are several methods for production of such bioactive scaffolds carrying different biomolecules which include: non-covalent adsorption, coaxial electrospinning or emulsion electrospinning. Emulsion electrospinning allows for biomolecule incorporation within the polymer solution prior to electrospinning, resulting in a dispersion of the molecule randomly in the fibers.

Methods:

Electrospun DegraPol meshes were produced, either by pure DegraPol or by a water-in-oil emulsion. Parameters such as weight % of DegraPol in the solvent, flow rate as well as voltage were varied. Fiber diameter as a function of those parameters was determined. Porosity, water contact angle and biomechanical properties (Young modulus, strain at break and tensile stress) of these meshes were assessed. Release kinetics of two model compounds (fluorescein (FL) and fluorescein isothiocyanate-conjugated bovine serum albumin (FITC-BSA)) were determined for different sets of fabrication conditions.

Results:

Fibers produced by emulsion electrospinning were significantly thinner compared to pure DegraPol fibers. Fiber diameters increased with increasing flow rate for both, pure and emulsion electrospun meshes. Pure and emulsion electrospun scaffolds (with FITC-BSA incorporated) were hydrophobic in nature with water contact angles from 104.61 ± 1.49 to 124.86 ± 2.87 . Biomechanical properties varied remarkably when pure and emulsion electrospun meshes were compared; strain at break was 660 % for emulsion spun meshes, while it was 1300 % for pure DegraPol meshes. Tensile stress of emulsion electrospun scaffolds also decreased (0.13 ± 0.01 MPa) when compared to pure DegraPol scaffolds (0.36 ± 0.04 MPa). The release of FITC-BSA within 14 days ranged from 85.93 ± 8.07 % for 12 wt % DegraPol up to 90.71 ± 5.11 % for 8 wt % DegraPol.

Conclusion:

Emulsion electrospun DegraPol meshes allow protein release in a sustained controlled manner. As such, they can be designed for specific applications in regenerative medicine where a controlled release of biological molecules is needed.

F. Kivrak-Pfiffner¹, C. Waschkes², Y. Tian³, A. Woloszyk⁴, M. Calcagni¹, P. Giovanoli¹, M. Rudin², J. Buschmann¹

A new *in vivo* MRI method to non-invasively monitor and quantify the perfusion capacity of 3D-biomaterials grown on the chorioallantoic membrane of chick embryos

Division of Plastic Surgery and Hand Surgery, University Hospital Zurich, 8091 Zurich, Switzerland¹, Institute for Biomedical Engineering, ETH and University of Zurich, 8093 Zurich, Switzerland², Visceral and Transplant Surgery, University Hospital Zurich, 8091 Zurich, Switzerland³, Institute of Oral Biology, University of Zurich, 8091 Zurich⁴

Introduction:

Adequate vascularization in biomaterials is essential for tissue regeneration and repair. Current models do not allow easy analysis of vascularization of implants *in vivo*, leaving it a highly desirable goal. A tool that allows to monitor the perfusion capacity of such biomaterials non-invasively in a cheap, efficient and reliable *in vivo* model would hence add great benefit to the research in this field.

Methods:

We established, for the first time, an *in vivo* Magnetic Resonance Imaging (MRI) method to quantify the perfusion capacity of a model biomaterial, DegraPol® foam scaffold, placed on the embryonic avian chorioallantoic membrane (CAM) *in ovo*. Perfusion capacity was assessed through changes in the longitudinal relaxation rate before and after injection of a paramagnetic MRI contrast agent, Gd-DOTA (®Dotarem, Guerbet S.A.). Relaxation rate changes were compared in three different regions of the scaffold, i.e. at the interface to the CAM, in the middle and on the surface of the scaffold

Results:

The highest relaxation rate changes, and hence perfusion capacities, were measured in the interface region where the scaffold was attached to the CAM, whereas the surface of the scaffold showed the lowest relaxation rate changes. A strong positive correlation was obtained between relaxation rate changes and histologically determined vessel density ($R^2 = 0.983$), which corroborates our MRI findings.

As a proof-of-principle, we measured the perfusion capacity in different scaffold materials, silk fibroin either with or without human dental pulp stem cells. For these, 3 – 4 times larger perfusion capacities were obtained compared to DegraPol®; demonstrating that our method is sensitive to reveal such differences.

Conclusion:

A novel *in vivo* method for analyzing the perfusion capacity in 3D- biomaterials grown on the CAM is presented, enabling the determination of the perfusion capacity of a large variety of bioengineered materials.

P. Jirkof¹, P. Cinelli², A. Tourvieuille³, M. Arras¹

Buprenorphine for pain relief in mice: repeated injections vs sustained release depot formulation

Division of Surgical Research, University Hospital of Zurich, Zurich, Switzerland¹, Division of Trauma Surgery, University Hospital Zurich, Zurich, Switzerland², Humanvet, Chemin des clochetons 8, 1004 Lausanne, Switzerland³

Introduction:

Sustained release formulations of analgesic drugs are promising alternatives to repeated drug injections.

Methods:

Here, we compared a sustained release formulation of buprenorphine (2.2mg/kg; SB), with a standard protocol of three injections of buprenorphine (0.1mg/kg/8 hours; Temgesic) in mice. Buprenorphine serum concentration and analgesic action (thermal sensitivity) were determined in healthy mice. Additionally, the pain relief properties of both protocols were assessed after laparotomy using physiological and ethological measures of pain and recovery.

Results:

Serum concentrations and thermal sensitivity tests indicated duration of action of at least 4 hours (but less than 8 hours) with the Temgesic protocol, and 24–48 hours with SB. Behavioural and clinical parameters indicated at least partial pain relief after surgery with both protocols. Observed side effects of buprenorphine independent of the protocol were increased activity, disturbed circadian rhythm and several abnormal behaviours. A tendency for decreased food and water intake as well as body weight reduction was also seen. Body weight decreased significantly in animals that received three injections of Temgesic, regardless if surgery was performed or not ($p=0.015$; $p=0.023$), hinting at a stress response towards this frequent intervention.

Conclusion:

In conclusion, an application interval of 8 hours (Temgesic) appears too long and might lead to repeated periods with insufficient analgesia in animals undergoing lasting and/or substantial pain after surgery. In comparison to the standard protocol, SB provided a long-lasting, assured analgesia without possible stressful repeated injections in a standard surgical model, with only limited and acceptable behavioural side effects.

J. Müller¹, C.J. Bockisch², G. Bertolini¹, D. Straumann¹, A. Tarnutzer¹

Spatial orientation in patients with chronic unilateral vestibular deficits

Neurology, University Hospital Zurich, Zurich¹, Otorhinolaryngology, Neurology and Ophthalmology, University Hospital Zurich, Zurich²

Introduction:

Acute unilateral vestibular deafferentation (UVD) is linked to sudden vertigo/dizziness, gait imbalance, nausea, nystagmus, and motion intolerance. Within days to a few weeks patients usually experience significant recovery with little or no impairment in daily activities despite persistent vestibular hypofunction in the majority of cases. One cornerstone of vestibular function is the percept of the direction of gravity, which is shifted strongly towards the lesioned side acutely. Whether normalization of verticality perception parallels clinical recovery has not been studied in roll tilted positions and results when upright were mixed. The aim of this study was to quantify verticality perception in the roll-plane in patients with persistent UVD, either affecting the superior and inferior vestibular nerve (CVN) or being restricted to the superior nerve (SVN).

Methods:

Semi-circular canal function and otolith function was quantified by use of 3D-video-head-impulse testing and vestibular-evoked myogenic potentials. In 11 patients with chronic UVD (aged 54 ± 17 years, mean ± 1 SD, CVN=7, SVN=4, time after lesion= 18 ± 16 months), the subjective visual vertical (SVV) was measured repetitively in different whole-body roll-tilt orientations (0° , $\pm 45^\circ$, $\pm 90^\circ$). Adjustment errors and trial-to-trial variability were determined and compared to results from 15 healthy control subjects (aged 46 ± 14 years). Results from patients with left-sided lesions (n=6) and right-sided lesions (n=5) were pooled.

Results:

When upright, the patients demonstrated a significant ($p=0.003$, two sample t-test, Bonferroni-corrected) shift in SVV of $3.9 \pm 2.1^\circ$ towards the lesioned side (controls: $-0.1 \pm 1.1^\circ$). When roll-tilted $\pm 45^\circ$, adjustments were significantly ($p=0.041$) shifted from accurate (controls) towards roll under-estimation, when roll-tilted $\pm 90^\circ$, roll under-estimation further increased in the patients (without reaching significance, $p=0.15$). These shifts tended to be larger when rolled to the lesioned side and were similar between the SVN group and the CVN group. Trial-to-trial variability was only slightly increased in the patients and did not depend on the side of the lesion.

Conclusion:

Verticality perception in patients with chronic UVD remained abnormal when upright and roll-tilted over an average of 18 months, indicating incomplete central compensation of imbalanced otolith input. We noted similar changes in SVV in case of isolated utricular loss (SVN group) and combined utricular and saccular (CVN group); whether this indicates a dominant role of the utricle in verticality perception or is only due to the small sample size remains to be investigated further. We conclude that implementing SVV measurements while roll-tilted in the clinical setting enhances the characterization of vestibular deficits and may help identifying more subtle deficits in verticality perception in patients with chronic UVD.

Need for Drug-Drug Interaction Alerts Triggered by Prolonged QTc Intervals

Research Centre for Medical Informatics, University Hospital, Zurich¹

Introduction:

It is a challenge for physicians to identify clinically significant drug-drug interactions (DDIs) and to adapt medications accordingly. This study focussed on QT-prolonging DDIs (QTpDDIs). QT interval prolongation is associated with torsades de pointes (TdP), a potentially life-threatening ventricular tachycardia. Our aim was to analyse the frequency of QTpDDIs and to examine how the physicians reacted to significant QT interval prolongations.

Methods:

We included the data of all inpatients admitted to the University Hospital Zurich from 12/1/2009 to 12/31/2011, except for those exclusively hospitalized in intensive care.

DDIs were identified based on a commercially available knowledge base (Galdat, e-mediat, Switzerland), including only the top three DDI severity levels. Drug prescriptions for optional administration were excluded.

The QT intervals were extracted from automated measurements embedded in digitally available electrocardiograms at rest (ECGs) and were corrected for heart rate (QTc). Significant QTc interval prolongation was defined as a QTc interval >500 ms or as an increase of the QTc interval of >50 ms compared with the last QTc interval measured prior to the DDI.

Results:

We analysed the medication in 76,467 patients and identified 2,738 QTpDDIs in 2,085 patients.

For 670 patients ECGs were available in the 4 weeks prior to the onset of DDI. ECGs measured during the DDIs were present for 342 patients, including 137 patients with ECGs in both periods.

52 QTpDDIs were started in 43 patients despite a significant QTc interval prolongation observed in the ECGs within 4 weeks prior to their onset.

61 QTc intervals measured in 50 patients during QTpDDIs were significantly prolonged: 49 QTc intervals exceeded 500 ms, 24 QTc intervals were increased by >50 ms, and both criteria were met in 12 ECGs.

The actions taken after obtaining ECGs showing a significant QTc interval prolongation during QTpDDIs were: (1) stopping all QTpDDIs within 24 hours (52.5%), (2) changing at least one QTpDDIs within 24 hours (8.2%), and (3) continuing all QTpDDIs without any change for at least 24 hours (39.3%), 48 hours (27.9%), or 72 hours (21.3%).

Conclusion:

QTpDDIs were associated with a significant QTc interval prolongation in 14.6% of the patients exposed. Therapy was adapted according to the guidelines in 60.7% of these interval prolongations. However, for 20 out of 50 patients the drugs associated with prolonged QTc intervals were not adjusted within 24 hours and remained unchanged even after 72 hours in 21.3% of the patients. Furthermore, 7.8% of all QTpDDIs were started despite the presence of a significant QTc interval prolongation. Thus, the medication was often started or continued without any changes despite the risk of TdP and of sudden cardiac arrest.

The lack of knowledge about QTpDDIs and not being aware of recent ECG findings may contribute to the fact that physicians start or continue QTc interval prolonging prescriptions despite contraindications. We therefore suggest automated assistance by (1) computer-triggered reminders for ECG monitoring at onset of and during QTpDDIs and (2) computer-triggered alerts when DDIs are started or continued unchanged despite documented significant QTc interval prolongations.

M. Samardzija¹, P. Geiger¹, M. Barben¹, C. Grimm¹

Blue light-induced cone cell death and edema formation in the retina of the *R91W;Nrl^{-/-}* mouse

Lab for Retinal Cell Biology, Department of Ophthalmology, University of Zurich, Zurich¹

Introduction:

Little is known about the mechanisms underlying macular degenerations, mainly for the scarcity of adequate experimental models to investigate cone cell death. In the absence of the NRL transcription factor, photoreceptor progenitor cells differentiate into cells resembling blue-cones in the mouse retina. However, the all-cone retina of *Nrl^{-/-}* mice is characterized by severely abnormal cone photoreceptor layering with abundant rosette-like structures and aberrant retinal vasculature. Recently, we generated *RPE65_{R91W};Nrl^{-/-}* (*R91W;Nrl^{-/-}*) double mutant mice, which express a mutant RPE65 protein with a 9-fold reduced production of 11-*cis*-retinal. Owing to the resulting reduced chromophore levels, *R91W;Nrl^{-/-}* mice display a well-ordered all-cone retina with a normal retinal vasculature and a strong photopic function that generates useful vision.

Methods:

We exposed *R91W;Nrl^{-/-}* and *wt* mice to toxic levels of blue light and analyzed their retinas at different time-points post-illumination (up to 10 days). Methods of analysis included ELISA, OCT, funduscopy, light and electron microscopy, immunofluorescence, Western blotting and real-time PCR.

Results:

TUNEL-positive (dying) retinal cells were detected in both *R91W;Nrl^{-/-}* and *wt* mice as early as 24 h post-illumination. However, while exposure of *wt* mice resulted in massive pyknosis only in a focal region in the outer nuclear layer, exposure of *R91W;Nrl^{-/-}* mice led to pyknotic nuclei also within the inner nuclear layer. RPE lesions that regularly occurred in *wt* mice were not observed in *R91W;Nrl^{-/-}* mice. This was probably due to the reduced extent of cellular debris formed in *R91W;Nrl^{-/-}* retinas, which could then readily be digested by the phagocytic activities of the RPE and microglia/macrophages. Indeed, microglia/macrophage infiltration at the site of injury was observed in both models, but was more pronounced in the all-cone retina of *R91W;Nrl^{-/-}* mice. Additionally, retinal vascular leakage was detected *in vivo* in light-exposed *R91W;Nrl^{-/-}* mice but not in *wt* mice. This was accompanied by retinal swelling and the appearance of cystoid spaces in both inner and outer nuclear layers of *R91W;Nrl^{-/-}* mice indicating edema in affected areas. However, retinal swelling was transient, and 10 days following light exposure signs of edema or leakage were no longer observed in *R91W;Nrl^{-/-}* mice.

Conclusion:

Collectively our data suggest that blue light exposure of *R91W;Nrl^{-/-}* mice induces cone cell death but also disrupts the inner blood-retinal barrier. Macular edema in humans is a result of diffuse capillary leakage and microaneurysm within the macula. Blue light exposure of the *R91W;Nrl^{-/-}* mouse could therefore be used to study molecular events preceding edema formation in a cone-rich environment, and thus potentially help to develop treatment strategies for edema-based complications in macular degenerations.

M. Shilaih¹, A. Marzel¹, J. Schüpbach⁵, J. Böni⁵, S. Yerly², T. Klimkait⁴, V. Aubert³, H. Günthard¹, R. Kouyos¹

Targeting the Unknown Unknowns: Characterization of HIV Positive Patients not Enrolled in the Swiss HIV Cohort Study (SHCS)

Infectious Diseases and Hospital Epidemiology, University Hospital Zurich, Zurich¹, Laboratory of Virology and AIDS Center, Geneva University Hospital, Geneva², Division of Immunology, Lausanne University Hospital, Lausanne³, Department of Biomedicine and Surgery, University Hospital Basel, Basel⁴, Swiss National Center for Retroviruses, University of Zürich, Zürich⁵

Introduction:

Adequate coverage of marginalized populations is essential for containment of the HIV pandemic and beyond. A unique opportunity to assess the presence of such populations in the SHCS is provided by a database of all genotypic resistance tests performed in Switzerland, which includes both SHCS enrolled and non-cohort patients.

Methods:

A maximum likelihood phylogenetic tree was built using 11130 SHCS and 2875 Swiss non-SHCS sequences, pooled with 27803 non Swiss background sequences from the Los Alamos database. Ethnicity and risk group were inferred for non-SHCS patients using phylogenetic proximity. Multivariate logistic regression was applied to determine factors associated with forming a separate introduction outbreak.

Results:

Non-B subtype (odds ratio 3.0; 95% C.I 2.8-3.3), female gender (1.4; 1.3-1.6), non-white ethnicity (2.8; 2.5-3.1) and heterosexual orientation (1.7; 1.5-1.8), were all significantly associated with not being represented in the SHCS cohort.

We found 344 purely non-SHCS Swiss transmission clusters, however, the largest outbreak was small (7 patients). Non-SHCS and SHCS patients overlap strongly, where 53% and 70% of SHCS and non-SHCS sequences respectively, were parts of mixed clusters. Non-SHCS patients were less likely to be part of transmission clusters compared to SHCS patients (0.79, 0.72-0.87).

Conclusion:

Our data suggests that migrants and immigrants might be underrepresented in the SHCS. The limited size and number of outbreaks of non-SHCS patients implies that no major HIV outbreak in Switzerland was missed by the SHCS. This study demonstrates the potential of sequence data to assess the representativeness of cohort studies.

C. Schori¹, SH. Ahanger¹, K. Evans², E. Levine², C. Grimm¹

Investigation of the neuroprotective role of Müller glia cell specific activation of a hypoxic response

Lab for Retinal Cell Biology, Dept. Ophthalmology, University of Zürich, Zürich, Switzerland¹, Department of Ophthalmology and Visual Sciences, John A. Moran Eye Center, University of Utah, Salt Lake City, Utah²

Introduction:

We previously showed that a rod-specific hypoxic response protects photoreceptors only marginally against damage, whereas systemic hypoxic preconditioning is strongly protective *in vivo*. Since Müller cells (MCs) can protect photoreceptors in normoxia by the production of cytokines and growth factors, we are testing whether MCs might be responsible for the protection mediated by hypoxic preconditioning.

Methods:

A conditionally immortalized mouse MC line (ciMC) was either exposed to hypoxia (0.2% O₂) or treated with siRNA to specifically inactivate the von Hippel Lindau (*Vhl*) gene. The cellular response to the treatments was analyzed by Western blotting and real-time PCR. MCs expressing GFP (GFP(+)) were isolated by FACS from dissociated retinas of *Rbp1-GFP* mice subjected to hypoxia (6h, 7% O₂) and analyzed by real-time PCR. Mice lacking *Vhl* in MCs were generated by the Cre-LoxP system using a tamoxifen-inducible *Rbp1-CreER* mouse line.

Results:

Hypoxia, or siRNA-mediated inactivation of *Vhl* in ciMC6 cells stabilized hypoxia-inducible factor 1A (HIF1A) *in vitro* and upregulated expression of hypoxia response genes such as adrenomedullin (*Adm*), vascular endothelial growth factor (*Vegf*) and others. Pools of GFP(+) cells isolated from hypoxic retinas were strongly enriched with MCs and showed increased expression of *Adm*, *Vegf* and erythropoietin (*Epo*). Hypoxia-induced expression of *Vegf* was detected in GFP(+) but not in GFP(-) cell pools where it was below detection threshold. *Adm* and *Epo* were upregulated by hypoxia in both pools, as was the expression of fibroblast growth factor 2. The consequences of the MC specific inactivation of *Vhl* are currently under investigation.

Conclusion:

Müller cells respond to reduced oxygen levels or to an inactivation of *Vhl* by an increased expression of hypoxia responsive genes *in vitro* and *in vivo*. Therefore, Müller cells can appropriately react to reduced oxygen levels and may thus be part of the neuroprotective response induced by hypoxic preconditioning *in vivo*. Consequences of an artificial activation of this response by the inactivation of *Vhl* in MCs will be tested in the light damage paradigm and in a model of inherited retinal degeneration.

A. Wyss¹, T. Raselli¹, K. Atrott¹, I. Frey-Wagner¹, A. Sailer², G. Rogler¹, B. Misselwitz¹

Role of EBI2 and Oxysterols in the Development of Intestinal Lymphoid Structures and Colon Inflammation

University Hospital Zurich, Zurich¹, Novartis Institutes for BioMedical Research, Basel²

Introduction:

Two types of lymphoid structures exist in the colon, colonic patches (CLP) and solitary intestinal lymphoid tissues (SILT). The process of lymphoid structure formation is dependent on lymphoid tissue inducer cells and the lymphotoxin signaling pathway, which includes the interaction between a variety of chemotactic factors and their ligands. Epstein Barr virus induced gene 2 (EBI2) is a G-protein coupled receptor expressed on immune cells. The EBI2 ligand 7 α ,25-Dihydroxycholesterol is produced by two enzymes, CH25H and CYP7B1. EBI2 and its oxysterol ligands can mediate migration, positioning and differentiation of B cells within secondary lymphoid organs but have not been implicated in immune development or the pathogenesis of colitis.

Methods:

Using a whole mount approach the colons of 12-week old EBI2^{-/-} mice and their wildtype littermates were stained to determine the number of B cell follicles. T-cell transfer colitis was induced by transferring naïve T cells from wildtype or EBI2^{-/-} mice to immunodeficient RAG2^{-/-} mice. The mice were examined 6 weeks after transfer. DSS colitis was induced by administration of 2-3% dextran sodium sulfate (DSS) for 7 days (acute) or 4 cycles of 7 days interspersed with 10 day recovery periods (chronic) in EBI2^{-/-} mice and wildtype controls.

Results:

EBI2^{-/-} mice showed significantly less B cell follicles within the colon than littermate wildtype controls ($p < 0.05$). The difference was restricted to smaller lymphoid structures, pointing to an anomaly in SILT development in the EBI2 knockouts. In T-cell transfer colitis, endoscopic severity of colitis was stronger after transfer of EBI2^{-/-} T cells compared to controls. Similarly, in CH25H^{-/-} mice histological changes were significantly stronger in chronic DSS colitis compared to wildtype controls ($p < 0.05$). Furthermore, in acute and chronic experimental colitis, mRNA for CYP7B1 and CH25H were upregulated in the colon ($p < 0.01$), suggesting increased oxysterol production in the inflamed gut. A similar up-regulation of CH25H was found in rectal biopsies of ulcerative colitis patients.

Conclusion:

Our results point to a role of EBI2 during development of intestinal lymphoid structures. Oxysterol production is likely increased in the inflamed gut of humans and mice and knockout of EBI2 and CH25H affected the severity of colitis in some experimental mouse models of colitis. These findings establish a role for EBI2 and oxysterols in the maturation of the gut immune system and in the pathophysiology of inflammatory bowel diseases.

T. Raselli¹, A. Wyss¹, K. Atrott¹, I. Frey-Wagner¹, A. Geier², A. Sailer³, G. Rogler¹, B. Misselwitz¹

Role of EBI2 and Oxysterols in the Pathogenesis of Fatty Liver Disease

Gastroenterology and Hepatology, University Hospital Zurich, Switzerland¹, Medical Clinic and Policlinic II, University Hospital Würzburg, Germany², Novartis Institutes for Biomedical Research, Basel, Switzerland³

Introduction:

Non-alcoholic steatohepatitis (NASH) is the most frequent liver disease in industrialized countries, but the underlying pathophysiological process is not completely understood. Several lines of evidence suggest a role of oxysterols in NASH pathogenesis, which for now remains poorly defined. Epstein Barr virus induced gene 2 (EBI2) is involved in B cell differentiation and was shown to stimulate the migration of B cells and dendritic cells in vitro and in vivo and might modify the inflammatory response in NASH. 7 α ,25-dihydroxycholesterol (7 α ,25-OHC) has recently been identified as a high-affinity ligand for EBI2. We are aiming to clarify the role of EBI2, 7 α ,25-OHC and its synthesizing enzymes (CYP7B1 and CH25H) in hepatic inflammation and fibrosis.

Methods:

We investigated the role of EBI2 and CH25H in NASH pathogenesis using a mouse feeding model. Knockout mice with a defective EBI2-7 α ,25-OHC-system (EBI2^{-/-}, CH25H^{-/-}) and wildtype littermate controls were fed ad libitum with a high fat high sugar diet (HFD) for 20 weeks. Liver inflammation was assessed using an established NASH score.

Results:

After 20 weeks of HFD EBI2^{-/-} and CH25H^{-/-} mice displayed stronger liver inflammation compared to wildtype littermate controls. In a single EBI2^{-/-} animal, with a very high NASH activity score (NAS), high expression markers of liver fibrosis (alpha smooth muscle actin and TIMP metalloproteinase inhibitor 1) was observed. mRNA expression of CH25H was upregulated in EBI2^{-/-} animals with a high expression of tumor necrosis factor and a high NAS, indicating an increased oxysterol production during NASH.

Conclusion:

Our data suggest a protective role of EBI2 and oxysterols in NASH pathogenesis, possibly by recruiting immunosuppressive dendritic cells into the inflamed liver. Our model allows studying the interplay between inflammatory molecules and oxysterols and might lead to new therapeutic options in NASH.

I. Leonardi¹, A. Gerstgrasser¹, F. Nicholls², B. Tewes³, R. Greinwald³, G. Rogler¹, I. Frey-Wagner¹

Administration of *T. suis ova* protects immunocompetent rabbit from DSS colitis, but is detrimental to immunosuppressed individuals.

Gastroenterology and Hepatology, University Hospital Zurich, Zurich¹, Central Biological Laboratory, University Hospital Zurich, Zurich², Research and Development, Dr. Falk Pharma GmbH, Freiburg (D)³

Introduction:

Immunomodulation by helminths can be used to prevent and treat immune-related diseases. Clinical trials in IBD with *T. suis ova* (TSO) have shown promising results but the underlying mechanisms and the safety in immune suppressed patients have not been investigated so far. We used a rabbit model of colitis to study the efficacy, mechanisms and safety of TSO therapy in immunocompetent and immunodeficient animals

Methods:

NZW rabbits received 3x2500 TSO (d1, 14, 21, i.g). Colitis was induced at d26 with 0.1% DSS for 5 days. Symptoms were monitored daily and rabbits were sacrificed at d35. Lamina propria mononuclear cells (LPMC) and epithelial cells (EC) were isolated from caecal biopsies, for RNA extraction and genome wide expression analysis. For immunosuppression, treatment with cyclosporine (100 ul/kg/day p.o) and Methylprednisolone (1 mg/kg/day p.o) was started 14d prior to the first TSO treatment and continued until d35.

Results:

TSO treatment significantly reduced the weight loss during colitis (% day10/day0, TSO: +4.23±0.98 vs. vehicle: -0.25±1.22; n=8 per group) and reduced the disease activity index (DAI) at d35 from 1.6±0.8 (vehicle) to 0.7±0.2 (TSO). TSO partially protected the caecal mucosa from the DSS-induced morphological changes and reduced the extent of lymphocyte infiltration into the intestinal epithelium and into the lamina propria. Expression profiling showed that the effect of TSO mainly influenced LPMC by dampening innate inflammatory and Th17 responses and by down regulating cell-adhesion pathways. In contrast, TSO treatment exacerbated the DSS induced colitis in immunosuppressed rabbits. In particular, the weight loss increased from -0.15±1.20 (vehicle, n=8) to -3.10±1.60 (TSO, n=9). Further, histological examination revealed the presence of larvae in the caecal mucosa and a worsening of the histology score by 50%.

Conclusion:

We show that TSO ameliorates the development of colitis in immunocompetent rabbits, where it modulates LPMC immune responses. However, this preventive effect is lost in immunocompromised animals, where TSO treatment exacerbates the colitis.

G. Klinke¹, M. Rohrbach⁵, R. Giugliani², P. Burda⁵, M. Baumgartner⁵, C. Tran³, M. Gautschi⁴,
D. Mathis¹, M. Hersberger¹

LC-MS/MS BASED ASSAY AND REFERENCE INTERVALS IN CHILDREN AND ADOLESCENTS FOR OXYSTEROLS ELEVATED IN NIEMANN-PICK DISEASES

Clinical Chemistry and Biochemistry and Children's Research Center, University Children's Hospital, Zurich¹, Medical Genetics Service, HCPA, Departement of Genetics, UFRGS, Porto Alegre², Center for Molecular Diseases, Lausanne University Hospital, Lausanne³, Paediatric Endocrinology, Diabetology and Metabolism, University Children's Hospital Bern, Bern⁴, Division of Metabolism and Children's Research Center, University Children's Hospital Zurich, Zurich, Switzerland⁵

Introduction:

Niemann-Pick type C (NP-C) is a rare progressive neurodegenerative lipid storage disorder with heterogeneous clinical presentation and challenging diagnostic procedures. Recently oxysterols have been reported to be specific biomarkers for NP-C but knowledge on the intra-individual variation and on reference intervals in children and adolescents are lacking.

Methods:

We established a LC-MS/MS assay to measure Cholestan-3 β , 5 α , 6 β -triol (Triol) and 7-Ketocholesterol (7-KC) following Steglich esterification. To assess reference intervals and intra-individual variation we determined oxysterols in 148 children and adolescents from 0-18 years and repeat measurements in 19 of them.

Results:

The reported method is linear ($r > 0.99$), sensitive (detection limit of 0.03 ng/mL for Triol, 0.54 ng/mL for 7-KC) and precise, with an intra-day imprecision in the reference intervals of 4.8% and 4.1%, and an inter-day imprecision of 7.0% and 11.0% for Triol and 7-KC, respectively. Recoveries for 7-KC and Triol range between 93 % and 107 % in the reference intervals. The upper reference limit obtained for Triol is 40.40 ng/mL (CI: 26.42-61.73 ng/mL) and 75.01 ng/mL for 7-KC (CI: 55.52-102.50 ng/mL), with no age dependency. Both oxysterols have a broad intra-individual variation of 46% for Triol and 52% for 7-KC. Nevertheless, all Niemann-Pick patients showed increased Triol levels including Niemann-Pick type A and B patients.

Conclusion:

The LC-MS/MS assay is a robust assay to quantify Triol and 7-KC in plasma with well documented reference intervals in children and adolescents to screen for NP-C in the pediatric population. In addition our results suggest that especially the Triol is a biomarker for all three Niemann-Pick diseases.

C. Naegeli¹, T. Zeffiro², A. Weilenmann¹, K. Hassanpour¹, M. Schick¹, A. Jaillard⁴, M. Piccirelli⁵, M. Rufer¹, R. Pitman³, S. Orr³, C. Mueller-Pfeiffer¹

The neural correlates of autonomic stress sensitization in posttraumatic stress disorder

Department of Psychiatry and Psychotherapy, University Hospital Zurich, Zurich¹, Neural Systems Group, Massachusetts General Hospital, Boston, MA², Department of Psychiatry, Massachusetts General Hospital and Harvard Medical School, Boston, MA³, CHU de Grenoble⁴, Inst. Of Neuroradiology, University Hospital Zurich, Zurich Switzerland⁶

Introduction:

Stress sensitization of the nervous system is believed to play an important role in the development of PTSD after a traumatic event and may underlie PTSD symptoms such as hypervigilance and exaggerated startle responses. Despite compelling evidence for autonomic stress sensitization in PTSD as provided by peripheral psychophysiological studies, its neural basis remains largely unknown. The loud-tone procedure, which consists of presenting a series of 95 dB loud tones in a task-free situation, is one of the established paradigms for measuring autonomic stress sensitization in PTSD.

Methods:

In an ongoing fMRI-study, PTSD subjects and trauma-exposed healthy subjects engage in a loud-tone-like procedure that presents 500 msec, 95 dB pure-tone or white-noise stimuli.

Results:

As a preliminary result, we observed heightened heart rate responses to pure tones and white noise stimuli in PTSD subjects ($p = 0.18$ and $p = 0.005$, respectively) in a subsample of 6 PTSD and 9 healthy subjects.

Conclusion:

Further peripheral and central physiological results will be presented of this ongoing study.

M. Toeteberg-Harms¹, L. Jozic², J. Magner², J. Funk¹

IOP Lowering Efficacy of Phacoemulsification Cataract-Extraction with Intraocular Lens Implantation alone (phaco) versus plus Excimer Laser Trabeculotomy (phaco-ELT) versus plus ab interno Trabeculotomy with the Trabectome® (phaco-AIT) – 1 Year Results.

Department of Ophthalmology, University Hospital Zurich, Zurich, Switzerland¹, Eye Clinic Ballindamm, Hamburg, Germany²

Introduction:

The aim of this study is to compare the IOP lowering efficacy among the three procedures within a follow-up period of 1 year.

Methods:

This is a prospective case-controlled comparative series. Inclusion criterion was diagnosis of mild and moderate open-angle glaucoma or ocular hypertension with a coexisting and visual impairing cataract. Only one eye of each patient was included, and if both eyes underwent the procedure, one was randomly chosen. Eyes underwent either phaco alone or combined phaco-ELT or phaco-AIT. Primary outcome measures were IOP, number of hypotensive medications (AGD), and Kaplan-Meier survival. Definition of failure was IOP >21mmHg or <20% reduction of IOP below baseline, hypotony (IOP ≤5mmHg), or loss of light perception vision.

Results:

38 eyes (16 OD = 42.1%; 17 males = 44.7%; mean age 76.0±7.4 years, preop IOP = 16.7±3.8 mmHg; preop AGD = 1.1±0.6) in the phaco, 105 eyes (58 OD = 55.2%; 38 males = 36.2%; mean age 74.8±6.0 years; preop IOP = 17.8±4.3 mmHg; preop AGD = 1.4±0.7) in the phaco-ELT, and 102 eyes (54 OD = 52.9%; 25 males = 24.5%; mean age 74.3±4.9 years; preop IOP = 19.3±4.6 mmHg; preop AGD = 1.3±0.8) in the phaco-AIT group were included ($P = 0.375$; $P = 0.045$; $P = 0.271$; $P = 0.004$; $P = 0.207$ respectively). At 1 year, IOP was lowered by 1.5±4.0 mmHg in the phaco alone group, by 4.3±5.6 mmHg in the phaco-ELT group, and by 5.3±4.5 mmHg in the phaco-AIT group, respectively. AGD were lowered by 0.1±0.8 in the phaco alone group, by 0.9±0.8 in the phaco-ELT group, and by 0.8±0.7 in the phaco-AIT group, respectively. The difference in IOP and AGD from baseline to 1 year was highly significant ($P < 0.001$) when comparing the phaco-ELT or phaco-AIT group with the phaco alone group, but not significant comparing the phaco-ELT with the phaco-AIT group ($P > 0.05$). Mean time to failure was 13.2±0.4 months in the phaco alone, 20.6±1.0 months in the phaco-ELT, and 12.9±0.6 months in the phaco-AIT group ($P < 0.001$).

Conclusion:

The phaco-ELT and phaco-AIT groups had significantly lower mean IOP and required fewer AGD compared with the phaco alone group. Mean IOP and AGD were not significantly different in the phaco-ELT and phaco-AIT groups. However, mean time to failure was significantly longer in the phaco-ELT group. The phaco-ELT and phaco-AIT groups had significantly lower mean IOP and required fewer AGD compared with the phaco alone group. Mean IOP and AGD were not significantly different in the phaco-ELT and phaco-AIT groups. However, mean time to failure was significantly longer in the phaco-ELT group.

A. Palla¹, M. Rohrbach², M. Baumgartner², A. Klein³, D. Straumann¹, C. Bockisch⁴

Evaluation of a video-oculographic system for the examination of saccadic eye movements in a 3-year old boy with Niemann-Pick Type C Disease

Department of Neurology, University Hospital Zurich¹, Division of Metabolism, Childrens research Centre, University Children's Hospital Zurich, Switzerland², Division of Child Neurology, University Children's Hospital Zurich, Switzerland³, Department of Neurology, University Hospital Zurich; Department of Ophthalmology, University Hospital Zurich; Department of Otorhinolaryngology, Head and Neck Surgery, University Hospital Zurich⁴

Introduction:

Niemann-Pick disease type C (NPC) is a rare, inherited, and fatal disease associated with impaired intracellular lipid trafficking and progressive neurovisceral symptoms. NPC may present from infancy through adulthood. In NPC patients, impaired saccadic eye movements are one of the most reliably present neurological signs. During infancy, however, they are often overlooked due to limitations in the child's cooperation and in the eye tracking equipment and testing paradigms not primarily developed for assessing children. The purpose of this study was to evaluate the suitability of the EyeSeeCam, a video-oculographic device for eye movement recording, in a child afflicted with NPC.

Methods:

Horizontal and vertical saccades were recorded with the EyeSeeCam in a three year old male NPC child and an age-matched healthy female control.

Results:

Main sequence characteristics (peak velocity versus saccade amplitude) of horizontal saccades could successfully be analyzed in both children. Measurements of vertical saccades were successful in the healthy control but failed in the patient because of eye blinks that accompanied saccades.

Conclusion:

The major advantage of the EyeSeeCam as a non-invasive video-based eye tracking system compared to more invasive eye measurement methods is counteracted in young children by the necessity of increased cooperation. The blinks that prevented accurate data recording of vertical saccades in the patient occur reflexively and are likely a strategy to inhibit brainstem omnipause neurons, thereby releasing saccades.

Y. Achermann¹, B. Tran³, M. Kang², J. Harro², M. Shirliff²

Immunoproteomic identification of in vivo-expressed *Propionibacterium acnes* proteins in a rabbit biofilm infection model

*University Hospital Zurich, Division of Infectious Diseases and Hospital Epidemiology, Zurich, Switzerland*¹, *Department of Microbial Pathogenesis, School of Dentistry, University of Maryland, Baltimore, USA*², *Department of Pharmaceutical Sciences, School of Pharmacy, University of Maryland, Baltimore, Baltimore, USA*³

Introduction:

Propionibacterium acnes is primarily known as a human skin commensal but can also act as an invasive pathogen causing implant-associated infections. In order to resolve these types of *P. acnes* infections, implants must be removed due the presence of an established biofilm that is recalcitrant to antibiotic therapy. In order to identify those *P. acnes* proteins expressed *in vivo* during a biofilm infection, we established a rabbit model of implant-associated infection with this pathogen.

Methods:

P. acnes biofilms were anaerobically grown on dextran beads that were then inoculated into the left tibia of rabbits. At four weeks post-inoculation, *P. acnes* infection was confirmed by radiograph, histology, culture, and PCR. In addition, *in vivo*-expressed and immunogenic *P. acnes* proteins were identified by matrix assisted laser desorption/ionization – time of flight tandem mass spectrometry (MALDI-TOF MS) after separation by two dimensional gel electrophoresis and Western blot using serially harvested rabbit sera samples.

Results:

Radiographs and histology demonstrated disruption of the normal bone architecture in animals with culture and/or PCR confirmed infections. A total of 23 immunogenic proteins were identified, therefore 13 proteins including an ABC transporter protein were upregulated in both planktonic and biofilm modes.

Conclusion:

We successfully adapted a common rabbit model of implant-associated infection for *P. acnes* to identify *P. acnes* proteins expressed during a chronic biofilm-mediated infection. Further studies are needed to evaluate the potential of these proteins for either a diagnostic test or a vaccine to prevent biofilm infections caused by *P. acnes*.

V. Pham¹, C. Chassard¹, C. Braegger², C. Lacroix¹

Trophic chain of lactate in infant's gut revealed by a novel functional approach

Department of Health Sciences and Technology, Institute of Food, Nutrition and Health, Laboratory of Food Biotechnology, ETH Zürich, Zürich¹, Division of Gastroenterology and Nutrition, University Children's Hospital Zurich, Zürich²

Introduction:

The colonization process of the infant gut microbiota is crucial for the present and future health of infants. However, little is known about the sequence of colonization, abundance and diversity of different functional bacterial groups in the infant gut. The present study investigated the colonization pattern of healthy infant gut microbiota using a combination of cultural and molecular methods, focusing on the functional groups of microbes contributing to a healthy trophic chain, and the fate of lactate as an important intermediate.

Methods:

Faecal samples were obtained from 40 healthy infants at 2 weeks, 1, 3, and 6 months after delivery. Functional groups of microbes were investigated using a combination of cultural and molecular methods (qPCR and high-throughput Illumina sequencing).

Results:

Our results indicated that a dense microbiota had established in all infants after 2 weeks of life (total bacteria: 11.9 log g⁻¹ faeces). The lactate producing bacteria population was dominated by *Bifidobacterium*, which reached 9.3 log g⁻¹ after 2 weeks and slightly decrease in the next 6 months. Other lactate producing populations were also detected after 2 weeks, including *Lactobacillus* (6.4 log g⁻¹) and *Bacteroides* (7.6 log g⁻¹). Interestingly, there was an uneven distribution of *Bacteroides* levels in the first 2 weeks of life and infants could be classified into two groups: one harboured high levels of *Bacteroides* (9.3 log g⁻¹), whereas the other showed significant lower levels (5.7 log g⁻¹).

We were able to detect early colonization of different groups that are able to reutilize lactate. *Veillonella* dominated the ecological niche at high levels after 2 weeks (7.8 log g⁻¹) and strongly increased to 9.0 log g⁻¹ after 6 months. Lactate-utilizing sulphate-reducing bacteria (SRB) population, which are involved in the pathogenesis of colonic diseases, already reached adult level of 6.3 log cfu g⁻¹ at week 2 and gradually increased to 7.2 log cfu g⁻¹ after 6 months. The lactate-utilizing bacteria non-SRB population increased from 2 weeks (5.8 log cfu g⁻¹) to 6 months (7.1 log cfu g⁻¹) but remained significantly lower than adult levels. *Eubacterium hallii*, detected after 2 weeks (7.0 log g⁻¹), remained stable over time and represented one of the predominant butyrate producers in the infant gut.

We demonstrated the strong impact of mode of delivery on predominant LPB and LUB. C-section delivered infants harbored significantly higher levels of *Veillonella* at 1m (P=0.009) and lower levels of *Bacteroides* during the follow-up period (P<0.001).

Interestingly, sequencing data revealed a shift in colonization pattern of lactate-utilizing propionate-producers between 2w and 6m of life; i.e. an increasing abundance of *Veillonella* and decreasing abundance of *Propionibacterium*.

Conclusion:

Our data revealed for the first time the complexity of early colonization until 6 months of age and the competition between functional groups involved with lactate production and reutilization. The competitive interactions among functional microbes could cause microbial and metabolic dysbiosis which may directly impact on infant gut health.

E. Saponara¹, G. Seleznik¹, R. Buzzi¹, F. Baschieri², H. Farhan², O. Pertz³, A. Caflisch⁴, K. Grabliauskaite¹, R. Graf¹, S. Sonda¹

Intracellular serotonin regulates cytoskeletal remodeling at the base of pancreatic acinar-to-ductal-metaplasia formation

Swiss HPB Center, Visceral & Transplantation Surgery, University Hospital Zurich¹, Biotechnology Institute Thurgau, Department of Biology, University of Konstanz², Department of Biomedicine, University of Basel³, Department of Biochemistry, University of Zurich⁴

Introduction:

Pancreatic ductal adenocarcinoma (PDAC) is the most frequent and lethal pancreatic cancer initiated by persistent lesions called acinar-to-ductal metaplasias (ADMs). Noteworthy, ADM formation mainly depends on cytoskeletal remodeling of acinar cells. After showing that intracellular serotonin (5-hydroxytryptamine, 5-HT) regulates actin re-arrangements in acinar cells, we investigated whether 5-HT regulates the cytoskeletal remodeling critical for ADM and pre-malignant lesion formation.

Methods:

Several biochemical and imaging approaches, acinar and human pancreatic cancer cell lines, primary pancreatic fibroblasts, an in vitro 3D culture model of ADM formation and 5-HT deficient mice were utilized to identify the molecular mechanisms at the base of 5-HT-dependent cytoskeletal remodeling. The therapeutic potential of selective 5-HT transporter inhibitors (SERTi) was evaluated in vivo in transgenic mice harbouring KrasG12D mutation which spontaneously form ADM and pre-malignant lesions

Results:

In vivo and in vitro analyses showed that intracellular 5-HT is required for Rac1 activation, a key regulator of cytoskeletal remodeling. Inhibition of 5-HT transport with SERTi in vitro inhibited ADM formation, reduced cell migration, increased cell adhesion and perturbed lipid metabolism without reducing cell viability. Importantly, in vivo treatment of KrasG12D mice with SERTi significantly reduced the formation of ADM and pre-malignant lesions without associated drug toxicity.

Conclusion:

Our data clearly indicate that cytoskeletal remodeling regulated by intracellular 5-HT is critical for the formation of ADM lesions. Given the role of ADMs as precursors of PDAC, we propose a novel therapeutic strategy which might complement current PDAC treatments.

E. Unterleutner¹, F. Barchiesi¹, B. Imthurn¹, R. Dubey¹

Differential Role of AKT-pathway in Mediating the Growth Effects of GPER in Human Coronary Arterial Smooth Muscle Cells and Human Umbilical Vein Endothelial Cells

Clinic For Reproductive Endocrinology , University Hospital Zurich, Zurich¹

Introduction:

Animal and human studies suggest that Estradiol (E2) induces vasoprotective actions, by improving endothelium dependent relaxation of vessels and inducing endothelial cell growth and repair. Moreover, it inhibits smooth muscle cell proliferation and migration – associated with vasoocclusive disorders. The molecular mechanisms via which it mediates these effects remain unclear. We have previously shown that E2 induces endothelial growth and capillary formation. Moreover, the effects of E2 on capillary formation are mimicked by its non-permeable analogue, BSA-tagged E2. Based on these findings, we hypothesize that E2- effects are potentially mediated via the newly discovered membrane bound estrogen receptor GPER. Hence, in the present study, we assessed whether E2 stimulates the capillary formation in HUVECs and reduces cell proliferation in HCASMCs via GPER. Finally, we explored the role of PI3K/AKT, a prominent angiogenic and proliferative pathway, in mediating the effects of E2.

Methods:

The role of GPER in E2-regulated capillary formation was assessed using 2D-matrigel based capillary assay. The cell proliferation was quantified by using cell counting. Cells were treated with the specific GPER-agonist (G1), -antagonist (G15), E2, ER-unspecific antagonist (ICI), PI3K-inhibitor LY292400 (LY) and GPER siRNA. Cell proliferation was induced with platelet-derived growth factor-BB (PDGF). Western Blotting was used to evaluate changes in AKT phosphorylation and the efficiency of GPER silencing siRNA transfection.

Results:

Treatment with the specific GPER-agonist G1 (10nm) and with E2 (10nm) significantly induced capillary formation in HUVECs. The stimulatory effects of both G1 and E2 were significantly abrogated in the presence of the specific GPER-antagonist G15 (100nm) or the ER-antagonist ICI (100nm). Cell proliferation of HCASMCs was induced with PDGF (20ng/ml) and could be significantly reduced with G1 (250nm) or E2 (250nm). These inhibitory effects on cell proliferation could be reversed using G15 (1µm) or ICI (1µm). GPER expression was significantly suppressed following siRNA transfection (50nm) for 72h. In HUVECs with GPER knockdown, stimulation with both G1 (10nm) and E2 (10nm) did not induce capillary formation, whereas capillary formation was significantly induced in the respective control. In HCASMCs with GPER knockdown, G1 (250nm) did not inhibit cell proliferation, whereas it significantly reduced it in the respective control. Both HUVECs and HCASMCs express AKT, an important pro-vasculogenic and -proliferative protein. G1 (10nm) differentially regulated the phosphorylation of AKT in the two cell types: it up-regulated the phosphorylation of AKT in HUVECs and reduced PDGF-induced AKT phosphorylation in HCASMCs. The stimulatory effects of G1 on pAKT in HUVECs were blocked by G15 (100nm), ICI (100nm), LY (5µm) and GPER knockdown. Upon treatment with LY (5µm) the effect of G1 on the capillary formation was lost. The inhibitory effect of G1 (250nm) on cell proliferation in PDGF-treated HCASMCs was mimicked by LY (5µm).

Conclusion:

Our findings provide evidence that GPER plays an important role in mediating differential effects of E2 on capillary formation and on smooth muscle cell proliferation. Importantly, the activation of the proliferative pathway PI3K/AKT by GPER in HUVECs and inhibition of PI3K/AKTs in HCASMCs seems to play a key role in mediating its vasoprotective actions. In conclusion, it is suggested that the use of GPER specific agonist may facilitate endothelial recovery thereby promoting vascular protection.

S. Burnos¹, O. Schmid¹, T. Fedele¹, N. Krayenbühl¹, J. Sarnthein¹

Quantifying the relationship between SEP and evoked high frequency oscillations (HFO) under anesthesia

Klinik für Neurochirurgie, Universitätsspital Zürich¹

Introduction:

The somatosensory evoked potential (SEP) of the medianus nerve elicits a N20 component and a high-frequency oscillation (HFO, >500 Hz). Here we investigate the feasibility of intraoperative subdural HFO recordings and the temporal and spatial relationship between N20 and HFO.

Methods:

During neurosurgical interventions in 7 anesthetized patients, the medianus SEP was recorded (11 recordings, 52 channels) from subdural electrode strips to localize the central sulcus. Depending on surgical restrictions, the strips were placed directly on sensory cortex or motor cortex or both.

Results:

The SEP response consisted of the two distinct spectral components N20 (<250 Hz) and HFO (721±70 Hz) in the time-frequency domain. The HFO maximum amplitude appeared at the same or an adjacent electrode contact as the N20 maximum in 10 of 11 recordings. HFO amplitude was proportional to N20 amplitude over patients. The N20 amplitude decayed with a larger spatial extent (exponential space constant 5.2±4.0 cm) than the HFO amplitude (2.4±1.9 cm, p<0.05). The HFO peak (21.4±1.8 ms) preceded the N20 (23.2±1.4 ms, p<0.05) by up to 8 ms.

Conclusion:

HFOs in response to medianus stimulation can be recorded under conditions of anesthesia. Since we recorded highly localized HFO bursts, the HFO bursts must be of cortical origin even if they precede the N20 component.

M. Barben¹, C. Schori¹, C. Grimm¹, M. Samardzija¹

Cone pathophysiology under chronic hypoxia

Lab for Retinal Cell Biology, Department of Ophthalmology, University of Zurich, Zurich¹

Introduction:

The recently generated *Rpe65^{R91W};Nrt^{-/-}* (*R91W;Nrt^{-/-}*) double-mutant mice express only cone photoreceptors in a well-layered and functional retina, and facilitate the investigation of cone-degenerative diseases, such as age-related macular degeneration (AMD). Since hypoxia has been postulated to be important in the etiology of AMD, we analyzed the effect of a chronic hypoxia-like response on cone pathophysiology. We hypothesized that a cone-specific inactivation of von Hippel Lindau protein (VHL) in *R91W;Nrt^{-/-}* mice leads to a long-term activation of HIF transcription factors enabling transcription of HIF target genes, and results in age-dependent retinal degeneration.

Methods:

We ablated *Vhl* specifically in cones of the all-cone *R91W;Nrt^{-/-}* mouse using the Cre-LoxP system (*BPcre;R91W;Nrt^{-/-};Vhl^{fl/fl}* (= *cone^{ΔVhl}*)). *cone^{ΔVhl}* mice were analyzed at 4, 6, 8, 12 and 26 weeks of age, and compared to age-matched *R91W;Nrt^{-/-};Vhl^{fl/fl}* control mice. Stabilization of HIF1A and differential regulation of HIF1 target genes were tested by Western blotting and real-time PCR. Photoreceptor degeneration and cellular structure in the retina were evaluated by light microscopy and TUNEL staining, respectively.

Results:

Based on data from ZsGreen-reporter mice, recombination by BPcre led to the inactivation of the floxed *Vhl* gene in most S-cones, but also in M-cones, and few other retinal cells of *cone^{ΔVhl}* mice. HIF1A was stabilized and expression of HIF1 target genes such as adrenomedullin and vascular endothelial growth factor were induced in retinas of normoxic *cone^{ΔVhl}* mice. Importantly, cone-specific ablation of *Vhl* resulted in a strong retinal degeneration with most cones lost at 26 weeks of age.

Conclusion:

Here, we employed the all-cone *R91W;Nrt^{-/-}* mouse to analyze the reaction of cones to a chronic hypoxia-like response, a feature that may be part of AMD pathology. Our results indicate that chronic activation of HIF transcription factors induces cone degeneration leading to loss of vision. However, further analysis is required to understand the underlying molecular pathways that lead to cone cell death. Ultimately, these results could assist in the development of therapeutical approaches for the treatment of cone-related diseases that suffer from reduced oxygenation of photoreceptors.

L. Abela², K. Steindl¹, L. Simmons², D. Mathis³, M. Papuc¹, B. Oneda¹, B. Schmitt⁴, G. Wohlrab⁴, J. Kröll⁵, R. Schmid⁶, T. Iff⁷, T. Schmitt-Mechelke⁸, R. Asadollahi¹, L. Crowther², C. Bühler⁹, O. Sass³, M. Hersberger³, P. Joset¹, A. Rauch¹, B. Plecko²

Metabolic and genetic research into early onset epileptic encephalopathies

Institute of Medical Genetics, University of Zurich, Schlieren, Switzerland¹, Division of Neuropediatrics, University Children's Hospital Zurich, Zurich, Switzerland², Division of Clinical Chemistry and Biochemistry, University Children's Hospital Zurich, Zurich, Switzerland³, Division of Epilepsy and Clinical Neurophysiology, University Children's Hospital Zurich, Zurich, Switzerland⁴, Swiss Epilepsy Center, Zurich, Switzerland⁵, Division of Pediatric Neurology, Cantonal Hospital Winterthur, Winterthur, Switzerland⁶, Private Practice Neuropediatrics, Zurich, Switzerland⁷, Division of Neuropediatrics and Developmental Medicine, Cantonal Children's Hospital, Lucerne, Switzerland⁸, Division of Metabolism, University Children's Hospital, Zurich, Switzerland⁹

Introduction:

Early onset epileptic encephalopathies (EE) represent a heterogeneous group of rare disorders that constitute a major diagnostic and therapeutic challenge and the majority of patients still remain without a clear diagnosis. Recent research has unravelled a growing number of inherited inborn errors of metabolism but also sporadic de novo mutations in neuronal genes as the underlying causes of EE. Due to the rarity of the single disease entities knowledge on clinical phenotypes is very limited. We apply a combined “omics” approach to unravel the etiologic background of EE.

Methods:

Study inclusion criteria were defined as following: i) onset of epilepsy before age 4 years, ii) difficult to treat seizures for more than 6 months iii) mental retardation iv) normal microarray and normal sequencing of the SCN1A gene. Exclusion criteria constitute morphological changes involving brain cortex. From April 2013 until December 2014, we included 63 patients with early onset EE of unclear etiology. The Division of Epilepsy and Neuropediatrics at the Kinderspital Zurich cares for the majority of these patients and holds detailed long-term records of seizure semiology and ictal EEGs. Neurometabolic analysis included evaluation of biomarkers including aminoacids in plasma, alpha-amino adipic semialdehyde, pipercolic acid, vitamin compounds, a culture of lymphoblast cell line for further studies and an untargeted metabolomics analysis. Genetic analysis included high-resolution chromosomal microarray testing and whole-exome sequencing in index patients and parents by means of next generation sequencing.

Results:

Detailed clinical and pedigree analysis was collected from all patients and entered into the study database. Targeted biochemical analysis and newly established vitamin B6 profiling and AASA testing revealed normal results for the study cohort. Untargeted plasma metabolome analysis was so far performed in 36 patients and identified a novel plasma biomarker for spermine synthase deficiency. Exome analysis is ongoing and so far identified relevant mutations in known disease genes in 58%, and in novel candidate genes in 25% of patients.

Conclusion:

Identification of patients with known genetic defects will contribute to delineate the phenotypic spectrum of these rare entities. Targeted and untargeted biochemical analysis will identify treatable causes of metabolic encephalopathies and reveal novel diagnostic biomarkers. Whole exome sequencing has the potential to identify novel genes involved in early onset epileptic encephalopathies, that can be further studied on a functional level in cell cultures. Ultimately, this study will translate into a better patient care due to improvements in disease recognition and management.

-. Seidl¹, -. Leimer¹, -. Furrer¹, -. Senn¹, -. Holzmann-Bürigel¹, -. Palheiros Marques¹, -. Matt¹, S. Zinkernagel¹

USA300 methicillin resistant *Staphylococcus aureus* in Zurich, Switzerland between 2001 and 2013

Division of Infectious Disease and Hospital Epidemiology, University Hospital of Zurich¹

Introduction:

USA300 methicillin-resistant *Staphylococcus aureus* (MRSA) is the most prevalent MRSA in the United States of America (USA) and a global epidemic threat. The aim of this study was to investigate the prevalence of this highly virulent MRSA clone at the University Hospital Zurich.

Methods:

MRSA strains isolated at the University Hospital Zurich, Switzerland have been collected and PFGE typed since 1992. These strains were retrospectively compared to the PFGE pattern of the USA300 strain JE2. All isolates with a respective PFGE pattern were *spa*-typed and tested for the presence of the arginine catabolic mobile element (ACME) and Panton-Valentine Leucocidin (PVL) genes.

Results:

The first MRSA strain with a USA300 PFGE pattern was isolated in 2001 from a patient visiting from the US. It was a *spa*-type t008 and carried PVL and ACME genes. The USA300 strain has represented between 0% (in 2002) and 9.2% (in 2012) of all MRSA isolates in our hospital. Various USA300 subtypes were identified based on either the PFGE pattern, the *spa*-type or absence of either the PVL or ACME genes. All the USA300 strains including the variants ($n=47$) accounted for 5.6% of all MRSA isolates that were typed between 2001 and 2013 and reached a maximum of 14.5% in 2009. They predominantly caused skin and soft tissue infections (74.4 %).

Conclusion:

USA300 has been present in our hospital for over twelve years. In contrast to the US it has not become the predominant MRSA clone. Strict hospital hygiene measurements are key in preventing USA300 strains from spreading in Zurich and Switzerland in general.

R. Zuellig¹, T. Hornemann², A. Othman², A. Hehl³, H. Bode², T. Güntert⁴, O. Ogunshola⁴, E. Saponara⁵, K. Grabliauskaite⁵, J. Jang⁵, U. Ungethüm⁵, Y. Wei², A. Von Eckardstein², R. Graf⁵, S. Sonda⁵

Deoxysphingolipids, a novel biomarker for type 2 diabetes, are cytotoxic for insulin-producing cells.

Division of Endocrinology, Diabetes and Clinical Nutrition, University Hospital Zurich¹, Institute for Clinical Chemistry, University Hospital Zurich², Institute of Parasitology, University of Zurich³, Institute of Veterinary Physiology, University of Zurich⁴, Departement of Visceral and Transplantation Surgery, University Hospital Zurich⁵

Introduction:

Irreversible failure of pancreatic beta cells is the main culprit in the pathophysiology of diabetes mellitus, a disease that is now a major global epidemic. Recently, elevated plasma levels of deoxysphingolipids, including 1-deoxysphinganine, have been identified as novel biomarkers for the disease. In this study, we analyzed whether deoxysphingolipids directly compromise the functionality of pancreatic beta cells.

Methods:

Effects of deoxysphingolipids were investigated in insulin-producing Ins-1 cells and primary islets. Cell functionality was analyzed by biochemical methods and flow cytometry. Cytoskeletal alterations were imaged by confocal microscopy. Activation of Akt, p38MAPK, JNK, and expression of Rac1 and RhoA were determined by immunoblotting. Levels of mRNA and composition of sphingolipid species were quantified by real-time PCR and mass spectrometry, respectively.

Results:

Treatment with 1-deoxysphinganine induced dose-dependent cytotoxicity with senescent, necrotic and apoptotic characteristics and compromised glucose-stimulated insulin secretion of beta cells. In addition, 1-deoxysphinganine altered cytoskeletal dynamics, resulting in intracellular accumulation of filamentous actin and activation of the RhoGTPase Rac1. Moreover, 1-deoxysphinganine selectively up-regulated ceramide synthase 5 expression and was converted to 1-deoxy-dihydroceramides, without altering normal ceramide levels. Inhibition of intracellular 1-deoxysphinganine trafficking and ceramide synthesis improved the viability of the cells, indicating that the intracellular metabolites of 1-deoxysphinganine contribute to its cytotoxicity. Analyses of signaling pathways identified JNK and p38 MAPK as antagonistic effectors of cellular senescence.

Conclusion:

Our results revealed that 1-deoxysphinganine is a cytotoxic lipid for insulin-producing cells, suggesting that the increased levels of this sphingolipid observed in diabetic patients may contribute to the reduced functionality of pancreatic beta cells. Thus, targeting deoxy-sphingolipid synthesis may complement the currently available therapies of diabetes.

A. Maric¹, C. Lustenberger¹, E. Werth¹, J. Leemann¹, R. Huber², C. Baumann¹, R. Poryazova¹

Slow Wave Activity and Vigilance Changes after Acute Sleep Deprivation and Chronic Sleep Restriction

Department of Neurology, University Hospital Zurich, Zurich¹, Child Development Center and Pediatric Sleep Disorders Center, University Children's Hospital Zurich, Zurich²

Introduction:

Acute sleep deprivation (aSD) and chronic sleep restriction (cSR) impair vigilance. Increased slow wave activity (SWA) during sleep is a well-established marker of sleep pressure resulting from prolonged wakefulness.

We aimed at directly comparing the effects of aSD and cSR on vigilance, subjective sleepiness and SWA.

Methods:

6 male subjects underwent 40 hours of aSD and 7 nights of cSR (5h instead of 8h sleep/night). We compared the maximal change in first hour SWA (power density in the 1.25-4.5 Hz range, 128 EEG electrodes), during the recovery nights after aSD and cSR relative to a baseline night. We assessed vigilance in the afternoons before the respective nights, using the psychomotor vigilance task (PVT), i.e. speed and number of lapses (reaction times >500ms; transformed: $\sqrt{x+\sqrt{(x+1)}}$), and subjective sleepiness by the Stanford Sleepiness Scale.

Results:

The maximal SWA increase after aSD ($+102.0 \pm 30.2\%$, mean \pm SD) was significantly higher ($p < 0.01$) than after cSR ($+37.0 \pm 9.8\%$). Subjective sleepiness increased after aSD ($+1.7 \pm 1.2$; $p < 0.05$) and cSR ($+2.0 \pm 1.3$; $p < 0.05$), reaching equal levels ($p = 0.58$). In the PVT, speed was reduced to comparable values ($p = 0.95$) after aSD ($-0.6 \pm 0.4\text{s}^{-1}$; $p < 0.05$) and cSR ($-0.4 \pm 0.3\text{s}^{-1}$; $p < 0.05$). The increase in lapses was significant after aSD ($+2.2 \pm 1.6$; $p < 0.05$), but not after cSR ($+0.8 \pm 1.6$; $p = 0.29$), with a trend for more lapses after aSD ($p = 0.08$).

Conclusion:

The higher impact of aSD on SWA and lapses in vigilance are contrasted by comparable effects of aSD and cSR on psychomotor speed and subjective sleepiness. Further data analysis in this ongoing study, i.e. topographical distribution of SWA changes, inter-individual differences, or the course of cSR might lead to novel insights in the underlying mechanisms of these seemingly discrepant findings.

A. Maric¹, C. Lustenberger¹, J. Leemann¹, E. Werth¹, A. Tarnutzer¹, A. Pangalu³, R. Huber², C. Baumann¹, R. Poryazova¹

Vigilance and Cortical Excitability after Acute Sleep Deprivation and Chronic Sleep Restriction

Department of Neurology, University Hospital Zurich, Zurich¹, Child Development Center and Pediatric Sleep Disorders Center, University Children's Hospital Zurich, Zurich², Department of Neuroradiology, University Hospital Zurich, Zurich³

Introduction:

Acute sleep deprivation (aSD) impairs vigilance and increases cortical excitability. Chronic sleep restriction (cSR) results in similar vigilance impairments as observed after aSD, but the effect on cortical excitability in cSR is unknown. We therefore aimed at investigating the changes in vigilance and cortical excitability after aSD and cSR.

Methods:

8 subjects underwent 1 night of aSD and 7 nights of cSR (5h instead of 8h sleep/night). We assessed vigilance using the psychomotor vigilance task (PVT), i.e. reaction speed and number of lapses (reaction times >500ms; transformed: $\sqrt{x} + \sqrt{x+1}$). As a measure of cortical excitability we used early evoked cortical activation (ECA) in response to single-pulse transcranial magnetic stimulation (TMS), i.e. the integrated area under the rectified curve (30-80ms after TMS-pulses). We analyzed data obtained in the afternoon, when circadian modulations are expected to be smaller than during the wake-maintenance zone in the early evening.

We performed a two way repeated measures ANOVA for all parameters above with the factors *time point* (baseline vs. after sleep loss) and *intervention* (cSR vs. aSD). Post-hoc comparisons were performed where effects were significant ($p < 0.05$).

Results:

Post-hoc analysis revealed that speed decreased after aSD ($-0.5 \pm 0.1 \text{ s}^{-1}$, $p < 0.01$) and cSR ($-0.4 \pm 0.1 \text{ s}^{-1}$, $p < 0.01$), while lapses and ECA were increased after aSD (lapses: $+4.2 \pm 1.0$, $p < 0.01$; ECA: $+35.2 \pm 36.7\%$, $p < 0.05$) and cSR (lapses: $+2.1 \pm 1.0$, $p = 0.05$; ECA: $+28.5 \pm 23.3\%$, $p < 0.05$), when compared to corresponding baseline levels. There were more lapses after aSD compared to cSR ($+3.0 \pm 0.8$, $p < 0.05$).

Conclusion:

Impaired vigilance is accompanied by increased cortical excitability after aSD, as well as after cSR. This electrophysiological measure may provide the means to investigate the underlying mechanisms of vigilance and other cognitive impairments due to sleep loss which is common in our 24/7 society. Moreover, using this perturbational approach may allow to directly examining neuronal functioning in patients with altered vigilance and/or sleep pressure.

M. Dietrich¹, R. Zuellig¹, B. Hemmings², G. Spinas¹, R. Lehmann¹, O. Tschopp¹, M. Niessen¹

Specific and redundant roles of PKB α /AKT1 and PKB β /AKT2 in human pancreatic islets

Division of Endocrinology, Diabetes and Clinical Nutrition, University Hospital of Zurich, Switzerland¹, Friedrich Miescher Institute (FMI) for Biomedical Research, Basel, Switzerland²

Introduction:

Loss of PKB α or PKB β in mice results in increased or decreased glucose tolerance, respectively, whereas loss of PKB γ has no effect. The regulation of β -cell mass is normal in these mouse models. The aim of this study is to test how PKB isoforms regulate proliferation, growth, apoptosis, and insulin production in human islets.

Methods:

Human islets (7 donors) were obtained from the Juvenile Diabetes Research Fund and the European Consortium for Islet Transplantation's "Islets for Research Distribution Program". Intact or dissociated islets were cultured on extracellular matrix-coated dishes. PKB α or PKB β were overexpressed from adenoviral vectors. Proliferation and apoptosis were assessed by BrdU incorporation and TUNEL staining, respectively. Insulin secretion (GSIS) and insulin content were assessed in intact islets. Insulin was measured by ELISA. At least 50 intact islets or 2000 cells from dissociated islets in triplicate were evaluated. Data were normalised to GFP control and. Analysis of variance (ANOVA) with Bonferroni's post hoc test was used for multiple-comparisons. Results were considered to be statistically significant when P value was < 0.05 *; $P < 0.001$ **; $P < 0.001$ *** .

Results:

In intact islets, PKB α increased overall proliferation more than PKB β (3.64 ± 0.78 fold vs. 1.41 ± 0.2 ($P < 0.05$)) while only PKB α increased β -cell proliferation in dissociated islets (PKB α : 3.53 ± 0.4 fold $P < 0.05$). β -cell size increased by PKB α - (1.56 ± 0.09 fold ($P < 0.005$)) and PKB β -overexpression (1.5 ± 0.08 fold ($P < 0.005$)). Incubation with IL-1 β induced apoptosis in intact islets (2.36 ± 0.33 fold, $P < 0.05$), which could be prevented by PKB α overexpression ($P < 0.05$). IL-1 β did not induce apoptosis in dissociated islets. PKB α overexpression decreased basal apoptosis of β -cells significantly (0.47 ± 0.05 fold, $P < 0.001$). Furthermore, PKB α overexpression increased the percentage of insulin-positive cells ($+10.4\% \pm 2.4\%$ ($P < 0.01$)), whereas the insulin content or GSIS were not affected after overexpression of PKB α and PKB β .

Conclusion:

The present data suggest that PKB α may be more potent than PKB β in regulating human islet mass, as it protects β -cells from apoptosis and increases the percentage of β -cells to non- β -cells. The potency of IL-1 β to induce β -cell apoptosis is likely to depend on cellular interactions in intact islets.

D. Perisa¹, A. Kaech², L. Rohrer¹, A. Von Eckardstein¹

The Adventures of High Density Lipoproteins In Endothelial Cells

Institute for Clinical Chemistry, University Hospital Zürich, CH-8952 Schlieren, Switzerland¹, Center for Microscopy and Image Analysis, University of Zürich, CH-8057 Zürich, Switzerland²

Introduction:

Atherosclerosis results from a progressive accumulation of lipids in the arterial intima leading to plaque formation. Epidemiological studies show an inverse association of high density lipoprotein (HDL) cholesterol with cardiovascular events. HDL and its main apolipoprotein A-I (ApoA-I) have multiple anti-atherogenic functions. Some of them are exerted within the vessel wall, notably the classical function of HDL, namely the mediation of cholesterol efflux from macrophage foam cells. To get access to the intima and the lipid-laden macrophages, HDL has to pass the endothelial barrier.

Methods:

To elucidate the itinerary of ApoA-I and HDL through endothelial cells (ECs), we investigated the cellular localization of ApoA-I and HDL, which was labelled either fluorescently, or with 1.4 nm Nanogold by using fluorescent microscopy and electron microscopy (EM), respectively. For EM, we used high pressure freezing to avoid artefacts and lipid extraction. Nanogold was detected by silver enhancement after fixation in OsO₄.

Results:

HDL as well as ApoA-I are taken up by ECs, and ApoA-I and HDL co-localize indicating the same route of trafficking. We compared the trafficking of ApoA-I and HDL with Transferrin and Albumin, which were used as tracers for clathrin- and caveolin-mediated endocytosis, respectively. Both pathways showed partial colocalization indicating a non-classical pathway for HDL trafficking.

Further experiments showed that HDL is targeted neither to lysosomes nor to the Golgi nor to the endoplasmic reticulum. Only a small amount can be detected in early endosomes (Rab5) and endosome to trans-golgi network (Rab9), but not at all with late endosomes (Rab7), the recycling endosomes (Rab11a) or vesicles involved in trans-Golgi network sorting (Syntaxin6). EM ultrastructure showed HDL to be located mainly in multivesicular bodies.

We performed pharmacological inhibitions and found that HDL uptake is cytoskeleton dependent but only weakly affected by blocking the fluid phase uptake with Amiloride or EIPA. Neither did we observe any colocalization of HDL with dextran as the marker of fluid phase uptake.

HDL was found to stimulate its own uptake into ECs. We identified several HDL and/or ApoA-I induced changes in the phosphorylation of signaling molecules, which however still remain to be linked to HDL endocytosis.

Conclusion:

In conclusion HDL transport into and through ECs seems to follow a non-classical trafficking route. It appears to be regulated by positive rather than negative feedback.

REGULATION OF THE ACTIVITY OF MAMMALIAN SERINE PALMITOYLTRANSFERASE

Department for Molecular Biomedical Research, VIB, Ghent, Belgium¹, Institute of Clinical Chemistry, University Hospital Zürich²

Introduction:

Serine Palmitoyltransferase (SPT) typically catalyzes the condensation of palmitoyl-CoA and L-serine, the first step in *de novo* sphingolipid synthesis. Several missense mutations in SPT are associated with hereditary sensory and autonomic neuropathy type 1 – HSAN1. HSAN1 is an autosomal dominant peripheral neuropathy, characterized by a loss of sensation mainly in distal limbs. Mutations in SPT subunits lead to a shift in the substrate preference of SPT from L-serine to L-alanine which results in the production of atypical 1-deoxy-sphingolipids (dSLs). Due to the lacking C1-hydroxyl-group dSLs cannot be degraded by the canonical catabolic pathway.

Studies in yeast demonstrated that SPT activity is tightly regulated by a metabolic feedback loop, mediated by Orm1 and Orm2 proteins. At high cellular sphingolipid levels Orm proteins bind to SPT and inhibit its activity. Low sphingolipid levels, in contrast, lead to phosphorylation of Orm proteins, which results in their dissociation from SPT and activation of the enzyme. However, the role of ORM proteins in regulating SPT activity in mammalian cells is not yet understood. In contrast to yeast, mammalian cells express three Orm isoforms (ORMDL1-3) and phosphorylation sites found in yeast are not conserved in the mammalian orthologs. We were therefore interested to see if a similar metabolic feedback inhibition also exists in mammalian cells.

Methods:

SPT activity was measured by incorporation of isotope-labeled substrates (deuterated ¹⁵N,³H L-Serine and ²D L-Alanine). To examine the regulatory effect of exogenously provided sphingolipids from the growth medium, cells were cultured in the presence of fetal bovine serum (FBS) and delipidated FBS. The cells were incubated for 24h, after which collected and followed by with liquid/liquid extraction were analyzed using liquid chromatography–mass spectrometry (LC-MS). The SPT activity was measured by quantifying the production of *de novo* sphinganine and sphingosine after hydrolysis of total sphingolipids, which were detected on the MS by a shift in mass over charge *m/z* of (+3 Da).

Results:

SPT activity did not change in HEK293 cells overexpressing ORMDL1-3 compared to empty control cells. A similar experiment was performed using MEFs in which ORMDL3 expression was abolished. In the KO cells *de novo* synthesis was not increased compared to wild type.

Increasing amounts of the membrane permeable C6-Ceramide (C6Cer), sphingomyelin and the free sphingoid bases – sphinganine and sphingosine were added to HEK293 cells to increase intracellular levels of sphingolipids. As a result, SPT activity decreased the most upon addition of C6Cer. An inverse correlation between the amount of the *de novo* formed sphingolipids and increasing levels of C6Cer was observed. This indicates that increasing levels of C6Cer inhibit SPT activity.

Different HSAN1-causing-mutations in SPT affect differently SPT activity. While mutation in SPTLC1 C133W does not affect SPT activity, S331F results in a several-folds increase in SPT activity. HEK293 cells that are overexpressing SPTLC1, C133W and S331F were treated with increasing amounts of C6Cer. Inhibition pattern was similar to control cells for HEK293 cells overexpressing SPTLC1 and C133W – upon increasing levels of C6cer added, *de novo* production of sphingolipids decreased. But this was not the case for S331F overexpressing cells.

Conclusion:

These results indicate that the role of the individual ORMDL isoforms in regulating SPT activity might be redundant and possibly depends on the cellular or metabolic context. Increasing levels of C6Cer seems to inhibit SPT activity, which indicates that mammalian system is similar to yeast. HEK SPTLC1 p.S331F mutation is possibly deregulated as it escaped the inhibition by resisting to C6Cer addition.

Z. Mahdi¹, B. Stieger¹

In vitro interaction of drugs with canalicular lipid transporters

Clinical Pharmacology and Toxicology, University Hospital Zürich¹

Introduction:

Canalicular bile formation is maintained by the simultaneous activities of three ABC-transporters: BSEP (Bile Salt Export Pump or ABCB11), ABCB4 (or MDR3) and ABCG5/G8. Dysfunctions in the biliary cholesterol–bile salt–phospholipid secretion (e.g. an increased ratio of cholesterol to bile salts or phospholipids) lead to cholestasis or result in crystallization of cholesterol followed by cholelithiasis. The aim of this project is the development of a cell-based and polarized model system to test the hypothesis that some drugs may induce cholestatic liver disease by specifically interfering with biliary lipid secretion and to identify such inhibitors/stimulators.

Methods:

Stably transfected LLC-PK1 cell lines (overexpressing human NTCP, BSEP, ABCB4 and ABCG5/G8) are cultured on Transwell® plates. In the Transwell® system cells grown on the filter are polarized, i.e. the basolateral membrane faces the lower compartment and the apical membrane faces the upper compartment. Detection and polar localisation of the transport proteins was accomplished by immunohistochemistry and Western blots. Functionality of the transporters was verified using radioactively (e.g. ³H-taurocholate and ¹⁴C-cholesterol) or fluorescently (NBD-phosphatidylcholine) labelled substrates. The substrates were added to the basolateral or apical compartments and the transported amounts were measured in the opposite compartment. Albumin was used as an acceptor to stimulate efflux. Lipid secretion was also chemically analysed by thin-layer-chromatography.

Results:

Western blots and immunohistochemistry indicate that LLC-PK1 cells (BNMG cell line) overexpress all three ABC transporters and that NTCP is overexpressed in the basolateral membrane while BSEP, ABCB4 and ABCG5/G8 are overexpressed in the apical membrane, as is the case in human hepatocytes.

Functional transport assays using radioactively or fluorescent labelled substrates demonstrate that the model cell line displays a vectorial transport of bile salt (³H-taurocholate) and phosphatidylcholine (NBD-PC), from the basolateral to the apical compartment.

Currently, we are at the stage of testing the effect of candidate drugs on lipid secretion by applying the generated model. Our experiments show that the antimycotic agent itraconazole inhibits phosphatidylcholine secretion into the apical compartment as previously reported by another group.

Conclusion:

We have successfully established an *in vitro* model for canalicular bile salt and lipid secretion. A chemical-based and a fluorescence-based lipid efflux assay were established. The fluorescence-based assay is faster and has a good reproducibility. The chemical-based assay which has the advantage of allowing the measurement the endogenous lipids still needs additional refinements of the lipid acceptor used, e.g. by using lipid-depleted albumin to reduce the background and increase the reproducibility of the measurements.

We will use this model to characterize the effect of drugs suspected to interfere with canalicular bile salts and lipid transporters. This knowledge will help us to better understand the relation between drugs and cholestasis and may help to identify potential therapeutic agents for gallstone disease.

N. Naenni¹, D. Schneider¹, C. Hämmerle¹, R. Jung¹, J. Hüsler¹, D. Thoma¹

Randomized controlled clinical study evaluating two membranes for guided bone regeneration

Center of Dental Medicine, Clinic of Fixed and Removable Prosthodontics and Dental Material Science, Zürich¹

Introduction:

To test whether there are differences regarding peri-implant guided bone regeneration in terms of clinical and radiological outcomes between two membranes.

Methods:

In 27 patients, 27 implants were placed in single-tooth gaps in the anterior area of both maxilla and mandible. All implants had a buccal dehiscence defect of at least 3mm. These defects were augmented using demineralized bovine bone mineral and randomly covered with either a resorbable membrane (RES, n=12) or a titanium-reinforced non-resorbable membrane (N-RES, n=15). The horizontal thickness (buccally) of the augmented area was assessed (baseline). Following primary wound closure, a cone-beam computed tomography (CBCT) was taken. At 6 months, a second CBCT was performed, a full thickness flap elevated, and the horizontal thickness re-measured. Linear measurements were performed on CBCTs assessing the augmented area.

Results:

At baseline, the clinical horizontal thickness at implant shoulder was 3.38mm mean (SD=0.51; RES) and 2.85mm mean (0.63; N-RES). At 6 months, these values amounted to 1.95mm (0.88; RES) and 2.85mm (1.16; N-RES) and the changes were statistically significant ($p < 0.001$ Kenward-Roger). High resolution CBCT analyses revealed a decrease from baseline to 6 months at the implant shoulder of a median -0.72mm (mean -0.83 SD 0.82 RES) and a median of -0.07mm (mean -0.15 SD 0.37 N-RES). These changes were statistically significant between the groups ($p = 0.009$ Wilcoxon).

Conclusion:

Both treatment modalities were clinically and radiologically effective in regenerating bone on the buccal side of dental implants but changes over time and differences between the groups were statistically significant.

M. Schmid¹, J. Marti-Jaun¹, M. Bühler¹, M. Herová¹, M. Hersberger¹

Polymorphisms in SOCS 1 and 3 and Human Coronary Artery Disease

Division of Clinical Chemistry and Biochemistry and Children's Research Center, University Children's Hospital Zurich, Zurich¹

Introduction:

Atherosclerosis is a multifactorial disease that is characterized by chronic inflammation at every stage, from initiation to progression, and eventually plaque rupture. Suppressors of cytokine signaling (SOCS) are a family of intracellular proteins playing a role in the physiological regulation of hormone and cytokine-mediated homeostasis. The SOCS proteins prevent excessive immune activation by negatively regulating the Jak/STAT pathways. We hypothesized that polymorphisms in SOCS 1 and 3 may differently affect the negative feedback loop and hence influence the degree of immune activation and the course of coronary artery disease (CAD).

Methods:

We therefore screened the SOCS1 and the SOCS3 genes for polymorphisms and investigated the association of 7 polymorphisms each with angiographically documented CAD in a case control study (n=496).

Results:

None of the polymorphisms was significantly associated with CAD but rs33977706 in SOCS1 and rs7207782 in SOCS3 showed borderline associations with CAD using an additive genetic model. In addition, rs33977706 in SOCS1 was associated with hsCRP levels in controls.

Conclusion:

Taken together, our data argue that rs33977706 in SOCS1 and eventually rs7207782 in SOCS3 may be associated with plasma inflammation markers and with CAD.

I. Jelcic¹, I. Jelcic¹, C. Kempf², F. Largey¹, R. Planas¹, S. Schippling¹, H. Budka², M. Sospedra¹, R. Martin¹

Brain-infiltrating JC virus-specific CD8⁺ effector T cells counteract CD4⁺ T cell immune escape of neurotropic JC virus variant

Neuroimmunology and Multiple Sclerosis Research Section, Department of Neurology, University Hospital Zurich, 8032 Zurich¹, Institute of Neuropathology, University Hospital Zurich, 8091 Zurich²

Introduction:

Infections of the central nervous system with JC virus (JCV) can cause cytolytic destruction of oligodendrocytes or granule cell neurons resulting in demyelination or cerebellar atrophy, respectively. The knowledge about components of the immune system that are involved in resolution of JCV-infected granule cell neurons is still scarce. We had the unique opportunity to study the prominent T cell infiltrate from a cerebellar biopsy of a case of natalizumab-associated granule cell neuronopathy (GCN).

Methods:

Isolation and expansion of cerebellum-infiltrating T cells during immune reconstitution allowed us to perform for the first time detailed analyses including the dissection of the antigen specificity, T cell receptor repertoire and functional phenotypes of brain-infiltrating JCV-specific T cells. Additional sequential cerebrospinal fluid samples were used to analyze immune responses and viral titers during evolution from GCN to GCN-IRIS.

Results:

JCV viral load dropped only slowly despite immune reconstitution. Detailed analyses of cerebellum-infiltrating T cells revealed impaired CD4⁺ T cell responses against the identified JCV variant, caused by viral mutations in the JCV major capsid protein VP1. This immune escape of the JCV variant appears to be compensated by massive clonal expansion of polyfunctional CD4-expressing CD8⁺ effector T cells with exquisite specificity for conserved regions of JCV large T antigen.

Conclusion:

Our findings highlight the importance of both CD4⁺ and CD8⁺ T cell subsets for combating JCV efficiently and provide novel insights about virus-host interactions during neuronal infection with a JCV variant, including the modulation of CD4⁺ T cell responses by mutations in the viral capsid protein VP1 and the multiple effector functions of JCV-specific CD8⁺ T cells for combating JCV-infected neurons.

I. Alecu¹, A. Othman¹, A. Von Eckardstein¹, T. Hornemann¹

Elucidating Novel Metabolic Pathways of the Neurotoxic 1-Deoxysphingolipids

Institute for Clinical Chemistry, University Hospital Zürich, 8091 Zürich, Switzerland¹

Introduction:

Sphingolipids (SLs) are a highly diverse class of lipids with important roles in plasma membrane biology and as lipid-signaling molecules. Serine palmitoyltransferase (SPT) catalyzes the first step in the *de novo* synthesis of SLs, normally forming sphinganine (SA) from the condensation of serine and palmitoyl-CoA, which is further downstream converted to sphingosine (SO). Under certain conditions SPT can also use alanine, which then forms a class of atypical 1-deoxysphingolipids (1-deoxySLs). Due to the missing C1 hydroxyl group, 1-deoxySLs are not metabolized to complex SLs nor degraded by the canonical pathways.

Pathologically elevated 1-deoxySLs are a hallmark of the inherited neuropathy HSAN1 (hereditary sensory and autonomic neuropathy 1), which is caused by several missense mutations in SPT. Clinically, there is a high level of similarity between HSAN1 and diabetic sensory polyneuropathy (DSN). We showed recently that 1-deoxySL levels are also significantly increased in the plasma of patients with type 2 diabetes mellitus (T2DM), which indicates that they may also be involved in the pathology of DSN. Little is known about the metabolism of 1-deoxySLs. In this project we aim to investigate the metabolism of 1-deoxySLs in order to help elucidate the underlying pathomechanism in neuropathies such as HSAN1 and DSN.

Methods:

We performed pulse chase experiments in which cells were incubated with deuterium-labeled 1-deoxySA for 2 hours, after which they were chased for 0, 1, 4, 8, 24, and 48 hours in unsupplemented growth medium. Samples were then acid/base hydrolyzed and analyzed by LC-MS. We used high resolution accurate mass spectrometry and metabolic profiling workflows using XCMS and Sieve to identify unknown 1-deoxySL-metabolites.

Results:

The levels of labeled 1-deoxySA decreased over time to approximately 25% of the starting concentration at 48 hours. This decrease in the 1-deoxySA was not compensated for by the increase in the downstream 1-deoxySL metabolites, and none of these metabolites were recovered in the medium. This indicates that the 1-deoxySA is being converted to yet unknown downstream metabolites. By comparing all of the metabolites and their amounts at time point 0 and 48 hours using Sieve metabolic profiling software, we were able to identify 3 novel 1-deoxySL metabolites coming from the deuterium-labeled 1-deoxySA. Two of these metabolites have an extra hydroxyl group added, however not at the C1 position as in the canonical sphingolipids. Upon blocking conversion of 1-deoxySA to 1-deoxySO using Fumonisin B1, we found that the levels of all 3 new metabolites greatly decreased. Therefore these 3 metabolites are formed downstream of 1-deoxySO, which is currently the last known product in the 1-deoxySL metabolic pathway. Furthermore, the formation of these new downstream 1-deoxySL metabolites appears to be cell type specific, as these lipids could not be found when performing the same experiments in HEK and HepG2 cells, although the total 1-deoxySL levels still decreased with time.

Conclusion:

1-DeoxySLs are not in fact dead-end metabolites, as is the current assumption. They disappear with time when they are externally added, perhaps being degraded via a pathway involving hydroxylation at a different position on the carbon chain than C1. Different cell types appear to have different pathways/enzymes for metabolizing 1-deoxySLs, providing a clue that the varying degrees of toxicity seen in different cell types, such as neuronal cells, could arise from the disturbance or complete absence of the metabolic pathway downstream of 1-deoxySO. In the future it would be important to analyze these new metabolites in HSAN1 and DSN patients in order to try to elucidate the pathomechanism in these conditions.

L. Rigassi¹, F. Federica¹, B. Imthurn¹, R. Dubey¹

Role of microRNA-221 in mediating the protective action of Estradiol in vascular cells

Clinic for Reproductive Endocrinology , Department of Obstetrics and Gynecology, University Hospital Zürich, Zürich¹

Introduction:

Recent studies provide evidence that microRNAs (miRNAs) are involved in many clinically relevant biological and pathophysiological processes. They regulate cell differentiation, proliferation, migration and apoptosis in many cell types, including the cardiovascular system. Vascular remodeling associated with cardiovascular disease involves endothelial cell (EC) damage/dysfunction and abnormal growth of smooth muscle cells (SMCs). Several miRNAs, including microRNA-221 (miR-221), are known to influence both EC function and SMC growth. Estrogens are known to protect women against vasocclusive disorders by promoting endothelial repair/recovery and inhibiting SMC growth. Thus, it is feasible that processes associated with vasoprotection and vascular repair are mediated by miRNA modulation. Hence, we hypothesize that the vasoprotective actions of estradiol (E2) may in part be mediated via modulation of miRNAs. In the present study we investigated the role of miR-221 in mediating the protective action of E2 in vascular cells.

Methods:

To investigate the miR-221 expression, human coronary artery SMCs (HCASMCs) and human umbilical vein ECs (HUVECs) were treated with or without E2 (10nM-1uM) prior to small RNA extraction and RT-qPCR. Both cell types were then transfected with miR-221 mimics or antimirs, to assess the miR-221 role using different functional assays. Cell counts and a BrdU ELISA kit were employed to study the proliferation of HCASMCs. Matrigel microvessel formation and scratch assay were used to investigate the cell function of HUVECs. Western Blotting was performed to inspect protein expression.

Results:

Treatment of HUVECs with miR-221 mimic inhibited capillary formation and wound closure. Moreover, the expression of miR-221 was negatively regulated by E2 in HUVECs. This observation was further supported by the observation that downregulation of miR-221 by the antimir mimicked the protective effects of E2 by promoting the microvessel formation and the wound closure (scratch assay). In contrast, the overexpression of miR-221 by the mimic inhibited these processes. In HCASMCs, E2 decreased the PDGF-induced miR-221 levels in a concentration dependent manner. Similar to PDGF, the miR-221 mimic increased the cell number and the BrdU incorporation, as well as the expression of CyclinD1 protein. Surprisingly, the downregulation of miR-221 by the antimir did not significantly reduce the cell number. However, it inhibited the DNA synthesis and reduced CyclinD1 protein level, similar to the effects of E2 in these cells. Additionally, the inhibition of HCASMC proliferation and the induction of HUVEC function by E2 were reversed in the presence of the miR-221 mimic. These findings may indicate an important role for miR-221 in mediating the protective actions of E2 on the cardiovascular system.

Conclusion:

Here, we demonstrate a differential role of miR-221 in regulating growth of endothelial and smooth muscle cells. Overexpression of miR-221 increased SMC proliferation and impaired EC-induced capillary formation and wound healing. We further show that E2 negatively modulates miR-221 expression in HCASMCs and HUVECs and that miR-221 downregulation by the antimir mimics the effects of E2. Interestingly, the miR-221 mimic was able to reverse the E2 effects in both cell types, suggesting that miR-221 modulation may represent a novel mechanism by which E2 mediates its protective actions on the cardiovascular system.

L. Kurmann¹, L. Rigassi¹, F. Barchiesi¹, B. Imthurn¹, R. Dubey¹

Estradiol regulates miR-221 expression via both ER-dependent and ER-independent mechanisms.

Clinic for Reproductive Endocrinology, Department of Obstetrics and Gynecology, University Hospital of Zurich, Zurich¹

Introduction:

Several studies have shown a protective effect of estrogen regarding cardiovascular diseases. An important action of estrogen within the vessel wall is its growth-inhibitory effect on vascular smooth muscle cells (VSMCs). Indeed, excessive growth of VSMC is a crucial step in the pathogenesis of atherosclerosis and other cardiovascular diseases. Preliminary results from our lab provide evidence that estradiol modulates the expression of different miRNAs, some of which play an important role in regulating VSMC growth. For example, miR-221 is up-regulated in VSMCs upon stimulation with PDGF, a potent mitogen in the vasculature. Estradiol (E2) has been shown to inhibit PDGF-induced expression of miR-221. We hypothesize that the protective action of E2 on the vasculature is, in part, mediated via regulation of growth-promoting miRNAs, as for example miR-221. Whether these effects of estradiol are Estrogen Receptor (ER)-dependent or -independent is currently unknown. Using ER-agonists and -antagonists, we have assessed the role of the three different ERs (ER- α , ER- β and GPER) in regulating miR-221 expression. Moreover, using the estradiol metabolite 2-methoxyestradiol (2-ME) with no affinity for ER, we assessed the ER-independent regulation of miR-221 production.

Methods:

Isolated female HCASMCs were pretreated with different ER-agonists and -antagonists (100 nM / 500 nM) as well as 2-ME (1-3 μ M) 4h prior to PDGF treatment (20 ng/ml). The change in miRNA-expression was measured by RT-PCR 30h after treatment of the cells. Protein levels were analyzed on whole-cell lysates by Western Blot (48h after treatment of the cells). Growth studies were performed by Cell Count 6-8 days after treatment.

Results:

Treatment of VSMCs with PDGF induced miR-221 expression, whereas E2 down-regulated the PDGF-induced expression of miR-221. Mitogen-induced VSMC growth was significantly reduced by E2, its ER-agonists and 2-ME. The ER- α -agonist PPT mimicked the inhibitory effect of estradiol on PDGF-induced expression of miR-221 in VSMCs, whereas the ER- β - and GPER-agonists DPN and G-1, respectively, had no effect. This indicates that the effect of E2 on the PDGF-induced expression of miR-221 is mediated via ER- α and not via ER- β or GPER. This is supported by the finding that MPP, a specific ER- α -antagonist, reversed the inhibitory effects of E2 and PPT on miR-221 expression. Interestingly, PDGF-induced production of miR-221 was also attenuated by the estrogen-metabolite 2-ME, suggesting that ER-independent mechanisms may also be active.

Conclusion:

We demonstrate that E2 down-regulates PDGF-induced expression of growth promoting miR-221 in VSMCs via ER- α , but not ER- β or GPER. Moreover, the effects of E2 on miR-221 are mimicked by 2-ME, suggesting ER-independent regulation of miR-221. Down-regulation of miR-221 by ER- α but not ER- β and GPER mediates the growth inhibitory effects of E2 in VSMCs. Further studies are required to assess the molecular mechanisms mediating the differential effects of ERs on miR-221 expression.

S. Bender¹, A. Sharma¹, O. Riesterer¹, A. Broggin-Tenzer¹, M. Pruschy¹

Identification of ADAM17 as a Novel Target for Radiosensitization of Non–Small Cell Lung Cancer

Department of Radiation Oncology, University Hospital Zurich, Switzerland¹

Introduction:

The therapeutic response of ionizing radiation (IR) is imparted by genomic instability and DNA damage. However, IR also triggers multiple intracellular signaling processes as part of IR-induced stress responses that lead to the secretion of various para- and autocrine factors into the tumor microenvironment. Here we investigated treatment-dependent secretion of auto- or paracrine factors, which drive acquired rescue mechanisms and determine the overall radiation sensitivity of the tumor.

Methods:

Exhaustive large scale secretome analysis was performed using antibody arrays for a wide range of secretory factors. Secretion kinetics of selected factors were determined using ELISA across different established tumor cells and in murine blood serum, derived from irradiated tumor xenograft-carrying mice. Clonogenic survival and xenograft tumor growth delay assays were performed in response to IR in siRNA-targeted tumor cell lines or in combination with small molecular agents.

Results:

We performed an exhaustive IR-dependent secretome analysis (>300 factors) in lung carcinoma cells and investigated IR-induced expression and tumor cell secretion of the top hits, including amphiregulin, transforming growth factor- α and ALCAM. All these factors were secreted in a similar IR-induced time- and dose-dependent way from several non–small cell lung cancer (NSCLC) cell lines, indicative of a common upstream mechanism. No changes were observed at the transcriptional level implying potential modulation at the posttranslational level. Interestingly, irradiation induced a dose-dependent increase in cleavage of the proform of ADAM17 (A Disintegrin and metalloprotease domain 17), which resulted in enhanced ADAM17 activity and correlated with subsequent substrate shedding. IR-induced ADAM17 activation required both p38 mitogen-activated protein kinases (MAPKs) and Furins. siRNA mediated silencing of ADAM17 or targeting of ADAM17 with the small molecular inhibitor TMI-005 suppressed IR-induced shedding of these factors, down regulated ErbB-signaling in target cells, induced senescence and enhanced IR-induced cytotoxicity *in vitro* and *in vivo*. *Ex vivo* substrate analysis of murine blood serum derived from irradiated tumor xenograft-carrying mice correlate with our *in vitro* results.

Conclusion:

Our findings demonstrate that IR significantly activates ADAM17, which results in shedding of multiple survival factors, growth factor pathway activation and contributes to treatment resistance in NSCLC cells. We provide a sound rationale for positioning ADAM17 inhibitors as radiosensitizers to improve the treatment of NSCLC.

A. Broggin-Tenzer¹, F. Bachmann², V. Vuong¹, A. Messikommer¹, K. Nytko-Karouzakis¹, T. O'Reilly², H. Lane², M. Pruschy¹

The novel microtubule-destabilizing drug BAL101553 (prodrug of BAL27862) sensitizes a treatment refractory tumor model to ionizing radiation

Department of Radiation Oncology, University Hospital Zurich¹, Basilea Pharmaceutica International Ltd²

Introduction:

Microtubule-targeting agents (MTAs) are widely used for cancer treatment, both alone and in combination. BAL27862 is a novel microtubule-destabilizing drug with a dual action against human tumors; targeting tumor cells refractory to standard MTAs as well as tumor blood supply. The water soluble prodrug BAL101553 has completed Phase I clinical evaluation administered i.v. but is also orally bioavailable. We have investigated the effect of ionizing radiation (IR) in combination with BAL27862 in vitro in human cancer lines resistant to standard MTAs, and with BAL101553 in a genetically defined paclitaxel-, epothilone- and IR-refractory xenograft model. Different routes of BAL101553 administration were compared.

Methods:

Alamar blue/crystal violet proliferation, clonogenic survival and apoptotic death assays were performed in human lung carcinoma A459, b-tubulin-mutated A549EpoB40 and Pgp-overexpressing colon carcinoma SW480 cells. Antitumor response was determined in SW480- and A549EpoB40-derived tumor xenografts with BAL101553 administered i.v. (21.3mg/kg/wk) or p.o. (15mg/kg QDx5 or 38mg/kg/wk) and IR fractionated over a week (3x5Gy).

Results:

BAL27862 reduced the proliferation/survival of wild type A549 cells, paclitaxel/epothilone-resistant A549EpoB40 cells and paclitaxel-resistant SW480 cells with similar potency (anti-proliferative IC50s: 28nM, 22nM & 9nM, resp). BAL27862 combined with IR resulted in additive cytotoxicity with no apoptosis induction. In SW480 xenografts, BAL101553 exhibited antitumor activity when administered i.v or p.o., with daily and weekly oral administration eliciting equivalent antitumor responses (final $\Delta\%T/C$: 36 & 41, resp). Equipotent single i.v. bolus and daily p.o. BAL101553 regimens were identified which partially inhibited tumor growth ($\%T/C$: 66 & 52, resp) in microtubule stabilizing agent-resistant A549EpoB40 tumor xenografts, as did IR ($\%T/C$: 35). Interestingly, both BAL101553 regimens induced a profound antitumor effect when combined with IR, associated with almost complete tumor stabilization ($\%T/C$: 4 & 7, resp) over 5 weeks. Based on the in vitro data, involvement of tumor microenvironment in antitumor response to this combination is likely.

Conclusion:

BAL101553 single bolus (i.v.) or daily (p.o.) treatment regimens positively interact with IR in a human cancer model refractory to clinically relevant MTAs and IR, demonstrating the potential of this combination therapy for the treatment of cancer patients.

J. Kresoja-Rakic¹, G. Ziltener¹, L. Pecze², B. Schwaller², W. Weder³, R. Stahel¹, E. Felley-Bosco¹

MECHANISMS REGULATING CALRETININ EXPRESSION IN MALIGNANT PLEURAL MESOTHELIOMA

Universitätsspital Zürich Oncology Unit¹, Department of Medicine, University of Fribourg, Fribourg², Thoracic Surgery, University Hospital Zürich³

Introduction:

Calretinin (CR, CalB2) is a calcium binding protein used as a diagnostic and prognostic marker in malignant pleural mesothelioma (MPM). Currently nothing is known on its regulation in MPM cells. Our aim was to investigate the regulation of CR expression in MPM.

Methods:

CR levels were characterized in different MPM cell lines by WB and q-PCR. Several genomic sequences surrounding +1 (800 bp upstream and 58 bp downstream of the CR gene (*CALB2*) transcription start site (TSS)) were cloned into the pGL3-B reporter vector. Having defined the minimum sequence to drive CR expression, consensus sequences of potential functional transcription factors (TF) were identified and mutated. Methylation status of CalB2 promoter was also analyzed in TCGA database. In addition, the effect of modulating intracellular Ca²⁺ levels with ionomycin on the promoter activity, as well as on ERK and CREB activation were investigated. Intracellular Ca²⁺ levels were monitored with the recombinant fluorescent Ca²⁺ indicator GCaMP3.

Results:

CR mRNA levels were found to be highly correlated with protein expression levels in MPM cell lines. The sequence of 160 bp upstream of the TSS was sufficient to drive CR expression. By mutating consensus sequences of the predicted TF, we observed that E2F and NRF-1 binding to the *CALB2* promoter might be essential. This is in line with the observation that CR expression changed during cell cycle. Treatment with the hypomethylating agent 5-Aza-CdR did not change CR expression and analysis of TCGA database, confirmed that *CALB2* promoter is not hypermethylated in tumors compared with non-tumoral tissue. *CALB2* promoter activity was up-regulated upon ionomycin treatment. The selected ionomycin concentration evoked a transient Ca²⁺ signal that reflected the depletion of ER stores; ionomycin also increased CR expression and was associated with increased activation of ERK and CREB.

Conclusion:

CR expression in MPM appears to be mainly regulated at the transcriptional level and it is affected by cell cycle and changes in intracellular Ca²⁺ concentration.

M. Bombardo Ayats¹, E. Saponara¹, T. Reding Graf¹, R. Graf¹, S. Sonda¹

Epigenetic acetylation mechanisms are activated during progenitor cell-based regeneration in the adult pancreas.

Swiss HPB Center, Visceral & Transplantation Surgery. University Hospital Zurich.¹

Introduction:

Regeneration of pancreatic acinar cells is critical for the recovery of the injured organ following pancreatitis. This regenerative process involves an initial de-differentiation of acinar cells to a progenitor-like state followed by cell division and re-differentiation. This study investigates whether epigenetic mechanisms regulated by the activity of histone deacetylases (HDACs) drive the change in gene expression observed during pancreatic regeneration.

Methods:

Pancreatitis was induced by serial cerulein injections in wild type C57BL/6 mice. *In vivo*, analyses of acetylation levels, HDAC expression and activity, as well as the regenerative potential of pancreatic acinar cells were evaluated over a period of one week. *In vitro*, HDAC-dependent regulation of gene expression was investigated in AR42J cells during differentiation into mature secretory acinar cells.

Results:

Pancreatic regeneration following pancreatitis was characterized by a time-dependent increase of nuclear HDAC activity and up-regulation of selected members of class I HDACs. Increased HDAC activity correlated with decreased acetylation of nuclear proteins. The timing of these acetylation changes paralleled the up-regulation of progenitor markers and preceded cell proliferation. *In vitro* differentiation of AR42J cells revealed modulation of HDAC activity and nuclear acetylation levels. Pharmacological inhibition of class I HDACs reverted the expression of genes regulated during differentiation.

Conclusion:

Our *in vivo* and *in vitro* results suggest that epigenetic acetylation regulates the changes in gene expression observed during pancreatic regeneration and acinar cell differentiation. Current investigations using pharmacological inhibitors and genetic approaches aim to elucidate the role of selected HDACs *in vivo* and their potential to modulate pancreatic regeneration.

C. Corró¹, C. Razafinjato¹, A. Von Teichman¹, S. Dettwiler¹, V. Voung¹, P. Schraml¹, H. Moch¹, M. Rechsteiner¹

Cancer Stem Cells and Tumor Heterogeneity in Renal Cancer

Institute of Surgical Pathology, University Hospital Zürich 8091 Zürich, Switzerland¹

Introduction:

Clear cell renal cell carcinoma (ccRCC), the most common type of renal cancer, is characterized by asymptomatic manifestation in early stage and a poor response to radiotherapy and chemotherapy in metastatic stage. Recent research and publications showed that ccRCC is a very heterogeneous tumor with multiple key driver mutations, i.e. *VHL*, *PBRM1*, *BAP1*, and *SETD2*. However, which tumor subpopulation and driver mutation regulates tumor spreading and initiation of metastasis remains unresolved. Additionally, evidence for a stem cell like ccRCC subpopulation opened the question about the role and the mutational landscape of these selfrenewing and chemotherapy resistant cell type.

Methods:

To elucidate tumor heterogeneity in RCC, primary ccRCC cell lines were established for studying the mutational profile, the expression pattern on RNA and protein level in relation to proliferation, migration and invasion characteristics in *in vitro* and *in vivo* models. Furthermore, to investigate and further characterize genotype and phenotype of the cancer stem cell fraction, a sphere assay was set up.

Results:

Seventeen RCC cell lines were studied in terms of their mutational genetic profile by next generation sequencing. Multiple combinations of key driver mutations in *VHL*, *PBRM1*, *BAP1*, and *SETD2* genes were identified. As expected, mutations in *PBRM1* and *BAP1* were mutually exclusive whereas mutations in *PBRM1* and *SETD2* were appearing together as well as individually. Furthermore, the protein expression of *PBRM1* and *BAP1* was assessed by immunohistochemistry and western blot and was found correlating to the mutational status of the corresponding genes. To establish the sphere assay, four RCC cell lines were tested for different conditions: seeding cell number, medium recipe and low attachment plates. So far, only the A-498 cell line showed sphere formation capability. Invasion and migration properties for these cell lines were investigated as well. The 786-O cell line showed increased migration and invasion properties compared to the A-498 and RCC4 *VHL* cell line. Moreover, RCC4 wt did not respond at FBS as attracting factor but fibronectin. These cell lines will serve as model systems for *in vitro* and *in vivo* experiments next to the established primary cell lines. So far, eight RCC primary cell lines were established and maintained in culture. Four of them have already been analyzed by Sanger sequencing to obtain information about the genetic identity of each primary cell line to the primary tumor which they derived from. In all four cell lines the *VHL* mutation status was confirmed and only one showed the presence of a mutation in *VHL*. In addition, immunohistochemical markers such as PanCK a and b, *BAP1*, *PBRM1* and the cancer stem cell marker CD105, revealed similar expression patterns in both primary cell line and primary tumor tissue. Finally, different morphological and cell growth characteristics were evaluated while culturing. A decreased proliferative rate was observed by increasing passage numbers.

Conclusion:

Primary cell lines represent a valuable tool to characterize and investigate the genotype and phenotype of RCC *in vitro*. This may also help to identify cancer stem cell or cancer cell subpopulations giving rise to chemoresistance and metastatic potential, respectively.

Planas¹, M. Ortiz¹, Metz², Vilarrasa¹, Heesen³, Brück², Martin¹, Sospedra¹

Methodological Approach to Identify and Isolate Disease Relevant Brain-infiltrating T Cell Clones in Multiple Sclerosis Patients

Department of Neurology, University Hospital Zurich¹, Department on Neuropathology, University of Göttingen², Department of Neurology, University Hospital Hamburg-Eppendorf³

Introduction:

Multiple sclerosis (MS) is a chronic inflammatory demyelinating disease of the central nervous system considered to be mediated by T cells. Two main approaches have been employed to study pathogenic T cells in MS in the past. The first approach focused on the functional phenotype of peripheral blood T cells, which were generated with myelin proteins, but for which a pathogenic role was otherwise unclear. Based on the 'skewed' TCR repertoire of brain infiltrating T cells, the second approach focused on clonally expanded T cells identified by expressing particular TCRs. This second approach is not biased by assumptions about autoantigens and considers that clonally expanded T cells are probably disease relevant. However, the main limitation in the few reported studies was the inability to further characterize the functional phenotype and specificity of infiltrating T cells since only frozen autopsy tissue was available. At least one group currently attempts to "revive" brain-infiltrating T cells by expressing TCR alpha and beta chains in recombinant systems that may allow to dissect the specificity but most likely not the functional phenotype of the original T cell clones (TCC).

Methods:

Here we present a new strategy consisting in a) identifying clonally expanded, brain-infiltrating T cells from autopsy tissue of a MS patient, who died after very aggressive disease course and b) subsequent isolation of the relevant TCC from the patient's cerebrospinal fluid (CSF). An actively demyelinating lesion based on reduced density of myelinated fibers and myelin degradation products within infiltrating macrophages was identified. Using deep sequencing approaches, we sequenced the TCR variable beta (V-beta) chains expressed by T cells infiltrating this lesion.

Results:

We identified 312 different lesion-infiltrating TCC. Both CD4 (32%) and CD8 (68%) TCC were present and clonally expanded with frequencies up to 30%. In a following step, we were able to isolate 14 of the most frequent CD4+ and CD8+ TCC using as a cell source *in vitro* PHA-expanded CSF T cells. T cells expressing V-beta families of interest were sorted and cloned by limiting dilution.

Conclusion:

These TCC are currently being characterized for functional phenotype and antigen specificity by using a combination of two complementary unbiased methods, synthetic combinatorial peptide libraries and an autologous brain-derived cDNA library, which is expressed in suitable antigen presenting cells.

N. Leimer¹, C. Rachmühl¹, A. Bahlmann¹, M. Palheiros Marques¹, A. Furrer¹, K. Seidl¹, R. Schüpbach², A. Zinkernagel¹

Treatment of *Staphylococcus aureus* persisting infections by phagolysosome alkalization

Division of Infectious Diseases and Hospital Epidemiology, University Hospital Zurich, University of Zurich, Switzerland¹, Division of Surgical Intensive Care Medicine, University Hospital Zurich, University of Zurich, Switzerland²

Introduction:

The human pathogen *Staphylococcus aureus* often causes invasive and chronic infections such as endocarditis and osteomyelitis. Recurrence rates are high despite *in vitro* effective antimicrobial therapy because *S. aureus* can hide from extracellular active antibiotics and the host's innate immune system in privileged locations such as abscesses and host cells.

Relapsing *S. aureus* infections have been associated with the small colony variant (SCV) phenotype and/or non-replicating persisters. Both subpopulations are characterized by either slow growth and reduced metabolism (SCVs) or dormancy (non-replicating persisters), resulting in antibiotic inefficiency and recurrence of infections.

SCVs are often isolated from abscesses in which the pH is low. We hypothesized that *S. aureus* adapt to the low pH, resulting in shut down of metabolism, stop of growth and thus persistence.

Methods:

We assessed the effect of low pH on *S. aureus* colony phenotype *in vitro* by growing *S. aureus* in various pH media. Non-replicating persisters were assessed using fluorescence dilution of labeled bacterial cell wall.

The localization of *S. aureus* within infected host cells was investigated using a long-term cell culture infection model, confocal- and electron microscopy. The same long-term cell culture infection model was used to assess whether bacteria enter a persisting state while hiding within host cell phagolysosomes, where the pH is also low.

The potential of alkalizing agents (e.g. the anti-malaria drug chloroquine) on regrowth of persisting bacteria and enhanced antibiotic efficiency was investigated using *in vitro* and *in vivo* models.

Results:

We found that low pH induced SCVs and non-replicating persisters which were capable of regrowth. Within host cells, *S. aureus* was localized within phagolysosomes, characterized by low pH. The percentage of SCVs increased over time in intracellular persisting bacteria.

Treatment of infected host cells or mice with compounds that alkalize the pH of phagolysosomes led to growth resumption of intracellular persisting bacteria, resulting in a decrease of bacteria with the SCV phenotype.

Conclusion:

We showed that low pH, as found in abscesses and within phagolysosomes, induced the persisting *S. aureus* subpopulations SCVs and non-replicating persisters. Raising the pH of culture medium or of phagolysosomes by adding alkalizing agents resulted in regrowth of the persisting bacteria and reduced the number of SCVs.

Phagolysosomal alkalization thus may provide a novel additional therapeutic strategy for intracellular persisting staphylococcal reservoir eradication, thus preventing infection relapses.

A. Marzel¹, M. Shilaih¹, W. Yang¹, J. Böni², S. Yerly³, T. Klimkait⁴, V. Aubert⁵, H. Günthard¹, R. Kouyos¹, SHC. Swiss HIV Cohort Study⁶

Estimation of HIV-1 Transmission During Recent Infection in Switzerland

Division of Infectious Diseases and Hospital Epidemiology, University Hospital Zurich, Zurich, Switzerland.¹, Institute of Medical Virology, Swiss National Center for Retroviruses, Zurich, Switzerland.², Geneva University Hospital, Laboratory of Virology, Geneva, Switzerland.³, University of Basel, Department of Biomedicine–Petersplatz, Basel, Switzerland.⁴, University Hospital Lausanne, Division of Immunology and Allergy, Lausanne, Switzerland.⁵, The Swiss HIV Cohort Study, Zurich, Switzerland⁶

Introduction:

Knowing the fraction of transmissions attributable to recent HIV infections is essential for the success of Treatment-as-Prevention. This is because recently infected patients are often unaware of their HIV status and hence remain untreated and highly infectious

Methods:

A maximum-likelihood phylogeny was constructed from 121,306 HIV-1 pol sequences (21,471 sequences from 11,567 Swiss HIV Cohort Study (SHCS) participants and 99,835 sequences from the Los Alamos database). Swiss transmission clusters were identified using different combinations of intra-cluster genetic distance (1%, 1.5%, 2%, 2.5%) and bootstrap (50% to 100% by increment of 2%) thresholds, in order to determine the effect of those criteria. Seroconversion dates were estimated based on immunological markers, dates of HIV positive/negative tests, clinical symptoms and ambiguous nucleotides. Transmission clusters were classified as recent or chronic transmission based on the maximal time interval between the seroconversion dates of the cluster members. Logistic regression with adjustment for age, sex, risk group, HIV subtype, baseline RNA/CD4, time-to-ART and Chronic phase RNA viral load integral, was applied to identify, among transmitters, the risk factors associated with having transmitted in the recent or chronic phase.

Results:

Depending on the implemented phylogenetic threshold criteria, we identified between 50 to 271 transmission clusters with known seroconversion dates for all members. These clusters showed that:

1. The median fraction of transmission during recent infection was 42.2% (range 37%-56%) when recent infection was defined as the first year of the infection and 32% (range 28%-43%) for a six months definition
2. Stricter criteria for defining transmission cluster (higher bootstrap thresholds) were strongly associated with higher fractions of recent phase transmission.
3. The total viral load in the chronic phase (measured as the Chronic phase RNA viral load integral) was negatively associated with recent as opposed to chronic phase transmission, OR 0.43 (0.24-0.77). This effect was even stronger in the adjusted model OR 0.25 (0.1-0.67).

Conclusion:

Our data points to a high fraction of transmission during recent HIV infections in the SHCS. Moreover, we show that the total viral load in the chronic phase is a strong determinant of the transmission phase. These results are important to the pertinent debate on Treatment-as-Prevention as an "Endgame" strategy.

N. Lautenbach¹, L. Saleh², T. Sulser¹, A. Von Eckardstein², C. Poyet¹

Prevalence of PSA disturbance caused by heterophilic antibodies in plasma of patients

Department of Urology, University Hospital Zurich, Zurich¹, Institute for Clinical Chemistry, University Hospital Zurich²

Introduction:

The plasma concentration of prostate specific antigen (PSA) is of paramount importance for the detection and monitoring of patients with prostate cancer. We and others have reported false-high PSA levels due to the presence of heterophilic antibodies (hA). This interference can lead to severe overtreatment of patients. The prevalence of hAs has been reported to range from 3% to 40% in patient serum samples. However, the prevalence of altered PSA levels due to hA interference is unknown.

Methods:

From February to May 2014 we determined the recovery of PSA concentrations (as determined by a 3rd generation electrochemoluminescence assay (ECLIA) from Roche diagnostics) diluting patient samples with a standard serum of known PSA concentration. The expected and measured concentrations were noted. Samples with recoveries < 80% or >130% were retested and analyzed for hA.

Results:

1500 serum probes were consecutively analyzed. Four out of 1500 probes (0.27%) showed reproducibly disturbed recoveries of 826'333%, 3'123%, 63.2%, and 1.6%. After pretreatment of the patient sera with a blocking reagent for hAs (Scantibodies Laboratory, Santee, CA), 3 out of 4 samples showed normal recoveries. The fourth sample could not be reanalyzed because of lack of original sample material and patient's death.

Conclusion:

We conclude that about 0.3% of PSA determinations by the ECLIA of Roche diagnostics are disturbed by hA. Although a very rare event this interference puts a relevant amount of patients worldwide at risk of over- or underdiagnostics. Manufacturers and clinical laboratories should know the rates and kinds of interference for their PSA test used. In case of clinically implausible high or low PSA levels in a patient, clinicians should rule out sampling errors and repeat PSA tests by including determinations of recoveries and, if pathological, absorbing hA in the serum of the patients.

H. Richter¹, M. Michael², D. Andermatt³, R. Frigg³, P. Kronen⁴, K. Klein¹, K. Nuss¹, S. Ferguson⁵, U. Stöckle⁶, B. Von Rechenberg¹

Dynamization at the Near Cortex in Locking Plate Osteosynthesis by Means of Dynamic Locking Screws - An Experimental Study of Transverse Tibial Osteotomies in Sheep

Musculoskeletal Research Unit (MSRU), Equine Hospital, Vetsuisse Faculty, University of Zürich, Winterthurerstrasse 260, 8057 Zürich, Switzerland¹, Trauma Hospital Graz UKH, Göstinger Strasse 24, 8021 Graz, Austria², Synthes GmbH, Luzernstrasse 21, 4528 Zuchwil/Solothurn, Switzerland³, Veterinary Anaesthesia Services International, Zürcherstrasse 39, 8400 Winterthur, Switzerland⁴, Institute for Surgical Technology and Biomechanics, University of Berne, Stauffacherstrasse 78, 3014 Berne, Switzerland⁵, Berufsgenossenschaftliche Unfallklinik Tübingen, Schnarrenbergstrasse 95, 72076 Tübingen, Germany⁶

Introduction:

In these days Locking plates are often used in fracture fixation. During the last period of time delayed- or non-unions are reported complications after using locking screw fixation techniques. Delayed callus formation is a risk due to high rigidity especially at the near cortex. The aim of this animal study in sheep was to evaluate the effect of dynamization on bone-healing. Locking plate constructs were used with new 5.0-mm dynamic locking screws (DLS group), which allow near-cortex micromotion. In comparison, the second group used a more rigid construct utilizing standard bicortical locking-head screws (LS group). Due to nearly parallel interfragmentary micromotion within the fracture gap, DLS screws are able to modulate the stiffness of existing locking compression plate constructs.

Methods:

Twelve female sheep (six in each group) have been subjected a standardized diaphyseal tibial osteotomy (90°, 3-mm fracture gap). Stabilization was performed with a six-hole large-fragment pure-titanium locking compression plate and 6 screws in each group. In the first group dynamic locking screws (DLS) were used in comparison to locking head screws (LS) in the second group. Radiographs were made postoperatively and then weekly from week three until sacrifice (9th week). Sheep tibiae were harvested immediately after sacrifice and the surrounding soft tissues were dissected. Macroscopical, biomechanical, histological and radiographical assessments and micro-CTs were performed.

Results:

Results of macroscopic, histologic and radiographic assessments have been confirmed with biomechanical and micro-CT measurements. In the DLS group the tested specimens had a higher biomechanical stability, with a significantly greater maximum failure moment ([mean and SD as a percentage of intact]; DLS: 55.15 ± 20.65 ; LS: 26.80 ± 14.96 ; $p=0.021$). The DLS group had greater periosteal callus volume at the near cortex ([mean volume and SD as a percentage of the tibial shaft volume]; DLS: 36.21 ± 10.08 ; LS: 18.98 ± 8.61 ; $p=0.026$) and in the intercortical region ([mean volume and SD as a percentage of the bone volume of the tibial shaft]; DLS: 3.56 ± 0.52 ; LS: 2.64 ± 0.98 ; $p = 0.045$), as shown by micro-CT. The DLS group had significantly greater torsional stiffness ([mean and SD as a percentage of intact], DLS: 84.88 ± 13.51 ; LS: 58.89 ± 20.61 ; $p=0.027$).

Conclusion:

The present study involving transverse tibial osteotomies in sheep confirmed the hypothesis that controlled dynamization at the near cortex can be achieved by means of DLS. Results are controlled micromotion and nearly homogeneous interfragmentary strain at the fracture site. Using DLS in this study results in significantly more callus formation at the near cortex together with biomechanically more competent bone-healing compared with locking head screws. Although results from animals cannot be directly extrapolated to human clinical fracture situations, the potential clinical relevance appears obvious. Improved callus formation would substantially enhance patient mobility. It should be mentioned that fracture-healing in humans is influenced not only by the mechanical situation at the fracture gap but also by a number of other potential factors such as local impairment of blood supply, damage to soft tissue, stripping of the periosteum and poor bone biology. Our model is limited and

cannot reflect all of these factors. Multicenter clinical studies will be needed to clarify the value of DLS in improving the mechanical environment at the fracture site.

M. Kijanska¹, A. Marmaras², A. Hegglin¹, V. Kurtcuoglu², P. Giovanoli¹, N. Lindenblatt¹

In vivo and in vitro study of the wound healing properties of the silk-derived surgical scaffold SERI™

Division of Plastic Surgery and Hand Surgery, University Hospital Zurich / Switzerland¹, Institute of Physiology, University of Zurich, Switzerland²

Introduction:

Acellular dermal matrices (ADMs) are reliable and frequently used in soft tissue replacement during breast reconstruction procedures where they contribute to restoration of breast aesthetics. A successful outcome for breast reconstruction depends on many factors, such as surgery technique, the health of the patient, and the selection of the right ADM, among others. In addition, considering the complexity of the healing process and the risks associated with different types of matrices, it is important to investigate the properties of materials and their contribution to wound healing *in vivo*.

Methods:

The angiogenesis and the healing process after implantation of a knitted, silk-derived SERI™ Surgical Scaffold (Allergan) were examined using the dorsal skinfold chamber (DSC). Tissue was harvested on days 2,5,7,10,14,21 (n=5 per timepoint) after implantation and analyzed by immunohistochemistry as well as Scanning Electron Microscopy.

Results:

SERI™ Surgical Scaffold promoted a rapid revascularization of the wound. The wound gap was closed with granulation tissue containing developed capillaries 5 days after implantation. During the healing process early and late stages of inflammation were observed. These were characterized by infiltration of regenerating tissue by different subsets of leukocytes. Moreover, the SERI™ Surgical Scaffold was fully integrated within granulation tissue and collagen deposition significantly increased over time. Qualitative analysis of the regenerated vasculature by corrosion casting and scanning electron microscopy revealed a complex, angiogenic network of capillaries originating from the wound bed.

Conclusion:

Based on these findings and together with its user-friendly handling properties, the SERI™ Surgical Scaffold appears to be a very promising bioengineered material for use in reconstructive surgery.

U. Siler¹, E. Kuzmenko¹, R. Valencia¹, J. Reichenbach¹

A Clinical Phase I/II Gene Therapy Study for Chronic Granulomatous Disease

Division Immunology, University Children's Hospital Zurich and Children's Research Centre Zurich¹

Introduction:

X-linked chronic granulomatous disease (X-CGD) is a primary immunodeficiency caused by mutations in the phagocyte nicotinamide adenine dinucleotide phosphate (NADPH) oxidase subunit gp91phox. Patients suffer from recurrent life threatening infections with bacteria and fungi, often requiring bone marrow transplantation. In case no matched bone marrow donor is available, the only alternative treatment option is gene therapy of autologous hematopoietic stem cells.

Methods:

A recent Swiss-German clinical trial for X-CGD in our unit using a gamma-retroviral vector has demonstrated clear therapeutic benefits in four patients although complicated by enhancer-mediated mutagenesis and diminution of effectiveness over time due to silencing. In collaboration with other centers in Europe a new lentiviral SIN (self-inactivated) gene transfer vector has therefore been developed to improve safety and efficacy. In this vector expression of the therapeutic transgene is mediated by a chimeric promoter, restricting gp91phox expression to terminally differentiated phagocytes.

Results:

This vector results in high levels of gp91phox expression and normal NADPH oxidase activity in committed myeloid cells and granulocytes from transduced human X-CGD CD34+ cells.

Conclusion:

Based on these results the chimeric lentiviral SIN-vector was selected for large scale GMP-production in a joint effort between labs in Zürich, Frankfurt, London and Paris. An EU-FP7 funded clinical gene therapy phase I/II trial for pediatric and adult patients using this vector will start in Zürich in January 2015.

Frequent expression of PD-L1 in testicular germ cell tumors

University Hospital Zurich, Zurich, Switzerland¹

Introduction:

Testicular germ cell cancer has become curable even in the presence of metastatic disease. Nevertheless, about 10-15% of patients who fail cisplatin-based first-line or salvage therapies can only be treated with palliative intent and will eventually die of their disease.

Programmed Death Receptor 1 (PD-1) is a T cell regulator expressed on the surface of activated T cells, B cells, and macrophages. Its ligand, Programmed Death Receptor Ligand (PD-L1), is expressed on tumor cells, macrophages and T cells. The interaction of these two molecules negatively regulates immune responses. Of major interest is that inhibition of the interaction between PD-1 and PD-L1 can enhance T-cell responses in vitro and mediate clinical antitumor activity. The aim of this study was to analyze the expression of PD-L1 in testicular germ cell tumors to evaluate its potential as predictive marker for further therapeutic strategies.

Methods:

Immunohistochemistry was performed in 479 Formalin Fixed Paraffin Embedded specimens using a monoclonal rabbit antibody (E1L3N, Cell Signaling Technology, Inc. (CST) of Danvers, MA, USA) 1:1000 according to a standard protocol. An experienced surgical pathologist evaluated all tissue microarray spots on the computer monitor. Percentages of PD-L1 positive tumor cells and staining pattern were evaluated for each punch. PD-L1 expression was recorded if a membranous immunostaining signal on the tumor cell surface, cytoplasmic staining within the tumor cells or stromal staining was observed. Staining intensity was described as negative, weak or moderate to strong. To evaluate the overall tumor expression of non-seminoma the tumors with multiple specimens were considered PD-L1-positive if any specimen met these criteria.

Results:

PD-L1 expression was found in 151 out of 208 (73%) seminomas and in 78 out of 121 non seminomas (64%) (See Table 1). When focusing on the single tumor components PD-L1 expression was found in 161 out of 248 seminomatous components (69%), in 19 out of 48 (40%) yolk sac components, 7 out of 46 (13%) teratomas components, 8 out of 10 (80%) choriocarcinomas components and 53 out of 87 (61%) embryonal carcinoma components. In 20 out of 20 Intratubular germ cell neoplasia unclassified (IGCNU) and also in 20 out of 20 normal tissue specimens no single case exhibited PD-L1 expression. These results are listed in Table 1.

Conclusion:

Our study describes for the first time the frequent expression of PD-L1 in a large series of human testicular germ cell tumors. Clinical trials with antibodies blocking the PD1/PD-L1 pathway have been completed for a variety of solid tumors and demonstrated a high activity of these treatments in tumors expressing PD-L1. Therefore and based on our results, checkpoint inhibition with anti-PD1 and anti-PDL1 antibodies might represent an attractive approach in germ cell tumors without response to traditional chemotherapy.

J. Schneider¹, A. Luft¹, S. Wegener¹

Transcranial ultrasound predictors of recurrent ischemic stroke in symptomatic internal carotid artery occlusion

Neurology, University Hospital Zurich¹

Introduction:

Occlusion of the internal carotid artery (ICA) puts patients at risk of recurrent ischemic events due to hemodynamic compromise. Activation of secondary collateral pathways involving the ophthalmic artery or leptomeningeal collaterals has been postulated to be an indicator of exhausted primary collaterals involving the anterior or posterior communicating artery. These pathways can be assessed by transcranial duplex sonography. However, neither clinical nor ultrasound parameters have been established to predict recurrent ischemic events after internal carotid artery occlusion. Our goal was to characterize duplex parameters that could indicate patients at risk of recurrent ipsilateral ischemia.

Methods:

We screened our clinical database for patients with symptomatic ICA occlusion treated between 2009 and 2014. Collateral networks as well as flow velocities and indices in extra- and intracranial vessels were analyzed along with clinical and epidemiological characteristics. The Kruskal Wallis test was used for group comparisons. Predictors for recurrent ischemia were investigated using a stepwise linear regression analysis.

Results:

Of 72 patients, 18 (25%) experienced a recurrent ischemic event such as transient ischemic attack (TIA), retinal ischemia or stroke within the same vascular territory during the mean follow up of 9 months (range 1 – 108). Except for the presence of peripheral artery disease ($p=0.048$) and pretreatment with platelet inhibitors ($p=0.032$), none of the patient characteristics were significantly associated with a recurrent event; neither were stroke etiology or severity of stroke symptoms. However, flow within the ipsilateral middle cerebral artery (MCA)-M1 segment was significantly lower in patients who experienced a recurrent event at a later time point. Furthermore, flow (PSV) in the contralateral P2 segment of the posterior cerebral artery (PCA) was significantly increased in patients with recurrent event ($p=0.012$). In the stepwise linear regression analysis, PSV P2 and PSV M1 were significant predictors of a recurrent event.

Conclusion:

Low flow in the ipsilateral MCA indicates hemodynamic failure, whereas increases in contralateral P2 flow suggest activation of vertebrobasilar collaterals. Further refinement of these predictors in conjunction with clinical and imaging information has the potential to identify patients at risk of hemodynamic failure.

N. Echeverry¹, G. Ziltener¹, W. Weder², R. Stahel¹, E. Felley-Bosco¹

INHIBITION OF AUTOPHAGY SENSITIZES MALIGNANT PLEURAL MESOTHLIOMA CELLS TO DUAL PI3K/mTOR INHIBITORS

Laboratory of Molecular Oncology, University Hospital Zurich, Switzerland ¹, Division of Thoracic Surgery, University Hospital Zurich, Switzerland²

Introduction:

PI3K/mTOR pathway is deregulated in MPM. The aim of this study is to explore the therapeutic potential of two dual PI3K/mTOR inhibitors and to identify and target resistance mechanisms in order to induce cell death.

Methods:

Cell growth inhibition upon treatment of NVP-BEZ235 or GDC-0980 was assessed by MTT assay in 19 MPM cell lines. Down-regulation of PI3K/mTOR signaling was assessed determining AKT, S6 and 4E-BP1 phosphorylation. Two resistant and sensitive cell lines were selected. Autophagy induction was monitored by WB using LC3 and p62 autophagy markers. Inhibition of cell cycle and induction of cell death in combination treatment with chloroquine and NVP-BEZ235 or GDC0980 was determined using Annexin V and PI by FACS.

Results:

Sensitive and resistant cell lines were selected and confirmed in 3D systems. Sensitive cell lines showed G1 cell cycle arrest with both drugs but no cell death. All cell lines showed an increase of autophagy after drug treatment. The inhibition of autophagy by chloroquine in combination with NVP-BEZ235 or GDC-0980 showed a stronger effect in cell growth inhibition in both resistant and sensitive cell lines, inducing significant caspase independent cell death in 2D and more pronounced 3D systems.

Conclusion:

Autophagy appears to be one of the main mechanisms of cell death resistance against dual PI3K/mTOR inhibitors in MPM. Since this therapeutic option is under investigation in clinical trials (e.g. NCT00854152), these results may help interpreting their outcome, and suggest ways for intervention.

N. Shepherd¹, T. Zeffiro², K. Hassanpour¹, M. Claussen¹, A. Jaillard⁴, M. Piccirelli⁵, C. Mueller-Pfeiffer³

Attention in Posttraumatic Stress Disorder: Gaze registration and functional magnetic resonance imaging study of saccadic eye movements

Department of Psychiatry and Psychotherapy, University Hospital of Zurich, Zurich¹, Neural Systems Group, Massachusetts General Hospital, Boston, MA², Department of Psychiatry, Massachusetts General Hospital and Harvard Medical School, Boston, MA³

CHU de Grenoble⁴

Inst. Of Neuroradiology, University Hospital Zurich, Zurich Switzerland⁶

Introduction:

Posttraumatic stress disorder (PTSD) is a relatively frequent and potentially severe mental disorder, which develops in about 10 % of survivors in the aftermath of a traumatic event. Despite research advances over the past two decades, PTSD remains a treatment-refractory condition in more than one-third of cases, and further work is needed to improve the understanding of the pathophysiology and treatment of this disorder. With a prevalence of 1 - 4 % in Europe and the United States, the disorder is a major public health burden. Patients suffering from posttraumatic stress disorder (PTSD) are often more easily distracted and find it difficult to focus. An increased involuntary distractibility to trauma-specific or trauma-nonspecific negative stimuli is empirically proven. It is however uncertain if arbitrary, goal-oriented attention processes in a neutral context are impaired through PTSD.

Methods:

In an ongoing fMRI-study PTSD-patients and healthy trauma controls perform a goal-oriented task involving saccadic eye-movements. Previous studies have demonstrated that attention and saccades share neuronal substrates. Saccade latencies can be measured with eye-tracking devices in a relatively inexpensive and non-invasive fashion. Such measurements are not connected to any emotional content and as they cause little stress, they are therefore suitable for PTSD patients. Eye-tracking provides behavioral outcome measurements; these are supplemented with a neural method. Functional magnetic resonance imaging is used to test if saccades and attention share neuroanatomical correlates and if the activation of these is reduced in the case of PTSD.

Results:

In addition to many other symptoms, PTSD patients suffer from impaired concentration. Attention dysfunction in PTSD has been demonstrated in connection with emotional triggers but is also suspected to be independent of such triggers. The neural basis of PTSD remains unknown for the most part. Development of a neurobiological model for the cortical and cerebellar modulation of attention is valuable for a better understanding of PTSD and its impact on the performance of daily tasks.

In the preliminary results for a first subsample of 7 PTSD-patients and 10 healthy trauma controls we found a tendentially decreased reaction time in the PTSD-group for predictable saccades and an increased reaction time for unpredictable saccades (Group [PTSD, controls] x condition [predictable saccades, unpredictable saccades] interaction in two-factor ANOVA: $p = 0.069$).

Conclusion:

In our contribution we will present the behavioural and the main physiological results of this ongoing study. More knowledge about the changes in attention will be critical for the development of more sensitive and specific diagnostic tests, more effective early therapeutic interventions after traumatic events, and a generally more efficient treatment of PTSD.

M. Hugelshofer¹, M. Wurnig², A. Keller¹, A. Boss², A. Aguzzi³

Photothrombotic cortical lesions in the mouse brain: a suitable rodent model for ischemic stroke?

Neurosurgery, University Hospital Zürich, Zürich¹, Diagnostic Radiology, University Hospital Zurich, Zurich², Neuropathology, University Hospital of Zurich, Zurich³

Introduction:

Various rodent stroke models have been developed to mimic the most common clinical subtype of stroke, focal cerebral ischemia. In 1985, Watson and colleagues first described a method where focal ischemic cortical lesions were induced photochemically in rats. Recently, this model has been adapted also for mice. Photochemically induced cortical lesions also referred as "photothrombosis model", takes advantage of the photochemical reaction of systemically administered xanthene dye, Rose Bengal, upon focused tissue illumination. Oxidative stress was shown to cause acute endothelial damage in cortical microvasculature with subsequent platelet aggregation and thrombus formation. However, platelet activation and plasmatic coagulation were shown not to be a prerequisite for tissue damage in photochemically induced stroke, indicating that other mechanisms than thrombotic vessel occlusions are involved in the pathology. Hence, there is a compelling need for detailed analysis of the pathobiology of photochemically induced brain lesions which is necessary to assess the usefulness of this model as ischemic stroke model.

Methods:

Photothrombotic lesions were induced by i.p. administration of Rose Bengal dye and stereotactical transcranial illumination of the cortical target region by a focused cold light source. Lesion development was analysed over time by repeated anatomical and functional MRI scans in a 4.7 Tesla small animal scanner as well as histological and immunohistochemical stainings of brains.

Results:

Photothrombotic cortical lesions can be detected as hyperintense areas in the T2-weighted MRI. FAIR perfusion maps show near-complete cessation of blood flow in the injured cortical area during early hours after induction of photothrombosis. ADC maps confirmed highly restricted brain water mobility in the lesion center indicating early cytotoxic edema. Also, the hypointense signal in FLAIR imaging suggested overall increased water content of the lesion core. In contrast, brain water mobility is increased in the cortex adjacent to the lesion indicating vasogenic edema, whereas perfusion of this area is decreased. After 24 hours of lesion induction, T2 images showed an increase of lesion size and the lesion centre could be detected as hypointense area in T1 images. Perfusion of the lesion center was further decreased and the hypoperfused area expanded into the adjacent cortex increasing the affected area over time. At day two, maximal lesion expansion was recorded by T2 images, and the area of cytotoxic edema and hypoperfusion did not further progress between 24 and 48 hours, indicating a termination of infarct growth. MR-angiography (TOF-MRA) did not show occlusion of major cerebral arteries at any timepoint. Furthermore, T2* images did not suggest hemorrhagic transformation of photothrombotic lesions within seven days after lesion induction.

Histological analysis revealed sharply demarcated cortical lesions with parenchymal palor and rarefaction without affecting the underlying hippocampus. Neurons in the lesion centre showed nuclear pyknosis, eosinophilic cytoplasm and occasional fragmented nuclei indicative of apoptosis. These features correspond to the histological hallmarks of acute ischemic stroke in humans. Furthermore, immunohistochemical stainings for astrocytes and microglia showed strong macro- and microgliosis on the lesion border.

Conclusion:

We have confirmed that the photothrombotic stroke model in mice closely mimics several radiological and histological features of human ischemic stroke, and therefore could be used as a model to study focal cerebral ischemia. However, the chemical induction of massive oxidative stress accompanied by early extensive blood-brain barrier damage limit the usage of this model in translational research.

A. Hegglin¹, C. Schmidt⁴, M. McLuckie¹, D. Bezuidenhout³, S. Hoerstrup², N. Lindenblatt¹

Surface modified polyurethane discs promote early angiogenesis in skin defects

UniversitätsSpital, Zurich Division of Plastic and Reconstructive Surgery¹, Universitätsspital Zürich, Abt. Forschung Chirurgie², Division of Cardiothoracic Surgery, University of Cape Town, South Africa³, Clinic for Cardiovascular Surgery, University Hospital Zurich, Zurich, Switzerland⁴

Introduction:

In skin tissue regeneration, three-dimensional scaffolds are often regarded as the basis to guide and promote normal tissue growth and healing. Qualities such as scaffold material, growth factors, and pore size are critical in ensuring efficient revascularisation, and therefore adequate nutrient and oxygen supply. In this study, the biomaterial polyurethane (PU) has been heparin surface modified and coated with the angiogenic growth factor vascular endothelial growth factor (VEGF) to improve this particular process.

Methods:

PU discs (5.4mm diameter, 300 µm thickness, pore size 150 µm) were coated with heparin and implanted into male C57BL/6J mice. The influence of VEGF₁₆₅ on the vascularisation rate was assessed by intravital microscopy (IVM) in four groups (n=5) containing the following surface coatings (I): plain surface (uncoated), (II) heparin surface, (III) low concentration heparin (15.1mg/g) VEGF₁₆₅ (250 µg/ml) (IV), high concentration heparin (84.9mg/g) VEGF₁₆₅ (250 µg/ml). The modified dorsal skin chamber (MDSC) was employed in order to visualize the revascularisation process of the PU disc by IVM over a period of 21 days. Additionally, immunohistological analysis was performed for signs of inflammation (PU1) and apoptosis in relation to angiogenesis (Caspase 3-CD31 double staining).

Results:

High concentration heparin surface modified PU discs loaded with VEGF₁₆₅ showed a marked increase in angiogenesis and healing in comparison to the other experimental groups. Not only does revascularisation start as early as day 4, the process is completed earlier with faster wound closure and full integration of PU into the tissue. The remaining groups; uncoated PU, heparin - coated, and low concentration heparin VEGF₁₆₅ coated showed the first signs of vascularisation at later time points (days 7 and 14), reaching similar levels of vascularisation as the high concentration heparin VEGF₁₆₅ group on day 7. On day 21, regression of capillaries in all four groups was observed, starting as early as day 14 in the high concentration heparin VEGF₁₆₅ group. This regression correlates with detected endothelial-cell specific apoptosis.

Conclusion:

High concentration heparin coated PU discs loaded with VEGF₁₆₅ displayed faster angiogenesis in addition to earlier wound healing and vessel normalization. Coatings with lower heparin concentrations loaded with VEGF₁₆₅ did not reveal any improvement in comparison to the control groups. The use of VEGF₁₆₅ may be useful in applications where a rapid revascularisation is required.

E. Guenova¹, D. Ignatova¹, YT. Chang¹, R. Dummer¹, L. French¹, A. Cozzio¹

Malignant T cells inhibit anti-infectious immunity in cutaneous T cell lymphoma

Department of Dermatology, University Hospital Zürich, ZH, 8091 Zürich, Switzerland¹

Introduction:

Cutaneous T cell lymphoma (CTCL) is a heterogeneous group of skin-homing T-cell neoplasms which represent approximately 75% of all primary cutaneous lymphomas. Currently available drug therapies, when effective, simply control disease and the only option for curing CTCL is stem cell transplant. The median overall survival for patients with advanced stage IV CTCL is poor and generally only 2 to 5 years. Interestingly, patients with advanced CTCL are susceptible to additional types of cancer and die most commonly from infections. We hypothesized the existence inhibitory mechanisms that enable malignant T cells to suppress both anti-cancer and anti-infection innate and especially adaptive immunity in skin and blood of CTCL patients.

Methods:

Progression of cancer is generally believed to be highly dependent on escape from the control of the local immune system, and dendritic cells (DC) are essential in the process of immune surveillance of tumors. The main goal of this project is to perform ex-vivo screening of the CTCL extracellular interactome and to assess the type of immune control from dendritic cell subsets over benign T cells in CTCL individuals. Preliminary data are shown.

Results:

Malignant CTCL cells are a source of suppressive Th2 cytokines, such as IL-4, and progressive impairment of cellular immunity is a hallmark of the disease. IL-4 is known for its capacity to sustain Th2 cell differentiation, when acting directly on T cells, but can also initiate an IL-12 dependent negative regulatory feedback loop and initiate protective Th1 immune response when present during the initial activation of DC. The association of increased IL-4 production and, at the same time decreased IL-12 levels, with advanced stage CTCL suggests not only cytokines but also inhibitory cell surface molecules on malignant T cells to be an important mechanism of down-regulation of effective immune responses in CTCL.

Conclusion:

Our data point out towards an abrogated DC-T cell regulatory loop in patients with CTCL and suggests an immune escape mechanism that allows cancer cells to evade recognition from the innate immune system, and subsequently abrogate the differentiation of a protective non-malignant effector CD4+ T cell population. Alternative therapeutic activation of innate immune cells (e.g. DC), especially in combination of administration of co-inhibitory antagonists might overrule the potential inhibitory signals coming from malignant T cells in CTCL patients.

H. Klein¹, D. Simic¹, P. Giovanoli¹, J. Plock¹

Handling the complications of cosmetic surgery tourism - Analysis of cost effectiveness and potential treatment

Plastic, Reconstructive and Hand Surgery Department, University Hospital Zurich, Zurich¹

Introduction:

Cosmetic surgery tourism characterizes the phenomenon of people travelling abroad to access aesthetic surgery treatment. This growing trend is driven by the promise of lower costs, shorter waiting lists or the possibility to combine vacation with cosmetic procedures in a luxurious ambience. Problems arise when patients travel abroad and return with complications. Increasing numbers of individuals have presented to our department requesting treatment of such complications by the Swiss healthcare system. Despite increasing attention in academic and popular media in this debatable field, clarity regarding responsibility, efficacy of treatment, cost coverage and cost effectiveness is lacking. In this retrospective study, we set out to investigate the complications of cosmetic surgery tourism treated at our hospital as well as to analyze cost effectiveness.

Methods:

Between 2010 and 2013, we retrospectively included all patients presenting as emergency cases or as outclinic patients with complications arising from cosmetic surgery abroad. Concerned medical records were reviewed for patients' characteristics including performed operations, surgical complications, diagnostics and treatment. Furthermore, associated cost expenditure and DRG-related reimbursement were compared.

Results:

A total of 42 patients were identified. All patients were female with a mean age of 36.4 ± 10.1 years. Most operations were performed in South America (43%) and in Eastern or Middle Europe, respectively. Favoured procedures were breast augmentation (45.2%) followed by abdominoplasty (14.3%) and mastopexy (11.9%). Median time between the initial procedure abroad and presentation at our department was 25.5 ± 68.4 days (mode 15 days). Main complications were wound infections (33.3%) followed by wound healing disturbances (21.4%) and pain/discomfort (14.3%). The majority of the patients (80%) could be treated conservatively, while only 20% became inpatients. Overall costs were SFr 97'200, while DRG-related reimbursement reached the total of SFr 100'784.

Conclusion:

Despite warnings from professional bodies regarding associated risks, cosmetic surgery tourism has proven to be growingly popular. Surgical complications caused by this trend are unavoidable and need to be treated in the patients' home countries. Efficient diagnostics and treatment algorithms can make this emerging field of health care a profitable arrangement for local hospitals without overusing the social healthcare system.

F. Wehrle¹, B. Latal², R. O'Gorman³, C. Hagmann¹, R. Huber²

Reduced Sleep Spindle Activity May Reflect Impaired Thalamocortical Connectivity in Very Preterm Born Children and Adolescents

Division of Neonatology, University Hospital Zurich, Zürich¹, Child Development Centre, University Children's Hospital, Zurich², Center for MR Research, University Children's Hospital, Zürich³

Introduction:

The majority of very preterm infants survive without any severe neurodevelopmental impairments (e.g., cerebral palsy), however, up to 50% of all very preterm children and adolescents suffer from subtle cognitive, behavioural and academic deficits. Very preterm birth is frequently associated with altered development of the thalamocortical system. Sleep spindles, thalamocortically generated phasic oscillations between 12-15 Hz during non-rapid eye movement (NREM) sleep, reflect the integrity of the thalamocortical system. More sleep spindle activity has been reported to be associated with better cognitive abilities in healthy children. The current study aimed to investigate potential alterations in the topographical distribution of sleep spindle activity in very preterm children and adolescents.

Methods:

Thirty-six very preterm participants with a mean gestational age of 29.5 ± 2.1 [M \pm SD] weeks and without any severe brain injuries participated in the study at a mean age of 13.0 ± 1.7 years. Thirty healthy term-born peers (born at ≥ 37 weeks of gestation) were included in the control group with a mean age of 13.0 ± 2.0 years. All-night high-density sleep EEG (128 electrodes) was recorded in all participants. Power maps were calculated based on the average spindle activity of the first hour of NREM sleep.

Results:

Sleep efficiency was high in both groups (approximately 90%). The duration and architecture of sleep were not significantly different between the groups ($p > .30$). In a temporal/parietal cluster of four electrodes, very preterm participants exhibited significantly less spindle activity than their term-born peers (decrease of $9.9 \pm 1.0\%$, $p < .001$). Narrowing the frequency range revealed lower spindle activity in very preterm participants bilaterally in a widespread temporal/parietal region in the slow spindle frequency range.

Conclusion:

The reduction in sleep spindle activity in very preterm children and adolescents may indicate impairments in thalamocortical connectivity. Interestingly, the reduction in spindle activity was observed over brain areas involved in spatial information processing, language and calculation, cognitive domains which are frequently impaired in very preterm children. In the future, high-density sleep EEG may serve as a tool to better understand neuronal mechanisms underlying cognitive impairments in very preterm children and adolescents.

H. Klein¹, N. Fuchs¹, M. Calcagni¹, G. Huber², P. Giovanoli¹, J. Plock¹

Extending the limits – reconstructive microsurgery in the elderly

*Plastic, Reconstructive and Hand Surgery Department, University Hospital Zurich, Zurich¹,
Otorhinolaryngology Department, University Hospital Zürich, Zurich²*

Introduction:

Reconstructive microsurgery has evolved significantly over the last four decades. However indications have changed greatly over time and contraindications should be revisited frequently to keep the field cutting edge surgery. The aim of this paper was to review risk factors and outcomes in patients ≥ 78 years undergoing free flap reconstruction.

Methods:

We analyzed personal and surgical data, including anesthesiological preoperative risk assessment (ASA), comorbidities, operation time, complications and hospital stay in the period between 2010 and 2014.

Results:

We collected 18 patients with a mean age of 82.8 ± 5.1 years ranging from 78-96 years. A majority of these patients was undergoing facial and oral cancer resection ($n=13$), while the others underwent defect reconstruction in the upper and lower limb ($n=5$). An individual approach was chosen using muscular, fascio-cutaneous, and arterialized venous flaps. We had two flap losses. Five Patients underwent a one-stage procedure including cancer resection or debridement and immediate flap coverage. In two cases secondary coverage with a split thickness skin graft of the radial forearm flap donor site was necessary, after using a dermal substitute for coverage during the initial operation. The mean operative time was not longer than in younger patients. One patient died on the third postoperative day due to a cardiac event. Although the patients had multiple co-morbidities, they represent an average population of aged persons in a superior public health care system. One patient was classified ASA I, nine ASA II, five ASA III and three ASA IV preoperatively.

Conclusion:

While this may not necessarily be true for other countries, we conclude that reconstructive microsurgery under general anesthesia can be performed safely, reliably and predictably in the elderly. There may however be a selection bias as primarily people with a better health status over their lifespan may reach the 9th decade of life. Compared to the pertinent literature this is the oldest population analyzed so far.

F. Wehrle¹, B. Latal², R. O'Gorman³, C. Hagmann¹, R. Huber²

Working Memory Ability and Topographical Distribution of Sleep Slow Wave Activity in Children and Adolescents

Division of Neonatology, University Hospital Zurich, Zürich¹, Child Development Centre, University Children's Hospital, Zurich², Center for MR Research, University Children's Hospital, Zürich³

Introduction:

Working memory is the ability to simultaneously keep in mind and manipulate information. This ability has been found to rely on a neural network involving (pre-) frontal and parietal brain areas. Sleep slow wave activity (SWA, 1-4.5 Hz), the key characteristic of deep non-rapid eye movement (NREM) sleep, has been shown to be an indicator of cortical maturation and use-dependent changes in brain functioning. This study assesses maturational and/or use-dependent differences in SWA topography between children and adolescents with high vs. low working memory abilities, thus investigating a developmental period in which major improvements in this key cognitive process occur.

Methods:

Working memory was assessed in 40 subjects ($13.2 \pm .28$ years). Low vs. high performers were distinguished according to the group median. All-night high-density EEG (128 channels) was recorded. Power maps were calculated based on the average SWA of the first and last hour of NREM sleep.

Results:

Working memory scores were significantly different between the groups with 113.3 ± 1.63 and 97.8 ± 1.58 points in high and low performers respectively ($p < .01$). Sleep efficiency was high in both groups (approximately 90%). The duration and architecture of sleep were not significantly different between the groups ($p > .05$). High performers exhibited significantly more SWA than low performers over a prefrontal/frontal cluster of six electrodes (increase: $14.28 \pm 0.86\%$, $p < 0.05$). This pattern was stable across the night.

Conclusion:

Children and adolescents with better working memory abilities show more SWA in an area known to be involved in working memory performance. This may either reflect a more mature neural network underlying this key cognitive process or it may illustrate the increased use of working memory functions in these children and adolescents.

Cell cycle Induction of Dormant Hematopoietic Stem Cells by Thrombopoietin Mimetic but not G-CSF

Division of Hematology, University Hospital Zürich, Zürich¹

Introduction:

Hematopoiesis is sustained by lifelong self-renewing hematopoietic stem cells (HSCs) in bone marrow (BM). Quiescent HSCs are equipped with cell surface receptors to integrate extrinsic demand of blood cell production to hematopoiesis. Although some of these naturally existing regulatory pathways have been utilized in clinical settings, little is known about the influence of cytokine signaling on long-term HSC function.

Methods:

CFSE (5(6)-carboxyfluorescein diacetate N-succinimidyl ester) labeled HSC-containing Lin⁻cKit⁺Sca1⁺(LKS) cells were i.v. transferred into non-irradiated recipients (Takizawa et al., JEM 2011). One week after transplantation mice were i.p. administered with PBS or Flt3L, G-CSF (Filgrastim), CXCR4 antagonist (AMD3100), and TPO receptor (cMpl) agonist (Romiplostim). Three weeks after divisional tracking, cells in different divisional classes were analyzed, sorted by FACS, and transplanted into lethally irradiated mice followed by monthly blood analysis to test long-term self-renewal and lineage repopulation of donor cells.

To test, whether cytokines can activate HSPCs into cell cycle, and thus make them susceptible to chemotherapeutic drugs, we administered mice with cMPL agonist, G-CSF or PBS followed by sub-lethal treatment with 5-FU (5-fluorouracil), and monitored anemia development.

For cross-species validation, immunodeficient newborn mice were engrafted with CFSE-labeled human cord blood-derived CD34⁺ cells, containing HSPCs. PBS or cMpl agonist were injected and analyzed in the same manner as described above.

Results:

BM analysis after 3 week divisional chasing demonstrated that most of phenotypic murine HSCs (LKSFlt3⁻cMPL⁺) were in a 0-divided, dormant fraction in PBS treated animals, while in cMpl agonist treated animals all HSCs have undergone >2 divisions, accompanied by substantial expansion of phenotypic HSCs. Flt3L administration had no impact on 0-divided cells as did CXCR4-antagonist, while administration of Filgrastim reduced the number of dormant HSC by half.

Transplantation of 20 LKS Flt3⁻ cMPL⁺ cells with each divisional history (0-1x, 2-4x and >5x-divided) into lethally irradiated mice, revealed that most of HSCs with multi-lineage reconstitution were found in slow 0-1x and 2-4x divided cells in PBS treated controls (1 HSC in 18.7 and in 39.6 cells, respectively). In contrast cMpl agonist treated animals had much higher frequency of HSCs in 2-4x divided cells (1 HSC in 10.1 cells) while no cells were left in the 0-1x divided fraction. Importantly, in G-CSF treated animals, HSC activity was only detectable in slow 0-1x divided, but not at all in 2-4x or in >5divided fraction.

Combination of cMPL pretreatment with sub-lethal dose of 5-FU resulted in anemia and decreased survival compared to G-CSF and PBS-pretreated control mice, suggesting successful depletion of HSPCs.

Preliminary BM analysis demonstrated that phenotypic human HSCs (Lin⁻CD34⁺CD38⁻CD90⁺) proliferated and expanded upon cMpl agonist treatment as compared to PBS control.

Conclusion:

These results demonstrate that cMpl agonist treatment recruits dormant murine HSCs into self-renewal, leading to increased susceptibility to a chemotherapeutic drug. In contrast G-CSF does not induce HSC cycling. This also holds true for human HSCs xenografted in mice and thus indicates a conserved mechanism across species. cMPL agonist pre-application might be a potent way to sensitize normal and malignant HSCs to chemotherapy.

I. Tritschler¹, K. Seystahl¹, E. Szabo¹, G. Tabatabai², M. Weller¹

TGF-BETA INDUCES AND BMP SUPPRESSES VEGF RELEASE DEPENDING ON SMAD2/3 VERSUS SMAD1/5/8 SIGNALING IN GLIOBLASTOMA

Department of Neurology, University Hospital of Zurich, Zurich¹, Interdisciplinary Division of Neuro-Oncology, Departments of Vascular Neurology & Neurosurgery, Eberhard Karls University Tübingen, University Hospital Tübingen, Germany²

Introduction:

The transforming growth factor (TGF)-beta/bone morphogenetic protein (BMP) and vascular endothelial growth factor (VEGF) pathways have been attributed a major role in the pathogenesis in glioblastoma, but their interactions have remained poorly understood.

Methods:

We characterized TGF-beta/BMP pathway activity in nine long-term glioma cell lines (LTC) and 4 glioma-initiating cell lines (GIC) in relation to constitutive and exogenous TGF-beta/BMP-induced VEGF release.

Results:

As reflected by TGF-beta-induced SMAD2/3-phosphorylation and TGF- β /BMP-induced SMAD1/5/8 phosphorylation, glioma cells exhibit heterogeneous patterns of constitutive BMP/ TGF-beta pathway activation. Constitutive TGF-beta pathway activity accounts for up to 69% of constitutive VEGF release which is positively regulated by SMAD2/3 and negatively by SMAD1/5/8 signaling in a cell line-specific manner. Exogenous TGF-beta induces and exogenous BMP reduces VEGF release in most cell lines. Overall, TGF-beta regulates VEGF release by glioma cells in an ALK-5-dependent manner involving SMAD2, SMAD3 and SMAD1/5/8 signaling.

Conclusion:

This crosstalk between the TGF-beta and VEGF pathways may open up new avenues of biomarker-driven exploratory clinical trials. Beyond, BMP-dependent differentiation therapy as anti-glioma therapy may include VEGF-inhibitory effects.

A. Lutterotti¹, T. Brodie¹, C. Blumer¹, M. Kayser², R. Stenger², M. Foege¹, M. Sospedra¹, R. Martin¹

Antigen-specific tolerance in multiple sclerosis with myelin peptide-coupled red blood cells.

Department of Neurology, University Hospital Zurich, Zurich¹, Swiss Center for Regenerative Medicine, University and University Hospital Zurich, Zurich²

Introduction:

Induction of antigen-specific tolerance is a promising therapeutic strategy in autoimmune diseases, such as multiple sclerosis (MS). We have developed a therapeutic regimen employing autologous blood cells chemically coupled with seven myelin peptides to induce antigen-specific tolerance in MS patients. In recent a open label, single center, phase I, dose escalation trial of autologous peripheral blood mononuclear cells chemically coupled with seven immunodominant myelin peptides (MBP13-32, MBP83-99, MBP111-129, MBP146-170, PLP139-154, MOG1-20 and MOG35-55) the feasibility, tolerability and safety of this novel therapeutic approach was established (Lutterotti et al., 2013). In the current project we aim to assess the safety, tolerability and efficacy of antigen-coupled cell tolerance using red blood cells as tolerogenic carrier cells.

Methods:

An open label, dose escalation study will be performed in relapsing-remitting and secondary progressive MS patients who are off-treatment for standard therapies. All patients will have to show T cell reactivity against at least one of the myelin peptides used in the trial. Neurological, MRI, laboratory and immunological exams will be performed to assess the safety and tolerability, efficacy and in vivo mechanisms of action of this regimen. We will follow the overall patient immune response as well as responses to myelin antigens prior to and following the administration of peptide-coupled cells.

Results:

A automatized GMP manufacturing process for antigen-coupled red blood cells using a Miltenyi Clinimacs Prodigy is currently being developed. Regulatory documentation is being finalized with the aim to get approval for the trial in Q1 2015.

Conclusion:

The first-in-man clinical trial of autologous peptide-coupled red blood cells in MS patients, aims to assess the feasibility, tolerability, safety and preliminary efficacy of this novel therapeutic approach. Provided the phase I/IIa trial shows positive results with regard to the tolerizing effect, the approach has great potential for treatment of MS, but also other immune mediated disease with defined target antigens, transplantation tolerance and allergies.

S. Grossi¹, H. Beer¹

The molecular mechanisms underlying UVB-induced apoptosis of human primary keratinocytes

Dermatologische Klinik, Universitätsspital Zürich, Zürich¹

Introduction:

The ultraviolet B (UVB) fraction of solar irradiation is mainly adsorbed by the keratinocytes of the epidermis and represents the most carcinogenic spectrum of sunlight. Repeated UVB irradiation is able to cause DNA lesions that, if not correctly repaired, can lead to mutations and subsequently to cancer *in vivo*. Apoptosis of keratinocytes antagonizes the malignant transformation and is therefore a protective pathway. However, the pathway of UVB-induced apoptosis is only poorly characterized. Our group has recently reported that caspase-1 is required for UVB-induced apoptosis of cultured human primary keratinocytes. In UVB-irradiated keratinocytes apoptosis occurs independently of others inflammasome components and inflammasome activation, with the exception of caspase-4 whose expression is required. Reactive oxygen species (ROS) and cytoplasmic calcium (Ca²⁺) were identified upstream of caspase-1 and the anti-apoptotic B-cell receptor associated protein 31 (BAP31) downstream. BAP31 is cleaved by caspase-1 during UVB-induced apoptosis in human keratinocytes. The main goal of the project is the molecular characterization of the mechanism of UVB-induced apoptosis in human primary keratinocytes. We would like to elucidate the mechanism of caspase-1 activation in this process. Since caspases with a long amino terminal extension are activated in large multi-subunit complexes it is reasonable to speculate that such a complex does also exist for the activation of caspase-1. Therefore we would like to identify proteins that might serve as platform or scaffold for the activation of the protease. In addition we would like to further investigate the role of caspase-4.

Methods:

The identification of caspase-1 binding proteins will be performed through an affinity-based proteomic approach. We will overexpress FLAG-tagged caspase-1 through transduction of a lentiviral construct in human primary keratinocytes with a knock down of endogenous caspase-1. We will then pull down endogenous caspase-1-binding proteins using a matrix with immobilized FLAG-tag-specific antibody. Caspase-1 binding proteins will be identified through MS/MS. The screening of the identified candidate binding proteins will be performed through siRNA-mediated knock down of their expression in human primary keratinocytes, UVB irradiation and analysis of apoptosis. The role of caspase-4 will be further investigated *in vitro* through siRNA knock down and overexpression experiments.

Results:

We confirmed that FLAG-tagged caspase-1 can be immunoprecipitated using a matrix with immobilized FLAG-tag specific antibody. Overexpression of wild type FLAG-tagged caspase-1 in contrast to a dead mutant partially rescues caspase-1 UVB-induced apoptosis in caspase-1 knock down keratinocytes. However, the fraction of cells that is targeted by lentiviral transduction is low and selection of positive keratinocytes is hampered by the fact that these cells undergo terminal differentiation *in vitro* after some passages. This is not suitable for proteomic experiments, because a large protein amount is necessary for MS/MS analysis. The development of an alternative to this approach is required.

Conclusion:

Optimization of the experimental system is necessary. We are currently trying to establish the generation of human primary keratinocytes that stably overexpress FLAG-tagged caspase-1 in order to obtain the large amount of material needed for proteomic experiments. Since we confirmed that also THP-1 cells are dependent on caspase-1 for UVB-induced apoptosis these cells can be used as an alternative to human primary keratinocytes for proteomics.

Investigation of the role of caspase-4 in UVB-induced apoptosis is ongoing.

L. Simmons³, L. Abela³, K. Steindl¹, B. Schmitt², P. Joset¹, M. Papuc¹, L. Crowther³, A. Rauch¹, B. Plecko³

Untargeted clinical metabolomics reveals N-acetylspermidine as a biomarker for spermine synthase deficiency (Snyder-Robinson Syndrome).

Institute of Medical Genetics, University of Zurich, Schlieren, Switzerland¹, Division of Epilepsy and Clinical Neurophysiology, University Children's Hospital Zurich, Zurich, Switzerland², Division of Neuropediatrics, University Children's Hospital Zurich, Zurich, Switzerland³

Introduction:

Clinical metabolomics has emerged as a powerful tool to study how myriad stimuli (e.g. IEM, cancer, diabetes) affect human metabolism and health. Comparative statistical analysis of the untargeted, or global metabolic profile of a patient cohort versus that of a control cohort can reveal perturbation of metabolite levels/ fluxes in the diseased state. In recent years, metabolomics analysis has led to the discovery of many important biomarkers and has expanded our knowledge of disease and physiology at the molecular level.

Methods:

A cohort of patients with undiagnosed epileptic encephalopathy (EE) was analyzed against an age- and sex matched control cohort. Metabolomics data were acquired from blood plasma by untargeted ultra-pressure hydrophilic interaction liquid chromatography (HILIC) and high resolution accurate mass spectrometry (LC-MS). Data were collected in Xcalibur and preprocessed by SIEVE or XCMS. After data filtering, alignment and framing, individual features were mined against the Human Metabolome Database for annotation. Univariate- (e.g. MWW) and multivariate (e.g. PCA, OPLS-DA) data analysis were employed to determine differential expression levels of metabolites between experimental and control cohorts. Confirmation of metabolite identity was done by retention time and mass fragmentation pattern analysis against commercial standards.

Results:

Principal components analysis (PCA) was applied to the EE cohort data *ad hoc* to look for any natural clustering within the patient profiles in the absence of control data sets. Initial analysis gave a short list (i.e. outliers) comprising six individuals, which warranted further investigation. To date, a subset of two (twin) patients, displaying the most divergent metabolic profile have undergone complete analysis. Discriminant analysis of the twins' profiles against matched controls revealed a metabolic pattern corresponding to errors in polyamine metabolism. Complete data mining and univariate analysis found significantly elevated levels of N-acetylspermidine, a metabolite involved in spermine biosynthesis, in the EE twins. Targeted analysis of the spermine/ spermidine ratio in lymphoblast lysates indicated a defect in spermine synthase in this cohort subset. In parallel, a missense mutation in the spermine synthase gene was confirmed by whole-exome sequencing, thus confirming a diagnosis of the so called Snyder-Robinson Syndrome.

Conclusion:

The application of clinical metabolomics has: 1) identified a short list of patients from a larger cohort with undiagnosed epileptic encephalopathy, whose metabolic profiles warranted further investigation; 2) identified a subset of patients with a defect in polyamine metabolism; and 3) identified N-acetylspermidine as a novel biomarker for spermine synthase deficiency (Snyder-Robinson Syndrome).

Y. Valko², S. Rosengren³, H. Jung², D. Straumann², K. Landau¹, K. Weber²

A novel diagnostic tool for myasthenia gravis: ocular vestibular evoked myogenic potentials (oVEMP)

Department of Ophthalmology, University Hospital Zurich, Switzerland¹, Department of Neurology, University Hospital Zurich, Switzerland², Department of Neurology, Royal Prince Alfred Hospital, Sydney, Australia³

Introduction:

Diagnosing myasthenia gravis (MG) can be challenging, especially in patients with isolated ocular involvement, negative autoantibodies or the absence of the characteristic decrement in repetitive nerve stimulation. Ocular vestibular evoked myogenic potentials (oVEMP) are a recently developed non-invasive test that records electromyographic activity of extraocular muscles in response to otolith stimulation by vibration of the skull. Thus, originally, the test was designed to assess vestibular function. We adapted oVEMP to detect the decrement in extraocular muscles of MG patients.

Methods:

We prospectively examined 27 MG patients and 28 healthy control subjects. We applied vibration stimuli to the forehead and recorded activity of the inferior oblique muscle with two surface electrodes placed beneath the eyes. To identify the oVEMP parameters with the highest sensitivity and specificity, we evaluated the decrement over 10 stimulus repetitions at three different repetition rates (3Hz, 10Hz and 20Hz).

Results:

Mean ages of MG patients and controls were 58±17 and 47±20 years, respectively. Male gender was predominant in both groups (67% and 64%). Mean disease duration was 3.3±4.4 years (range 3 month to 20 years). All MG patients had ocular symptoms, including ptosis (100%) and diplopia (85%). Thirteen patients (48%) had pure ocular MG. Repetitive stimulation at 20Hz appeared to yield the best differentiation between MG patients and controls. Specifically, we found a bilateral decrement of >20% between the second stimulation and the mean value of the fifth to ninth stimulations in 17 MG patients (63%) but none of the controls ($p<0.001$), corresponding to a specificity and sensitivity of 100% and 63%, respectively. Among the 13 patients with isolated ocular MG, 10 (77%) showed a decrement (8 (62%) bilaterally, 2 (15%) unilaterally).

Conclusion:

The findings of our study demonstrate that the presence of a bilateral oVEMP decrement by more than 20% is highly specific for MG. Thus, oVEMP should be considered as an additional diagnostic tool in MG. This simple, non-invasive test can be implemented in any neuromuscular clinic.

D. Marino¹, J. Luginbühl ¹, A. Klar¹, E. Reichmann¹

Bioengineering Dermo-Epidermal Skin Grafts with Blood and Lymphatic Capillaries

Tissue Biology Research Unit, Dep. of Surgery, University Children's Hospital Zurich¹

Introduction:

The first bioengineered, autologous, dermo-epidermal skin grafts are presently undergoing clinical trials; hence, it is reasonable to envisage the next clinical step at the forefront of plastic and burn surgery, which is the generation of autologous skin grafts that contain vascular plexuses, preformed in vitro. As the importance of the blood, and particularly the lymphatic vascular system, is increasingly recognized, it is attractive to engineer both human blood and lymphatic vessels in one tissue or organ graft.

Methods:

We show here that functional lymphatic capillaries can be generated using three-dimensional hydrogels.

Results:

Like normal lymphatics, these capillaries branch, form lumen, and take up fluid in vitro and in vivo after transplantation onto immunocompromised rodents. Formation of lymphatic capillaries could be modulated by both lymphangiogenic and anti-lymphangiogenic stimuli, demonstrating the potential usefulness of this system for in vitro testing. Blood and lymphatic endothelial cells never intermixed during vessel development, nor did blood and lymphatic capillaries anastomose under the described circumstances. After transplantation of the engineered grafts, the human lymphatic capillaries anastomosed to the nude rat's lymphatic plexus and supported fluid drainage.

Conclusion:

Successful preclinical results suggest that these skin grafts could be applied on patients suffering from severe skin defects.

D. Lewandowska¹, O. Zagordi¹, A. Zbinden¹, M. Schuurmans², P. Schreiber³, F. Geissberger¹, J. Huder¹, J. Böni¹, C. Benden², N. Mueller³, A. Trkola¹, M. Huber¹

DIAGNOSIS OF AN ENTEROVIRUS C104 STRAIN IN A LUNG TRANSPLANT RECIPIENT BY HIGH-THROUGHPUT SEQUENCING

Institute of Medical Virology, University of Zurich, Switzerland¹, Division of Pulmonology, University Hospital, Zurich², Division of Infectious Disease and Hospital Epidemiology, University Hospital of Zurich³

Introduction:

Human Enterovirus (HEV) and Rhinovirus (HRV) species can cause a wide spectrum of diseases. Precise discrimination would be of advantage for disease monitoring particularly in immunocompromised individuals, as the clinical outcome and associated risks of HEV and HRV infections differ. With broadly reactive multiplex PCR systems currently employed in routine diagnostics, accurate differentiation of HEV and HRV can be problematic because of high homology between the viruses. Here, we report a case of a 51-year old individual with a protracted respiratory tract infection 4 months after lung transplantation for respiratory failure related to cystic fibrosis.

Methods:

Respiratory samples were analyzed by a commercial multiplex real-time PCR kit, which detects 18 different respiratory viruses and virus types (FTD Respiratory pathogens 21, Fast-track diagnostics, Luxembourg). Due to cross-reactivity issues of this assay, when both HEV and HRV are positive samples are recorded only as HEV positive. To resolve this unclear status of infection, we used a metagenomic approach by performing whole nucleic acid high-throughput sequencing of throat swabs from several time points. The metagenomic sequencing involved virus enrichment, whole nucleic acid extraction, random amplification, sequencing on the Illumina MiSeq platform and bioinformatic data analysis.

Results:

Based on the multiplex PCR results, following an initial HRV only positivity, the subsequent series of samples proved highly positive for HRV and additionally borderline for HEV, suggesting a possible dual infection or a HEV infection that is not properly detected by the kit with HRV cross-reactivity. Metagenomic sequencing analysis revealed infection with a rare Human Enterovirus C104 (HEV C104) closely related to the recently identified AK11 strain. HRV as the source of the highly positive PCR signal could be ruled out, as no HRV-sequences were detected. Using reference-based alignment we were able to recover full-length genomes. We identified sequence variation characteristic in the C104 group likely responsible for the low sensitivity of the multiplex PCR against this particular isolate. Additionally, metagenomic analysis identified co-infections with Polyomavirus KI and Torque Teno viruses in some of the samples.

Conclusion:

The metagenomic approach proved to be successful in both supporting the HEV diagnosis and clarifying potential viral co-infections. In some routinely used methods, rare or novel virus isolates might be missed due to sequence variation within virus strains and subtypes. High-throughput sequencing combined with metagenomic analysis holds great promise for adaptation in routine diagnostic use, hence opening the door for a new area in virus diagnostics and management of viral infections.

M. Nägele¹, A. Flammer¹, F. Enseleit¹, S. Roas¹, S. Cantatore¹, A. Hirt¹, P. Kaiser¹, M. Romanens², T. Lüscher¹, F. Ruschitzka¹, G. Noll¹, I. Sudano¹

Stress-Induced Vascular Dysfunction: Evaluation of Sympathetic Activity and Endothelial Function in Patients with Takotsubo Syndrome

Cardiology, Cardiovascular Center, University Hospital Zurich, Zurich¹, Cantonal Hospital and Vascular Risk Foundation, Olten²

Introduction:

Transient left ventricular apical ballooning syndrome or Takotsubo cardiomyopathy is an acute cardiac syndrome mimicking ST-segment elevation myocardial infarction. This syndrome is typically observed in patients experiencing sudden physical or emotional stress. The precise etiology and pathophysiology of this syndrome as well as its prognosis remains unclear. Aim of this study was to evaluate the vascular function and structure as well as sympathetic nervous activity in patients with Takotsubo syndrome and matched controls.

Methods:

22 patients with Takotsubo syndrome and 21 controls, matched for age, cardiovascular risk factors and medications were included in this prospective observational study. Flow-mediated vasodilatation (FMD) of the brachial artery at baseline and during stress tests was used as a marker for endothelial function. Arterial stiffness was evaluated by tonometric measurement of pulse wave velocity. Carotid atherosclerosis was assessed using ultrasound measurement of intima-media thickness and total plaque area. Sympathetic activation was measured using microneurography and quality of life was assessed using EQ-5 questionnaires.

Results:

Compared to controls, patients with Takotsubo syndrome had a significantly reduced endothelial function (FMD $3.0 \pm 1.7\%$ vs. $5.0 \pm 1.7\%$; $p=0.016$) and an increased sympathetic nervous activity (MSA 49.7 ± 27.5 vs. 28.7 ± 15.1 Burst/100HB, $p=0.04$). Cardiovascular risk factors (age, weight, glucose, lipid profile and physical activity), pharmacological therapies, pulse wave velocity, intima-media thickness, total plaque area and quality of life were similar between both groups.

Conclusion:

Our findings highlight the potentially important role of sympathetic activation and endothelial dysfunction in patients with Takotsubo syndrome.

F. Enseleit¹, S. Michels², M. Nägele¹, I. Sudano¹, M. Stahel², S. Zweifel³, O. Schlager¹, M. Becker², S. Winnik¹, A. Flammer¹, M. Neidhart⁶, N. Graf⁴, CM. Matter¹, B. Seifert⁵, T. Lüscher¹, F. Ruschitzka¹

Safety of VEGF Inhibitors in Age-Related Macular Degeneration (SAVE-AMD)

Cardiology, Cardiovascular Center, University Hospital Zurich, Zurich¹, Ophthalmology, Triemli Hospital, Zurich², Ophthalmology, University Hospital Zurich, Zurich³, Graf Biostatistics, Winterthur⁴, Biostatistics, Institute for Social and Preventive Medicine, University of Zurich, Zurich⁵, Rheumatology, University Hospital Zurich, Zurich⁶

Introduction:

Age-related macular degeneration (AMD) is the leading cause of blindness in the developed world. In the neovascular form (wet AMD), vascular endothelial growth factor (VEGF) plays an important pathophysiological role and intravitreal VEGF inhibitors such as ranibizumab or bevacizumab are an established therapy. While these agents can improve or stabilize vision, there is an ongoing debate whether the beneficial effects come at the cost of increased systemic cardiovascular events. The goal of the Safety of VEGF-Inhibitors in Age-related Macular Degeneration Trial (SAVE-AMD) was to study the cardiovascular effects of intravitreal VEGF inhibition in an interdisciplinary cardio-ophthalmological safety study.

Methods:

Prospective multi-center controlled clinical trial. Previously untreated patients with wet AMD and without known cardiovascular disease were recruited and randomized to intravitreal treatment with either ranibizumab or bevacizumab at 4 week intervals. Patients with non-neovascular (dry) AMD served as an untreated control group. Primary endpoint was the change in endothelial function, assessed non-invasively by flow-mediated dilatation (FMD) of the brachial artery, after 8 weeks and 12 months of treatment with VEGF inhibitors in patients with wet AMD compared to untreated patients with dry AMD. Secondary outcomes included evaluation of central retinal thickness (CRT), best-corrected visual acuity (BCVA), "Early Treatment Diabetic Retinopathy Study" (ETDRS) letters, 24-hour ambulatory blood pressure (ABP), pulse wave velocity, augmentation index, plasma levels of VEGF, thromboxane B2 (TXB2), prostaglandin E2 (PGE2) and 15-F2T-isoprostane, as well as measurement of platelet adhesion.

Results:

49 patients were included in the study, 24 in the wet AMD group and 25 in the dry AMD group. The study was prematurely terminated after review by the independent data safety and monitoring board due to a higher than expected rate of thromboembolic events. Three thromboembolic events were observed, all of which occurred in the wet AMD group treated with VEGF inhibitors (1 fatal stroke, 1 pulmonary embolism, 1 suspected transient ischemic attack). The primary outcome showed no significant differences in FMD after 2 or 12 months follow-up between the groups. Compared to baseline, treatment with VEGF inhibitors did not significantly affect FMD, changing from 4.7±2.4% at baseline, to 3.9±1.9% after 8 weeks (p=0.07) and to 5.1±2.0% after 1 year (p=0.93). Patients on intravitreal VEGF inhibitors demonstrated a significant mean reduction in CRT of 109.9 µm (p<0.001) and 77.6µm (p=0.002), as well as a mean increase in BCVA of 2.8 (p=0.338) and 4.2 (p=0.118) ETDRS letters at 2 and 12 month follow-up, respectively. In the wet AMD group, diastolic ABP dropped from 74±7 to 72±6 mmHg (p=0.03) and augmentation index increased from 30.4±7.2 to 36.5±9.3 after 12 months (p=0.02). No significant differences in pulse wave velocity, plasma VEGF, TXB2, PGE2, 15-F2T-isoprostane or platelet adhesion were found between the groups at baseline or follow-up.

Conclusion:

In this trial, intravitreal VEGF inhibition with ranibizumab or bevacizumab did not significantly impair endothelial, vascular or platelet function in patients with wet AMD. However, an unexpected rate of thromboembolic events led to premature termination of the trial.

K. Fritsch¹, P. Bourguine², S. Pigeot², E. Piccinini², I. Martin², M. Manz¹, H. Takizawa¹

In vivo maintenance of human hematopoietic stem cells and hematopoiesis by engineered bone organs

Division of Hematology, University Hospital Zurich and University of Zurich, Zurich¹, Department of Biomedicine and Surgery, University Hospital Basel, Basel²

Introduction:

Lifelong self-renewal and multilineage repopulation capacity of hematopoietic stem cells (HSCs) is maintained in a specialized microenvironment in the bone marrow (BM), the so-called “niche”. It has been revealed with genetically modified animals that the mouse HSC niche consists of multiple non-hematopoietic cell types, such as e.g. mesenchymal stromal cells (MSCs) that provide HSCs with various vital factors for their maintenance. However, little is known about the cellular and molecular components of the human HSC niche.

Methods:

We took a developmental tissue engineering approach that allows to differentiate human adult BM-derived MSCs into functional bone organs through ex vivo and in vivo endochondral ossification. Ex vivo differentiated human cartilage templates were implanted subcutaneously to immunodeficient mice, and 4 weeks later, third-party donor human cord blood (CB)-derived CD34+ cells were intravenously transplanted to reconstitute human hematopoiesis following sub-lethal irradiation. The implanted ossicles were isolated 3 months post CB transplantation and analyzed by flowcytometry to immunophenotype human HSC and hematopoiesis. To test the functionality of human HSPC in the ossicle, colony-forming unit assays (CFU) were performed with human CD34+ cells. To identify the putative human niche factors that are expressed in the ossicle and thus might be responsible for human HSC maintenance, total RNA were isolated from in vitro-expanded MSCs, in vitro-differentiated ossicles and in vivo-developed ossicles, and subjected to quantitative PCR.

Results:

Histological analysis at 3 months post implantation showed that human ossicles implanted into immunodeficient mice developed vascularization and mature bone in all the cases analyzed, recapitulating endogenous BM structure such as sinusoids and trabecular bones. The flowcytometric analysis showed comparable or better development of human hematopoiesis with phenotypic HSC and progenitor (HSPC) engraftment and maintenance in the human ossicles compared to mouse BM of the same recipient, suggesting full functionality of ectopic human bone organs. The CFU Assay revealed similar frequencies of human HSPCs maintained in the ossicles compared to human HSPC frequencies in same mouse BM. The gene expression profiling showed that in vivo-developed human ossicles express higher levels of CXCL12, Thrombopoietin and Wnt5b than the in vitro-expanded original MSCs and the in vitro-differentiated template, indicating in vivo human BM niche formation with pivotal HSC maintenance factors.

Conclusion:

Our data shows that adult BM MSCs develop ectopic bone organs in vivo through an endochondral ossification process that can support functional allogenic human HSPCs and hematopoiesis, possibly via local expression of human HSC niche factors. The functional human bone organ system that is transplantable and reengineerable will serve as a platform to study physiology and pathophysiology of human HSC niche in vivo.

M. Martin¹, J. Bonvini¹, S. Kuhn¹, T. Neff², B. Beck-Schimmer¹

SEVOFLURANE POSTCONDITIONING MIGHT REDUCE SEVERITY OF CARDIAC AND NON-CARDIAC COMPLICATIONS AFTER ELECTIVE CARDIAC VALVE SURGERY. RESULTS OF A 6 MONTH FOLLOW-UP

Institute of Anaesthesiology, University Hospital, Zurich¹, Institute of Anesthesiology, Kantonsspital Münsterlingen, Münsterlingen²

Introduction:

Anesthetic conditioning with volatile anesthetics has reduced ischemia-reperfusion injuries in various settings of pre- and postconditioning. In a recent randomized controlled trial from our center, including 102 patients undergoing elective cardiac surgery, we were able to show that a four hour sedation with sevoflurane in comparison to propofol upon arrival to the intensive care unit reduced myocardial damage, measured by troponin T levels on the first postoperative [1]. In order to assess the clinical long-term implications of these findings, we performed a 6-month follow up, focusing on cardiac and non-cardiac events.

Methods:

All patients who successfully completed the post-conditioning trial were included into this follow-up study, approved by the local ethical committee (KEK-ZH 2014-0040). Primary and secondary endpoints were assessment of Cardiac events (dysrhythmias, congestive heart failure and cardiac ischemia) and non-cardiac complications (pulmonary embolism, bleeding, infection, cerebral events and chronic kidney failure) resulting in diagnostic or therapeutic interventions. Data were retrieved from the hospital database, secondary care units and family doctors. Statistical analysis was performed using mixed linear models with propofol as the reference group.

Results:

Ninety-four of the 102 patients from the primary study were evaluated in this 6-month follow-up. Sixteen out of 41 (39%) patients in the sevoflurane and 19 patients out of 54 (36%) in the propofol group suffered from one or several cardiac events during the first 6 months after participating in the primary study ($p=0.75$). In 4 (9%) patients treated with sevoflurane vs. 7 (13%) patients treated with propofol non-cardiac events were reported ($p=0.61$). Therapeutic intervention (drugs, interventional treatment or surgery) was required only in 12 patients in the sevoflurane compared to 20 patients in the propofol group (OR: 0.24, CI: 0.04-1.43, $p=0.12$). Eleven patients in the propofol arm compared to only 2 patients in the sevoflurane group were hospitalized due to complication (OR 0.23, CI: 0.04-1.29, $p=0.10$).

Conclusion:

We document a similar number of adverse events (cardiac and non-cardiac) in patients treated with sevoflurane compared to propofol. Despite not reaching statistical significance, we observed less severe complications in the sevoflurane group (less need for treatment, fewer admissions to the hospital). Statistical significance might not have been reached because the original study was powered for biochemical surrogate markers and not for clinical outcomes.

References:

[1] Steurer MP et al: Crit Care. 2012 14;16(5): "Late pharmacologic conditioning with volatile anesthetics after cardiac surgery"

J. Vontobel¹, R. Liga¹, M. Possner¹, O. Clerc¹, F. Mikulicic¹, P. Veit-Heibach¹, E. Ter Voert¹, T. Fuchs¹, R. Buechel¹, P. Kaufmann¹

MR-based attenuation correction for cardiac FDG-PET on a hybrid PET/MR scanner: Comparison with standard CT attenuation correction

Nuklearmedizin, Universitätsspital Zürich¹

Introduction:

The aim of this study was to evaluate the feasibility of attenuation correction (AC) for cardiac FDG-PET using MR-based attenuation maps.

Methods:

We included 23 Patients with no known cardiac history undergoing whole-body FDG PET/CT imaging for oncologic indications on a PET/CT scanner using time-of-flight (TOF) and subsequent whole-body PET/MR imaging on an investigational hybrid PET/MR scanner. Data sets from PET/MR (with and without TOF) were reconstructed using MR AC and semi-quantitative segmental (20 segment model) myocardial tracer uptake (percent of maximum) was compared to PET/CT which was reconstructed using CT AC and served as standard of reference.

Results:

Excellent correlations were found for regional uptake values between PET/CT and PET/MR with TOF (n=460 segments in 23 patients; r=0.913; p<0.0001) with narrow Bland-Altman limits of agreement (-8.5% to +12.6%). Correlation coefficients were slightly lower between PET/CT and PET/MR without TOF (n=460 segments in 23 patients; r=0.851; p<0.0001) with broader Bland-Altman limits of agreement (-12.5% to +15.0%). PET/MR with and without TOF showed minimal underestimation of tracer uptake (-2.08% and -1.29% respectively), compared to PET/CT.

Conclusion:

Relative myocardial FDG uptake obtained from MR-based AC FDG-PET is highly comparable to standard CT-based attenuation corrected FDG-PET, suggesting interchangeability of both AC techniques.

C. Eberhardt¹, MC. Wurnig¹, A. Wirsching², C. Rossi¹, M. Rottmar¹, PS. Özbay¹, L. Filli¹, M. Lesurtel², A. Boss¹

Intravoxel incoherent motion analysis of abdominal organs: computation of reference parameters in a large cohort of C57Bl/6 mice

Institute for Diagnostic and Interventional Radiology, University Hospital Zürich, Zürich¹, Department of Visceral and Transplant Surgery, University Hospital Zürich, Zürich²

Introduction:

Diffusion-weighted MRI (DW-MRI) combined with Intravoxel Incoherent Motion (IVIM) analysis may be applied for characterization of organ lesions, assessment of diffuse parenchymal pathologies and therapy monitoring. The aim of this study was to determine reference parameters of the abdominal organs for translational research in a large cohort of C57Bl/6 laboratory mice.

Methods:

Anesthetized mice (n=29) were measured in a 4.7T small animal MR scanner with a diffusion-weighted echo-planar imaging sequence at the b -values 0, 13, 24, 55, 107, 260, 514, 767, 1020 s/mm². IVIM analysis was conducted on different abdominal organs i.e. liver, spleen, renal medulla and cortex, pancreas and small bowel with computation of the true tissue diffusion coefficient, the perfusion fraction, and the pseudodiffusion coefficient.

Results:

Mean values for the different organs are (in 10⁻³ mm²/s; in %; in 10⁻³ mm²/s): liver 1.15±0.14; 14.8±6.2; 50.28±33.21, spleen 0.55±0.12; 9.9±5.7; 24.46±17.31, renal medulla =1.50±0.20; 14.6±4.1; 35.50±18.01, renal cortex 1.34±0.18; 10.8±3.7; 16.74±6.74, pancreas 1.23±0.22; 20.1±7.5; 29.35±17.82, and small bowel 1.06±0.13; 16.5±3.6; 15.31±7.00.

Conclusion:

This systematic evaluation of murine abdominal organs with IVIM analysis allowed establishing IVIM reference parameters for future DW-MRI translational research studies on small animal disease models.

Transport of High-density lipoproteins (HDL) through endothelial cells*Institute of Clinical Chemistry, University Hospital Zürich, Schlieren¹***Introduction:**

Atherosclerosis is a progressive disease that is characterized by lipid accumulation in macrophages in the arterial wall. High density lipoproteins (HDL) and their main protein constituent and precursor, apolipoprotein A-I (apoA-I), exert several atheroprotective actions within the vascular wall. However, it is little understood how HDL and apoA-I leave the plasma compartment and pass the endothelial barrier to reach this extravascular space. We have previously found that aortic endothelial cells bind, internalize and resecret apoA-I and HDL by processes that are modulated by the ATP binding cassette transporters ABCA1 and ABCG1, respectively, as well as the scavenger receptor BI (SR-BI), and endothelial lipase. In course of time we found that these modulators do not colocalize with HDL during the transcytosis through endothelial cells. Hence, our current study is focused to identify the key interactors that facilitate for HDL internalization and transcytosis through endothelial cells.

Methods:

To identify the key interactors, high-throughput screening using a kinase drug inhibitory library containing 141 compounds was used. Endothelial cells isolated from human and bovine aortae were cultured in 384 well plates in a density of 6000cells/well. After 72hours the cells were incubated for 1hour with 7 different concentrations of each drug. Further HDL uptake and internalization was assessed by incubating cells for 1hour with Atto-594 fluorescent labelled HDL followed by washing and fixation with 2% Paraformaldehyde and subsequent staining of nuclei with Hoechst. The plates are finally processed using molecular devices wide-field fluorescence microscopy.

Results:

The primary analysis from image acquisition data will provide information regarding the localization of HDL in cytoplasmic compartments, signal intensity and number of fluorescent HDL spots with respect to the radial distribution between nucleus and plasma membrane. The secondary analysis will give high quality lead for multiple targets in relation to the effect of drugs that will be further verified using biochemical assays. Based on the data analysis of the hits with significant effects, siRNA targeting corresponding signal transduction kinase pathways will be studied.

Conclusion:

Our project will answer a key question on the pathogenesis of atherosclerosis, namely how HDL enter the vascular wall. This process is a pre-requisite for the mediation of anti-atherogenic functions of HDL and therefore a potential target for anti-atherosclerotic drug therapy.

J. M \ddot{u} nger¹, J. Meienberg¹, J. Crabb², A. Mauri², S. Gysi¹, C. Kaiser³, G. Barmettler³, J. De Vos⁴, I. Bhattacharya⁵, J. Courseau⁶, C. Giunta⁷, E. Bakker⁴, E. Battegay⁵, R. Jaeger⁶, E. Van Bavel⁴, E. Haas⁵, U. Ziegler³, M. Kopf⁸, S. Zeisberger⁹, E. Mazza², G. Matyas¹

Assessment of the Mechanical Stability of the Aorta in a Col3a1 Mouse Model

Center for Cardiovascular Genetics and Gene Diagnostics, Foundation for People with Rare Diseases, Schlieren-Zurich¹, Institute of Mechanical Systems, Swiss Federal Institute of Technology Zurich, Zurich², Center for Microscopy and Image Analysis, University of Zurich, Zurich³, Department of Biomedical Engineering and Physics, Academic Medical Center, University of Amsterdam, Amsterdam⁴, Research Unit, Division of Internal Medicine, University Hospital of Zurich, Zurich⁵, Fraunhofer Institute for Mechanics of Materials IWM, Freiburg⁶, Division of Metabolism, University Children's Hospital, Zurich⁷, Institute of Molecular Health Sciences, Department of Biology, Swiss Federal Institute of Technology Zurich, Zurich⁸, Swiss Centre for Regenerative Medicine, University of Zurich, Zurich⁹

Introduction:

Ehlers-Danlos syndrome vascular type (EDS IV) is a rare connective tissue disorder (1-2 in 100'000) characterized by translucent skin, easy bruising, and arterial, intestinal and/or uterine fragility. The most severe complication is the increased risk for rupture of the aorta, leading to life-threatening internal bleeding. EDS IV is inherited in an autosomal dominant manner and caused by mutations in the *COL3A1* gene, which encodes the alpha 1 chain of type III collagen, a fibrillar collagen expressed in walls of hollow organs. So far, only disease management and treatment of symptoms are available but no targeted therapy. Recently, a novel mouse model, which has true haploinsufficiency of *Col3a1* due to a spontaneous deletion, has been described. In heterozygous mice, this *Col3a1* deletion leads to reduced mechanical stability of the aorta and in ~28% of cases to spontaneous rupture of the aorta and thus to increased mortality similar to the phenotype of human patients. Our goal was to determine whether in this mouse model significant difference in mechanical stability of the thoracic aorta between heterozygous and wild-type animal can be measured and hence objectively characterized. This could allow us in the future to find substance(s) that will increase the mechanical stability of the aortic wall and therefore reduce mortality due to aortic dissection.

Methods:

The thoracic aorta from wild-type and heterozygous *Col3a1* mice was dissected and cleaned of adherent connective tissue. 1.5-mm-long sections of aortic arch as well as ascending and descending aorta were mounted on two 200- μ m diameter stainless steel wires on a TissuePuller (Danish Myo Technology). The mounted vessels were stretched radially until tissue damage and the maximum force (in mN) was recorded.

Results:

Maximum force at tissue damage was significantly lower in heterozygous *Col3a1* mice compared to age- and gender-matched wild-type animals in both the ascending and descending parts of the aorta. For both genotypes the mechanical stability of the aorta was decreasing, with increasing distance from the heart.

Conclusion:

We successfully developed a protocol for the assessment of the mechanical stability of mice aorta, which is suitable to detect significant differences between heterozygous and wild-type *Col3a1* mice. As a next step, we will test pharmacological substances for their potential to increase the mechanical stability of the aorta with the goal to find a targeted therapy that lowers the risk for potentially mortal aortic ruptures in EDS IV patients as well as patients with related genetic disorders.

R. Hasbala¹, L. Rohrer¹, P. Fotakis², V. Zannis², J. Parks³, A. Von Eckardstein¹

Characterization of ApoA-I and HDL metabolism in an endothelial specific ABCA1 deficient mouse model

Institute of Clinical Chemistry, University Hospital of Zürich, Zürich¹, Whitaker Cardiovascular Institute, Boston University School of Medicine, Boston, USA², Department of Pathology, Wake Forest School of Medicine, Winston-Salem, North Carolina, USA³

Introduction:

Atherosclerosis is a progressive disease that is characterized by lipid accumulation in macrophages in the arterial wall and leads to complications like heart attacks and strokes. Low plasma levels of high density lipoprotein (HDL) cholesterol as well as apolipoprotein A-I (ApoA-I) are associated with increased risk of coronary heart disease. HDL and ApoA-I must leave the circulation and pass the endothelium to exert their atheroprotective actions in the arterial wall. We previously demonstrated in vitro that the transendothelial transport of ApoA-I involves ATP-binding cassette transporter (ABC) A1 and secretion of lipidated ApoA-I particles. We hypothesize that ApoA-I transport is started by the ABCA1-mediated generation of a lipidated particle which is then transported by ABCA1-independent pathways.

Methods:

To investigate the role of the endothelial ABCA1 we are currently characterizing an ABCA1 transgenic Cre model expressing the Cre recombinase under the control of the Ve Cadherin gene to specifically target the endothelial cells (ABCA1e^{-/-}).

Results:

We analyzed the plasma lipid and glucose level of these ABCA1e^{-/-} mice with an endothelium-specific knock-out of ABCA1 when fed on a normal chow diet and a HFHC diet for 16 weeks. The ABCA1e^{-/-} mice did not differ from wild type mice by plasma levels of cholesterol or triglycerides but had lower glucose levels upon glucose tolerance testing. After injection of radio-iodinated ApoA-I, we found no difference in the decay of plasma radioactivity but a significantly reduced enrichment of the radiolabel in the aorta of ABCA1e^{-/-} mice as compared to wild type mice.

Conclusion:

Taken together the data show that the knock-out of ABCA1 is endothelium-specific, has no impact on the plasma lipoprotein profile including HDL but alters the accumulation of ApoA-I in the arterial intima.

R. Gerosa¹, S. Boettcher¹, M. Manz¹

The regulatory role of non-hematopoietic bone marrow cells in steady-state and during inflammation

University Hospital Zurich, Division of Hematology, Zurich¹

Introduction:

Hematopoiesis is a hierarchically organized system that produces all types of blood cells. This process is taking place within the bone marrow (BM) and the hematopoietic cells are surrounded by different types of supportive cells called the BM microenvironment. We set out to study how the BM microenvironment supports the hematopoietic system in adaptation to inflammation.

Methods:

To this end, wild-type (WT) mice were stimulated with lipopolysaccharid (LPS) or polyinosinic:polycytidylic acid (polyI:C) to mimic gram-negative bacterial or viral infection, respectively. Using CD45 and Ter119 to exclude hematopoietic cells, mesenchymal stromal cells (MSCs), a stromal cell population enriched for CXCL12 abundant reticular cells (CARs), and endothelial cells (ECs) can be identified by flowcytometry based on their different expression of Sca1, CD31 and CD140b. These various cell types were isolated and their gene expression profiles were determined and compared to steady-state WT mice using microarray analysis.

Results:

We revealed that *Il6* is significantly and specifically up-regulated during LPS stimulation by the cell population enriched for CARs. This was validated using quantitative PCR and changes in IL6 protein production were also analyzed by measuring IL6 protein levels at different time points after LPS injection.

Conclusion:

Future experiments using the Cre-loxP system will be aimed at determining which BM cell population is the main source of IL6. In summary, our preliminary data shows that *Il6* is mainly expressed following LPS treatment by BM resident CAR cells suggesting that *Il6* may play a role in regulating hematopoiesis during bacterial infection.

G. Gers Huber¹, A. Audigé¹, H. Rehrauer², R. Speck¹

Identification of IFN- α -stimulated candidate genes as novel HIV-1 restriction factors

Department of Internal Medicine, Division of Infectious Diseases and Hospital Epidemiology, Zurich¹, Functional Genomics Center, University of Zurich, Zurich, Switzerland²

Introduction:

IFN- α is able to block or decrease HIV-1 replication in several types of cells, including cell lines and primary cells. This is due to the upregulation of several interferon-stimulated genes (ISGs) which have anti-HIV-1 activity. Here we studied IFN-mediated inhibition of HIV-1 replication in MT4R5 and SupT1R5 cells with the aim of identifying the pathways involved in the inhibition of HIV-1 that could point to a non-identified cellular restriction factor.

Methods:

HIV-1 replication was assessed in MT4R5 and SupT1R5 cells with and without IFN- α treatment. HIV-1 reverse transcription products and integration were quantified to determine the step at which IFN- α inhibits HIV-1 replication. Next generation sequencing (NGS) was performed with RNAs from cells treated or not with IFN- α . HIV-1 replication was also assessed in MT4R5 and SupT1R5 cells in which the ISG MX2 was knockdown with shRNAs.

Results:

We observed a strong inhibition of viral replication at low concentrations of IFN- α in both cell lines. We determined that the inhibition occurs at early steps of the viral life cycle between reverse transcription and integration. NGS of total RNAs of the cells treated or not with IFN- α identified 162 upregulated genes in both cell lines upon IFN- α treatment. We analyzed the pathway maps, biological processes and process networks, in which these 162 genes are present, and obtained an enrichment in immune/defense response genes. We also compared the 162 upregulated genes with genes reported to be upregulated in previous studies and found that 44 of the 162 genes are widely reported in similar analyses of IFN- α treatment or HIV-1 infection. Finally, we showed that among the 162 upregulated genes, the newly identified restriction factor MX2 is present and enriched in the immune response pathways and networks. Although we successfully downregulated MX2 with shRNAs, we observed no decrease in IFN-mediated restriction.

Conclusion:

We identified 44 genes that are upregulated by IFN- α in our and previous studies. Lack of decrease of IFN- α -mediated restriction of HIV-1 replication in cells with knockdown of MX2 indicates that at least one of the other upregulated genes might be responsible for the inhibition of HIV-1 replication.

A. Richter¹, Ch. Woernle³, N. Krayenbühl³, S. Kollias², D. Bellut³

Affective symptoms and white matter alterations in brain tumor patients

Department of Psychiatry, University Hospital Zurich, Zurich¹, Department of Neuroradiology, University Hospital Zurich, Zurich², Department of Neurosurgery, University Hospital Zurich, Zurich³

Introduction:

Affective symptoms are frequent in brain tumor patients. The origin of such symptoms remains unknown; either focal brain injury or reactive emotional distress may be responsible. The objective of this study was to investigate potential correlations between depressive symptoms and anxiety with alterations in white matter in a population of brain tumor patients. We hypothesized that there would be alterations in FA which were dependent on the severity of affective symptoms, in brain regions known to be involved in affective processing.

Methods:

Thirty-nine patients with newly diagnosed supratentorial primary brain tumor underwent diffusion tensor imaging (DTI) scanning. Patients filled in the Beck Depression Inventory (BDI-1A) and examiners rated them on the Hamilton Depression Rating Scale (HDRS). State and trait anxiety were measured using the State-Trait Anxiety Inventory (STAI-G). Correlations between fractional anisotropy (FA) and psychological measures were assessed on a regions of interest (ROIs) basis; the defined ROIs corresponded to clearly specified white matter tracts.

Results:

The severity of depressive and anxious symptoms was correlated with FA in the left and right internal capsule; the correlation was stronger for the left hemisphere. Depressive symptoms were also associated with FA values in the right medial uncinate fasciculus and state anxiety was associated with FA values in the left medial and lateral uncinate fasciculus.

Conclusion:

This study suggests that affective symptoms in patients with brain tumors are associated with alterations in tissue integrity in WM tracts of brain circuits involved in emotional processing. One might go even further and suggest that the white matter changes we observed could be a plausible biomarker for affective symptom severity in brain tumor patients; cohort studies in this population would be needed to provide evidence to support this hypothesis. Affective symptoms occur predominantly in patients with lesions in the frontal cortex or in a subcortical location with anatomical links to frontal brain areas; this patient group should be checked for affective symptoms and treatment given where necessary.

Z. Song¹, E. Maurizio¹, B. Humar¹, R. Graf¹, PA. Clavien¹, Y. Tian¹

Melatonin Rescues Small for Size Liver Graft Failure in Mice

Department of Visceral and Transplant Surgery, University Hospital Zürich, Zürich¹

Introduction:

living donor liver transplantation (LDLT) is a good solution for liver donor shortage. However, small for size (SFS) syndrome which leads to graft failure impedes the development of LDLT. Melatonin is a strong antioxidant and shows protective effect on hepatocyte. The aim of this study is to investigate whether melatonin has protective effect after SFS liver transplantation in mice.

Methods:

Male C57BL6 mice were subjected to 60 min of 1/3 liver ischemia plus 2/3 hepatectomy of non-ischemia lobes (I/R+PH group) or liver ischemia plus extended hepatectomy (I/R+exPH group). Both groups were subdivided as melatonin group or control group depending on the treatment of melatonin or vehicle. Hepatic injury was determined by AST, ALT and histology. The regenerative cytokines and PCNA staining were examined by PCR and immunohistochemistry. Serum HMGB1 was measured by ELISA. Survival rate in each group was monitored.

Results:

In I/R+PH groups, more hepatic injury was observed in control group than melatonin group. Melatonin treated mice liver showed more PCNA positive cells and higher level of regenerative cytokines compared with the animals of control group. The expression of HMGB1 in the late time point was significantly suppressed by melatonin treatment compared with controls. In I/R+exPH groups, 7 days survival rate was 0% in control and 50% in melatonin treated groups.

Conclusion:

Melatonin rescues small for size liver graft failure by reducing ischemic reperfusion injury and promoting liver regeneration.

F. Largey¹, I. Jelcic¹, M. Sospedra¹, R. Garcea², R. Martin¹, I. Jelcic¹

The anti-VLA-4 monoclonal antibody natalizumab depletes intrathecal production of anti-JCV and -BKV antibodies, but not other antiviral antibodies

Neuroimmunology and Multiple Sclerosis Research Section, Department of Neurology, University Hospital Zurich, 8032 Zurich¹, Department of Molecular, Cellular, & Developmental Biology, and The Biofrontiers Institute, University of Colorado at Boulder, Colorado, USA²

Introduction:

Progressive multifocal leukoencephalopathy (PML) is caused by JC virus (JCV) and may occur in multiple sclerosis (MS) patients under natalizumab treatment (NAT). NAT is considered to hinder JCV-specific T cells from entering the brain and thereby to increase the risk for PML. NAT may also affect intrathecal B cell immunity, since oligoclonal bands (OCB) disappear from cerebrospinal fluid (CSF) in 17-67% of MS patients during NAT. However, it is not clear, if NAT influences the polyspecific intrathecal humoral immune response against e.g. measles (M), rubella (R) and/or varicella zoster (Z) viruses (MRZ reaction), which is found in 80-100% of MS patients and represents the most specific single marker for MS. Here, we analyzed, if the intrathecal production of antibodies against various viral antigens, particularly JCV, differs between MS patients before and during NAT.

Methods:

Serum and CSF from 15 MS patients were collected before NAT (V0) and after 12 (V12) and 24 months of NAT (V24). Samples were tested in capture ELISAs using measles, rubella, mumps, influenza, enteroviruses, herpes viruses and polyomaviruses (JC, BK, KI and WU virus) antigens in order to calculate the virus-specific CSF IgG antibody index (AI). An AI>1.5 indicates intrathecal synthesis of virus-specific antibodies. OCB of all samples were determined by isoelectric focusing.

Results:

Prevalence of intrathecal antibody synthesis was either unchanged or tended to slightly decrease under NAT when compared to untreated samples. Interestingly, AI_{JCV}>1.5 and AI_{BKV}>1.5 were detected in three out of 15 (20%) MS patients before NAT (V0), but were not detectable under NAT treatment. Such a remarkable decrease was not found for any other antigen tested (decreases ranging from 0%-10% only), including MRZ reaction. Furthermore, OCB in CSF of two patients completely disappeared under NAT. Loss of OCB did not correlate with loss of intrathecal antibody production.

Conclusion:

NAT seems not to generally inhibit intrathecal humoral immune responses since intrathecal antibody synthesis is still detectable under NAT. However, intrathecal antibody production against JCV and BKV is completely lost under NAT, suggesting a selective inhibitory effect. The potential of NAT to deplete specifically intrathecal anti-JCV antibody synthesis might add to PML development.

U. Lindert¹, M. Gnoli², L. Sangiorgi², M. Bedeschi³, M. Rohrbach¹, C. Giunta¹

Pathomechanism of a COL1A1 Signal Peptide Heterozygous Mutation Leading to Severe Osteogenesis Imperfecta

Division of Metabolism, Connective Tissue Unit, University Children's Hospital and Children's Research Center, Zurich¹, Department of Medical Genetics and Skeletal Rare Diseases, Rizzoli Orthopaedic Institute, Bologna², Medical Genetics Unit, Fondazione IRCCS Ca'Granda Ospedale Maggiore Policlinico, Milano³

Introduction:

Osteogenesis imperfecta (OI) is a disorder of connective tissue which is inherited in both a dominant and recessive manner. Most cases of OI are caused by autosomal dominant mutations in the genes encoding type I collagen (*COL1A1* and *COL1A2*). It is a heterotrimer consisting of two $\alpha 1(I)$ and one $\alpha 2(I)$ chains that fold in the rough-endoplasmic reticulum (rER) to form a triple helix of uninterrupted Gly-X-Y repeats. A foetus presenting at ultrasound examination with bowing and shortening of all long bones and a diagnosis of severe OI was aborted at the 22nd week of gestation. Post mortem examination showed facial anomalies, shortening and bowing of all long bones, camptodactyly of hands and club feet. X-rays showed gross demineralization of calvaria and facial bones, varying thickness and discontinuous beading of the ribs, distorted and irregularly ossified scapulae, slender and twisted long bones with fractures, confirming the suspected diagnosis of OI. An unusual heterozygous p.Gly22Arg disease variant at the the -1 position of the signal peptide cleavage site of *COL1A1* was identified. The signal peptide is required for cytoplasm/endoplasmic reticulum translocation of the nascent collagen α -chains; it is recognized by the signal recognition particle (SRP) and is subsequently cleaved by a signal peptidase. We set out to characterize the p.Gly22Arg mutation at the biochemical level, in order to gain insights into the pathomechanism leading to OI.

Methods:

Steady state biochemical analysis of *in vitro* produced collagens, and pulse-chase experiments on cultured fibroblasts aimed to investigate the production and secretion of collagens was investigated as previously reported. Electron microscopy analysis of cultured fibroblasts of the patient was performed using standard techniques. Immunofluorescent staining was performed on patient and control primary fibroblasts. Cells were co-stained for type I collagen (COL I) and either for the endoplasmic reticulum (ER) marker PDI or the Golgi marker GM130.

Results:

Production of procollagen I was reduced, and its secretion was slightly delayed. Furthermore, aberrant procollagen $\alpha 1(I)$ and $\alpha 2(I)$ chains were detected in the cell layer by pulse-chase analysis, suggesting the presence of both overmodified, as well as undermodified collagen chains. *In vitro* ultrastructural analysis of cultured fibroblasts showed the presence of enlarged ER-cisterns. Immunofluorescent staining aimed to test for accumulation of aberrant procollagen I chains in the ER, showed unexpectedly a punctuate staining that did not overlap with either ER- or Golgi markers. This suggests either a secretion block of aberrant collagen I molecules within cargo particles, or their lysosomal degradation.

Conclusion:

A heterozygous mutation in the signal peptide cleavage site of *COL1A1* causes a severe form of OI leading to: (i) reduced secretion of procollagen I by fibroblasts; (ii) intracellular retention of aberrant modified procollagen $\alpha 1(I)$ and $\alpha 2(I)$ chains; (iii) enlarged ER-cisternae and (iv) punctuate intracellular staining pattern not overlapping with ER-lumen or Golgi. Our results suggest that the mutation impairs cleavage and thus release of procollagen $\alpha 1(I)$ chains from the ER-membrane, and might interfere with ER-integrity; this hypothesis is supported by our observation of enlarged ER-cisternae by transmission electron microscopy. In summary our data point towards the retention of aberrantly folded procollagen I in the ER, its degradation within the cell, and possibly the involvement of ER-stress as pathomechanism leading to OI in the affected foetus.

T. Restin¹, M. Kajdi², M. Schläpfer¹, B. Beck-Schimmer¹

Sevoflurane improves junction properties of brain endothelial cells after hypoxia

University Hospital Zurich, Institute of Anesthesiology, Zurich¹, University of Zurich, Institute of Physiology, Zurich²

Introduction:

Sevoflurane is a volatile anesthetic known to reduce inflammatory response after hypoxic injury of the heart, liver and lung. Animal models suggest that sevoflurane reduces cerebral infarct size after ischemia, probably impacting on the blood brain barrier (BBB). How sevoflurane interacts with injured endothelial still has to be elucidated. We therefore analyzed the effect of sevoflurane on rat brain endothelial cells (RBE4) following hypoxia.

Methods:

RBE4 cells were exposed to hypoxia (0.2% O₂) for 24 hours, followed by a 4 hour reoxygenation with 21% O₂ with or without addition of 2.2% sevoflurane. Cellular DNA content (bisbenzimidazole) was measured. In order to assess permeability of the monolayer, RBE4 cells were cultured in Boyden chambers until confluency. Consequently the permeation of 40kD FITC dextran was determined. Immunostaining was performed using monoclonal mouse anti ZO-1 and anti-beta-Catenin antibodies to identify tight and adhesion junctions microscopically.

Results:

Hypoxia of 24 hours followed by a 4-hour reoxygenation significantly reduced DNA content of RBE4 cells by 20% ($p < 0.0001$), sevoflurane had no effect. Barrier function, determined by dextran permeability, was significantly impaired after hypoxia-reoxygenation (increased permeability of 2.5, $p < 0.0001$). It partially recovered with sevoflurane postconditioning (increased permeability of 1.6, $p < 0.001$). Tight junction organization was altered by sevoflurane treatment. Both ZO-1 and beta-Catenin were dislocated from the cellular membrane after reoxygenation with 21% O₂, while both junction proteins were better maintained under sevoflurane reoxygenation.

Conclusion:

Sevoflurane positively impacts on impaired endothelial barrier function and stabilizes junction proteins at the cellular membrane after hypoxic injury.

P. Schreiber¹, C. Benden², C. Berger⁷, J. Böni³, D. Braun¹, M. Felder⁴, F. Geissberger³, T. Güngör⁶, H. Günthard¹, M. Hoernes⁶, M. Huber³, D. Lewandowska³, K. Metzner¹, T. Müller⁵, D. Nadal⁷, J. Pavlovic³, J. Reichenbach⁶, J. Pachlopnik Schmid⁶, M. Schuurmans², R. Seger⁶, R. Weber¹, O. Zagordi³, A. Trkola³, N. Müller¹

Implementation of the multisite, multidisciplinary trial “Metagenomic profiling of viral infections for improved virus diagnostic and infectious disease management in immune compromised patients” into clinical daily routine

Infectious Diseases, University Hospital Zurich¹, Pneumology, University Hospital Zurich², Institute of Medical Virology, University of Zurich, Switzerland³, Clinical Trials Center, University Hospital Zurich, Zurich, Switzerland⁴, Nephrology, University Hospital Zurich⁵, Children's Research Center (CRC), University Children's Hospital Zurich, Div of Immunology/BMT, Zurich, Switzerland⁶, Children's Research Center (CRC), University Children's Hospital of Zurich, Zurich, Switzerland⁷

Introduction:

Connate or acquired immune deficiency renders individuals prone to infections with a broad range of potential pathogens representing a major challenge for conventional pathogen-specific diagnostic methods. Diagnostic approaches that allow simultaneous detection of known and new pathogens are urgently needed to ensure rapid diagnosis and initiation of directed therapies. In contrast to bacteria for which sequence based detection according to the conserved 16S rRNA gene is highly efficient, broad-range diagnosis of viruses is particularly difficult due to their heterogeneity. A metagenomic approach for virus detection using Next Generation Sequencing (NGS) may overcome some of these limitations. To probe the capacities of metagenomic virus profiling in clinical use, we designed clinical trials to evaluate the virus population in different immunocompromised settings.

Methods:

To encompass a wide spectrum of immunocompromised patients, the three trials aim at patients of the University Hospital Zurich (USZ) and the University Children's Hospital with both inborn and acquired immunodeficiencies. At the USZ, transplant patients are enrolled at time of transplantation (routine scenario) or with clinical symptoms compatible with a viral infection. Both situations are very demanding in terms of logistics. To ensure optimal support, caregivers of the target population were actively involved in the implementation. SOPs were adopted for the different patient groups and scenarios. At the infectious diseases outpatient clinic patients with primary or recent HIV infection are enrolled by treating physicians.

Feedback was used to optimize workflow. With support of the Clinical Trials Center an eCRF using SecuTrial was established and stepwise adjusted.

Results:

A total of 89 transplant recipients were enrolled so far: 26 lung transplant recipients and 18 kidney recipients (including 5 living kidney donors) are participating in the routine scenario (enrolment at time of transplant and regular follow-up thereafter). Symptomatic patients are divided in 41 lung transplant recipients, 2 kidney recipients and 2 patients with prior lung and kidney transplantation. A total of 199 blood, 189 urine, 156 stool, 150 throat swab and 5 broncho-alveolar lavage samples were collected from transplant recipients.

55 stool samples derived from HIV-infected patients were obtained (30 baseline samples, 17 week 24 samples, 8 week 48 samples).

At the University Children's Hospital 12 patients with primary immunodeficiencies were enrolled. 9 blood, 1 liquor, 1 BAL, 1 throat swab and 1 stool sample have been collected.

Conclusion:

A complex setting characterized by involvement of multiple sites (USZ, University Children's Hospital, Institute of Medical Virology) and within these sites participation of different wards and outpatient clinics requires rigorous organisation and motivation. Intensive teaching and a well-organized flow of samples with predefined and adapted SOPs and ready-to-use sample kits can achieve readiness 24/24 hours seven days a week, which is an essential prerequisite given that a relevant number of

transplantations are performed during nights or weekends. Investigators must keep an open attitude towards suggestions for improvement from all parties to enable feasible and convenient solutions. In addition close guidance of the patients by the treating physicians facilitates both enrolment and sampling (e.g. readiness of patients to send samples by mail). In terms of follow-up and particular the completeness of sampling these trials have achieved an excellent performance given the complexity and duration of the trials.

Successful implementation of true translational trials remains a logistical challenge and is only made possible through close collaboration of all involved parties.

E. Malagola¹, K. Schlesinger¹, E. Saponara¹, K. Grabliauskaite¹, T. Reding Graf¹, S. Sonda¹, R. Graf¹

Effect of thyroid hormone T3 in pancreatic acinar cells

VIS Klinik f. Viszeralchirurgie, University Hospital Zurich, Zurich¹

Introduction:

Recently, evidences of a mitogenic effect of 3,5,3'-triiodo-L-thyronine (T3) on rat pancreatic acinar cells were described. In the present work we tested the injection of T3 in adult mice in healthy condition or following cerulein-induced pancreatitis, to investigate the cells that actively respond to the T3 stimuli and the molecular mechanisms beyond.

Methods:

Wild type C57BL/6 mice were injected with T3 or cerulein or a combination of the two molecules. Levels of cell replication, inflammation and fibrosis were investigated through immunohistochemistry as well as gene expression analysis. Gene expression was tested through qPCR using the $\Delta\Delta Ct$ method. Protein serum levels were quantified through biochemical analyses

Results:

T3 injections, either alone or in combination with cerulein, stimulated division only of pancreatic acinar cells, while no mitogenic activity was found in islet or ductal cells. No sign of increased tissue damage, inflammation or fibrosis from T3 treatment was observed. Interestingly we noticed induction of β -catenin expression as well as a regulation of deiodinase 1-3 (DIOs) levels, which are responsible for both the activation and the suppression of thyroid hormone pathway. DIOs' expression was up-regulated also in pancreatitis samples.

Conclusion:

T3 robustly promotes cell cycle of acinar cells in both normal and injured pancreas, likely via activation of the β -catenin pathway. In addition, the evidence of a regulation of DIOs' expression during pancreatitis points out a putative patho-physiological role of endogenous T3 in pancreatic regeneration. Thus T3 administration may have a therapeutic role to improve the outcome of this severe disease.

M. Schanz¹, T. Liechti¹, O. Zagordi¹, E. Miho², S. Reddy², H. Günthard³, A. Trkola¹, M. Huber¹

High-throughput sequencing of human immunoglobulin variable regions with subtype identification

Institute of Medical Virology, University of Zurich, Zurich, Switzerland¹, Department of Biosystems Science and Engineering, ETH Zurich, Basel, Switzerland², Division of Infectious Diseases and Hospital Epidemiology, University Hospital Zurich, University of Zurich, Zurich, Switzerland³

Introduction:

The humoral immune response plays a critical role in controlling infection and the rapid adaptation to a broad range of pathogens depends on a highly diverse antibody repertoire. The advent of high-throughput sequencing technologies in the past decade has enabled insights into this immense diversity. However, not only the variable, but also the constant region of antibodies determines their *in vivo* activity. Antibody isotypes differ in effector functions and are thought to play a defining role in elicitation of immune responses, both in natural infection and in vaccination.

Methods:

We have developed an Illumina MiSeq high-throughput sequencing protocol that allows determination of the human IgG subtype alongside sequencing full-length antibody variable heavy chain regions. We thereby took advantage of the Illumina procedure containing two additional short reads as identifiers. By performing paired-end sequencing of the variable regions and customizing one of the identifier sequences to distinguish IgG subtypes, IgG transcripts with linked information of variable regions and IgG subtype can be retrieved.

Results:

We applied our new method to the analysis of the IgG variable region repertoire from PBMC of an HIV-1 infected individual confirmed to have serum antibody reactivity to the Membrane Proximal External Region (MPER) of gp41. We found that IgG3 subtype frequencies in the memory B cell compartment increased after halted treatment and coincided with increased plasma antibody reactivity against the MPER domain.

Conclusion:

The sequencing strategy we developed determines IgG subtype very reliably and is not restricted to analysis of IgG. It can be adopted for any Ig subtyping and beyond that for any research question where phasing of distant regions on the same amplicon is needed.

S. Dias¹, L. Regli¹, A. Keller¹

Oxidative stress modifies microvascular calcifications in brain

*Department of Neurosurgery, University Hospital Zurich, Switzerland*¹

Introduction:

Dementia caused by vascular dysfunction is the second most common form of dementia after Alzheimer's disease. However, the pathogenic mechanisms leading to vascular dysfunction and neurodegeneration are not well understood. Idiopathic basal ganglia calcification (IBGC) is a rare neurodegenerative disease characterized by microvessel-associated calcifications. Our recent work has pinpointed defects in the neurovascular unit (NVU), in particular pericytes and blood-brain barrier (BBB) dysfunction, as a potential cause for brain calcifications. Oxidative stress has been implicated in neuronal and vascular pathologies, and microarray analysis of microvasculature isolated from the brains of IBGC mouse models shows deregulated balance. Thus, our aim is to elucidate if oxidative stress modifies microvessel calcification in the brain.

Methods:

We have crossed an IBGC mouse model – *pdgfb ret/ret* with Nox2 knockouts. Nox2 is strongly upregulated on mRNA and protein levels in microvasculature of *pdgfb ret/ret* animals (unpublished observations). Brain tissue of *pdgfb ret/ret*, Nox2 knockout animals has been analyzed using various histological and immunohistological stainings. In addition to genetic modification of oxidative stress we are planning to feed mice with anti-oxidant supplements (N-acetyl-cysteine and hydroxytyrosol) and study the effect of dietary antioxidants on formation of microcalcifications in the brain of *pdgfb ret/ret* animals.

Results:

Our preliminary analysis of *pdgfb ret/re*; Nox2 knockout animals shows a reduction of the size and number of vessel-associated calcified lesions compared to *pdgfb ret/ret* animals.

Conclusion:

Our data provide the evidence that oxidative stress plays an important role in development of vessel-associated calcifications. Further experiments are directed towards understanding the mechanism by which oxidative stress modulates the development of vessel associated calcifications.

C. Van Niftrik¹, M. Piccirelli², O. Bozinov¹, J. Burkhardt¹, G. Esposito¹, S. Wegener³, A. Luft³, A. Pangalu², A. Valavanis², J. Fierstra¹, L. Regli¹

Assessment of cerebral autoregulation: a combined fMRI and ASL study

Neurochirurgie, Universitätsspital, Zürich¹, Neuroradiology, University Hospital Zürich, Zürich², Neurology, University Hospital Zurich, Zurich³

Introduction:

This study aimed to assess cerebrovascular hemodynamics in healthy subjects and patients with neurovascular disease. Patients with steno occlusive neurovascular diseases have an increased risk of ischemic stroke in the affected hemisphere. Cerebrovascular mapping is increasingly used to assess Cerebrovascular Reactivity (CVR) in neurovascular patients. Impaired CVR, measured with Blood-Oxygen-Level-Dependent (BOLD) MRI, is shown to be a marker for the risk of ischemic stroke. Although BOLD is mainly dependent on cerebral blood flow (CBF), the BOLD signal is in nature multi factorial. Arterial Spin Labeling (ASL), however, primarily measures CBF and allows for direct and independent quantification. We combined ASL cerebrovascular reactivity blood flow (CVR_{CBF}) measurements and BOLD MRI cerebrovascular reactivity (CVR_{BOLD}) measurements together with controlled prospective arterial CO₂ targeting using a prospective CO₂ gas blender (Respiract™) and demonstrate how these studies can complement each other for the assessment of the cerebrovascular autoregulation. CVR is defined here as either the percent BOLD signal change per mmHg CO₂ change or the percent CBF change per mmHg CO₂ change.

Methods:

A total of 8 healthy subjects (mean age 30.4±3.5) and 5 patients (mean age 57.4±13.7) with chronic steno occlusive diseases were studied on a 3T Siemens Skyra. To correct for possible ASL post-label-delay-time errors in patients, two separate acquisitions of 2D ASL were acquired during hypocapnia and hypercapnia. CO₂ was manipulated using a pre-programmed sequence. Post processing and analysis were done using SPM12, in-house scripts for Matlab and SPSS (22.0).

Results:

Baseline CO₂ values during BOLD acquisitions for healthy subjects and patients were (Mean± STD) 40.29±1.92 and 40.84±0.97 respectively and for the hypercapnic phase 47.76±1.4 and 48.78±1.18. Whole brain CVR_{BOLD} for healthy subjects was 0.248±0.045 and for patients 0.169±0.038. In patients, the affected hemisphere showed a mean CVR_{BOLD} of 0.125±0.028 compared to 0.184±0.049 in the unaffected hemisphere.

Mean hypocapnic CO₂ during the ASL acquisitions was 33.53±2.85 and 34.30±2.91 for healthy subjects and patients resp., during hypercapnia 47.77±2.94 and 48.92±1.73. Mean hypocapnic CBF was 74.63±9.30 and 58.19±13.64 and during hypercapnia 91.25±9.63 and 70.29±16.52. CVR_{CBF} of healthy subjects is 1.596±0.63 and for patients 0.901±0.610. A good spatial agreement was found on visual examination of the CVR_{BOLD} and CVR_{CBF} maps. Regions with reduced or negative CVR_{BOLD} also showed reduced CVR_{CBF}.

Conclusion:

Combining CVR_{BOLD} and CVR_{CBF} allows for a noninvasive complementary assessment of cerebral hemodynamics with high spatial agreement.

U. Nüesch¹, B. Volkmer¹, A. Mauracher¹, A. Urwyler¹, S. Vavassori¹, J. Pachlopnik Schmid¹

Role of TTC7 in the pathogenesis of combined immunodeficiency in hereditary multiple intestinal atresia

Children's Research Center (CRC), University Children's Hospital Zürich, Div of Immunology/BMT, Zürich, Switzerland¹

Introduction:

Hereditary Multiple Intestinal Atresia (MINAT; OMIM 243150) is a rare congenital disorder characterized by a variable number of atresias throughout the small and large intestine. The disease has been linked to various mutations in the tetratricopeptide repeat domain 7A (*TTC7A*) gene and is associated with a combined immunodeficiency (CID) with profound T cell lymphopenia, decreased numbers of naïve T lymphocytes and hypogammaglobulinemia.

Methods:

In our studies we employed the flaky skin mutant mouse (*TTC7^{fsn/fsn}*), a model carrying mutations in the mouse orthologue of *TTC7A*.

Results:

We observed smaller thymi with disrupted cortico-medullar demarcation at the age of 10 weeks from *TTC7^{fsn/fsn}* mice compared to wild-type littermates. Thymocyte numbers in *TTC7^{fsn/fsn}* mice were decreased while flow cytometry analysis showed increased percentage of CD4 and CD8 double negative but decreased double positive thymocytes. Considering the importance of reciprocal signalling between developing T cells and thymic stromal cells in thymopoiesis, we anticipated that the known role of TTC7 in trafficking phosphatidylinositol-4-kinase-III α (PI4KIII α) to the inner leaflet of the plasma membrane could be involved in controlling TCR signalling by influencing the levels of phosphatidylinositols. CD4⁺ T cells from *TTC7^{fsn/fsn}* mice stimulated *in-vitro* with mitogens, or antibody mediated TCR and CD28 costimulation, showed altered Th1 and Th2 cytokine secretion. Under the same stimulatory conditions, reduced levels of TCR signalling were seen when compared with wild-type CD4⁺ T cells.

Conclusion:

Our data suggest that mutations in *TTC7A* lead to defective T cell function and activation with improper thymic structuring and output due to deficient TCR signalling during thymopoiesis.

M. Meerang¹, K. Bérard¹, B. Bitanirwe¹, M. Friess¹, E. Felley-Bosco², A. Soltermann³, B. Vrugt³, B. Seifert⁴, R. Stahel², H. Moch³, W. Weder¹, I. Opitz¹

NF2 and Hippo Pathway Dysregulation as Predictors of Survival for Mesothelioma Patients Treated with Multimodal therapy

Division of Thoracic Surgery, University Hospital Zurich, Switzerland¹, Laboratory of Molecular Oncology, University Hospital of Zurich, Switzerland², Institute of Surgical Pathology, Department of Pathology, University Hospital Zurich, Switzerland³, Epidemiology, Biostatistics and Prevention Institute, Department of Biostatistics, University of Zurich, Switzerland⁴

Introduction:

Multimodal regimen including induction chemotherapy (CTX) followed by extrapleural pneumonectomy (EPP) provides variable outcome for malignant pleural mesothelioma (MPM) patients, highlighting a need for prognostic biomarkers and novel therapeutic candidates. Neurofibromatosis type 2 gene (NF2) is one of the most frequently deleted and mutated tumor suppressor genes in MPM. NF2 inactivation results in deleterious consequences involving in tumorigenesis such as Hippo pathway alterations. Nonetheless, NF2 expression status as well as its prognostic role has not been so far investigated in MPM. Here, we assessed the prognostic value of NF2 as well as Hippo pathway alterations employing survivin, one of Hippo pathway target genes, as a functional readout.

Methods:

145 samples of MPM patients intended to be treated with CTX followed by EPP were collected pre- and post-CTX and assembled in tissue micro arrays. Expression of cytoplasmic and nuclear NF2 and survivin, were evaluated by immunohistochemistry (H-score and labeling index, respectively). Marker expression (low vs high) was associated with overall (OS) and progression free survival (PFS).

Results:

Kaplan-Meier survival curves revealed an association between low cytoplasmic NF2 expression in pre-CTX tissues with shorter PFS (median PFS (months), low = 10.7 vs high = 15.3, $p=0.02$) and OS (median OS (months), low = 11.2 vs high = 23, $p=0.03$). In post-CTX tissues, low nuclear NF2 expression was also associated with shorter PFS (median PFS (months), low = 11.1 vs high = 14.4, $p=0.04$) and OS (median OS (months), low = 14.6 vs high = 22, $p=0.05$). High nuclear survivin labeling index in both pre- and post-CTX tissues was associated with shorter PFS (pre-CTX: Median PFS (months), low = 16.6 vs high = 10.3, $p=0.02$; post-CTX: Median PFS (months), low = 14.8 vs high = 12.6, $p=0.02$).

Conclusion:

Our results revealed a prognostic significance of nuclear and cytoplasmic NF2 expression loss and alterations of the Hippo pathway for shorter survival of MPM patients receiving multimodality treatment. These results also provide a rationale for targeted treatment against NF2/Hippo pathway alterations for MPM. In addition to their importance as prognostic biomarkers, NF2 and survivin expression may be further qualified as predictive biomarkers for targeted treatment.

S. Karlen¹, E. Eschmann¹, M. Schneemann², S. Weiler³, J. Blaser¹

Too frequent Methotrexate Administrations in Non-Oncological Therapies and Technical Challenges for Preventing Prescription Errors

Medical Informatics Research Centre, University Hospital, Zurich¹, Division of Internal Medicine, University Hospital, Zurich², Pharmacology and Toxicology, University Hospital, Zurich³

Introduction:

Methotrexate (MTX) is used in the treatment of many medical conditions such as cancer as well as autoimmune diseases. In addition, scheduling of doses varies widely, from cyclical protocols for cancer chemotherapy (including high MTX doses) to weekly for autoimmune diseases such as rheumatoid arthritis and psoriasis (usually as low-dose MTX). Due to this complexity misunderstandings sporadically lead to serious incidents for patients, e.g. when MTX is administered once every morning (mo) instead of once every Monday (Mo). Serious adverse drug events include haematological toxicity, nephrotoxicity or drug-induced liver injury.

Two cases of too frequent MTX administrations have been reported in 2014 to the Critical Incident Reporting System (CIRS) at the University Hospital Zurich (USZ). In this quality control study we analysed the incidence of too frequent administrations of MTX in non-oncological therapies. Subsequently, we designed concepts for assisting the computerized prescription order entry process in order to avoid too frequent MTX administrations.

Methods:

We included all inpatients admitted to the USZ from 12/2/2009 to 06/30/2014 and retrospectively analysed all MTX medication orders and administrations in the electronic health record. Medication data during intensive care stays were not available electronically and were therefore excluded. Prescriptions of MTX unambiguously linked to chemotherapy through oncological order sets were also excluded.

The remaining orders were analysed to identify patients with more than one administration prescribed per week. A clinician then scrutinized the list of patients based on their medical records to identify errors in the context of non-oncological MTX therapies.

A prescription error was defined as a failure in the treatment process that leads to, or has the potential to lead to, harm to the patient.

Results:

We analysed all medications administered to 113,894 inpatients. 2,341 MTX prescriptions were ordered to 802 patients. 1,093 prescriptions linked to chemotherapy order sets were excluded. 67 cases with more than one MTX administration per week were identified in the remaining 1,248 prescriptions. Manual scoring yielded that 53 of the 67 cases related to chemotherapies or special protocols.

The remaining 14 cases were identified as MTX prescription errors, including the 2 cases previously reported to CIRS: 5 errors resulted in too frequent administrations with 3 errors leading to major adverse events. The other 9 prescription errors did not reach the patients and were near misses only. Noteworthy was the observation that in 6 out of the 14 cases (43%) more than one MTX prescription was involved.

Conclusion:

On average, too frequent MTX administrations in non-oncological therapies were ordered for 3 patients per year (i.e. in 1.7% of all patients treated with MTX).

Computer-based clinical decision support may be useful to reduce these prescription errors. However, a real-time quality control check of individual prescriptions is insufficient. Overlapping and adjacent MTX prescriptions need to be considered as well as to reliably detect too short administration intervals.

K. Dräger¹, I. Bhattacharya¹, P. Seebeck⁵, U. Held², A. Azzi³, S. Brown³, M. Hall⁴, R. Humar¹, E. Bategay¹, E. Haas¹

Knockout of Rictor in adipocytes and brain increases mean arterial pressure and locomotor activity

Research Unit - Division of Internal Medicine, University Hospital Zurich, Switzerland¹, Horten Center for Patient-Oriented Research and Knowledge Transfer, University of Zurich, Switzerland², Chronobiology and Sleep Research Group, Institute of Pharmacology and Toxicology, ³, Biozentrum, University of Basel, Switzerland⁴, Zurich Center for Integrative Human Physiology, Switzerland⁵

Introduction:

The serine/threonine kinase mammalian target of rapamycin (mTOR) is a kinase found in two complexes: mTORC1 and mTORC2. The latter is characterized by the adaptor protein RICTOR and is activated by growth factors such as insulin. mTORC2 controls essential functions in white adipose tissue, while little is known about its role in perivascular adipose tissue (PVAT) surrounding most arteries. PVAT is an emerging regulator of the vascular tone and we have shown that mTORC2 is necessary for the physiological function of PVAT. In the present study, we assessed whether adipose and brain mTORC2 contributes to blood pressure regulation and locomotor activity.

Methods:

Rictor^{fl/fl} mice were crossed with C57BL/6J mice expressing CRE recombinase under the control of the *fabp4/aP2* gene promoter to generate *Rictor^{aP2KO}* mice. In all experiments, male mice (18-23 weeks old) were used. Control group consisted of littermates without the *cre* transgene, *Rictor^{fl/fl}*, termed henceforth control. Blood pressure recordings were performed using radiotelemetry, measuring hemodynamic and locomotor activity parameters over 7 days (n = 5-6). mRNA and protein levels were analyzed by performing qRT-PCR and Western Blot, respectively.

Results:

Blood pressure recordings revealed a significant increase in the 24-h average of mean arterial pressure (103.9 ± 1.1 vs. 98.5 ± 1.4 mmHg) and diastolic arterial pressure (94.6 ± 1.4 vs. 90.2 ± 0.6 mmHg) in *Rictor^{aP2KO}* mice, while systolic arterial pressure and pulse pressure were not significantly different between groups. Interestingly, physiological dipping of mean arterial pressure was strongly compromised in *Rictor^{aP2KO}* mice during dark period. Concurrently, active time and intensity of locomotor activity were increased in *Rictor^{aP2KO}* mice. Expression analysis revealed that *Rictor* was downregulated in brain and adipose tissue of *Rictor^{aP2KO}* mice. Differential expression of clock genes between groups was detected in adipose but not in brain tissue.

Conclusion: mTORC2 in adipose and brain tissue regulates mean arterial pressure and locomotor activity, possibly by affecting clock gene expression in adipocytes.

C. Waschkies¹, T. Reding Graf¹, G. Seleznik¹, U. Ungethuen¹, R. Graf¹

Magnetic Resonance Imaging of the Pancreas in a Transgenic Mouse Model of Pancreatic Carcinogenesis

Pancreatitis-Research Laboratory, Division of Visceral and Transplantation Surgery, University Hospital Zurich, Zurich¹

Introduction:

MRI has been appreciated in the clinical assessment of various pancreatic diseases such as pancreatitis and in the diagnosis of pancreatic cysts and tumors. However, only few preclinical studies infer upon MRI to assess and monitor pancreatic tissue changes in the commensurate animal models, mostly due to the inherently low conspicuity of the murine pancreas, its more amorphous presentation and splayed out position within the retroperitoneum and abdominal cavity.

Pancreatic inflammation is a risk factor for pancreatic ductal adenocarcinoma development in humans, and its initiation is linked to activating mutations in KRAS oncogene (p48+/Cre;Kras+/G12D, referred to as KC model here) with acinar cells undergoing ductal reprogramming through premalignant pancreatic intraepithelial neoplasia lesions, finally leading to tumor formation. Here we explore the potential of preclinical in vivo MRI to visualize the murine pancreas and assess changes associated with cellular transformations in this mouse model of pancreatic carcinogenesis.

Methods:

MR imaging was performed on a 4.7T/20 cm Bruker PharmaScan unit equipped with transmit/receive a 40 mm bird-cage resonator. Motion-gated T1-weighted FLASH sequences (TE/TR 5/410ms, FA 80°, NA 4, MTX 256x256) w/o fat suppression and Magnetization Transfer prepulses (1.5 kHz offset, 0.4 kHz bandwidth, 20, 40 and 60 uT pulse strength), and quantitative T2 images (MSME sequence, PD and T2 weighted, TE/TR 15 resp. 75/426ms, NA 4) were acquired in 11 image slices at a spatial resolution of 117x117x700um³. Two wildtype and KC mice underwent two MRI examinations, without and with prior oral contrast (10ml/kg paramagnetic ion rich blueberry fruit juice administered by oral gavage). During MRI mice were intubated, mechanically ventilated and maintained under 1.8-2% isoflurane anesthesia in a 1:5 oxygen:air mixture. Animals were placed supine onto a heated animal bed and fixed by adhesive tapes to reduce respiratory motion at the level of the pancreas. Throughout the MRI procedure body temperature of the animals was kept at 37°C and respiratory motion was continuously monitored.

Results:

High-resolution abdominal images were obtained from all animals. The pancreas was identified and outlined anatomically by locating the head of the pancreas using the posterior border of the stomach, spleen and kidney as anatomical landmarks and tracing it through subsequent posterior slices. In the KC mice the pancreas was found to be substantially enlarged and to extend laterally into the right side of the animal, confirmed by autopsy after the MRI examination. Contrast-enhancement with oral contrast agent facilitated delineation of the pancreas by providing contrast to surrounding intestinal structures. Furthermore, KC pancreatic mass presented as heterogenous in T2- and T1-weighted images. Conspicuous globular foci of <200um in diameter were distinguished in one KC animal and in ex vivo KC pancreas preparations, possibly depicting acinar and ductal metaplasia in this animal model. However, quantitative analysis of MRI tissue parameters such as T2, fat and macromolecular content were inconclusive.

Conclusion:

Robust imaging methods have been set up to visualize the murine pancreas. Yet, more quantitative measures of tissue transformation beyond anatomical presentation still remain to be established.

U. Graf¹, FA. Weber¹, E. Vollenweider², G. Wanner¹, H. Koseki⁴, J. Wong³, R. Santoro², P. Cinelli¹

The ubiquitin proteasome system regulates epigenetic remodeling in pluripotent cells

University Hospital Zurich, Division of Trauma Surgery¹, University of Zurich, Institute of Veterinary Biochemistry and Molecular Biology², Institute of Biomedical Sciences and School of Life Sciences, Shanghai Key Laboratory of Regulatory Biology, China³, Developmental Genetics Laboratory, RIKEN Center for Integrative Medical Sciences, Yokohama City, Japan⁴

Introduction:

Maintenance of pluripotency in embryonic stem cells (ESCs) relies on a complex interplay between transcription factors and epigenetic modifiers as well as microRNAs (miRNAs) non-coding RNAs (ncRNA) and components of the protein processing machinery like the ubiquitin proteasome system. Even though the functions of these different key players have extensively been studied, the mechanisms underlying their interplay remain largely elusive.

For the first time, we present data highlighting the importance of the ubiquitin proteasome system in mediating global epigenetic remodeling in pluripotent stem cells and its essential role in maintaining ESCs in a pluripotent self-renewing state. We show that Prame17 (Preferentially Expressed Antigen in Melanoma-like 7), a protein exclusively expressed in pluripotent cells, functions as a substrate recognition component of the proteasome system and mediates the targeted dose-dependent, rapid and reversible degradation of Ubiquitin-like, containing PHD and RING finger domains, 1 (UHRF1/Np95/ICBP90), a process which further leads to a drastic reduction of global DNA methylation and impairment of terminal differentiation in pluripotent cells.

Like Prame17, other members of the PRAME family are exclusively detected during distinct stages of the preimplantation development. Thus, it is possible that also other proteins of the PRAME family are involved in chromatin remodeling. Last but not least our data open a new vision in understanding the role of PRAME in cancer progression, since PRAME expression could confer stem cell properties to cancer cells by a similar mechanism described for Prame17.

F. Aimi¹, S. Georgiopolou¹, I. Kalus¹, F. Lehner¹, N. Lindenblatt², I. Bhattacharya¹, V. Gomes de Lima¹, E. Haas¹, M. Rüegg³, M. Hall³, E. Battegay¹, R. Humar¹

Deletion of endothelial Rictor (mTORC2) constrains extensive FGF2 -induced vascular remodeling and growth in vivo and disables endothelial network formation in vitro

Division of Internal Medicine, University Hospital, Zurich¹, Division of Surgical Research, University Hospital, Zurich², Biozentrum, University of Basel, Basel³

Introduction:

Blood vessels evolved to carry oxygen to distant organs. Not surprisingly, they are crucial for organ growth in embryos and for repair of wounded tissue in adults. But an imbalance in angiogenesis, the growth of new blood vessels, promotes malignancies and ocular and inflammatory disorders. Blocking endothelial signaling specifically promoting aberrant angiogenesis would be ideal to treat vascular-dependent pathologies. Here we explored endothelial signaling via mammalian target of rapamycin complex 2 (mTORC2) and its contribution to angiogenesis in vivo and in vitro.

Methods:

To assess distinct roles of mTORC2 in angiogenesis we disabled this complex by deleting two exons of the essential mTORC2 component Rictor by a Cre-lox approach. In vitro, lentiviral transduction of a constitutive Cre recombinase resulted in primary Rictor knockout endothelial cells that were used for several biochemical and cell biological analysis. In vivo, a Tamoxifen-inducible Cre recombinase that was expressed under a VE-Cadherin promoter delivered endothelial deficiency of mTORC2 in mice, which were used in two assays to assess vascular morphological changes, i.e. the dorsal skinfold chamber and the matrigel plug assay.

Results:

In vitro, Rictor knockout (ko) specifically disabled mouse aortic endothelial cells (MAECs) to form capillary-like networks on matrigel in response to FGF2, while VEGFA supported the formation of a stable network composed by MAECs with deficient mTORC2 signaling. Rictor ko MAECs cells did not display significant reduction in FGF2- or VEGFA-induced proliferation or migration. In response to FGF2 and VEGFA, Rictor ko strongly reduced Akt^{Ser473} phosphorylation and reduced PKC α activity by blunting total PKC α protein levels. No other signaling pathways were significantly affected by Rictor ko. In vivo, deletion of the essential mTORC2 component Rictor in the endothelium (Rictor^{i Δ ec}) of adolescent mice did not affect physiologic angiogenesis or blood vessel integrity. In contrast Rictor^{i Δ ec} specifically blocked extensive remodeling and capillary dilation when the dorsal skin capillary bed was stimulated with a high dose of FGF2. Similarly, Rictor^{i Δ ec} strongly reduced de novo angiogenesis into FGF2-loaded Matrigel plugs and prevented hemorrhage in adolescent mice. Preliminary results indicate increased levels of FGF2- but not VEGF-induced VEGFR3 message after Rictor ko in MAEC. Currently, FGF2- and VEGFA-induced transcriptomic and secretomic changes are assessed in Rictor ko versus control MAECs and might shed further light on the molecular mechanisms behind mTORC2-dependent angiogenic processes.

Conclusion:

Thus, here we demonstrate for the first time that deactivation of the mTORC2 multi-protein kinase in the endothelium by deleting the essential component Rictor severely impacts FGF2-induced vascular remodeling and de novo angiogenesis in vivo and endothelial network-formation in vitro.

S. Frese¹, M. Auer¹, E. Rushing², M. Toigo³, J. Petersen¹, H. Jung¹

Exercise effects in Huntington's disease

Department of Neurology, University Hospital of Zurich, Switzerland¹, Department of Neuropathology, University Hospital, Zurich², University Hospital Balgrist, University of Zurich, Zurich³

Introduction:

Huntington's disease (HD) is an relentlessly progressive neurodegenerative disorder based on CAG-triplet-expansion in the Huntingtin gene. Clinical hallmarks of HD are choreatic movement disorders, cognitive dysfunction and psychiatric alterations. Recently it was recognized that HD is not confined to the central nervous system, but also affects other tissues including muscle, leading to muscle wasting. In HD animal models, physical exercise delays the onset of symptoms and ameliorates cognitive impairment. However, in human HD patients the effects of exercise on disease progression has never been examined.

We investigated whether endurance training (ET) can stabilize and/or reverse the progression of motor and cognitive impairment, the decline of muscle structure and function, and whether ET ameliorates cardiovascular function in HD patients.

Methods:

Nine male HD patients (mean \pm SD, age: 59.3 ± 4.7 yrs; BMI: 25.6 ± 4.0 kg·m⁻²; CAG repeats: 39 - 44) and twelve male healthy controls (Ctrls, 51.7 ± 6.8 yrs; BMI: 26.2 ± 4.1 (kg·m⁻²) participated in this study. HD patients and Ctrls underwent a specific ET regimen for 6 months. Assessments were carried out immediately before (PRE) and after (POST) ET. In order to examine the natural course of the disease, HD patients were assessed 6 months ahead of the ET as well. Assessments included the UHDRS (Unified Huntington's Disease Rating Scale), a battery of neuropsychological tests, as well as histological and ultrastructural analyses of muscle tissue, body composition and functional tests.

Results:

HD patients with less than 44 CAG repeats (n=8) exhibited a significantly reduced disease progression during ET (-2.2 UHDRS-points) as compared to the observation period (+8.1 UHDRS-points). Neuropsychological tests revealed major cognitive deficits in HD patients, particularly regarding executive function, attention and attention related psychomotor coordination. Cognitive function was not significantly altered during ET. In all subjects (HD and Ctrls), body mass, BMI and lean mass were stable throughout the study. With ET, leg lean mass increased by 2.0 % and whole body fat decreased by 4.6 % in Ctrls (both $p < .05$; POST vs PRE), but not in HD patients. HD patients and Ctrls did response positively to ET regarding peak oxygen uptake (ml·kg⁻¹·min⁻¹) in the graded cycling exercise test (HD +12.5 %, Ctrls +9.9 %; both $p < .05$, POST vs PRE), peak power output (Watt·kg⁻¹; HD +19.0 %, $p < .01$, and Ctrls +19.2 %, $p < .001$; POST vs PRE), and time to exhaustion in the constant-load cycling exercise test (HD 126.2 %, Ctrls 113.2 %; both $p < .01$, POST vs PRE). All exercise physiological parameters exhibited a significant overall time difference, some an additional group difference. Muscle analyses of ragged red fibers, COX negative fibers and mitochondrial abundance did not reveal mitochondrial dysfunction in both groups.

Conclusion:

For HD patients with small CAG expansions, ET may be effective to slow disease progression, as assessed with the UHDRS, while no significant effects were seen for the entire group of HD patients. During the observation period, parameters for body composition and endurance capacity remained stable in HD patients. In addition, HD patients showed an increase in endurance capacity as indicated by an improvement in cardiovascular and muscular function.

V. Sennrich¹, A. Maric¹, J. Leemann¹, S. Weissengruber², C. Ruff², C. Baumann¹, R. Poryazova¹

Reduced Risk Aversion After Chronic Sleep Restriction But Not After Acute Sleep Deprivation

Department of Neurology, University Hospital of Zurich, Zurich¹, Department of Economics, University of Zurich, Zurich²

Introduction:

Various studies showed an effect of acute sleep deprivation (aSD) on risky decision making. Chronic sleep restriction (cSR) mirrors everyday life better than aSD. It is not yet clear if and how chronic sleep restriction (cSR) affects decision making behavior. Such sleep restriction particularly affects people in positions with vast responsibilities including managers, scientists, or politicians, where risky decisions could have far-reaching consequences. Our study investigates the influence of both aSD and cSR on decision making under conditions of risk and uncertainty.

Methods:

We studied decision making behavior under risk in eight healthy males. Their risk preferences were assessed prior to and after cSR (reduction of sleep duration from 8h/night to 5h/night over the period of one week) as well as prior to and after aSD (one night of total sleep deprivation). The risk task (RT, adapted from Levy and colleagues) allows the measurement of the model-free risk aversion ratio ($\frac{\sum(\text{chosen safe options})}{\sum(\text{chosen risk options})}$). A paired samples t-test was performed with $p < 0.05$ considered as significant.

Results:

The risk aversion ratio significantly decreased after cSR (mean \pm SD: $-32.9\% \pm 23.7\%$, $p < 0.05$). Meanwhile, no significant effects could be assessed for aSD ($13.7\% \pm 46.1\%$, $p = 0.789$).

Conclusion:

Preliminary results of our ongoing study indicate that risk aversive behavior is notably decreased after cSR. Therefore, cSR and aSD might have distinct effects on risk aversion. These findings are a first step towards understanding risk taking behavior under cSR.

M. Kirschner¹, Y. Cheng², N. Armstrong³, R. Lin², S. Kao², A. Linton², S. Klebe⁴, B. McCaughan⁵, N. Van Zandwijk², G. Reid²

MiR-Score: A 6-microRNA signature for prognosis in malignant pleural mesothelioma

Asbestos Diseases Research Institute, Sydney, Australia *since 15.11.2014 *Division of Thoracic Surgery, Isabelle Opitz/Walter Weder, Zürich¹, Asbestos Diseases Research Institute, Sydney, Australia², School of Mathematics and Statistics, University of Sydney, Sydney, Australia³, Department of Anatomical Pathology, Flinders Medical Centre, Adelaide, Australia⁴, Sydney Cardiothoracic Surgeons, RPA Medical Centre, Sydney, Australia⁵*

Introduction:

Prognosis for malignant pleural mesothelioma (MPM) is poor, and predicting the outcome of treatment is particularly difficult. Here we identified a 6-microRNA signature, the miR-Score, as novel prognostic factor for mesothelioma patients.

Methods:

Candidate microRNAs from microarray profiling of tumour samples long (median: 53.7 months) and short (median: 6.4 months) survivors were validated in 48 tumour samples from patients undergoing extrapleural pneumonectomy (EPP). Kaplan-Meier log ranking was used to further explore the association between microRNA expression and overall survival (OS). A microRNA expression signature for prediction of ≥ 20 months OS was built using binary logistic regression modelling. Performance of the signature (miR-Score) was evaluated by receiver operating characteristics curve analysis. The miR-Score was then independently validated in 43 tumour samples from patients undergoing palliative pleurectomy/decortication (P/D) surgery.

Results:

The miR-Score including 6 microRNAs, miR-21-5p, -23a-3p, -30e-5p, -221-3p, -222-3p and -31-5p, was able to predict a long survival with an accuracy of 92.3% in patients undergoing EPP and an accuracy of 71.9% in patients receiving palliative P/D. Score-positive patients showed increased median overall survival of 23 and 9 months for EPP and P/D, respectively. Hazard ratios for score-negative patients were 4.12 (95% CI: 2.03–8.37, $p=0.00001$) for EPP and 1.93 (95% CI: 1.01–3.69, $p=0.047$) for P/D. Furthermore, adding the miR-Score to a set of clinical factors (histology, age, gender) resulted in improved predictive accuracy in the independent validation cohort.

Conclusion:

This study has identified a novel microRNA signature, the miR-Score, which can accurately predict prognosis of MPM patients.

The miR-Score will now be validated in a large independent sample series of surgical specimens and diagnostic biopsies available to the Division of Thoracic Surgery, University Hospital Zurich. Mechanistical investigation of the functional relevance of the miR-Score microRNAs will also be performed in Zurich.

D. Heuberger¹, A. Franchini¹, R. Schuepbach¹

Thrombomodulin-thrombin complex activates pro-inflammatory signaling pathway via protease-activated receptor 2

Division of Surgical Intensive Care, University Hospital Zurich, Zurich¹

Introduction:

Protease-activated receptors (PARs) are G-protein coupled seven transmembrane proteins, sensing for extracellular proteolytic activity. Thrombin is the prototypical activator for three highly related receptors (PAR1, 3 and 4) whereas PAR2 was believed to uniquely be activated by proteases other than trypsin. We wondered whether thrombin recruited to the cell surface by thrombomodulin (TM) activates PAR2 and whether this activation drives inflammation.

Methods:

To determine whether co-receptors improve the efficiency of thrombin to cleave PAR2, a well-established PAR-cleavage reporter assay was used. It bases on chimeric PAR expression constructs that carry a secreted alkaline phosphatase (AP) tag at the extracellular N-terminus of PAR, allowing colorimetric measurement of PAR cleavage events. The AP-PAR2 construct alone or together with the co-receptor thrombomodulin were transiently overexpressed in HEK T293 cells and clotting proteases were tested for PAR cleavage efficiency. The induction of pro-inflammatory signaling pathway NF- κ B was measured in lung adenocarcinoma cell line A549 by interleukine-8 (IL-8) with immunoassays. The genes involved PAR1, PAR2 and thrombomodulin were silenced by transfection of A549 cells with small-interfering RNA (siRNA) molecules.

Results:

We found that PAR2 was cleaved by thrombin in presence of the cell surface co-receptor thrombomodulin. Incubation of the lung adenocarcinoma cells A549 constitutively expressing TM, PAR1 and PAR2 with thrombin sustained induction of IL-8 secretion, even if PAR1 or PAR2 were silenced by siRNA alone. Silencing both PAR1 and PAR2 however blunted effects of thrombin.

Conclusion:

Our experiments in overexpression systems supported that PAR2 can be cleaved and activated by thrombomodulin bound thrombin. In natively PAR2 expressing cells we provide evidence, that thrombomodulin-thrombin activation of PAR2 support pro-inflammatory stimuli. Since thrombin and PAR2 have been found to be key players in chronic inflammation we speculate that this pathway might be of therapeutically potential in inflammatory driven diseases.

P. Valko¹, B. Roschitzki², W. Faigle¹, J. Grossmann², C. Panse², P. Biro³, M. Dambach³, D. Spahn³, M. Weller¹, C. Baumann¹

In Search of CSF Biomarkers of Fatigue in Multiple Sclerosis. A Proteomic Study.

Department of Neurology, University Hospital of Zurich, Switzerland¹, Functional Genomic Center Zurich, 8057 Zurich, Switzerland², Institute of Anaesthesiology, University Hospital, Zurich³

Introduction:

Fatigue represents one of the most frequent and disabling complaints in patients with multiple sclerosis (MS). Our ability to offer a tailored treatment, however, is hampered by a fundamental lack of insight into the neurobiological mechanisms underlying this major symptom.

Methods:

To identify potential biomarkers of MS-related fatigue, we compared the cerebrospinal fluid (CSF) proteome of 20 MS patients with fatigue (MS-F), 20 MS patients without fatigue (MS-wo) and 20 healthy and non-fatigued control subjects (CS). After tryptic digestion, the samples were analyzed on a liquid chromatography – mass spectrometry (LC-MS). Protein identification was performed using the Mascot search algorithm and LC-profile alignment and quantification was done using three different analytic approaches, including Progenesis LC-MS software package and spectral counting. Fatigue was assessed with the Fatigue Severity Scale; scores were > 5 in the MS-F groups, and < 3 in the MS-wo group. Candidate proteins showing differential levels between groups were subjected to Western blot analysis, in order to validate the results obtained by mass spectrometry.

Results:

In summary, we identified a total of 591 CSF proteins. By application of the two different analytic approaches, we found 9 proteins that showed different CSF levels among the three groups as well as between the two MS groups (Alpha-1-antichymotrypsin, Neural cell adhesion molecule L1-like protein, Protein kinase C-binding protein NELL2, Neurosecretory protein VGF, Reelin, Peptidyl-glycine alpha-amidating monooxygenase, Voltage-dependent calcium channel subunit alpha-2/delta-1, Receptor-type tyrosine-protein phosphatase zeta, Thy-1 membrane glycoprotein). Seven additional proteins showed differential abundance in the CSF of the two MS groups in both analytic approaches (Zinc-alpha-2-glycoprotein, Beta-2-glycoprotein 1, Tyrosine-protein phosphatase non-receptor type substrate 1, Chitinase-3-like protein 1, Neurotrimin, N-acetylmuramoyl-L-alanine amidase, Protein NOV). Using Western blot, we found the same group differences for the following candidate proteins: Protein kinase C-binding protein NELL2, Reelin, and Neural cell adhesion molecule L1-like protein. In all of them, protein levels were lowest in MS patients with fatigue.

Conclusion:

Our findings suggest that CSF proteomic pattern analysis has the potential to identify biomarkers of fatigue. Here, we identified several candidate proteins and validated the differential levels of three of them by a second method. These proteins are involved in the regulation of synaptic plasticity and energy homeostasis and it seems therefore plausible that decreased levels may contribute to fatigue.

L. Macrea¹, D. Spahn¹, K. Maurer¹

Pain-Out - Quality of postoperative pain management in lung surgery. A survey study.

Institute of Anesthesiology / Interdisciplinary Pain Clinic / Pain Research Unit¹

Introduction:

Every year, surgery is performed on over 40 million patients in Europe. Data registries with standardized data collection are optimal for the continuous measurement of the quality of postoperative pain, benchmarking of results and improvement of treatment quality. In patient having thoracic surgery 10-50% will develop a chronic pain condition. We compared postoperative outcomes for patients with any type of lung surgery (LS) with other participating hospitals in the pain-out data base.

Methods:

After informed consent, patients with any type of LS (thoracotomy, thoracoscopy) were recruited from thoracic surgery (TS) wards the first postoperative day and questioned about their pain condition. Pain-Out questionnaires / methodology was used. We report only on the results of the pain-out outcome questionnaire (pain severity, interference, emotional impairment, adverse effects and perception of care) Obtained results were compared by ranking with the existing benchmark groups in the pain-out data base.

Results:

We included 147 LS patients (63% men) which were compared with the benchmark group of 144 thoracic surgery patients ranked in eight groups. The mean worst pain score was 5.7 (SD=2.8) 5th rank. Mean percentage of time with severe pain was evaluated at 25.7% (SD=22.2) 8th rank. Pain interference with activities in bed or out of bed was evaluated on 0-10 scale. Interference with activities out of bed was 3.3 (SD=2.5) both were ranked 4th. Pain effect on mood and emotions was assessed on 0-10 scale. Pain induced anxiety was 2.7 (SD=2.7) 5th rank and pain induced helplessness was 2.9 (SD=3.1) 7th rank. Postoperative nausea and drowsiness was evaluated on a 0-10 scale. Nausea score was 2.1 (SD=3.1) 8th rank and drowsiness 2.2 (SD=2.7) 2nd rank. 16% of patients would have preferred to receive more pain treatment (6th rank). Satisfaction with the result of pain treatment was evaluated on a 0-10 scale and was 8.2 (SD=2.4) 8th rank.

Conclusion:

Postoperative pain in lung surgery is a major issue and many patients report on high pain scores and with long lasting pain periods. Side effects (nausea) is despite the low scores a issue comparing to the benchmark. Pain induced emotional impairment was adequate. Satisfaction with the pain treatment was lower than in the benchmark groups. This evaluation showed that improvements should be done in the postoperative pain process.

B. Vrugt¹, E. Felley-Bosco², S. Simmler¹, M. Storz¹, M. Friess³, A. Soltermann¹, W. Weder³, H. Moch¹, I. Opitz³

Changes in biomarker profil and dedifferentiation during progression of malignant pleural mesothelioma

Institute of Surgical Pathology, University Hospital Zurich, Zurich¹, Laboratory of Molecular Oncology, University Hospital Zurich, Zurich², Division of Thoracic Surgery, University Hospital Zurich, Zurich³

Introduction:

Malignant pleural mesothelioma (MPM) is a highly aggressive tumor arising from the mesothelial lining of the pleural cavity. The recurrence rate of the tumor is high and therefore we evaluate the prognostic impact of morphological and immunohistochemical changes in MPM during disease progression.

Methods:

Clinical characteristics and histological samples of 48 patients with MPM (36 epithelioid, 8 biphasic and 4 sarcomatoid) were investigated. Tissue microarrays were constructed from paraffin-embedded tissue samples taken before therapy, during cytoreductive surgery and at the time point of tumor recurrence. Immunohistochemical stainings for calretinin, cytokeratin 5/6 (CK5/6) and Wilm's tumor-1 (WT-1) as well as the biomarkers mesothelin, osteopontin, and fibulin-3 were performed and staining intensity and percentage of positively stained tumor cells scored semiquantitatively. The results were compared with clinicopathological characteristics of the patients including overall survival (OS). To determine the prognostic value of the markers at the different timepoints a multivariate analysis including all factors that were significant in univariate analysis was performed.

Results:

Not surprisingly patients with epithelioid MPM (n=36) in the diagnostic biopsy had a significantly better OS (30 months; 95% confidence interval (CI): 23-38 months) in comparison to patients with biphasic (n=8) (17 months; 95% CI: 13-23 months) and sarcomatoid MPM (n=4) (5 months; 95% CI: 3-8 months) respectively (p<0.0005). In the group with epithelioid MPM in the diagnostic biopsy the expression of calretinin (p=0.01), CK5/6 (p=0.02), membranous (p=0.02) and cytoplasmic mesothelin (p=0.03) and fibulin-3 (p=0.006) significantly decreased during the course of the disease. In contrast no significant alterations in the immunoreactivity of WT1 and osteopontin were noticed. Low calretinin and high fibulin-3 expression in the pretreatment samples was significantly associated with shorter OS (p=0.045 and 0.004 respectively). On multivariate analysis, high fibulin-3 in diagnostic biopsies was found to be an independent prognosticator of poor survival (p=0.02).

In 33% of patients with the initial diagnosis of epithelioid MPM, histological comparison of the pretreatment samples with the surgical specimens and tissue samples at recurrence revealed a transition towards a biphasic or sarcomatoid growth pattern. This dedifferentiation was associated with significantly decreased expression of calretinin (p=0.02), membranous (p=0.03) and cytoplasmic mesothelin (p=0.04) in the recurrent tumor as well as a shorter overall survival (p=0.007).

Conclusion:

In patients with epithelioid MPM, disease progression is accompanied with decrease in calretinin, mesothelin and fibulin protein expression. Both high fibulin-3 expression in pretreatment samples and dedifferentiation are independent predictors of a shorter OS.

J. Mata Pavia¹, D. Wyser¹, A. Kalyanov¹, C. Germanier², M. Rudin², M. Wolf¹

Hypoxia Measurements on Mice with Near-infrared Optical Tomography (NIROT) and Fluorescence Molecular Tomography (FMT)

University Hospital Zürich, Neonatology¹, ETH Zürich²

Introduction:

The oxygenation state of tumors has a strong impact on the survival rate of patients. Previous studies have demonstrated that the survival rate is about 40% lower for patients suffering from hypoxic tumors than for patients with normoxic tumors. However, there is no established method to measure tumor oxygenation in clinical practice. Fluorescence molecular tomography (FMT) is capable of detecting the hypoxic state of tumors by measuring the light emission of a fluorescence protein that is produced under hypoxic conditions and expresses the amount of hypoxia inducible factors (HIF) in the cells. However, FMT can only be employed in preclinical research with small animals, since the use of fluorescence dyes in humans is still a topic under study. Near-infrared optical tomography (NIROT) is a non-invasive method that has been employed in studies with humans to measure the oxygenation state of tissue. NIROT measures the absorption spectra of hemoglobin in blood, from which the oxygen saturation in tissue can be calculated.

Methods:

We present, to our knowledge, the first combined FMT and NIROT setup for small animal imaging. The goal of this setup is to compare measurements performed with FMT and NIROT to gain knowledge about how the oxygenation state of tumors and HIF expression correspond to better understand the behavior of tumors under hypoxic conditions. A novel NIROT reconstruction algorithm employing wavelength normalization is also presented. The wavelength normalization reduces the constraints of the algorithm on the accuracy of the model that is being employed.

Results:

Hypoxia measurements on two mice, both containing subcutaneous tumors, were performed. The obtained results validated the novel algorithm and hypoxia measurements obtained with NIROT and FMT could be compared. A good correspondence was observed between the hypoxia measurements obtained with the two methods.

Conclusion:

We were able to show that both methods are able to determine the location of hypoxic tissue on mice under certain conditions. The presented results pave the way towards new experiments in which the HIF expression will be studied for different tissue oxygenation states.

T. Reding¹, G. Seleznik¹, A. Dittmann¹, A. Perren², R. Graf¹

Gastrokine as a novel potential biomarker for premalignant pancreatic lesions

Swiss HPB (Hepato-Pancreatico-Biliary) Centre, Department of Visceral and Transplant Surgery, Zurich University Hospital, Zurich¹, Institute of Pathology, University of Bern²

Introduction:

Gastrokine (GKN1-3) is a secreted auto-/paracrine protein in the gastric mucosa which shows growth factor or 'cytokine-like' activity toward gastric epithelial cells. GKN expression is so far believed to be almost exclusive to the stomach, except for trace levels in the uterus and placenta and scattered expression in the duodenum. In the stomach, GKN expression is confined to the gastric epithelium, where individual paralogs (GKN1-3) manifest remarkable cell-type-specific localization on different mucus-secreting epithelial lineages. Definitive physiological functions have not been formally ascribed to GKNs; however, the limited published evidence suggests fundamental roles in regulating gastric epithelial homeostasis and tumor suppression. While current research focusses on the exploration of tumor-suppressive properties of GKN1 regarding gastric tumors, nothing is known about GKN expression and function in other organ systems. Within the frame of a whole genome microarray analysis of a mouse model for pancreatic carcinogenesis (KrasxPtf1a), we have found gastrokines strikingly upregulated in the pancreas.

Methods:

The aim of the study is to investigate gastrokine expression and function during pancreatic carcinogenesis. Microarray results were confirmed by RT-PCR in different mouse models (pancreatitis and pancreatic carcinogenesis). Gastrokine expression was visualized by immunohistochemistry. Presence of Gastrokine in mouse pancreatic juice was shown by proteomic analysis.

Results:

Gene expression analysis showed high gastrokine expression during mouse pancreatic carcinogenesis, and in human patients with pancreatic malignancies. Gkn expression in normal pancreas was undetectable, and in samples with pancreatic inflammation a mild, insignificant elevation was identified. Immunohistochemistry revealed strong gastrokine expression in premalignant PanIN lesions. GKN1 was abundant in the cytoplasm of dysplastic epithelium whereas GKN2 was localized on associated inflammatory cells. Elisa and proteomics analysis in mouse confirmed the secretion of GKN1 into pancreatic juice but not serum.

Conclusion:

We identified for the first time gastrokine expression in neoplastic human and mouse pancreatic tissues. GKN expression is specific for premalignant PanIN lesions and it is secreted into the pancreatic juice during pancreatic carcinogenesis. Therefore, gastrokine could serve as a potential biomarker for early pancreatic pre-neoplastic lesions.

G. Seleznik¹, T. Reding¹, A. Perren², E. Diamantis², M. Heikenwaelder^{*3}, R. Graf^{*1}

Lymphotoxin Promotes Acinar Cell Reprogramming and Accelerates Pre-neoplastic Conversion in Kras Induced Pancreatic Tumorigenesis

Swiss HPB (Hepato-Pancreatico-Biliary) Centre, Department of Visceral and Transplant Surgery, Zurich University Hospital, Zurich ¹, Institute of Pathology, University of Bern², Institute for Virology, Helmholtz-Centre Munich, Germany³

Introduction:

Pancreatic inflammation is a well-known risk factor for pancreatic ductal adenocarcinoma (PDAC) development in humans. PDAC initiation is linked to activating mutations in KRAS oncogene. Pancreatic acinar cell transdifferentiation results in acinar-to-ductal metaplasia (ADM), which can give rise to pancreatic intraepithelial neoplasia (PanIN), the most common PDAC precursor.

Methods:

The aim of the study is to explore the inflammatory mechanisms promoting ADM and PanIN development. We established a new genetic model (LTKC) by intercrossing $p48^{+/Cre};Kras^{+/G12D}$ (KC) model for pancreatic tumorigenesis, to a transgenic mouse developing spontaneous pancreatitis, due to Lymphotoxin (LT) overexpression.

Results:

Lymphotoxin overexpression in mice harbouring an activating Kras mutation in the pancreas (LTKC) dramatically accelerates the development of premalignant PanIN lesions compared to KC animals. Already after 6 weeks extensive ADM and PanIN development are observed in LTKC mice. This coincides with significant upregulation of inflammatory genes and increased Ras activity. These molecular and phenotypic changes were observed around 16 weeks in Kras animals. *In vitro* experiments show that LT overexpression in wt acinar cells is sufficient to initiate spontaneous transdifferentiation. Furthermore, acinar cells derived from LTKC animals form ADMs significantly faster than acini from KC animals. Pharmacological inhibition of LTbR signalling mitigated inflammatory environment and moderated PanIN development in both KC and LTKC models.

Conclusion:

We conclude that Lymphotoxin may contribute to the initiation PDAC precursor formation: By (1) inducing inflammatory environment and by (2) regulating cell autonomous acinar transdifferentiation, leading to accelerated PanIN development.

J. Krützfeldt¹, A. Mizbani¹

Identification of microRNAs involved in the activation of adult skeletal muscle stem cells

Endocrinology and Diabetes, University Hospital of Zurich, Zurich¹

Introduction:

Skeletal muscle has the ability to regenerate efficiently after heavy exercise or damage. This process is shown to be dependent on the proper function of muscle adult stem cells, named satellite cells or myogenic progenitors (MP). Upon injury these cells exit the quiescent phase and proliferate, making both myoblasts and undifferentiated cells which reconstitute the stem cell pool.

MicroRNAs (miRNAs) are a class of small noncoding RNAs that downregulate the expression of their target genes by inhibiting translation or inducing degradation of mRNA. It is getting increasingly evident that miRNAs are essential regulatory factors in the muscle regeneration process.

The aim of this study is to identify novel miRNAs involved in skeletal muscle regeneration and also investigate their relevance to the known muscular diseases such as Duchenne muscular dystrophy (DMD). With further understanding of the involved pathways, we hope to find targets for treating diseases related to impaired muscle regeneration, like muscular dystrophies, sarcopenia, and fibrosis.

Methods:

We use cardiotoxin (CTX) injections into Tibialis anterior (TA) muscles of mice as a model for muscle regeneration. MPs were sorted from regenerating and also adult skeletal muscle, and the RNA was subjected to Illumina deep sequencing. Regulated miRNAs were identified and their tissue specificity and expression levels in regenerating and adult skeletal muscle were examined by northern blot analysis and q-RT-PCR. The role of candidate miRNAs for proliferation of myoblasts was examined in vitro and in vivo by EdU assay. Inhibition and overexpression of miRNAs was done in myoblast cultures using transfection with antagomirs and miRNA mimics, respectively. Histological characterization of regenerating muscle with inhibited miRNA was done by H&E staining and immunofluorescence on tissue sections. Finally, transcriptome profile of cultured myoblasts with and without inhibition of miRNA was determined by RNA-seq to find the significant changes in gene expression and identify the miRNA targets. The serum miRNA levels in mdx mice at different ages were measured using spike-in synthetic miRNA as normalizer, as well as serum Creatine kinase levels using a specific kinetic assay.

Results:

Based on the data from initial screenings we selected one miRNA (pre-myomiR-1) for its remarkable enrichment in activated MP, freshly isolated or cultured in vitro. Our findings indicate that inhibition of this miRNA in regenerating muscle could downregulate early myogenic regulatory factors and upregulate adult muscle markers, suggesting a potential role in preventing premature differentiation of myoblasts. So far we observed no difference in proliferation rate of MP after inhibition of the miRNA. Several candidate target genes are identified and are being further investigated. The pre-myomiR-1 level in sera and skeletal muscle of mdx mice over a range of different ages shows a trend similar to skeletal-muscle-specific miRNA miR-206. This suggests the use of pre-myomiR-1 as a disease progression marker in DMD.

Conclusion:

We identified a novel miRNA significantly upregulated in skeletal muscle progenitors early after their activation. The expression of this miRNA in proliferating myoblasts is much higher than all other tissues tested. Our functional studies so far suggest a role for this miRNA in regulating the onset of differentiation in proliferating myoblasts. Our preliminary data on mdx mice shows promise of using it as a diagnostic biomarker for DMD. This will be examined on the DMD patients.

T. Gorski¹, J. Krützfeldt¹

Adipogenic potential and UCP1 expression in monoclonal colonies of skeletal muscle fibro-adipogenic progenitors

Endocrinology and Diabetes, University Hospital of Zurich, Zurich¹

Introduction:

While white adipocytes (WAs) store lipids in response to excessive energy intake, brown adipocytes (BAs) dissipate energy as heat due to the presence of uncoupling protein 1 (UCP1) in the mitochondrial inner membrane, increasing whole-body energy expenditure. Additionally, pockets of adipocytes expressing UCP1, called beige adipocytes, are found in white adipose tissue depots and there is evidence that fibro-adipogenic progenitors (FAPs) from skeletal muscle of Sv/129 mice can differentiate into BAs. Increasing the amount and activation of BAs or beige adipocytes in skeletal muscle could constitute a new means of treating obesity. The present study assessed the adipogenic potential and UCP1 expression of monoclonal colonies of FAPs from different skeletal muscles of obesity-prone C57Bl/6 and obesity-resistant Sv/129 mice.

Methods:

Skeletal muscle tissue was excised from adult Sv/129 and C57Bl/6 mice. To investigate possible differences between FAPs residing in muscles with different fiber-type content, skeletal muscles were separated into two samples: one containing only M. soleus (SOL, enriched for type-1 fibers), and other containing the remaining muscles from the hind limbs (HL). Samples were digested with collagenase and FAPs (CD31⁻CD45⁺α7 integrin⁺Sca1⁺) were single-sorted into 96-well plates using fluorescence-activated cell sorting. After reaching confluence or after 21 days in culture, growth medium was replaced by adipogenic induction medium (containing 10% fetal bovine serum, 1% antibiotics, 5 ug/ml insulin, 125 uM indomethacin, 5 uM dexamethasone, 0.5 mM isobutylmethylxanthine, 1 nM T3, 1 uM rosiglitazone) for 2 days, followed by culture in adipogenic differentiation medium (10% fetal bovine serum, 1% antibiotics, 5 ug/ml insulin, 1 nM T3, 1 uM rosiglitazone) for 5 days. Finally, cells were stimulated with 10 uM forskolin for 4 h. Adipogenesis was assessed through microscopy and colonies were classified as adipogenic (more than 20% of cells differentiated into adipocytes), fibrogenic (no cells differentiated into adipocytes) or mixed (few cells – less than 20% – differentiated into adipocytes). Expression of UCP1 was analyzed through Western blotting.

Results:

In total, 315 colonies were analyzed; 9% of them were adipogenic, 63% were fibrogenic and 29% were mixed. When the muscle group from which FAPs were isolated was considered, a tendency for higher percentages of adipogenic colonies in SOL (13%) than in HL (4%) was observed. This tendency seems to be more pronounced in Sv/129 (SOL: 21% adipogenic, 21% mixed and 59% fibrogenic colonies; HL: 8% adipogenic, 26% mixed, 66% fibrogenic colonies) than in C57Bl/6 mice (SOL: 3% adipogenic, 32% mixed and 65% fibrogenic colonies; HL: 0% adipogenic, 38% mixed and 63% fibrogenic colonies). The percentage of adipogenic colonies was higher in Sv/129 (15%) than in C57Bl/6 mice (1%). Of all colonies analyzed, only one (from SOL of a Sv/129 mouse) expressed UCP1, at a very low level compared to brown adipose tissue.

Conclusion:

Although a 7-days brown adipogenic treatment results in differentiation of FAPs into WAs in many monoclonal colonies of FAPs from C57Bl/6 and Sv/129 mice, formation of BAs was rather a rare event. Genetic background and muscle from which FAPs are isolated can play a role in FAP differentiation. It remains to be defined if the formed WAs are able to express UCP1 in response to treatment with browning agents.

A. Hartung¹, J. Krützfeldt¹

A high-throughput screen to identify microRNAs which influence human skeletal muscle metabolism

*Endocrinology and Diabetes, University Hospital of Zurich, Zurich*¹

Introduction:

Skeletal muscle is responsible for the major part of insulin stimulated whole body glucose disposal and plays an important role in the pathogenesis of insulin resistance. The decrease in insulin sensitivity correlates with metabolic inflexibility of skeletal muscle cells. Recently, the role of mitochondria has gained interest in explaining this metabolic disturbance. Different studies have shown that mitochondrial function is impaired during insulin resistance and that muscles of type 2 diabetic patients have less mitochondria than healthy individuals. The regulation of mitochondria mass and function are complex and dependent on multiple factors at the transcriptional level as well as regulatory mechanism at the post-transcriptional level.

MicroRNAs (miRNA) are small non-coding RNAs which are able to modulate gene expression by post-transcriptional mechanism. They have recently emerged as key regulators of metabolism but only little is known how miRNA affect mitochondrial function in regard to insulin resistance.

The aim of this project is to perform an unbiased approach to identify novel miRNAs which could be potent regulators of skeletal muscle metabolism.

Methods:

Fluorescent activated cell sorting (FACS) was used to isolate primary myoblast from human muscle biopsies. Myoblast were differentiated into myotubes and transfected via RNAiMax in a 384 well plate format. Insulin resistance was induced by treating myotubes with TNFalpha (20 ng/ml) for 24 h. Mitochondrial membrane potential was measured by JC-1 and metabolic activity by alamarBlue®. To perform a high-throughput screen the Janus pipetting robot coupled to a fluorescence plate reader (Perkin Elmer) will be used.

Results:

We developed a functional high-throughput screen. Culture and transfection condition of primary human myotubes in a 384 well format were optimized. Two high-throughput compatible readouts which could be run subsequently in the same assay were confirmed. JC-1 to analyze mitochondrial membrane potential and alamarBlue® to measure metabolic activity. Additionally, to perform this assay also in an insulin resistant phenotype, human myotubes were treated with TNFalpha. Insulin resistance was determined by a decrease in insulin stimulated Akt-phosphorylation at Ser473 as well as a reduction in metabolic activity measured by alamarBlue®.

Conclusion:

We have designed and optimized a bidirectional high-throughput screen to identify miRNAs which regulate mitochondria and metabolic activity of healthy and insulin resistant primary human myotubes. This assay will allow us to screen for relevant miRNAs from two different human microRNA libraries containing 2019 miRNA-mimics and inhibitors each (mirBase V19). Our studies could lead to new possibilities for the treatment of insulin resistance and diabetes.

D. Rittirsch¹, E. Wanner¹, V. Schoenborn¹, S. Märsmann¹, P. Cinelli¹, C. Werner¹, H-P. Simmen¹, G. Wanner¹

Role of the heme degradation pathway in systemic inflammation after multi-system injury

University Hospital Zurich, Division of Trauma Surgery¹

Introduction:

Trauma and tissue damage trigger an inflammatory response required for postinjury regeneration and tissue repair. In severe trauma, overwhelming systemic inflammation (SIRS) can result in additional damage to the host cells and the development of multi-organ failure (MOF) and sepsis. In the present study, we hypothesized based on transcriptomic screening analyses that activation of the heme degradation pathway is closely linked to the inflammatory response and contributes to adverse events during trauma-induced SIRS.

Methods:

Blood samples were collected from 115 patients with multiple injury (injury severity score ISS \geq 17 points) over a period of 21 days after trauma. Isolated RNA samples were analyzed for gene expression changes as a function of time. In a first step, a subset of the patient cohort (n=10) was screened by microarray technology. Based on explorative gene set analysis using DAVID and the gene expression pathway analysis software GeneGO, components of heme degradation pathway were identified as the pathway, in which the strongest changes occurred. In a second step, samples from all patients with complete data sets (n=67) at all time points were selectively analyzed for transcription of haptoglobin (HP), CD163, heme oxygenase-1 (HMOX-1), and biliverdin reductase A and B (BLVRA, BLVRB) by quantitative RT-PCR and correlated with clinical outcome parameters. For assessment of the severity of SIRS a novel scoring system was developed.

Results:

Transcription rates of the components of the heme degradation pathway HP, CD163, HMOX-1 and BLVR collectively showed robust changes following trauma, with considerable interindividual differences. Patients who received mass transfusions of packed red blood cells (RBCs) showed more severe levels of SIRS than patients without hemorrhagic shock which was associated with an increased length of stay on the ICU. On the transcriptional level, the severity of SIRS was reflected by the expression of HP, as were the changes in SIRS severity between specific time points (delta SIRS). Moreover, strong upregulation of the anti-inflammatory heme degradation pathway was associated with the incidence of infectious complications, including sepsis. Among all parameters analyzed, HP and the BLVRA/BLVRB ratio were identified as the most promising biomarkers for assessment of the activation level of the heme degradation pathway in trauma-induced SIRS.

Conclusion:

In the present study, we demonstrate for the first time that activation of the heme degradation pathway, which may be triggered by release of free heme after transfusion of RBCs in particular, affects the inflammatory response after severe trauma and thereby contributes to increased susceptibility to infectious complications. These findings are likely to have direct implications for the treatment strategy of severely injured patients since the underlying pathophysiology needs to be taken into account in order to minimize the risk for second hit damages and secondary complications.

C. Egger¹, S. Lukas¹, C. Waschkies², R. Martin¹, M. Rudin², S. Schippling¹

Using the afferent visual pathway model to quantify neurodegeneration in Multiple Sclerosis and experimental autoimmune encephalomyelitis – A translational optical coherence tomography (OCT) and diffusion-tensor-imaging (DTI) approach

Department of Neurology, University Hospital Zürich¹, Institute for Biomedical Engineering, University and ETH Zürich²

Introduction:

Multiple sclerosis (MS) is an inflammatory and neurodegenerative disease of the central nervous system in which several pathological mechanisms lead to neuro-axonal loss. Although disease subtypes are characterized by significant clinical and pathological heterogeneity, visual impairment is common in MS with 20% of patients presenting with visual impairment as a primary symptom (Miller et al., 2005). Frequently, episodes of MS-related acute optic neuritis are followed by structural retinal damage that can be quantified in vivo using optical coherence tomography (OCT) (Costello et al. 2006, Petzold et al. 2010). Since alterations in optic nerve as well as retina were also described in a mouse model of MS (Sun et al., 2007; Horstmann et al. 2013) investigating structural damage in the visual system might hold promising potential of quantifying neurodegenerative changes in a translational approach. Loss of retinal nerve fiber layer (RNFL) as well as ganglion cell layer (GCL) assessed by OCT and post-processing segmentation of macular images have shown to correlate densely with functional visual impairment as well as MRI-detected brain atrophy in MS patients (Walter et al. 2012; Young et al. 2013). In combination with diffusion-tensor-MRI (DTI), which might provide information about the integrity of the optic nerve, nearly the entire optic tract can be assessed as regards its structural integrity. Aim of this project is to evaluate feasibility and reliability of OCT and DTI in the quantification of neurodegenerative changes in the visual system of MS patients and EAE mice.

Methods:

To investigate the diffusion properties and therewith integrity of the optic nerve, chiasm and optic tract in mice, two EPI-DTI-sequences with 60 or 30 directions (TE = 35ms, TR = 2000ms) were tested in small group of C57BL/6 mice. Human DTI data have been acquired using a standard-MS-MRI-protocol. The data-set was examined regarding the resolution in the area of interest and the need of optimization.

At the time of submission of the abstract OCT (Micron IV, Phoenix Research Lab, Pleasanton CA, USA) has been performed in a group of C57BL/6-Tg(Tcra2D2,Tcrb2D2)1Kuch/J (2D2) mice using a circular scan (1 B-Scan, 512 A-Scans) around the optic nerve head (ONH) and a volume scan (512 B-Scans, 512 A-Scans) covering the ONH. Post-processing was carried out using ORION™ Software (Voxelon LLC, Pleasanton CA, USA) to segment retinal layers.

For human OCT imaging (SPECTRALIS OCT, Heidelberg Engineering, Heidelberg, Germany) latest scan protocols were used. Peripapillary circle scans (1 B-Scan, 1536 A-Scans), a star scan (24 B-Scans, 768 A-Scans) covering the ONH and a volume scan (61 B-Scans, 768 A-Scans) of the macula were acquired. System built in software was used to quantify retinal layers.

Results:

DTI (fractional anisotropy, axonal -, and radial diffusivity) of the visual system was shown to be feasible in mice. Repeated measures proved ON fractional anisotropy to be highly reproducible (six time points, three animals) with an averaged FA value of 0.829 (+0.039/-0.046) and an averaged intragroup stdev. of 0.024. A proof of concept study, reproducing the results of Sun et al., is ongoing. OCT assessments in mice were feasible, a reproducibility study is yet ongoing.

Conclusion:

While human OCT already belongs to the standard readouts at the USZ for MS-patients with visual pathway pathology and the optimization of the human DTI-sequence for optical pathway imaging is yet ongoing, OCT of the murine retina and DTI of the murine visual system have been established. Our results provide the methodological background, against which a multimodal imaging approach as

applied here may assist in assessing neurodegeneration in EAE and human MS using the afferent visual pathway as a model.

C. Razafinjatovo¹, M. Rechsteiner¹, Q. Zhong¹, P. Wild¹, P. Schraml¹, H. Moch¹

Comprehensive investigation of the mutational landscape in clear cell Renal Cell Carcinoma and its correlation to treatment response

Institute of Surgical Pathology, Department of Pathology, University Hospital Zurich, Switzerland¹

Introduction:

Sporadic renal cell carcinoma (RCC) is the most frequent malignant tumor arising from the kidney. RCC can be divided into different subtypes from which clear cell Renal Cell Carcinoma (ccRCC) is the most frequent and aggressive form. Treatments include surgery, immuno- and chemotherapy but are still suboptimal. Formation of ccRCC is thought to be closely connected to the functional loss of the von Hippel-Lindau (VHL) tumor suppressor gene which is mutated in up to 70% of the cases. Several other genes, such as PBRM1, SETD2 and BAP1, have been recently found to be altered in ccRCC as well. The possible existence of mutational patterns specific for the clear cell subtype and their impact on the patients' response to therapy are unclear.

Methods:

In this study, we used the IonTorrent technology on the Ion Proton instrument and the Ion AmpliSeq™ Comprehensive Cancer Panel. We focused first on 18 genes including VHL, HIF1A, PDGFB, PDGFA, PDGFRA, PDGFRB, PBRM1, SETD2, BAP1, KDM6A, KDM5C, NFKB1, EGFR, TP53, CARD11, TSC1, MTOR, and PTEN. The experiment was conducted on 17 human kidney cell lines and 33 nephrectomy samples. The ccRCC patients were treated with Tyrosine Kinase Inhibitors, mTOR inhibitors or immunotherapy after surgery: 18 patients presented with progressive disease, nine had stable disease and six had regressive disease. Sequencing data were analysed using the Ion Reporter variant caller and the Integrative Genomics Viewer visualization tool. Total variants found were filtered based on two main criteria: a coverage higher than 50 reads and an allele ratio higher than 30%.

Results:

Nine of the ccRCC cell lines showed variants (90%, 9/10) and four of the other subtypes cell lines were mutated (80%, 4/5). The genes showing the most variants were VHL (64%, 11/17), BAP1 (23%, 4/17), SETD2 (12%, 2/17) and PDGFR (12%, 2/17). All patients showed a variant in at least one of the selected genes. The genes with the highest mutation rates were VHL (79%: 26/33), SETD2 (39%: 13/33), PBRM1 (33%: 11/33) and BAP1 (12%: 4/33). We are currently investigating the impact of the variants on the treatment response.

Conclusion:

Deciphering individual mutation maps may give rise to the pathways being altered in ccRCC, thus revealing new therapeutic options.

M. Neidert¹, D. Kowalewski³, F. Wolpert², S. Stevanovic³, L. Regli¹, M. Weller², G. Eisele²

The natural HLA ligandome of glioma stem-like cells: Another step towards peptide-based immunotherapy

*Department of Neurosurgery, University Hospital Zurich, Switzerland*¹, *Department of Neurology, University Hospital Zurich, Switzerland*², *Department of Immunology, Institute for Cell Biology, University of Tübingen, Germany*³

Introduction:

The human leukocyte antigen (HLA) ligandome is the showcase of a cell's protein content and the level at which the immune system monitors cells for pathological alterations.

Glioblastoma is the most frequent and the most malignant primary brain tumor. Despite advances in radiotherapy and chemotherapy, the prognosis of glioblastoma remains poor. In recent years, there is growing evidence for the presence of glioma-initiating cells within glioblastomas exhibiting stem cell properties, which are named glioma stem-like cells (GSC). In a hierarchical tumor model, GSC are supposed to have important functions in the initiation, maintenance, and resistance of glioblastoma and therefore warrant evaluation as a possible target for immunotherapy. Exclusively- or over-expressed proteins in GSC are expected to serve as tumor-associated antigens (TAA). TAA give rise to HLA-bound peptide ligands which are recognized by T cells. They are believed to be suitable targets for T cell-based immunotherapy.

The aim of this project is the large-scale analysis of HLA ligands (peptides) of GSC and freshly resected solid glioblastoma samples as a novel source for defining candidates for peptide-based immunotherapy.

Methods:

Pellets of GSC lines (GS-2, GS-5, GS-9) culture-expanded in neurobasal medium or snap frozen freshly resected glioblastoma samples are used to produce a cell lysate. Immunoprecipitation of the HLA-peptide complexes from this lysate is performed using the HLA-A, B, and C specific antibody W6/32 (HLA class I) coupled to cyanogen bromide-activated sepharose columns followed by acidic elution, size exclusion ultrafiltration and lyophilization. Isolated peptides are sequenced using a liquid chromatography and tandem mass spectrometry setup (LC-MS/MS). Peptides are annotated to specific HLA allotypes by taking the HLA type of the patient into consideration as well as known binding motifs of different allotypes. Peptide sequences are assigned to their corresponding source protein using the Basic Local Alignment Search Tool.

Results:

The HLA ligandome analysis of GSC pellets (GS-2, GS-5, GS-9) yielded 3871 peptides derived from 3587 source proteins. A total of 4059 peptides derived from 2985 source proteins were isolated and sequenced from freshly resected solid glioblastoma samples (n=6). When compared to a comprehensive HLA ligandome database of normal human tissues including normal brain, 340 source proteins were exclusively represented on the ligandome of GSC, 51 proteins were represented on both GSC and solid glioblastoma, and 145 source proteins were specific for solid glioblastoma. The immunogenicity of candidate peptides is currently under investigation by priming T cells of healthy donors followed by Enzyme Linked Immuno Spot Assays (ELISpot) and tetramer stainings.

Conclusion:

HLA-bound peptides presented exclusively on GSC or on both GSC and differentiated glioblastoma cells are promising targets for immunotherapy. The characterization of the HLA ligandome of GSC is only the first, but an important step in a translational approach towards a patient-individualized, peptide-based immunotherapy addressing the glioblastoma stem cell niche.

G. Strittmatter¹, L. French¹, H. Beer¹

Keratinocytes, the Inflammasome and Viral Infection

Dermatology, University Hospital, Zurich¹

Introduction:

Inflammasomes are multiprotein immune complexes, which induce an inflammatory response upon sensing of different stress signals. This effect is mainly mediated by activation and secretion of the proinflammatory cytokines prointerleukin(IL)-1 β and -18. Both cytokines have been implied in the defense against Herpes simplex virus (HSV)-1 in mouse models. HSV-1 is a common human pathogen, which is able to establish lifelong latency in neural ganglia. Infection of epithelial cells, such as keratinocytes, in the course of primary infection but also after reactivation of the virus from latency, results in a lytic cycle with release of newly generated virions. Human keratinocytes, although not professional innate immune cells, express functional inflammasome complexes and can respond to certain danger or pathogen associated molecular patterns by inflammasome activation. Here, we assessed whether keratinocytes are able to respond to infection with the double-stranded DNA viruses Modified vaccinia Ankara (MVA) and HSV-1 by initiating inflammation.

Methods:

We infected human primary keratinocytes with MVA, wild type, UVB-inactivated, or replication-deficient HSV-1 *in vitro* and assessed inflammasome activation in these cells by ELISA and Western blotting. RNAi-mediated knockdowns of gene expression were used to investigate the involvement of different inflammasome components in sensing of the viral infection. Infection rates and replication were analyzed using flow cytometry and qPCR-based quantification of viral DNA, respectively. In addition, we established an *ex vivo* infection model of human epidermis with HSV-1. Viral infection was analyzed in this case by immunohistochemistry.

Results:

Here we report that infection of human primary keratinocytes with MVA or HSV-1 induced secretion of mature IL-1 β and -18 in a time- and dose-dependent manner. The secretion was dependent on several inflammasome complexes including the AIM2 and NLRP3 inflammasomes. Whereas prestimulation of keratinocytes with interferon (IFN)- γ moderately increased MVA-induced IL-1 β secretion, it was essential for substantial cytokine secretion caused by HSV-1 infection. HSV-1 suppressed both proIL-1 β expression and secretion, which was dependent on viral gene expression as we could show by infection with UVB-inactivated virus and a mutant virus lacking ICP27, a gene involved in transcriptional activation of several other viral genes. IFN- γ priming was able to restore HSV-1-suppressed proIL-1 β expression and secretion. Most importantly, IFN- γ strongly suppressed viral replication in keratinocytes.

Conclusion:

Our results suggest that, comparable to herpesviridae infection in mice, human keratinocytes might be involved in control of HSV-1 replication in human skin by a positive feedback loop of keratinocyte-derived IL-1/IL-18 and IFN- γ expressed by immune cells.

K. Schilcher¹, A. Zinkernagel¹

Impact of subinhibitory concentrations of clindamycin on biofilm formation and matrix composition in *Staphylococcus aureus*

*Infectious Diseases and Hospital Epidemiology, University Hospital Zurich, Zurich*¹

Introduction:

Staphylococcus aureus is a Gram-positive bacterium responsible for acute life threatening infections as well as chronic infections as found in association with foreign bodies. Foreign body infections are characterized by biofilms. The biofilm matrix produced by *S. aureus* consists of polysaccharides, proteins and extracellular DNA (eDNA). Typically the eDNA of the biofilm matrix is partially degraded by the *S. aureus* nuclease Nuc1. This partial degradation is crucial for structuring the biofilm and dissemination of bacterial cells in mature biofilms. In addition amyloid fibres phenol soluble modulins (PSMs) are crucial for the development of mature biofilms. Biofilm associated infections are very difficult to treat since antibiotics and antimicrobial peptides barely penetrate through the biofilm matrix. This results in an antibiotic diffusion gradient and subsequently in subinhibitory antibiotic concentrations within the biofilm. It was previously shown that subinhibitory concentrations of clindamycin lead to upregulation of certain bacterial virulence factors. We aimed to investigate whether subinhibitory concentrations of clindamycin affect the matrix composition of *S. aureus* biofilms.

Methods:

S. aureus strains were grown for 18 and 36 hours in 96-well plates for static biofilm assays in presence and absence of clindamycin. Biofilm mass was measured with a photometer after staining with crystal violet. eDNA was isolated from sonicated biofilms by enzymatic digestion and phenol:chloroform extraction and subsequently visualized on agarose gel with ethidium bromide. Altered gene expression of *pmsβ* upon clindamycin exposure was assessed by quantitative RT-PCR (qRT-PCR).

Results:

S. aureus biofilms grown in presence of clindamycin subinhibitory concentrations formed a thicker biofilm compared to biofilms grown without clindamycin. The observed difference correlated with increased levels of eDNA. The increase in biofilm production was independent of the Nuc1 repression by clindamycin since the *S. aureus* Nuc1 mutant showed an increase in biofilm mass when grown in presence of clindamycin compared to the same mutant grown without clindamycin. We observed an approximately 40-fold upregulation of *pmsβ* gene expression in biofilms grown in presence of subinhibitory concentrations of clindamycin.

Conclusion:

Exposure to subinhibitory concentrations of clindamycin, which is routinely used to treat foreign body infections, lead to increased *S. aureus* biofilm formation. The increased biofilm mass correlated with increased eDNA levels in the biofilm. However we clearly showed that this was not due to Nuc1 repression by clindamycin subinhibitory concentrations. The observed upregulation of *pmsβ* upon clindamycin exposure is a potential mechanism for the increase in biofilm mass that is currently under investigation. This study provides the basis for further research on PSMs and eDNA as potential drug targets against biofilm-associated staphylococcal infections.

T. Wälchli^{1,2,3}, A. Wacker¹, J. Shiu⁴, S. Pantasis¹, H. Schneider⁵, J. Vogel⁶, V. Vogel⁴, M. Schwab³, M. Weller⁵, O. Bozinov², K. Frei^{1,2}, L. Regli², S.P. Hoerstrup¹

Nogo-A and S1PR2 as novel regulators of developmental and tumor angiogenesis in the CNS

Group of CNS Angiogenesis and Neurovascular Link, and Physician-Scientist Program, Swiss Center for Regenerative Medicine and Division of Surgical Research, and Neuroscience Center Zurich and Division of Neurosurgery, University and University Hospital Zurich, and Department of Health Sciences and Technology Swiss Federal Institute of Technology (ETH) Zurich, Zurich, Switzerland¹, Division of Neurosurgery, University Hospital Zurich, Zurich, Switzerland², Brain Research Institute, University of Zurich and Department of Health Sciences and Technology, Swiss Federal Institute of Technology (ETH) Zurich, Zurich, Switzerland³, Laboratory of Applied Mechanobiology, Department of Health Sciences and Technology, Swiss Federal Institute of Technology Zurich, Zurich, Switzerland⁴, Division of Neurology and Laboratory of Molecular Neurooncology, University Hospital Zurich, Zurich, Switzerland⁵, Institute of Veterinary Physiology, Vetsuisse Faculty, University of Zurich, Zurich, Switzerland⁶

Introduction:

Glioblastomas are among the most common brain tumors, associated with a poor prognosis. One hallmark of glioblastoma growth is angiogenesis, the formation of new blood vessels. Classical approaches to target glioblastoma angiogenesis – for instance using the anti-VEGF-A antibody bevacizumab (Avastin®) – have not led to the desired improvement of patient survival. Accordingly, there is a great interest in identifying novel regulators of brain tumor angiogenesis.

There is emerging evidence that the patterning of neural and vascular networks in health and disease (e.g. brain tumors) are governed by common mechanisms, through guidance molecules acting on the neural growth cone as well as on the endothelial tip cell. The membrane protein Nogo-A is mainly expressed in the central nervous system (CNS) and has well-known functions as a very potent, myelin-derived neurite outgrowth inhibitor and as a regulator of axonal growth in the CNS. Recently, we have identified a new, unexpected function for Nogo-A as a negative regulator of angiogenesis in the developing CNS. Interestingly, the Nogo-A specific receptor has recently been identified as the Sphingosine 1-Phosphate-Receptor 2 (S1PR2).

Based on these exciting findings, the two main objectives for this project are as follows:

Investigation of a potential role for the ligand-receptor pair Nogo-A and S1PR2 for angiogenesis during CNS development and in brain tumors, with a special emphasis on glioblastoma.

Further investigation of the molecular mechanisms underlying the effects of Nogo-A and S1PR2 during developmental CNS and in brain tumor angiogenesis, including ligand-receptor interaction, downstream signaling pathways as well as interaction with the VEGF-VEGFR2-Dll4-Jagged-Notch pathway.

Methods:

To address the question whether Nogo-A and S1PR2 regulate glioblastoma angiogenesis, we use a combination of *in vivo* and *in vitro* techniques, namely:

in vivo: Genetically modified mice (Nogo-A^{-/-}, S1PR2^{-/-}), orthotopic glioma mouse models, human tissue samples and tissue microarray, immunofluorescence, laser scanning confocal microscopy

in vitro: Isolated human and mouse microvascular endothelial cells, qRT-PCR, Western blot analysis, migration experiments, spreading experiments, current molecular and cellular techniques

Results:

So far, we could show that Nogo-A is expressed in vicinity of growing blood vessels and endothelial tip cells expressing S1PR2 during mouse and human brain development *in vivo*. At the functional level, the number of endothelial tip cells was significantly increased in Nogo-A^{-/-} as well as in S1PR2^{-/-} mice, indicating a negative regulatory role for this ligand-receptor pair *in vivo*. During mouse and human glioblastoma angiogenesis, Nogo-A showed a perivascular expression pattern whereas S1PR2 was expressed on the glioblastoma vasculature. In mouse gliomas, S1PR2 was upregulated within the tumor as compared to the surrounding brain tissue and in vicinity of brain tumor endothelial tip cells.

Moreover, Nogo-A inhibited the adhesion, spreading, migration and filopodia- and lamellipodia of primary murine brain-derived microvascular endothelial cells (MVECs) as well as of human glioblastoma-derived MVECs *in vitro*. Interestingly, these effects were – at least in part – mediated by the Nogo-A receptor S1PR2. Mechanistically, we have obtained preliminary results indicating that Nogo-A-S1PR2 signaling interacts with VEGF-A-VEGFR2-Dll4-Jagged-Notch signaling *in vitro*.

Conclusion:

Our data indicate a negative regulatory role for Nogo-A-S1PR2 in mouse and human developmental brain- and glioblastoma angiogenesis.

P. Zanoni¹, L. Rohrer¹, A. Von Eckardstein¹

Development of a genome-wide siRNA screening as a tool to unveil new players in liver HDL holoparticle uptake

Institute of Clinical Chemistry, University Hospital of Zurich¹

Introduction:

Plasma HDL levels inversely correlate with the risk of developing cardiovascular disease. The uptake of circulating HDL by the liver is the most important step in regulating their plasma levels and in mediating some of their biological effects. To fully understand this internalization mechanism though we need to discover virtually all the molecular players and the regulatory proteins involved in it. The availability of new genome-wide siRNA libraries, liquid handling robots and high throughput microscopes allows now to directly visualize the internalization of lipoproteins in liver cells and how it changes when the expression levels of thousands of genes are selectively modulated via RNA interference.

Methods:

In this work, we present our effort to optimize conditions for a genome-wide siRNA screening aimed to study the internalization of fluorescently-labeled HDL by Huh-7 cells.

Results:

We focalize on the optimization of reverse transfection conditions, the choice of appropriate internal controls and the development of a microscopy assay in a 384 well plate format.

Conclusion:

Our data represent a first step towards a genome-wide siRNA screening aimed to reveal new players involved in HDL holoparticle uptake in the liver. The hits generated through this approach could be exploited as pharmacological targets to modulate HDL function.

BONE MARROW INJURY AND ITS CONSEQUENCES ON HEMATOPOIETIC RECONSTITUTION FOLLOWING RADIATION CONDITIONING AND HEMATOPOIETIC CELL TRANSPLANTATION

Klinik für Hämatologie, Universitätsspital Zürich, Schmelzbergstrasse 12, 8091, Zürich Switzerland¹

Introduction:

Allogeneic hematopoietic cell transplantation (HCT) following chemo/radiotherapy conditioning remains the only treatment option for many malignant and a variety of benign hematologic disorders. Immune cells of the donor are critical for tumor control, a phenomenon referred to as graft-versus-leukemia (GVL) effect. However, donor immune cells, specifically T cells, also target host tissues and can induce a clinical syndrome called graft-versus-host disease (GVHD). GVHD is one major cause of morbidity and mortality following allogeneic HCT, and thus impedes the success and broader application of HCT. Acute GVHD of the skin, the liver and the intestines is well characterized and is one major cause of morbidity and mortality following allogeneic HCT. In contrast, little attention is paid to the subclinical effects of alloreactive T cells on the bone marrow microenvironment and how structural damage of the marrow could affect blood formation and leukemia control. Rather, with regards to hematopoietic reconstitution and immune function, donor T cells are generally believed to be beneficial for the recovery following HCT. We challenge this hypothesis and study here the effects of conditioning and allogeneic HCT on the bone marrow microarchitecture and hematopoietic reconstitution using flow cytometry and 3D-confocal microscopy.

Methods:

Here we use mouse models of lethal and sublethal total body irradiation (TBI) conditioning, in some experiments followed by allogeneic HCT (C3H.SW (H2b) into C57BL/6 (H2b)). Hematopoietic reconstitution and changes to the microarchitecture of the stromal cell compartment were assessed by flow cytometry and 3D-confocal microscopy at several time points (up to 2 months) post-transplant.

Results:

To this point we determined in a baseline experiment, examining the damage of the conditioning regimen alone, that in B6-mice by day 4 after both, lethal (950 cGy) and sublethal (475 cGy) TBI there were no residual Lin⁻Sca1⁺cKit⁺ hematopoietic stem cells (HSC) detectable; however, in mice given sublethal TBI HSC started to recover by day 14. Regarding the non-hematopoietic, stromal compartment on day 4 post lethal and sublethal TBI there appeared to be an increased proportion of endothelial cells (CD45⁻Ter119⁻Sca1⁺CD31⁺). In terms of 3D-bone imaging, morphologically by day 4 early signs of destruction of the extracellular matrix were detectable manifesting as vasodilation of the sinusoids; by day 7-10 adipocytes appeared and ultimately dominated the hollow spaces between the completely destructed extracellular matrix and severely vasodilated sinusoids. Around day 14 in mice given sublethal irradiation extracellular matrix and sinusoids started to recover and adipocytes disappeared. Ultimately, at 2 months post TBI there was complete recovery of the bone marrow microenvironment similar to healthy controls.

These experiments set the basis for the currently ongoing studies transplanting allogeneic hematopoietic grafts (containing donor HSC plus donor immune cells, including alloreactive donor T cells) compared with transplantations of congenic grafts. Preliminary data here show even more distinct marrow hypocellularity following transplantation of alloreactive T cells than sublethal irradiation alone induces.

Conclusion:

In summary, hematopoiesis is a 3D process involving the interactions between the blood cells and their environment. GVH-related damage of the stromal microarchitecture can influence hematopoietic reconstitution following allogeneic HCT significantly, and should therefore be further investigated.

P. Cheng¹, O. Shahkova³, D. Widmer¹, D. Zingg³, S. Frommel², B. Belloni¹, M. Raaijmakers¹, O. Eichhoff¹, S. Goldinger¹, R. Santoro², S. Hemmi⁴, K. Hoek¹, L. Sommer³, R. Dummer¹, M. Levesque¹

Methylation dependent SOX9 expression mediates invasion in human melanoma cells and is a negative prognostic factor in advanced melanoma

Dermatology Clinic, University Hospital Zürich, Zürich, Switzerland¹, Institute of Veterinary Biochemistry and Molecular Biology, University Zurich, Switzerland², Institute of Anatomy, University of Zurich, Zürich³, Institute of Molecular Biology, University of Zürich, Switzerland⁴

Introduction:

Melanoma is the most fatal skin cancer displaying a high degree of molecular heterogeneity. Phenotype switching is a mechanism that contributes to melanoma heterogeneity by altering transcription profiles for the transition between states of proliferation/differentiation and invasion/stemness. As phenotype switching is reversible, epigenetic mechanisms, like DNA methylation, could contribute to the changes in gene expression.

Methods:

RNA microarray and DNA microarray were performed for RNA expression and DNA methylation respectively on 10 melanoma cell cultures. Integrative analysis of methylation and gene expression datasets of five proliferative and five invasion melanoma cell cultures revealed two distinct clusters.

Results:

SOX9 was methylated and lowly expressed in the highly proliferative group. SOX9 overexpression resulted in decreased proliferation but increased invasion *in vitro*. In a B16 mouse model, sox9 overexpression increased the number of lung metastases. Transcriptional analysis of SOX9-overexpressing melanoma cells revealed enrichment in epithelial to mesenchymal transition (EMT) pathways. Survival analysis of the TCGA melanoma dataset showed that metastatic patients with high expression levels of SOX9 have significantly worse survival rates. Additional survival analysis on the targets of SOX9 revealed that a majority of SOX9 down-regulated genes have survival benefit for metastatic patients.

Conclusion:

Our genome wide DNA methylation and gene expression study of 10 early passage melanoma cell cultures revealed two phenotypically distinct groups. One of the genes regulated by DNA methylation between the two groups was SOX9. SOX9 induces melanoma cell invasion and metastasis and decreases patient survival. A number of genes down regulated by SOX9 have a negative impact on patient survival. In conclusion, SOX9 is an important gene involved in melanoma invasion and negatively impacts melanoma patient survival.

Y. Kok¹, V. Vongrad¹, M. Shilaih¹, H. Kuster¹, R. Kouyos¹, H. Günthard¹, K. Metzner¹

HIV-1 Integration Sites in Macrophages and CD4⁺ T Cells are Distinct

Department of Infectious Diseases and Hospital Epidemiology, University Hospital Zurich, Zurich¹

Introduction:

The host genetic surroundings of integrated HIV-1 provirus have great impact on the activity of the HIV-1 LTR. Thus, HIV-1 integration site (IS) studies will contribute to the understanding of how to reactivate latent HIV-1 provirus, a currently pursued approach to eradicate the latent reservoir. Analysis of *in vivo* HIV-1 IS in macrophages is not feasible as it is too invasive to obtain them from HIV⁺ patients. Moreover, IS analysis in monocyte-derived macrophages (MDMs) has only been done *in vitro* and was never compared to CD4⁺ T cells within the same experimental settings. In this study, we compared and characterized HIV-1 IS in treated HIV-1⁺ patients' MDMs and activated CD4⁺ T cells infected *ex vivo* with the patients' autologous primary HIV-1 isolates.

Methods:

A total of 7 patients from the Zurich Primary HIV Infection study were selected based on the following inclusion criteria: (i) Successful viral suppression for ≥ 2 years and (ii) Efficient replication of autologous primary HIV-1 isolates in donors' MDMs. Patients' autologous HIV-1 and the clonal HIV-1_{JR-FL} strain were used. HIV-1 IS were amplified with optimized non-restrictive linear amplification-mediated PCR, and sequenced using next generation sequencing technology. Sequencing reads were subjected to high quality trimming and mapped to the human genome. Gene clustering was done using the online bioinformatics tool DAVID. Fischer's exact test was used for statistical analysis.

Results:

A total of 1160 unique HIV-1 IS were analysed. As expected, HIV-1 favours integration into introns of genes. However, autologous HIV-1 was less likely to integrate into introns of genes in MDMs compared to CD4⁺ T cells ($p < 0.01$). Significant difference was not observed between autologous HIV-1 and HIV-1_{JR-FL} in MDMs for all genetic features examined. Consistently, analysis with DAVID showed that 37.5% versus 15.8% of enriched gene clusters (DAVID enrichment score ≥ 1.3) in MDMs infected with HIV-1_{JR-FL} and CD4⁺ T cells infected with autologous HIV-1, respectively, overlap with those in MDMs infected with autologous HIV-1. Additionally, we have identified 12 genes in which at least 3 different HIV-1 IS are found between cell types and/or HIV-1 strains. 5 of these genes form an enriched cluster associated with catabolic processes and 3 have been found previously in clonally expanded CD4⁺ T cells *in vivo*.

Conclusion:

HIV-1 IS patterns between MDMs and CD4⁺ T cells are distinct. Nonetheless, MDMs and CD4⁺ T cells have common hotspots for HIV-1 integration.

A. Scherer¹, J. Böni², W. Yang¹, R. Kouyos¹, S. Yerly³, T. Klimkait⁴, H. Günthard¹

HIV-1 Drug Resistance among ART-Experienced Patients in the Swiss HIV Cohort Study between 1999 and 2013

University Hospital Zürich, Division of Infectious Diseases and Hospital Epidemiology¹, University of Zürich, Switzerland², Geneva University Hospitals, Geneva³, University of Basel, Basel⁴

Introduction:

Patients infected with HIV-1 viruses carrying drug resistance mutations have limited treatment options. Therefore it is important to monitor time trends of emergence of HIV-1 drug resistance at a population level.

Methods:

We studied the presence of HIV-1 drug resistance among 11,148 patients from the Swiss HIV Cohort Study (SHCS) who were treated with antiretroviral treatment (ART) between 1999 and 2013. A total of 8,152 genotypic resistance tests were performed among 3947 ART-experienced patients (>120 days on ART). Patients were categorized in three groups based on their first-line ART: 1) historic ART included single class therapies or dual class therapies with one nucleoside reverse transcriptase inhibitor (NRTI), 2) historic combination ART (cART) included unboosted protease inhibitors (PI) and at least two NRTIs and 3) potent cART included treatments with ≥ 3 drugs which contained NRTIs, non-nucleoside reverse transcriptase inhibitors, ritonavir-boosted PIs, entry inhibitors or integrase inhibitors. HIV-drug resistance was defined as the presence of ≥ 1 major mutation defined by IAS-USA 2014.

Results:

The number of ART-experienced patients in the SHCS increased from 4621 in 1999 to 8105 in 2013. The number of patients with historic first-line ART/cART steadily decreased due to loss-of-follow-up or death whereas the percentage of actively participating patients with potent first-line cART increased from 5.9% in 1999 to 61.0% in 2013. The number of patients detected with ≥ 1 drug resistance mutation remained stable within the last 10 years (about 2000 patients) but the proportion of ART-experienced patients detected with a mutation decreased substantially from 34.7% in 2003 to 24.2% in 2013 ($p < 0.001$). In 2013, 974 patients had single-class drug resistance (12.0%), 721 (8.9%) dual-class drug resistance and 265 (3.3%) triple-class drug resistance. Most patients with dual and triple-class drug resistance started their treatment with historic ART, 52.3% and 71.1%, respectively. Triple-class resistance was very rarely detected among patients who started with potent first-line cART (0.4% in 2013) but was increasing among patients with first-line historic ART (0.1% in 1999 to 10.8% in 2013, $p < 0.001$). Transmitted drug resistance is becoming more important in proportion to acquired drug resistance. The fraction of transmitted drug resistance mutations contributing to the overall drug resistance of ART-experienced patients was 14.7% in 1999 and continuously increased to 27.8% ($p < 0.001$) in 2013 (not to be confused with the transmission rate of drug resistance which did not increase since the last 15 years).

Conclusion:

Our study demonstrates that the emergence of drug resistance can be minimized in a setting with new potent therapies and close monitoring. Multiple-class resistance remains mainly a problem for patients who have once received historic ART. This population has limited treatment options and should be observed carefully to avoid the transmission of drug-resistant viruses.

A. Rafiei¹, H. Takizawa³, Y. Saito², M. Manz¹

Establishment of a human B-RAF^{V600E} mutated LCH model in humanized mice

Department of Hematology, Universitätsspital, Zürich¹, Kobe University Graduate School of Medicine, Kobe, Japan², Kumamoto University, Kumamoto, Japan³

Introduction:

Langerhans cells histiocytosis (LCH) disease was assumed for the past 40 years to be a pathologic reactive process with the epidermal Langerhans cells (LC) being the cell of origin of this disease. However, this malignancy was recently redefined to be a neoplastic transformation due to the identification of high frequency mutations in MAPK pathway-related genes. Also a somatic mutation in the *B-RAF* gene (*B-RAF*^{V600E}) was detected in more than 50% of the LCH lesions. The high frequency of the *B-RAF*^{V600E} mutation in LCH disease indicates a central role for this kinase in the pathogenesis of this malignancy. However, the cellular origin of LCH and the mechanism of transformation is still unclear. In recent studies we found that the expression of *B-RAF*^{V600E} in distinct hematopoietic compartments defines the stage and the clinical risk in LCH disease; Whereas the expression of *B-RAF*^{V600E} in differentiated dendritic cells (DC) resembled low risk disease, the expression of this mutant in DC precursors was associated with high risk disease. The aim of this study is to create a xenograft mouse model, in order to model the disease and identify the blood-borne LCH-initiating cells. We recently generated MISTRG mice that express multiple human myeloid cytokines. Thus, these mice might be suitable for the development and support of myeloid neoplasia and are used for the experiments.

Methods:

HeLaHR-5 cells were infected lentivirally using synthetic bidirectional promoter vector harboring luciferase (as control) or *B-RAF*^{V600E} constructs and western-blot analysis was performed in order to investigate the effect of *B-RAF*^{V600E} on the phosphorylation status of Erk1/2 proteins. CD34⁺ cells isolated from cord blood samples were infected lentivirally with luciferase or *B-RAF*^{V600E} vectors in the presence of supportive growth factors. For colony forming unit (CFU) assay CD34⁺ cells were plated in M4230 medium and scored microscopically after 14 days for colony formation. The *In vivo* experiments were performed by the injection of transduced CD34⁺ intrahepatically into newborn MISTRG mice, which were sublethally irradiated previous to transplantation. Adult mice were analyzed subsequently for investigating the development of LCH-like disease.

Results:

Here we show that the expression of *B-RAF*^{V600E} constitutively activates the MAPK kinase pathway by measuring the phosphorylation status of Erk1/2 proteins. Also our preliminary *in vivo* data reveal that the lentivirally infected CD34⁺ cells harboring control vector or *B-RAF*^{V600E} engraft and proliferate successfully in 3rd generation of humanized mice. The rate of engraftment of *BRAF*^{V600E} cells seemed to be higher than the mice transplanted with control vector.

Conclusion:

The preliminary data obtained in this study indicate that the application of a synthetic bidirectional promoter expressing *B-RAF*^{V600E} enables the expression of this gene in CD34⁺ human cells. The CD34⁺ cells harboring *B-RAF*^{V600E} are able to engraft and proliferate in the 3rd generation of humanized mice and this should enable us to investigate the pathogenesis and the biology of LCH.

Q. Zhong¹, M. Gabrani², T. Guo³, P. Schüffler⁴, R. Aebersold³, H. Moch¹, P. Wild¹

Computational profiling of heterogeneity reveals high concordance between morphology and proteomics-based methods in prostate cancer

Institute of Surgical Pathology, University Hospital Zurich, Zurich¹, IBM Research-Zurich, Ruschlikon², Institute of Molecular Systems Biology, ETH, Zurich³, Department of Computer Science, ETH, Zurich⁴

Introduction:

Tumor heterogeneity is widely acknowledged as a critical hurdle for personalized medicine. However, the complexity of intra- and inter-tumor heterogeneity has not been fully investigated. We aim to explore tumor heterogeneity by integrating morphological and proteomics data. We model prostate cancer intra- and intertumor heterogeneity at the morphological level, using a novel computational workflow, and compare quantitative profiling of image-based morphological heterogeneity with proteomic measurements of the same tissues.

Methods:

We have collected a cohort of 39 prostate cancer patients with different degrees of tumor grade evaluated by Gleason score, and constructed a tissue microarray (TMA), followed by H&E staining. We developed a computational workflow that generates mathematical models for intra- and inter-tumor heterogeneity. More specifically, we used scale-invariant feature transform (SIFT) to model the tissue morphology, and developed a computational geometry algorithm to model the tissue topology. For the same cohort, we further punched out fresh frozen tissues from different regions for proteomic analysis using a cutting-edge methodology termed pressure cycling technology (PCT), coupled with SWATH-mass spectrometry (SWATH-MS). We then analyzed and compared the heterogeneity at the morphological and proteomic level.

Results:

We used our image-based computational workflow to mathematically represent each sample of the 39- patient cohort with multiple TMA cores per patient (non-tumorous and tumor regions of different Gleason scores, 105 cores in total). In the proteomic analysis of the same dataset, we quantified over 3000 proteins. In silico analysis of generated morphological and proteomic data matrices by statistical testing revealed a high concordance (measured by probabilistic model distance) between the morphological-based and proteomic-based profiling of tumor heterogeneity.

Conclusion:

Our integrative analysis of tumor heterogeneity demonstrates a strong association between the phenome and proteome of prostate cancer specimens, contributing to the development of personalized therapy for patients.

Comparable whole exome sequence data from FFPE and snap-frozen skin samples*Department of Dermatology, Universitätsspital, Zurich¹***Introduction:**

In dermatology, multiple skin conditions have been shown to follow Blaschko's lines, the patterns of cell migration during embryological development. Several of these diseases have been demonstrated to be caused by genetic factors such as a *de novo* somatic mutation causing a cutaneous mosaicism. Thus, genetic investigation of skin biopsies in affected areas and subsequent comparison to germline DNA should allow identification of underlying genetic risk factors. In preparation for a study involving one of these conditions, namely linear localized scleroderma, we asked what biopsy types are suitable for this type of study.

The most frequently available types of biopsies are formalin fixed and paraffin embedded (FFPE) samples that are suitable for immunohistology. A drawback of this mode of preservation is that the DNA in these samples accumulate changes mainly the deamination of cytosine to deoxyuracil. This process results in non-reproducible and misleading sequencing artefacts therefore extra-stringent quality controls have to be in place to ensure accuracy. Snap-freezing of biopsies in liquid nitrogen keeps DNA intact and might thus be a better starting material.

Here we asked whether the quality and quantity of DNA extracted from FFPE and snap-frozen tissue is comparable, also in terms of coverage during sequencing and if FFPE samples show more sequencing artefacts.

Methods:

To investigate this, non-tumorous skin samples (n = 3) were cut in two, half fixed in formalin and embedded in paraffin, the other half was snap frozen. The GeneRead FFPE kit (Qiagen) was used to extract DNA from the FFPE samples with a treatment step with the UDG (uracil-DNA glycosylase) enzyme. The corresponding snap frozen samples were extracted using QIAamp DNA Blood Mini kit (Qiagen). In multiple studies on tumours, FFPE samples are used as starting material for whole exome sequencing (WES). Previous studies have shown that after the FFPE samples have been treated with UDG, this deamination step is reversed resulting in sequencing artefacts being reduced by up to 93%.

Results:

Quantity of DNA of snap-frozen material was significantly higher (average of 1.755 µg vs 1.515 µg FFPE). After shearing of DNA, fragment size was comparable and the library preparation flawless for both types of samples. In 91.45% of bases, 20x coverage was achieved in both sample types. We did not see more C>T variants in FFPE than in snap-frozen which would indicate presence of formalin-induced artefacts. Finally, we sought to compare with paired genotype calling whether the genotypes match between FFPE and snap-frozen tissue. VarScan was used to call somatic mutations and the FFPE samples were designated as the "tumor" whilst the snap-frozen samples were labelled "healthy tissue". This resulted in only 1-2 somatic mutations in each pair of tissue from the same patient.

Conclusion:

All the measures so far have shown comparable quality of FFPE and snap-frozen material, therefore we conclude that both sample types are valid and can be used together in one study. We will therefore continue the study using the above methods to a collected cohort of linear localized scleroderma patients including both FFPE and snap frozen samples.

K. Deml¹, S. Merkelbach-Bruse², H. Künstlinger², K. Albus², M. Ihle², K. König², L. Heukamp⁵, J. Wolf⁴, R. Büttner², HU. Schildhaus³

Genetic and phenotypic diversity of BRAF mutations in lung cancer

Institute of Surgical Pathology, University Hospital Zurich, Zurich, Switzerland¹, Institute of Pathology, University Hospital Cologne, Cologne, Germany, as part of the Lung Cancer Group Cologne (LCGC)², Institute of Pathology, University Hospital Göttingen, Göttingen, Germany³, Department I of Internal Medicine, Centre of Integrated Oncology Köln-Bonn, University of Cologne, Cologne, Germany, as part of the Lung Cancer Group Cologne (LCGC)⁴, Institut für Hämatopathologie Hamburg, Hamburg, Germany⁵

Introduction:

BRAF mutations have been identified as a potential therapeutic target in a variety of human cancers. Our aim was to determine clinical, morphologic and molecular characteristics of *BRAF* mutated lung cancer samples.

Methods:

2529 consecutive lung cancers were tested for *BRAF* mutations as part of a comprehensive genetic characterization. Immunohistochemical staining for the V600E mutation was carried out in a subset of cases.

Results:

56 tumors harbored a *BRAF* mutation, among them 54 (96.4%) adenocarcinomas, one (1.8%) squamous and one sarcomatoid carcinoma (1.8%). We identified five different mutational subtypes in exon 11, including one newly described in this report. Among thirteen different mutational subtypes in exon 15 five are here reported for the first time.

Conclusion:

Having evaluated the so far largest series of unselected lung cancers we could determine the frequency of *BRAF* mutations at 2.2% and show that *BRAF* mutations occur predominantly in solid and acinar subtypes of adenocarcinomas. The spectrum of *BRAF* mutations in pulmonary carcinomas is broader than previously thought with only 39.3% accounting for the V600E subtype (1% of all cancers).

O. Clerc¹, B. Kaufmann², M. Possner², R. Liga², J. Vontobel², F. Mikulicic², C. Gräni², D. Benz², B. Herzog², O. Gämperli², P. Kaufmann², R. Büchel²

Long-term prognostic performance of prospectively ECG-triggered low-dose coronary CT angiography

Department of Cardiology, University Hospital Zurich¹, Cardiac Imaging, Department of Nuclear Medicine, University Hospital Zurich²

Introduction:

This study aims at assessing the long-term prognostic performance of low-dose 64-slice coronary CT angiography (CCTA) using prospective ECG triggering in patients with known or suspected coronary artery disease.

Methods:

We retrospectively included 434 patients undergoing low-dose CCTA with prospective triggering (CCTA-PT), stratified according to maximal coronary lesions in CCTA-PT: normal, non-obstructive lesions (luminal narrowing <50%), obstructive stenosis (luminal narrowing ≥50%) and previously revascularized patients. Coronary artery calcium score (CACS) was also recorded. Follow-up was performed using hospital records and telephone interviews regarding major adverse cardiac events (MACE), defined as cardiac death, non-fatal myocardial infarction or need for elective revascularization. Revascularizations within 6 weeks after CCTA-PT were excluded because they were potentially triggered by scan findings. Kaplan-Meier analysis, Cox regressions and receiver operating characteristic (ROC) curves were performed for prediction of MACE.

Results:

Mean effective radiation dose from CCTA-PT was 1.7 ± 0.6 mSv. At baseline, 153 (35%) patients had normal arteries, 87 (20%) non-obstructive lesions, 131 (30%) obstructive stenosis and 34 (8%) were previously revascularized. Twenty-nine (7%) patients were lost to follow-up. After a median follow-up of 6.1 years, MACE occurred in 0% of normal patients, in 6% with non-obstructive lesions, in 30% with obstructive stenosis and in 39% of revascularized patients. Multivariate Cox analysis identified obstructive stenosis and CACS as independent MACE predictors ($p < 0.001$). Area under ROC curve was significantly higher for CCTA-PT than CACS.

Conclusion:

Low-dose CCTA-PT has an excellent prognostic performance with a warranty period of at least 6 years for patients with normal coronary arteries.

O. Clerc¹, M. Possner², R. Maire³, R. Liga², T. Fuchs², S. Dougoud², J. Stehli², J. Vontobel², F. Mikulicic², C. Gräni², D. Benz², B. Herzog², R. Büchel², P. Kaufmann², O. Gämperli²

Is left bundle branch block a predictive factor of coronary artery disease?

Department of Cardiology, University Hospital Zurich¹, Cardiac Imaging, Department of Nuclear Medicine, University Hospital Zurich², Specialist for Cardiology and Flight Medicine, Private Practice, Männedorf³

Introduction:

Left bundle branch block (LBBB) is considered an unfavorable prognostic marker in patients with underlying heart disease. Testing for coronary artery disease (CAD) is often prompted by incidental LBBB finding, but published studies disagree about a significant association between LBBB and CAD. We therefore assessed the association of LBBB with previously unknown CAD in patients undergoing coronary CT angiography (CCTA).

Methods:

We enrolled 818 patients (mean age 57.2±11.1 years, 106 LBBB patients and 712 controls) without known CAD, cardiomyopathy, severe valvular disease or congenital heart disease who underwent 64-slice CCTA at our institution. Image quality was assessed on a 4-point scale for each coronary segment. Comparison of CAD prevalence (defined as ≥50% coronary stenosis) was performed using triple case-matching for pre-test probability (based on age, gender and typicality of symptoms) in 101 LBBB patients and 303 matched controls.

Results:

There was no difference in obstructive CAD prevalence between LBBB patients (n=101) and matched controls (n=303) (15% versus 16%, p=0.88). Similarly, no significant differences were found in the number of cardiovascular risk factors (CVRF), stenosis severity, CAD extent, non-obstructive disease and vessel-based analysis between both groups. Image quality was very high in LBBB patients and comparable to controls. On multivariate analysis, age, gender, typical angina and CVRF, but not LBBB (p=0.94), emerged as significant and independent predictors of obstructive CAD.

Conclusion:

CAD prevalence is similar in LBBB patients at low-to-moderate pretest probability compared to controls matched for age, gender, symptom typicality and cardiovascular risk factors. CCTA is a useful imaging modality in LBBB patients providing comparable image quality to non-LBBB controls.

J. Stehli¹, O. Clerc¹, T. Fuchs², S. Dougoud², M. Possner², R. Liga², J. Vontobel², F. Mikulicic², C. Gräni², D. Benz², P. Kaufmann²

Impact of Monochromatic Reconstructions from Single-Source Dual-Energy Coronary CT Angiography on Stenosis Evaluation. A Comparison to Invasive Angiography.

Department of Cardiology, University Hospital Zurich¹, Cardiac Imaging, Department of Nuclear Medicine, University Hospital Zurich²

Introduction:

In coronary CT angiography (CCTA), stenosis evaluation is limited by artefacts such as blooming. Monochromatic reconstructions from single-source dual-energy CCTA were shown to reduce image noise and improve image quality. The aim of this study was to analyse the impact of monochromatic CCTA reconstructions on stenosis quantification using invasive coronary angiography (ICA) as standard of reference.

Methods:

Patients who were referred for clinically indicated assessment of coronary artery disease without known stent implantation or bypass graft surgery underwent CCTA and ICA within 4 months. Standard polychromatic CCTA images as well as 8 monochromatic series between 50 and 140 keV were reconstructed. Luminal narrowing of coronary lesions was measured in all CCTA reconstructions and compared to ICA with quantitative coronary angiography (QCA). Plaque composition was determined by CCTA.

Results:

Of 37 patients with a mean age of 63.4 years and a broad range of BMI (19.9 - 45.5 kg/m²), 124 lesions were studied. Throughout all reconstructions, CT measurements showed a significant correlation with QCA ($P < 0.001$), except for 50 keV. Calcified and mixed lesions were generally overestimated and soft plaques underestimated by CCTA. In stepwise regression, reconstructions with 90 keV showed the best correlation to QCA (coefficient 0.9, $P < 0.001$, adjusted R^2 0.9). Analysis by plaque composition suggested a superior performance of reconstruction at 90 keV for calcified plaques and at 140 keV for soft plaques.

Conclusion:

Comparing monochromatic and polychromatic images, reconstruction at 90 keV showed the best correlation with ICA for analysis of coronary lesions. Thus, monochromatic reconstruction appears as a promising technique to refine the diagnostic performance of CCTA.

P. Kambakamba¹, M. Linecker¹, K. Slankamenac¹, M. DeOliveira¹

The value of retrieved lymph node number for Perihilar Cholangiocarcinoma Staging

Department of Surgery, Swiss HPB & Transplantation Center, University Hospital Zurich, Zurich, Switzerland

Objective:

The purpose of this systematic review was to evaluate the number of retrieved lymph nodes for staging of patients undergoing surgery for perihilar cholangiocarcinoma (PHC).

Nodal status is an important prognostic factor for survival in PHC. A certain benchmark of lymph node retrieval (LNR) is necessary in order to guarantee a significant lymph node staging and to avoid under staging. However the required minimum number of retrieved lymph nodes remains unclear for PHC. The 7th AJCC TNM edition increased the requirement for the histologic examination of lymph nodes in PHC patients from 3 to 15. The relevance of such recommendation appears to be arbitrary and questionable.

Methods:

The MEDLINE, EMBASE, and The Cochrane Library databases were systematically screened up to December 2014.

Results:

725 abstracts were screened and twenty studies were included for analysis, comprising 3986 patients. The cumulative median LNR was 7 (2- 24). A median LNR ≥ 15 was reported in 9% of PHC patients and could only be achieved in extended lymphadenectomy. Subgroup analysis revealed a median LNR of 7 (range 7-9) detected the most lymph node positive (N+) patients and showed the lowest risk for under staging patients. In contrast LNR ≥ 15 did not increase detection rate of N+ patients.

Conclusions:

The systematic analysis revealed LNR ≥ 7 is adequate for prognostic staging, while LNR ≥ 15 does not improve detection of patients with tumor positive lymph nodes.

S. Salemi¹, A. Mortezaei¹, T. Sulser¹, D. Eberli¹

The Role of Autophagy in the Differentiation of Adipose Derived Stem Cells to Functional Smooth Muscle Cells for Urologic Tissue Engineering

¹Laboratory for Urologic Tissue Engineering and Stem Cell Therapy, Department of Urology, University Hospital Zurich, Switzerland.

Introduction

Tissue engineering using smooth muscle cells may provide a treatment option for diseases with smooth muscle pathology such as bladder dysfunction, urinary incontinence, and erectile dysfunction. As autologous smooth muscle cells (SMC) should not be harvested from organs with end-stage disease and tissue regeneration requires large amount of functional SMCs, there is a need for other cell sources. Adipose derived stem cells (ADSC) can be harvested easily and can be differentiated into SM tissue. We have shown that autophagy, a conserved lysosomal degradation pathway, is required for cell survival and differentiation of human blood and skin SC. ADSC undergoing differentiation to SMC efficiently remodel their cytoskeleton and shape in an energy-consuming process. We investigated the functional role of autophagy during differentiation and remodeling of ADSCs to SMC *in vitro*.

Methods:

Rat ADSCs were characterized by immunocytochemistry (ICC) and FACS. ADSC were induced towards SMC using MCDB induction medium for 1 to 6 weeks. The changes in gene and protein expression level for SMC specific markers: calponin, smoothelin, α -SMA, MyH11; and autophagy genes: LC3, Atg5, Beclin1, were investigated by ICC and WB.

Results:

Upon induction, up regulation of Atg5-Atg12 and free Atg5 was observed during 4 - 6 weeks. This was supported by an increase in conversion of cytosolic LC3I to membrane-bound LC3II protein. At the same time the contractile proteins calponin, MyH11 and smoothelin were up regulated during 1 - 3 weeks and decreased after 5 - 6 weeks of differentiation detected by WB and ICC.

Conclusion:

Our study demonstrates that autophagy plays an important role in ADSC differentiation to SMC. This finding might lead to novel supporting strategies for ADSC use in clinics, since autophagy can be easily influenced by FDA approved drugs.

S. Salemi, D. Keller, M. Rottmar, T. Sulser, D. Eberli

Synergistic effects of combining undifferentiated adult stem cells and differentiated cells for the engineering of functional bladder smooth muscle tissue.

Laboratory for Urologic Tissue Engineering and Stem Cell Therapy, Department of Urology, University Hospital Zurich, Switzerland.

Introduction:

Engineered tissues for bladder augmentation or substitution would allow circumventing the side effects of using bowel tissue for reconstruction. Tissue engineering using a combination of cells may provide novel approach for functional reconstruction. Adipose derived stem cells (ADSC) might be a key instrument to bioengineer contractile bladder tissue when differentiated to smooth muscle cells (SMC). However, it is uncertain whether these cells maintain their cell faith long term in vivo. It is our aim to evaluate different combinations of cells to improve the bladder tissue formation, by improving the microenvironment and cell-to-cell interactions.

Methods:

We have characterised rat ADSCs and optimally differentiated them to SMC (3 weeks) prior to subcutaneous injection into nude mice. Cells were injected in different combinations (ADSC, ADSC + differentiated ADSC, SMC, differentiated ADSC + SMC). The tissue formation was followed by MRI and PKH labelling. The formed tissue was analysed for contractile proteins measuring gene and protein expression by using RT-qPCR, Western Blot and immunohistochemistry.

Results:

In all experimental conditions, the PKH positive cells could be detected after 4 weeks, indicating the presence and survival of engineered tissues in vivo. MRI was able to visualize the engineered SM tissue over the study period. Collagen without cells showed no signal and was absorbed quickly. The tissue size differed between the experimental conditions with tissues grown from cells with 3 week ex vivo differentiation showing the largest constructs with good correlation in histology. Differentiated ADSC showed positive upregulation of smooth muscle makers (Calponin, Smoothelin, MYH 11 and α SMA) similar to bladder derived SMC.

Conclusion:

The presented research offers key information on survival and functionality of bioengineered smooth muscle tissue grown using differentiated ADSC in combination with differentiated cells. This approach could help to engineering contractile bladder tissue for future clinical application.

D. Haralampieva^{1,2,4}, S. Salemi¹, T. Betzel², I. Dinulovic³, S. Kramer², S. Ametamey², C. Handschin³, T. Sulser¹, D. Eberli^{1,4}

Metabolic Tracking Of Muscle Precursor Cells For Muscle Tissue Engineering by PET Imaging

1 Laboratory for Tissue Engineering and Stem Cell Therapy, Department of Urology, University Hospital, Zurich, Switzerland *2* Institute of Pharmaceutical Sciences, ETHZ, Zurich, Switzerland *3* Biozentrum, University of Basel *4* Zurich Center for Integrative Human Physiology (ZIHP)

Introduction

Regenerative medicine offers an alternative using autologous stem cell therapy for skeletal muscle reconstruction. In this study we investigated the possibility of using a mutated dopamine D2-receptor (D2R) and PET Imaging for precise localization and long-term *in vivo* tracking of the implanted cells for skeletal muscle engineering. Furthermore we established the implementation of a PET tracer for hypoxia measurement, thereby gaining more read-outs about the survival and metabolism of the implanted cells. This technology could be used for a wide variety of questions in muscle tissue engineering.

Methods:

Human muscle precursor cells (hMPCs) were isolated from muscle biopsies and expanded. The cells were genetically modified to express a mutated D2R, as D2R tracers are already used in clinics. The infected hMPCs were characterized via immunocytochemistry and FACS using muscle-specific markers and visualized with PET with specific tracer for dopamine receptors, as well as with a hypoxia tracer.

Results:

For the *in vivo* evaluation 30 million modified hMPCs were suspended in collagen and injected s.c. in nude mice. After 2 and 4 weeks the newly-formed muscle tissues were visualized by PET and harvested for autoradiography, histology and histomorphometry.

Transduction of hMPCs allowed precise detection by PET Imaging *in vitro*. The morphology after harvesting revealed no differences to non-transduced cells, confirming that using modified hMPCs does not alter the muscle phenotype or contractility.

PET Imaging of engineered muscles allowed cell tracking after transplantation and provided us with additional insights about their survival *in vivo*, by showing a significant decrease in hypoxia levels with time. Autoradiography confirmed the presence of the transduced cells in the engineered tissue.

Conclusion:

PET Imaging may offer a novel method for non-invasive visualization and metabolic read-outs of autologous stem cells after injection for future treatment of sphincter deficiency, by engineering new muscle fibers.

M. Rottmar^{1,2}, D. Keller², A. Boss¹, D. Eberli²

Monitoring of in vivo fiber formation of muscle precursor cells via magnetization transfer (MT)-MRI

¹ *Department of Urology, UniversityHospital Zurich, Switzerland*

² *Institute of Diagnostic and Interventional Radiology, UniversityHospital Zurich, Switzerland*

Cell based therapies using e.g. muscle precursor cells (MPCs) show great promise to treat stress urinary incontinence. However, for the translation of such approaches into clinics, non-invasive in-vivo imaging modalities are needed. Magnetization transfer (MT)-MRI provides contrast based on the presence of macromolecules such as proteins and lipids. Therefore, the aim of this study was to assess the muscle fiber formation of hMPCs *in vivo* using MT-MRI in a mouse model in correlation to histology and immunohistochemistry.

hMPCs were mixed with collagen and injected subcutaneously into nude mice and monitored via MRI (4.7 T scanner) for 4 weeks. A 3D-spoiled gradient-echo sequence (TR/TE 20.4ms/4.7ms) was applied with/without a systematically varied MT prepulse (off-resonance frequency 50Hz to 37'500Hz, flip angle 800°). The engineered muscle tissue was assessed by histology, immunohistochemistry and western blot.

At 1'750Hz, MT measurements showed magnetization transfer ratios (MTR) of 27.8% at day 1, decreasing to 18.1% at day 3, before increasing to 23.4%, 38.9% and 49.9% at days 7, 14 and 21, respectively; approximating the MTR of 64.3% from the skeletal muscle reference. A similar trend could be observed over a range of tested off-resonance frequencies. Cell differentiation and myofiber formation could be confirmed by histology, immunohistochemistry and western blot.

hMPCs form muscle tissue *in vivo* and MT-MRI allows to directly assess muscle fiber formation as a measure of the myogenic differentiation process. The results will be transferable to the clinical setting as a non-invasive biomarker for the assessment of muscle tissue regeneration in patients.

Conference Location

University Hospital Zurich
Grosser Hörsaal Ost
Rämistrasse 100
8091 Zürich

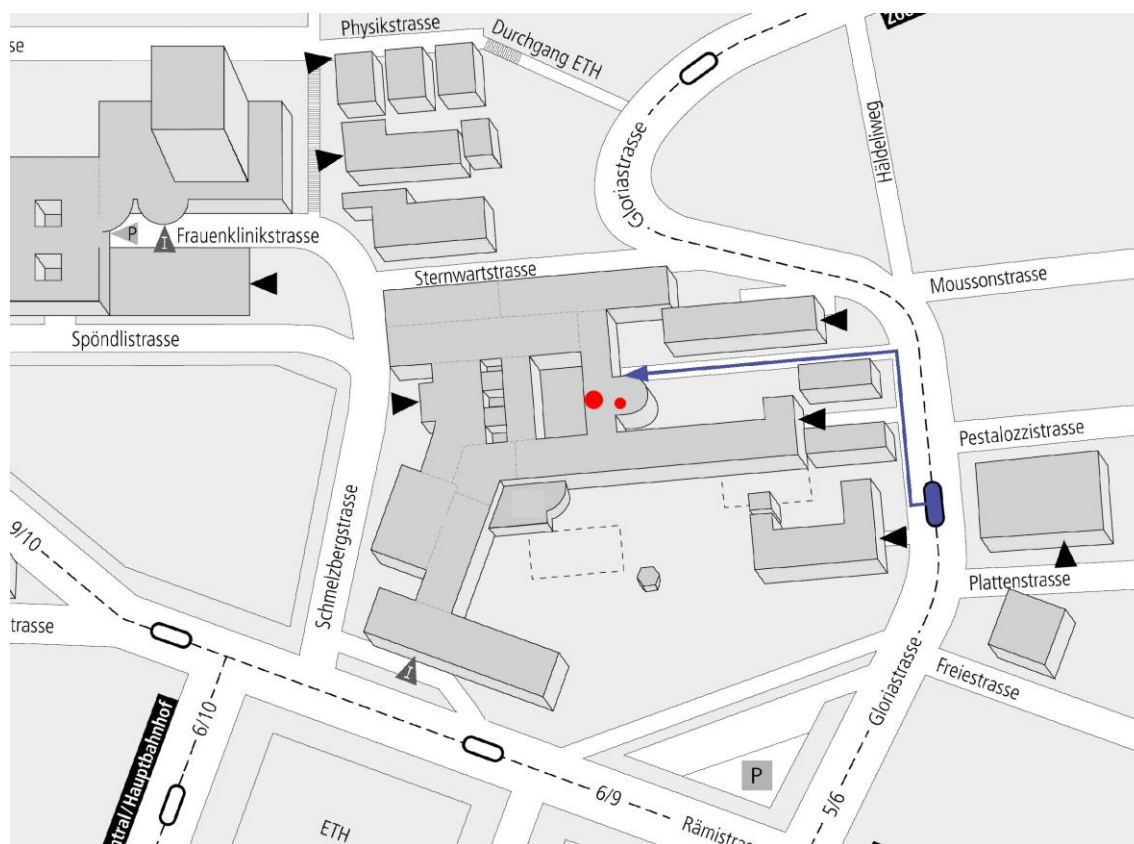
Contact Address

Prof. Dr. med. Gregor Zünd
Direktor Forschung und Lehre
Managing Director ZKF
UniversitätsSpital Zürich
gregor.zuend@usz.ch

phone: +41 (0) 44 634 55 00

fax: +41 (0) 44 634 55 03

Secretary office: +41 (0) 44 634 55 01



UniversitätsSpital
Zürich



Universität
Zürich^{UZH}